

Acute bilirubin toxicity causes hearing loss through presynaptic degeneration at a central glutamatergic synapse

A thesis submitted for the degree of
Doctor of Philosophy
at the University of Leicester

By

Martin D. Haustein

Department of Cell Physiology and Pharmacology
and MRC Toxicology Unit
University of Leicester

March 2011

ACUTE BILIRUBIN TOXICITY CAUSES HEARING LOSS THROUGH PRESYNAPTIC NEURODEGENERATION AT A CENTRAL GLUTAMATERGIC SYNAPSE

Martin D. Haustein

Severe neonatal jaundice causes bilirubin encephalopathy with complications such as ataxia, delayed neurodevelopment and deafness. The hair cells in the cochlea are spared suggesting central damage but the underlying mechanisms for this hearing loss are unknown. Utilising the Gunn rat model of hyperbilirubinemia I investigated the detrimental effect of high levels of bilirubin on the hearing system, using electrophysiological and imaging techniques combined with in vivo and in vitro studies of the auditory brainstem. My studies have focussed on synaptic transmission between the well characterised giant synapse called the calyx of Held and its target, the principal neuron of the Medial Nucleus of the Trapezoid Body (MNTB), as a model synapse.

In vivo auditory brainstem responses (ABR) revealed a significant loss of sound-evoked brainstem activity and increased thresholds after homozygous Gunn rats were exposed to elevated bilirubin levels. Extracellular field potential recordings from the MNTB in vitro using multi-electrode arrays showed impaired synaptic transmission. Whole-cell patch-clamp recordings from MNTB neurons confirmed that their electrophysiological properties remain essentially normal. Significantly, synaptic stimulation failed to elicit EPSCs from the giant synapse, with only smaller synaptic inputs being activated in homozygous Gunn rats exposed to elevated bilirubin levels. Multiphoton imaging of dextran-rhodamine labelled calyces in living brain slices revealed degeneration of the presynaptic terminals in Gunn rats exposed to high bilirubin. Electron microscopic images confirmed the loss of the presynaptic terminals observed in living tissue with no sign of degeneration in postsynaptic neurons. The use of neuronal nitric oxide synthase antagonist 7-nitroindazole protected the ABRs and the synaptic transmission in the MNTB. This implicates nitric oxide as playing a key role in bilirubin-induced neurodegeneration of the presynaptic terminals.

This research demonstrates for the first time that deafness associated with jaundice is fundamentally a neurodegenerative disease and suggests some novel therapeutic strategies.

ACKNOWLEDGEMENTS

First and foremost I want to thank God for giving me a hope beyond this life.

I am grateful to a number of people who made this PhD a memorable experience and provided expertise, encouragement and friendship through the course of this project:

My supervisor Prof. Ian D. Forsythe, for taking me on as a PhD student and securing the funding for the project, for finding the right balance between challenging and encouraging me and sharing his year-long experience with me. Deafness Research UK for funding my PhD scholarship.

Pauliina, for her love, friendship and for wanting to marry me.

My parents, for constant encouragement and support throughout my studies.

Christoph, for being the greatest brother in the world and for constantly supplying me with new and excellent music to listen to.

Paul and Velina Jordan, for their friendship and hospitality especially during the last months of the write-up.

Jessica and Alexander Seager and Adam Tozer, for their help with proof-reading several chapters of this thesis and for their friendship.

The members of the Forsythe lab for critical comments, fruitful discussions and joyful elevenses and 5 o'clock tea breaks with lots of biscuits, cakes, laughter and friendly banter.

I am indebted to and gladly acknowledge the help of:

Dr. Jörn Steinert for help with Ca^{2+} Imaging, advise on data and statistical analysis and for sharing tips and tricks of patch-clamping; David Read for sharing his microscopy expertise with me, helping to set up the multi-photon laser microscope and assisting with analysis of 3D z-stacks and electron microscopic images; Dr. Alistair Fryatt for teaching me how to perform ABR recordings; Drs. Robert Fern and Andy Smith for sharing their expertise on electron microscopy and bilirubin, respectively and for being on my PhD committee; DBS staff for looking so well after the Gunn rat colony and their help with the anaesthesia during ABR recordings.

DECLARATION

The work in this thesis is my own, and includes several collaborative projects, outlined below.

Simultaneous whole-cell patch-clamp and extracellular recordings from AVCN bushy cells were conducted with Marei Typlt. Calcium-Imaging experiments were carried out with Dr. Jörn R. Steinert. Perfusion fixation of the rats for electron microscopy was conducted with David J. Read. He also assisted with the double-blind analysis of the EM measurements and the analysis of the 3D z-stacks acquired through multi-photon imaging. Tissue samples for electron microscopy were prepared by Judy McWilliam and Tim Smith. The EM images were selected and recorded with the assistance of Dr. David Dinsdale. The first ABR recordings were performed with the help and under the supervision of Dr. Alistair Fryatt. ABR recordings in the presence of 7-NI and on Wistar rats were done together with Dr. Nadia Pilati.

Parts of this thesis have been previously published in Steinert *et al.*, 2008, Typlt *et al.*, 2010 and Haustein *et al.*, 2010.

TABLE OF CONTENTS

ABSTRACT	I
ACKNOWLEDGEMENTS	II
DECLARATION	III
TABLE OF CONTENTS	IV
TABLE OF FIGURES	VII
1. INTRODUCTION	1
1.1 HYPERBILIRUBINAEMIA, NEONATAL JAUNDICE AND BILIRUBIN ENCEPHALOPATHY (KERNICTERUS)	1
1.1.1 <i>A brief history of research on hyperbilirubinaemia</i>	1
1.1.2 <i>Bilirubin formation and hyperbilirubinaemia</i>	3
1.1.3 <i>Neonatal jaundice and bilirubin encephalopathy (kernicterus)</i>	7
1.1.4 <i>The Gunn rat model of hyperbilirubinaemia</i>	11
1.2 THE AUDITORY SYSTEM	12
1.2.1 <i>Sound transduction in the inner ear</i>	12
1.2.2 <i>Architecture of auditory brainstem</i>	13
1.2.3 <i>Processing of spatial information in the auditory brainstem</i>	16
1.3 ION CHANNELS AND NEUROTRANSMISSION.....	20
1.3.1 <i>Ligand-gated ion channels</i>	20
1.3.2 <i>Voltage-gated ion channels</i>	22
1.4 AIMS AND OBJECTIVE	25
2. MATERIAL AND METHODS	26
2.1 THE GUNN RAT MODEL OF HYPERBILIRUBINAEMIA	26
2.1.1 <i>Use of Gunn rats in this thesis</i>	30
2.2 AUDITORY BRAINSTEM RESPONSES (ABRs).....	32
2.3 PREPARATION OF <i>IN VITRO</i> BRAIN SLICES FROM THE MNTB	34
2.3.1 <i>Preparation of in vitro brain slices from the AVCN</i>	38
2.4 MULTI-ELECTRODE ARRAYS (MED64)	39
2.5 PATCH-CLAMP RECORDINGS	43
2.6 CALCIUM-IMAGING	45
2.7 DEXTRAN-LABELLING AND MULTI-PHOTON-IMAGING	47
2.7.1 <i>Dextran labelling</i>	47
2.7.2 <i>Multi-photon imaging</i>	48

2.8	ELECTRON MICROSCOPY	53
3.	RESULTS FROM MULTI-ELECTRODE ARRAY (MEA) AND AUDITORY BRAINSTEM RESPONSE (ABR) RECORDINGS	56
3.1	EXTRACELLULAR MULTI-ELECTRODE ARRAY (MEA) RECORDINGS	56
3.1.1	<i>Effects of temperature on the evoked field potential in the MNTB.....</i>	<i>60</i>
3.1.2	<i>Pharmacological characterisation of the evoked field potential in the MNTB.....</i>	<i>61</i>
3.1.3	<i>Long-term recordings of the evoked field potential in the MNTB at 32°C ..</i>	<i>69</i>
3.2	AUDITORY BRAINSTEM RESPONSES	77
3.2.1	<i>The effect of sulfadimethoxine on the evoked field potential in the MNTB at 32°C</i>	<i>83</i>
3.2.2	<i>Summary and Conclusions:.....</i>	<i>86</i>
4.	PATCH-CLAMP RESULTS	88
4.1	PATCH-CLAMP RECORDINGS IN THE MNTB	88
4.1.1	<i>Synaptic Stimulation</i>	<i>89</i>
4.1.2	<i>Voltage-Clamp.....</i>	<i>90</i>
4.1.3	<i>Current-Clamp.....</i>	<i>92</i>
4.1.4	<i>Miniature EPSCs</i>	<i>94</i>
4.2	PATCH-CLAMP RECORDINGS IN THE AVCN.....	96
4.2.1	<i>Summary and Conclusions:.....</i>	<i>100</i>
5.	RESULTS FROM IMAGING, LIGHT AND ELECTRON MICROSCOPY	101
5.1	CALCIUM-IMAGING	101
5.2	ANTEROGRADE DEXTRAN-LABELLING OF CALYCES OF HELD.....	103
5.3	LIGHT AND ELECTRON MICROSCOPY	106
5.3.1	<i>Cerebellum</i>	<i>106</i>
5.3.2	<i>Medial Nucleus of the Trapezoid Body</i>	<i>109</i>
5.3.3	<i>Cochlear Nucleus</i>	<i>114</i>
5.3.4	<i>Summary and Conclusions:.....</i>	<i>120</i>
6.	NITRIC OXIDE AND BILIRUBIN NEUROTOXICITY.....	121
6.1	THE NNOS BLOCKER 7-NITROINDAZOLE (7-NI) LEADS TO A PARTIAL RESCUE OF THE ABRs & MEA RECORDINGS	123
6.1.1	<i>Summary and Conclusions:.....</i>	<i>127</i>
7.	SUMMARY OF RESULTS	128

8. DISCUSSION.....	132
8.1 MEA RECORDINGS.....	133
8.1.1 <i>The effects of temperature on evoked field potentials in the MNTB</i>	133
8.1.2 <i>Pharmacological characterisation of evoked MNTB field potentials</i>	134
8.2 AUDITORY BRAINSTEM RECORDINGS	138
8.3 MEA RECORDINGS FROM ACUTE BRAINSTEM SLICES OF TREATED JJ-GUNN RATS...	139
8.4 PATCH-CLAMP RECORDINGS	141
8.5 CALCIUM-IMAGING	144
8.6 DEXTRAN LABELLING AND LIVE MULTI-PHOTON IMAGING.....	146
8.7 LIGHT AND ELECTRON MICROSCOPY IN THE CEREBELLUM	147
8.8 LIGHT AND ELECTRON MICROSCOPY IN THE MNTB.....	148
8.9 LIGHT AND ELECTRON MICROSCOPY IN THE VCN	150
8.10 PRESYNAPTIC DEGENERATION	153
8.11 THE ROLE OF NITRIC OXIDE (NO) IN BILIRUBIN-INDUCED NEURODEGENERATION	156
8.11.1 <i>Practical challenges of working with 7-NI in vivo</i>	156
8.11.2 <i>Nitric oxide and neurotoxicity</i>	158
8.11.3 <i>Astrocytes and bilirubin-induced neurotoxicity</i>	161
8.12 SUMMARY:	165
REFERENCES	166
LIST OF ABBREVIATIONS	

TABLE OF FIGURES

FIGURE 1.1 THE FORMATION OF BILIRUBIN. 4

FIGURE 1.2 SCHEMATIC DRAWING OF THE AUDITORY BRAINSTEM. 15

FIGURE 1.3 PROCESSING OF SPATIAL INFORMATION IN THE AUDITORY BRAINSTEM. 17

FIGURE 2.1 THE PHENOTYPE TELLS THE GENOTYPE OF HOMO- AND HETEROZYGOUS GUNN RATS. 31

FIGURE 2.2 SCHEMATIC DRAWING OF A RODENT BRAIN..... 35

FIGURE 2.3 SCHEMATIC DRAWING OF THE AVCN BRAIN SLICE PREPARATION..... 39

FIGURE 2.4 OVERVIEW OF THE COMPONENTS OF THE MED RECORDING SYSTEM. 41

FIGURE 2.5 ACUTE BRAIN SLICE ON MEA AND STIMULUS PARADIGM. 41

FIGURE 2.6 PRINCIPLES OF MULTIPHOTON LASER MICROSCOPY. 49

FIGURE 2.7 CHOOSING CELLS FOR EM ANALYSIS. 55

FIGURE 3.1 DEFINITION OF A CHARACTERISTIC MNTB EVOKED FIELD POTENTIAL AS RECORDED WITH MEAS. 58

FIGURE 3.2 EXAMPLE TRACE OF A CHARACTERISTIC MNTB FIELD POTENTIAL RECORDED WITH MEA. 59

FIGURE 3.3 EFFECTS OF TEMPERATURE ON THE EVOKED FIELD POTENTIAL IN THE MNTB. 61

FIGURE 3.4 THE EFFECT OF TETRODOTOXIN (TTX) ON THE EVOKED MNTB FIELD POTENTIAL..... 62

FIGURE 3.5 THE EFFECT OF Ca^{2+} FREE ACSF ON THE EVOKED MNTB FIELD POTENTIAL. . 63

FIGURE 3.6 THE EFFECT OF DNQX ON THE EVOKED MNTB FIELD POTENTIAL. 64

FIGURE 3.7 THE EFFECT OF AP-5 ON THE EVOKED MNTB FIELD POTENTIAL. 65

FIGURE 3.8 THE EFFECT OF DENDROTOXIN-I (DTX-I) ON THE EVOKED MNTB FIELD POTENTIAL..... 66

FIGURE 3.9 THE EFFECT OF TETRAETHYLAMMONIUM (TEA) ON THE EVOKED MNTB FIELD POTENTIAL..... 67

FIGURE 3.10 THE EFFECT OF BAY 41-2272 AND SODIUM NITRO-PRUSSIDE (SNP) ON THE EVOKED MNTB FIELD POTENTIAL. 68

FIGURE 3.11 VARIABLE EFFECTS OF FREE BILIRUBIN (20 μ M) ON MNTB FPs IN MEAS AT ROOM TEMPERATURE. 71

FIGURE 3.12 MEA RECORDINGS IN THE MNTB ARE STABLE FOR 2 HOURS AT 32°C. 72

FIGURE 3.13 FREE BILIRUBIN (20 μ M) LEADS TO REDUCED FIELD POTENTIAL AMPLITUDES IN THE MNTB AT 31°C. 73

FIGURE 3.14 MEA RECORDINGS FROM THE MNTB ARE STABLE FOR OVER 4H AT 32°C. 75

FIGURE 3.15 FREE BILIRUBIN HAS NO EFFECT ONTO EVOKED MNTB FIELD POTENTIALS IN SLICES OF JJ-GUNN RATS AT 32°C. 76

FIGURE 3.16 THE INDUCTION OF BILIRUBIN-TOXICITY THROUGH SULFADIMETHOXINE LEADS TO DECREASED ABRs IN JJ-GUNN RATS. 79

FIGURE 3.17 SULFADIMETHOXINE DOES NOT AFFECT ABRs IN WISTAR RATS..... 81

FIGURE 3.18 ABR THRESHOLDS FOLLOWING 'CLICK' STIMULI IN WISTAR AND JJ-GUNN RATS BEFORE AND AFTER SULFA-TREATMENT. 82

FIGURE 3.19 ABR THRESHOLDS FOLLOWING PURE-TONE STIMULI IN WISTAR AND JJ-GUNN RATS BEFORE AND AFTER SULFA-TREATMENT. 83

FIGURE 3.20 SULFADIMETHOXINE DOES NOT IMPAIR SYNAPTIC TRANSMISSION IN THE MNTB OF WISTAR RATS..... 84

FIGURE 3.21 SULFADIMETHOXINE INDUCED BILIRUBIN TOXICITY LEADS TO INCREASED SYNAPTIC DELAY AND REDUCTION OF THE C₂ AMPLITUDE. 85

FIGURE 4.1 THE GIANT CALYCEAL EPSC IS COMPROMISED IN PRINCIPAL MNTB NEURONS FROM TREATED RATS. 90

FIGURE 4.2 CURRENT-VOLTAGE RELATIONSHIPS IN CONTROL AND TREATED NEURONS SHOW NO EFFECT OF HIGH BILIRUBIN LEVELS ON POTASSIUM CHANNELS..... 91

FIGURE 4.3 HYPERBILIRUBINAEMIA DOES NOT CHANGE ACTION POTENTIAL PROPERTIES... 93

FIGURE 4.4 MINIATURE EPSCs ARE NOT CHANGED BY HYPERBILIRUBINAEMIA. 94

FIGURE 4.5 HYPERBILIRUBINAEMIA DOES NOT CAUSE SIGNIFICANT CHANGES IN THE PROPERTIES OF MINIATURE EPSCs. 95

FIGURE 4.6 CURRENT-CLAMP RECORDING OF A AVCN BUSHY NEURON..... 96

FIGURE 4.7 COMPARISON OF *IN VIVO* AND *IN VITRO* SINGLE-UNIT RECORDINGS FROM THE AVCN..... 97

FIGURE 4.8 PHARMACOLOGY REVEALS PRE- AND POSTSYNAPTIC ORIGIN OF COMPONENTS IN COMBINED INTRA- AND EXTRACELLULAR RECORDINGS. 99

FIGURE 5.1 BILIRUBIN DOES NOT CHANGE INTRACELLULAR CALCIUM CONCENTRATIONS. 102

FIGURE 5.2 MULTIPHOTON IMAGING REVEALS PRESYNAPTIC DEGENERATION IN TREATED GUNN RATS. 105

FIGURE 5.3 LIGHT MICROSCOPIC IMAGES FROM FIXED CEREBELLAR BRAIN SLICES SHOW ABERRANT PURKINJE CELLS IN JJ-GUNN RATS..... 108

FIGURE 5.4 ELECTRON MICROSCOPIC IMAGES FROM THE CEREBELLUM OF CONTROL AND TREATED RATS..... 109

FIGURE 5.5 LIGHT MICROSCOPIC IMAGES OF THE MNTB SHOW NO DIFFERENCES BETWEEN CONTROL AND TREATED RATS. 111

FIGURE 5.6 ELECTRON MICROSCOPIC IMAGES FROM THE MNTB OF CONTROL AND TREATED RATS..... 112

TABLE OF FIGURES

FIGURE 5.7 ELECTRON MICROGRAPHS OF MNTB PRINCIPAL NEURONS REVEAL NO SIGNS OF POSTSYNAPTIC DEGENERATION BUT CONFIRM LOSS OF PRESYNAPTIC PROFILES IN TREATED JJ-GUNN RATS.	113
FIGURE 5.8 LIGHT MICROSCOPY REVEALS DIFFERENCES BETWEEN THE VCN OF CONTROL AND TREATED GUNN RATS.	117
FIGURE 5.9 ELECTRON MICROSCOPIC IMAGES OF THE VCN FROM CONTROL GUNN RATS (A-D) AND TREATED GUNN RATS (E-H) SHOW STARK SIGNS OF NEURODEGENERATION..	118
FIGURE 5.10 ELECTRON MICROSCOPY REVEALS DIFFERENCES IN VCN BUSHY NEURONS BETWEEN CONTROL AND TREATED JJ-GUNN RATS.	119
FIGURE 6.1 PROTECTION FROM BILIRUBIN-INDUCED HEARING LOSS BY THE NNOS ANTAGONIST 7-NITROINDAZOLE (7-NI).	128
FIGURE 6.2 THE NNOS ANTAGONIST 7-NI DECREASES THRESHOLD ELEVATION BY SULFA IN JJ-GUNN RATS.	129
FIGURE 6.3 MEA RECORDINGS FROM ACUTE BRAINSTEM SLICES OF 7-NI TREATED GUNN RATS SHOW PROTECTED SYNAPTIC DELAY TIMES BUT DECREASED C ₂ AMPLITUDES.	130

1. Introduction

In the first part of this chapter a brief overview of the history of research on hyperbilirubinaemia will be given, followed by a description of the process of bilirubin formation before the clinical features of severe hyperbilirubinaemia and bilirubin encephalopathy are explained. In the second part, the auditory system is introduced with a particular focus on the role of the medial nucleus of the trapezoid body (MNTB) within the brainstem circuits. Subsequently, it will be explained how spatial information is processed at the level of the auditory brainstem, and some of the ion channels that are relevant for faithful action potential propagation in the MNTB will be briefly described.

1.1 Hyperbilirubinaemia, neonatal jaundice and bilirubin encephalopathy (kernicterus)

1.1.1 A brief history of research on hyperbilirubinaemia

In 1875, Johannes Orth described a striking yellow staining of the basal ganglia, hippocampus and cerebellum in what was probably the first pathological examination of brains from infants who died after severe jaundice (Orth, 1875). Christian G. Schmorl coined the term ‘kernicterus’ (meaning ‘yellow kernel’) in his paper in 1904, referring to the yellow staining of the basal ganglia and in the brainstem in autopsied brains from jaundiced infants (Hansen, 2000). When Becker and Vogel published their literature review in 1948, they already listed a total of 46 cases of kernicterus which had been pathologically examined

(Becker & Vogel, 1948). In addition, they presented further 7 autopsy case studies of kernicterus they had found in their own hospital, confirming the initial findings of Orth and Schmorl.

In 1952, Crigler and Najjar described a hereditary form of non-haemolytic jaundice leading to kernicterus (Crigler & Najjar, 1952), which was later named after them. Clinical observations led to the conclusion that sulfonamides displace bilirubin into tissues, including the brain and thereby increasing mortality rates and incident rates of kernicterus (Silverman *et al.*, 1956). Prior to this, in 1934, Charles J. Gunn discovered the rodent model organism, named 'Gunn rat' after him, which is still utilised to study hyperbilirubinaemia (Gunn, 1938). Lathe and Walker demonstrated that a liver enzyme deficiency in Gunn rats and human babies underlies elevated bilirubin levels in the blood (Lathe & Walker, 1958). The same enzyme deficiency was found in patients with Gilbert's syndrome (Arias & London, 1957). Initially, blood exchange transfusion was used to decrease blood bilirubin levels (Lathe, 1955). Later it was discovered that exposure of babies to light is positively correlated with decreasing bilirubin levels and reduced incidence of kernicterus, and phototherapy was proposed as a non-invasive treatment for elevated bilirubin levels (Cremer *et al.*, 1958; Dobbs & Cremer, 1975).

Extensive studies on Gunn rats showed that they mimic the Crigler-Najjar syndrome (inherited, non-haemolytic, same enzyme deficiency) in particular and severe neonatal jaundice in general (Schmid *et al.*, 1958; Blanc & Johnson, 1959; Johnson *et al.*, 1959; Johnson *et al.*, 1961; Shapiro, 1988; Shaia *et al.*, 2005).

In 1966, Diamond and Schmid showed that it is free bilirubin (i.e. unconjugated bilirubin, not bound to albumin) that enters the brain and not the conjugated form (Diamond & Schmid, 1966). Although free and not total bilirubin concentration in the blood is the best predictor for auditory neuropathy and bilirubin encephalopathy (Nakamura *et al.*, 1985; Amin *et al.*, 2001; Ahlfors & Parker, 2008; Ahlfors *et al.*, 2009) it is not yet widely used in clinical settings (Ahlfors, 2010).

In the late 1980s and 1990s, several groups demonstrated that free bilirubin can impair transmitter uptake into synaptic vesicles (Vazquez *et al.*, 1988; Ochoa *et al.*, 1993) and also that bilirubin interacts with (Leonard *et al.*, 1989) and can diffuse through cell membranes (Zucker *et al.*, 1999) and disrupt them (Rodrigues *et al.*, 2002a; Rodrigues *et al.*, 2002b). More recently, studies on neuronal and glial cultures showed that free bilirubin does not affect neurons and glia cells to the same extent (Notter & Kendig, 1986; Silva *et al.*, 2002; Brito *et al.*, 2008b), that bilirubin impairs neurite outgrowth (Fernandes *et al.*, 2009) and that nitric oxide and NMDA receptors are involved in bilirubin-induced neurotoxicity (Brito *et al.*, 2010).

1.1.2 Bilirubin formation and hyperbilirubinaemia

The human body produces about 300mg of bilirubin per day (Berk *et al.*, 1969), of which over 85% stem from haemoglobin (London *et al.*, 1950) and a smaller fraction from other sources of haem such as myoglobin or cytochromes. While the globin is degraded into amino acids, the haem group is degraded via biliverdin to bilirubin (Figure 1.1). Bilirubin is lipophilic and is bound to albumin in

the blood. It needs to be conjugated in the liver by the enzyme uridine-diphosphate-glucuronyl-transferase (UDP-GT) before the now more water-soluble, conjugated form (Figure 1.1) can be excreted in the bile (Bosma, 2003).

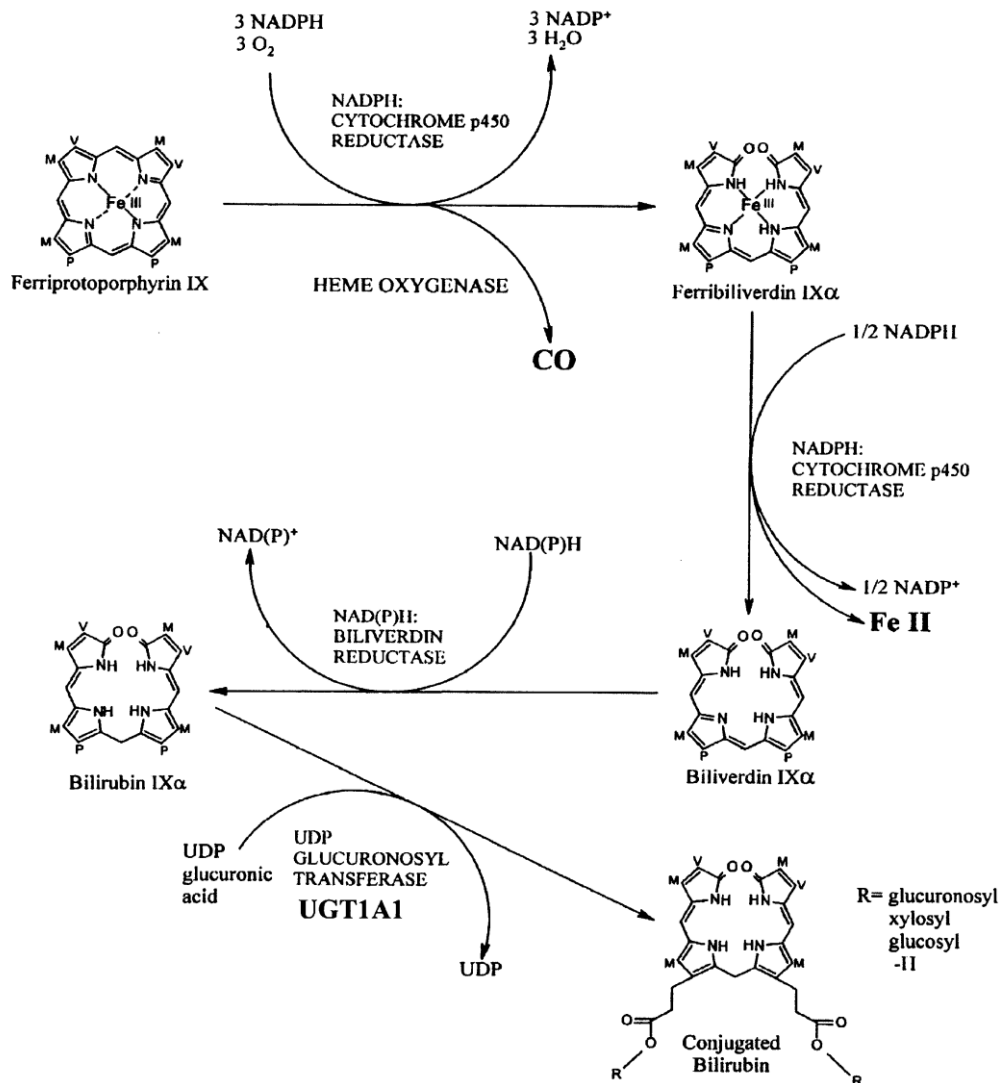


Figure 1.1 The formation of bilirubin.

Reprinted from *Journal of Hepatology* 38, Bosma, PJ: Inherited disorders of bilirubin metabolism, p107-117, Copyright (2003) with permission from Elsevier.

While birds and reptiles stop the degradation reaction chain at biliverdin, thereby saving two energy-consuming steps, mammals do not. The reason might be that, although it is costly to make bilirubin, it can be used by cells as an antioxidant (Stocker *et al.*, 1987; Dore *et al.*, 1999) and nitric oxide

scavenger (Mancuso *et al.*, 2003). Although the tissue concentration of bilirubin is only ~20-50nM (<0.1% of glutathione concentrations, a well-established cytoprotectant) (Baranano *et al.*, 2002), it protects cells from damage against nearly 10,000x higher concentrations of H₂O₂ (Baranano *et al.*, 2002).

In humans, 15 UDP-glucuronyl-transferases in the endoplasmic reticulum perform the detoxification process of over 350 compounds (Tukey & Strassburg, 2000), making them water-soluble and therefore excrete-able.

Hyperbilirubinaemia occurs when blood bilirubin levels are increased above normal. Concentrations of 0-0.03mg/dl for conjugated bilirubin and 0.2-1.9mg/dl for total bilirubin (conjugated plus unconjugated) are regarded as 'normal' in humans (MedlinePlus Encyclopedia). Marked signs of hyperbilirubinaemia, such as yellow sclera or skin, appear above 2.5-3mg/dl total bilirubin. This can occur in obstructive jaundice where the bile duct is blocked and conjugated bilirubin cannot flow into the intestine. It can also be an increase in unconjugated bilirubin as a result of high erythrocyte turn-over rate, e.g.: haemolytic jaundice, including Rhesus factor incompatibility. In such cases, UDP-GT cannot conjugate all the new bilirubin. This may also occur in non-haemolytic jaundice in neonates where UDP-GT enzymes do not yet work properly; or there can be genetic causes for elevated bilirubin-levels, i.e. reduced enzyme activity of UDP-GT in Gilbert's and Crigler-Najjar syndrome (Crigler & Najjar, 1952).

In Gilbert's syndrome, which affects about 5-10% of the population, the enzyme activity of UDP-glucuronyl-transferase 1A1 (UGT1A1) is reduced to about 30% of activity in healthy humans (Bosma *et al.*, 1995; Koiwai *et al.*, 1995). This is due to a heterozygous missense mutation in the gene for UGT1A1 (Aono *et al.*,

1995; Koiwai *et al.*, 1995). Depending on whether the mutation occurs in the promoter region or the gene itself, it will cause the milder or the more severe form, respectively (Monaghan *et al.*, 1996). Generally, patients with Gilbert's syndrome have normal conjugated bilirubin blood levels but slightly elevated total bilirubin levels (Aono *et al.*, 1995). Hence unconjugated bilirubin levels are elevated and can increase even more when under stress. In patients suffering from Crigler-Najjar syndrome the mean total bilirubin values are between 16 ± 5 mg/dl (Strauss *et al.*, 2006) to 24.5mg/dl (Crigler & Najjar, 1952) (normal: 0.2-1.9mg/dl), with a range from 15-45mg/dl for individuals (Crigler & Najjar, 1952; Cornelius & Arias, 1972; van der Veere *et al.*, 1996). These patients produce virtually no UDP-GT enzymes, due to a mutation in the gene that encodes UGT1A1 (Strauss *et al.*, 2006). Brain damage and/or death due to kernicterus are seen frequently in these patients (Crigler & Najjar, 1952; van der Veere *et al.*, 1996). Their continually monitored clinical care – especially in the early years – must include phototherapy, blood exchange transfusions and avoidance of drugs that displace bilirubin from albumin into tissues to prevent kernicterus. In absence of UDP-GT enzymes, alternative pathways are used to excrete bilirubin (Schmid & Hammaker, 1963), e.g. involving the oxidation of bilirubin and cytochrome P450 (Abu-Bakar *et al.*, 2005; de Matteis *et al.*, 2006).

1.1.3 Neonatal jaundice and bilirubin encephalopathy (*kernicterus*)

Hyperbilirubinaemia is common in newborns, affecting about 60% of all well term babies and 80% of preterm babies (National Collaborating Centre for Women's and Children's Health, 2010; Rennie *et al.*, 2010).

Severe hyperbilirubinaemia and its sequelae are still a problem in developing countries, e.g. Pakistan (Tikmani *et al.*, 2010), Iraq (Hameed *et al.*, 2011) or India (Mukhopadhyay *et al.*, 2010) as well as developed ones, e.g. the United Kingdom (Manning *et al.*, 2007), Canada (Sgro *et al.*, 2006), Italy (Dani *et al.*, 2011) or Denmark (Ebbesen, 2000; Ebbesen *et al.*, 2005).

Kernicterus – or bilirubin encephalopathy, as it is now called – is a condition in which high bilirubin levels lead to – transient or persistent – brain damage.

As kernicterus was initially a pathological diagnosis, it does require the examination of the brain of the deceased patients. Human autopsy studies of patients who died from kernicterus repeatedly found the same brain regions affected: the cerebellum, the basal ganglia, the hippocampus, the auditory brainstem (Becker & Vogel, 1948; Crabtree & Gerrard, 1950; Dublin, 1951; Gerrard, 1952; Fenwick, 1975; Ahdab-Barmada & Moossy, 1984; Perlman *et al.*, 1997).

More babies survive severe hyperbilirubinaemia these days due to improved intensive care. In recent literature the classic term kernicterus, initially describing to yellow staining of distinct nuclei in the brain by bilirubin, and the newer term bilirubin encephalopathy – which does not require an autopsy of the brain for a diagnosis – are used more and more interchangeably. Clinicians differentiate between acute bilirubin encephalopathy with transient neurological

deficits and chronic bilirubin encephalopathy or kernicterus with lasting brain damage (Kaplan & Hammerman, 2005; Shapiro *et al.*, 2006).

Children developing kernicterus suffer from severe neurological impairments (Maimburg *et al.*, 2009). Typical symptoms range from hearing impairment or deafness over dental enamel dysplasia, impaired upward gaze, cerebral palsy and spasticity to death (American Academy of Pediatrics Subcommittee on Neonatal Hyperbilirubinemia, 2001; Harris *et al.*, 2001; Kaplan & Hammerman, 2005; Shapiro *et al.*, 2006). The incidence rate for kernicterus in the USA is about 1.5/100,000 newborns (Burke *et al.*, 2009), 1.3/100,000 in Denmark (Maimburg *et al.*, 2009) and 0.9/100,000 in the UK (Manning *et al.*, 2007). There are about 7 cases of kernicterus per year in the UK (Manning *et al.*, 2007).

Neonatal jaundice can be treated with phototherapy and, in more severe cases, blood exchange transfusions. There is no evidence at the moment that prolonged phototherapy increases the risk for melanomas (skin cancer) in later life (Brewster *et al.*, 2010). However, the authors of this report suggest longer studies for follow up are needed to rule out any possible long-term effects. Exchange transfusions have been shown to improve hearing impairment after hyperbilirubinaemia in human babies, as measured with auditory brainstem responses (ABRs) (Nwaesei *et al.*, 1984; Kuriyama *et al.*, 1986). From a follow-up study testing severely jaundiced babies 3 years after birth there is evidence that, if fast and aggressive treatment in form of phototherapy and blood exchange transfusion is provided, the changes in auditory brainstem responses (ABRs) might only be transient although 3 cases with elevated ABR thresholds remained (Wong *et al.*, 2006). Hyperbilirubinaemia without kernicterus, if treated

quickly, does not lead to persistent hearing loss (Thoma *et al.*, 1986), demonstrating that prompt and aggressive treatment can protect from life-long sequelae. However, negative neurodevelopmental outcomes such as motor impairment can persist even if fast and aggressive treatment is provided (Chen *et al.*, 2006).

High serum levels of bilirubin (de Vries *et al.*, 1987) and prolonged exposure to these high concentrations (de Vries *et al.*, 1985) increase the risk for sensorineural hearing loss in human babies. Low birth weight is a contributing factor for babies to suffer from hearing loss after hyperbilirubinaemia (Bergman *et al.*, 1985; de Vries *et al.*, 1985). Prematurity, low birth weight and total bilirubin concentrations of 10-14mg/dl or higher are also associated with impaired motor skill and development (Scheidt *et al.*, 1977). A recent Swedish cohort study showed that hyperbilirubinaemia in newborns is still a risk factor for neonatal morbidity at gestational ages between 30-34 weeks (Altman *et al.*).

Hearing loss in human babies with neonatal jaundice/kernicterus is indicated by absent or decreased ABR amplitudes and delayed ABR components (Chisin *et al.*, 1979; Kaga *et al.*, 1979; Perlman *et al.*, 1983; Rhee *et al.*, 1999). In human babies, a retrocochlear site of damage is assumed as ABRs and oto-acoustic emission tests (OAE) indicate that hair cells are intact (Chisin *et al.*, 1979; Rhee *et al.*, 1999; Saluja *et al.*, 2010), although the auditory nerve may be damaged (Chisin *et al.*, 1979; Kaga *et al.*, 1979). Before functional hearing test such as ABRs were available, early work already suggested neonatal jaundice as a cause for deafness (Crabtree & Gerrard, 1950; Gerrard, 1952; Fenwick, 1975).

The autopsy of 2 cases of deaf or severely hearing-impaired humans with a history of kernicterus/neonatal jaundice revealed highly degenerated neurons in ventral and dorsal cochlear nuclei (Gerrard, 1952).

Auditory neuropathy/auditory dys-synchrony (AN/AD) describes a condition in which ABRs of patients are abnormal but OAE tests are normal (Starr *et al.*, 1996), indicating functional hair cells. Many jaundiced babies who are not deaf but have hearing impairments could be diagnosed with AN/AD, with some studies reporting AN/AD in between 46% (Saluja *et al.*, 2010) to over 50% (Nickisch *et al.*, 2009) of severely jaundiced newborns with hearing impairments. However, there still are some cases of jaundiced neonates and children in which the diagnosis of sensineuronal loss hearing means that the hair cells are damaged. This is indicated by lower OAE amplitudes (Silva & Martins, 2009) and distorted or absent OAEs (Sheykholeslami & Kaga, 2000; Oysu *et al.*, 2002).

Recent studies from Brazil (Botelho *et al.*, 2010) and India (Mukhopadhyay *et al.*, 2010) demonstrated that hyperbilirubinaemia is still a risk factor for hearing impairment in children. Despite the long-known association of hyperbilirubinaemia with hearing impairment (Chisin *et al.*, 1979; Kaga *et al.*, 1979; Bergman *et al.*, 1985; Nakamura *et al.*, 1985) surprisingly little is known today about the mechanisms of how bilirubin leads to hearing loss.

Studies from the United States, Canada and Denmark on infants that suffered from moderate to severe hyperbilirubinaemia, which did not trigger bilirubin encephalopathy, show a higher incidence rate in developing cognitive and

mental problems (Juul-Dam *et al.*, 2001), e.g. attention-deficit disorder and autism in later life (Jangaard *et al.*, 2008; Buchmayer *et al.*, 2009; Maimburg *et al.*, 2010). However the link between autism and hyperbilirubinaemia is currently disputed (Croen *et al.*, 2005). Lower concentrations of bilirubin that do not lead to kernicterus could still be potentially harmful for development in later life (Shapiro, 2010), usually manifested in reduced IQs and abnormal ABRs (Özmert *et al.*, 1996). There is also a statistically significantly higher incidence of schizophrenia in patients with Gilbert's syndrome (Miyaoka *et al.*, 2000), adding weight to the argument that persistent low levels of bilirubin could be harmful.

1.1.4 The Gunn rat model of hyperbilirubinaemia

The Gunn rat, which is an animal model for hyperbilirubinaemia, shows characteristics similar to severely jaundiced human babies. As in humans, the Gunn rat model shows decreased ABRs, signs of damage and neurodegeneration in the auditory brainstem (Shapiro, 1988; Conlee & Shapiro, 1991; Shapiro & Conlee, 1991; Shaia *et al.*, 2005) and has been proposed as a model for auditory neuropathy/auditory dys-synchrony (Shaia *et al.*, 2005).

The Gunn rat will be described in more detail in chapter 2.

1.2 The auditory system

1.2.1 *Sound transduction in the inner ear*

Sound waves arrive through the auditory canal at the tympanic membrane and cause it to vibrate. The vibration gets amplified through the ossicles (malleus, incus and stapes) and deflects the round window of the cochlea. This deflection leads to a vibration which in form of a travelling wave runs along the basilar membrane through the fluid-filled cochlea. On the basilar membrane along the cochlea sits the organ of Corti which contains the hair cells. Three rows of outer hair cells act as a cochlear amplifier, influencing the stiffness and thereby frequency-specificity of the cochlea (Fettiplace & Hackney, 2006). One row of inner hair cells (IHC) converts the fluid oscillation into action potentials (AP). The movement of the tectorial membrane deflects the stereocilia of the IHC. This deflection causes a depolarisation of the IHCs through influx of calcium and potassium ions. This depolarisation leads to transmitter release from IHC onto afferent fibres of type I spiral ganglion cells. Action potentials are then propagated along the axons of the type I spiral ganglion cells (i.e. the auditory nerve), which innervate the cochlear nucleus.

The cochlea resonates at high frequencies at the base (close to the oval window) and at low frequencies at the apex. This frequency encoding by place is called tonotopy and is a feature preserved throughout the hearing system (Kandler *et al.*, 2009). The volume of sound is encoded by AP firing rates.

1.2.2 Architecture of auditory brainstem

From the inner hair cells, action potentials are conducted along the auditory nerve fibres to the cochlear nucleus (CN), the first auditory processing station (Figure 1.2). The CN can be roughly divided into the ventral part (VCN) and the dorsal part (DCN). Neurons of the DCN mainly project to the lateral lemniscus and inferior colliculus (Figure 1.2). The VCN is home to a number of different cell types such as octopus cells, multipolar or stellate cells, granule cells, spherical and globular bushy cells (Helfert *et al.*, 1991; Cant & Benson, 2003), with spherical and globular bushy cells and stellate cells mainly located in the anterior part (AVCN) and octopus cells and stellate cells in the posterior part (PVCN). Neurons in the CN are damaged in conditions of severe hyperbilirubinaemia (Dublin, 1974; Jew & Williams, 1977; Jew & Sandquist, 1979). Electrophysiological recordings from VCN bushy neurons of jaundiced homozygous Gunn rats showed increased synaptic delays (Zhang *et al.*, 1989). For clarity, because they are the main input to the superior olivary complex (SOC) and therefore most important for this thesis, the description will focus on spherical bushy cells (SBC) and globular bushy cells (GBC).

The *in vivo* AP firing patterns to sound stimuli are “primary-like” (Pfeiffer, 1966b) for both SBC and GBC (Helfert *et al.*, 1991). This is most likely because both bushy cell types receive large synapses from the auditory nerve called endbulbs of Held (Held, 1893), allowing for a high-fidelity transmission of APs. In patch-clamp recordings all bushy cells fire 1-3 APs following current injection and display a characteristic ‘sag’ at hyperpolarising currents (Oertel, 1983; Cao *et al.*, 2007).

SBCs have a spherical soma with a few dendrites that branch out into a bush-like structure, giving the cells their name. GBCs have a similar morphology, however, GBCs have a bigger dendritic tree and the somata are more ovoid than in SBCs (Tolbert & Morest, 1982). SBCs are located towards the ventral tip of the AVCN, while GBCs are closer to the point at which the auditory nerve fibres enter into the CN (Helfert *et al.*, 1991).

The auditory nerve fibres form large synapses called endbulbs of Held onto globular and spherical bushy cells, both of which project to different parts of the superior olivary complex (SOC). The globular bushy cells of the AVCN send axons across the midline to form huge presynaptic terminals called the calyx of Held (Held, 1893) (Tolbert *et al.*, 1982; Spirou *et al.*, 1990; Kuwabara *et al.*, 1991) (Figure 1.2). Their recipients are the principal neurons of the medial nucleus of the trapezoid body (MNTB) which receive one giant calyceal terminal. Spherical bushy cells on the other hand innervate the ipsilateral medial and lateral superior olive (MSO and LSO, respectively, see Figure 1.2) and contralateral MSO (Helfert *et al.*, 1991).

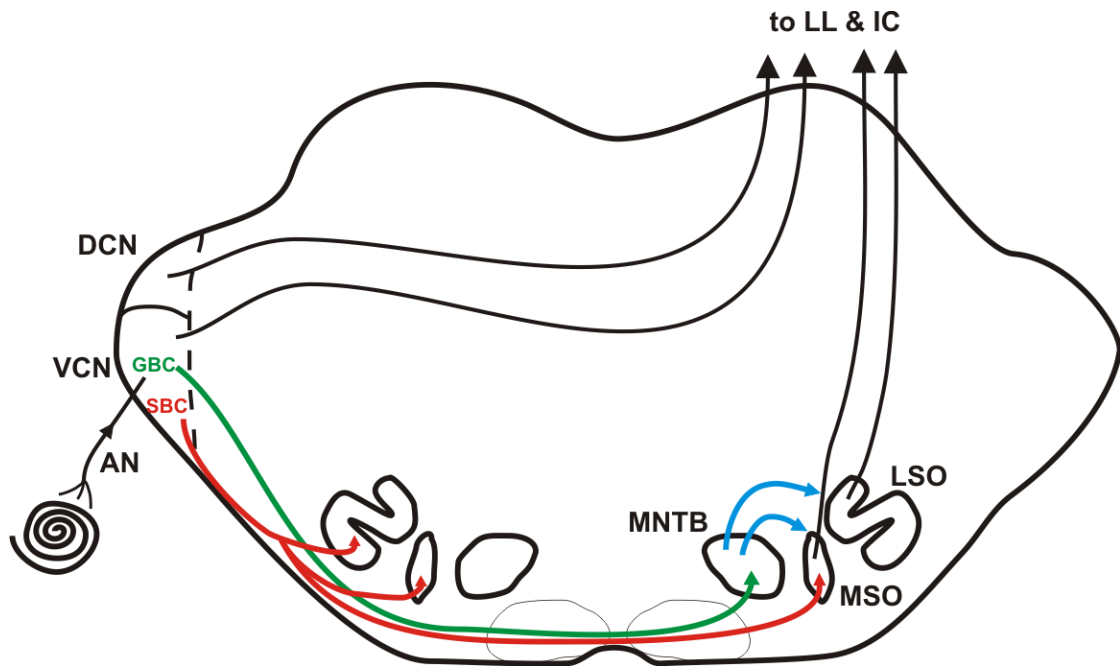


Figure 1.2 Schematic drawing of the auditory brainstem.

The cochlear nucleus receives information from the cochlea via the auditory nerve fibres. Globular bushy cells of the VCN project to the contralateral MNTB. Spherical bushy cells project to ipsilateral MSO & LSO and to contralateral MSO. The MNTB sends inhibitory projections to MSO & LSO which in turn project to LL and IC. Other neurons in the CN also innervate higher order auditory nuclei such as the lateral lemniscus and the inferior colliculus. AN= auditory nerve, DCN= dorsal cochlear nucleus, GBC= globular bushy cell, IC= inferior colliculus, LL= lateral lemniscus, LSO= lateral superior olive, MNTB= medial nucleus of the trapezoid body, MSO= medial superior olive, SBC= spherical bushy cell, VCN= ventral cochlear nucleus.

The MNTB projects mainly to MSO (Adams & Mugnaini, 1990) and LSO (Bledsoe *et al.*, 1990; Wu & Kelly, 1992), which in turn innervate higher order auditory nuclei such as the lateral lemniscus and the inferior colliculus (see Figure 1.2). The latter send information via the medial geniculate body to the auditory cortex (Helfert *et al.*, 1991). In the interest of clarity and because this nucleus was investigated in more detail, a more detailed description of the MNTB and its role in the auditory brainstem is given below.

1.2.3 Processing of spatial information in the auditory brainstem

Spatial information is completely lost during sound transduction because the only parameters encoded at the cochlea are frequency and intensity of sound. Therefore, spatial information has to be regained by other means. To retrieve this spatial information, information from both ears (i.e. binaural information) is required. Therefore, information is needed about signal differences between the two ears (i.e. interaural), e.g. interaural time differences (ITD) and interaural level differences (ILD). When the sound arrives at the head laterally from the left or right it will reach one ear earlier than the other (ITD). In the same way, the ear facing the sound source will detect sound with a higher intensity than the ear facing away from the source because the sound intensity is refracted and reflected by the head (ILD). For ITD a comparison is made of different phases of excitatory inputs from both cochleas in the MSO (via ipsi- and contralateral VCN, Figure 1.3d). That fibres and neurons show phase-locked activity has already been described at the stage of the cochlea. This phase-locking property of firing neurons is preserved and in the MSO the summation of phase-locked activity or the lack thereof between the two ears is compared to determine the localisation of the sound source at the horizontal plane (azimuth, Figure 1.3f). A summation i.e. being in phase¹ will lead to a maximal firing rate (Figure 1.3b). Inhibitory inputs from MNTB act to narrow the time window in which the comparison is carried out in the MSO and so help to make the detection more precise. As the precision for phase-locked activity is best at low frequencies (below 3kHz), for higher frequencies (above 3kHz) the differences in loudness

¹ An example for being in phase: tuning a guitar string with the help of a tuning fork. When both are at the same frequency, then they are in phase, resulting in maximal resonance and vibration.

or intensity are used to detect the place of the sound object at the azimuth (Grothe, 2000). These ILDs are computed for the first time in the LSO. ILDs are determined by comparison of ipsilateral excitatory and contralateral inhibitory inputs (from the VCN and from the MNTB, respectively; Figure 1.3c) (Kotak *et al.*, 1998). This means that the louder a sound on the ipsilateral side of the LSO is, the higher the AP firing rate will be and the louder a sound from the contralateral side of the LSO is, the lower the firing rate (Figure 1.3a).

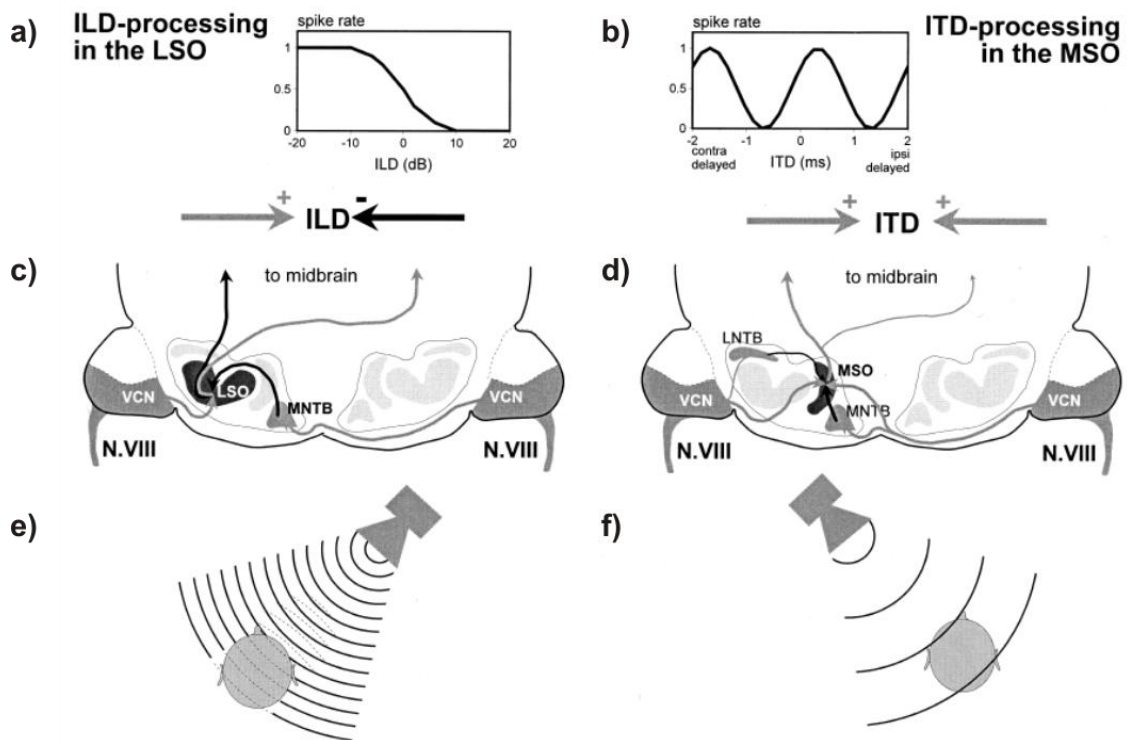


Figure 1.3 Processing of spatial information in the auditory brainstem.

The processing of interaural level difference (ILD) in the LSO is displayed on the left side and the processing of the interaural timing difference (ITD) in the MSO on the right side. The lower panel illustrates that distinct features of sound (e): intensity, f): timing) that –depending on the place of the sound source- differ between ears are used for regaining spatial information of the sound source. The middle panel shows the main areas of the superior olivary complex in the auditory brainstem and the position of and the inputs to the LSO (c) and MSO (d). a) ILDs are determined by comparison of excitation and inhibition (arrows). The spiking rate is higher the louder the received sound on the left hand side is and gets lower the louder the sound on the right hand side gets. b) ITDs are determined by comparison of the time difference at which the sound arrives at left and right cochlea. N.VIII= auditory nerve, VCN= ventral cochlear nucleus, LNTB= lateral nucleus of the trapezoid body, MNTB= medial nucleus of the trapezoid body, MSO= medial superior olive, LSO= lateral superior olive, grey arrows= excitatory projections, black arrows= inhibitory projections. Reprinted from *Progress in Neurobiology* 61, Grothe B: The evolution of temporal processing in the medial superior olive, an auditory brainstem structure. p581-610, Copyright (2000) with permission from Elsevier.

With its central role in the computation of ILD and ITD, the MNTB is for many other reasons an interesting research subject. Its anatomical structure shows characteristics which attracted investigators interested in synaptic transmission and modulation. The axons of globular bushy cells from the anterior ventral cochlear nucleus (AVCN), which themselves receive their input directly from the 8th nerve via a large presynaptic terminal called the Endbulb of Held (Held, 1893; Lenn & Reese, 1966; Ryugo *et al.*, 1996; Nicol & Walmsley, 2002), give rise to the chalice-shaped presynaptic endings terminating on the principal neurons of the contralateral MNTB (Friauf & Ostwald, 1988; Kuwabara *et al.*, 1991; Smith *et al.*, 1991; Smith *et al.*, 1998). These calyceal terminals were first described by the German anatomist Hans Held and are now named after him (Held, 1893). Since the presynaptic terminals are so big that they embrace the principal neurons like an open hand clasps a fist, it has been possible to perform *in vitro* patch-clamp recordings from the presynaptic site (Forsythe, 1994; Barnes-Davies & Forsythe, 1995) and even from pre- and postsynaptic sites simultaneously on a single-cell basis (Borst *et al.*, 1995; Takahashi *et al.*, 1996; Borst & Sakmann, 1998; Kimura *et al.*, 2003).

With firing rates of up to 800Hz (Taschenberger & von Gersdorff, 2000) the MNTB is an amazing example of high fidelity synaptic transmission in the auditory system. All the connections from the VCN to LSO, MSO and MNTB are glutamatergic. The postsynaptic principal neurons express AMPA and NMDA receptors (Forsythe & Barnes-Davies, 1993).

In the MNTB there is a signal inversion as the principal neurons of the MNTB are glycinergic (Bledsoe *et al.*, 1990; Wu & Kelly, 1992; Suneja *et al.*, 1995; Wu

& Kelly, 1995; Kotak *et al.*, 1998; Smith *et al.*, 2000) and GABAergic (Adams & Mugnaini, 1990; Kotak *et al.*, 1998). As the MNTB innervates both the ipsilateral MSO (Adams & Mugnaini, 1990) and LSO (Bledsoe *et al.*, 1990; Wu & Kelly, 1992) this means: the greater the excitation that arrives at the MNTB from the contralateral ear the more the MSO and LSO are inhibited by the MNTB.

The MNTB is also one of the generators of waveform III in ABRs (Melcher *et al.*, 1996a). It has been shown to have reduced size (Conlee & Shapiro, 1991; Shapiro & Conlee, 1991) in hyperbilirubinaemia in homozygous Gunn rats and decreased expression of calcium-binding protein parvalbumin (Spencer *et al.*, 2002) but no changes in calbindin-expressing levels were found (Spencer *et al.*, 2002).

It is of interest what happens at pre- and postsynaptic sites – especially for questions concerning modulation of activity by either excitation or inhibition of these sites – but it is difficult to perform patch-recordings in brain slices from animals older than 18 days. Multi-electrode arrays may bridge this gap and give useful insight, for this method can provide high spatial and temporal resolution, generate large amounts of data in relatively short time, and provide insight into a larger area/network of neurons than is possible with patch-clamp recordings.

1.3 Ion channels and neurotransmission

Without ion channels, the very fast information transmission and processing in the nervous system is unthinkable. Ion channels facilitate neuronal excitation (in form of APs) by means of voltage-gated ion channels along axons and neurons and by ligand-gated ion channels at chemical synapses. Channels of both ion channel families allow the flow of ions across cellular membranes along electrochemical gradients. Ion channels open their ion gating pores either after sensing a voltage-change or after the binding of a neurotransmitter. In the following sections, ligand-gated and voltage-gated ion channels and their role in the MNTB will be briefly described.

1.3.1 Ligand-gated ion channels

Ligand-gated ion channels include a variety of ion channels united by the feature that their opening is dependent on the binding of a ligand. This can be compounds such as glutamate, glycine, γ - amino butyric acid (GABA), ATP or acetylcholine. They also vary in their number of subunits e.g. glutamate receptors (Glu-R) have 4 subunits, whereas nicotinic acetylcholine receptors (nACh-R) have 5.

Since it has been known for some time that the synaptic transmission at the calyx of Held is glutamatergic (Grandes & Streit, 1989; Banks & Smith, 1992) and that both NMDA and AMPA receptors (NMDA-R and AMPA-R) are involved (Forsythe & Barnes-Davies, 1993), the function of NMDA and AMPA receptors will be briefly mentioned here.

AMPA and NMDA receptors are ionotropic receptors, which means they are permeable for cations such as sodium, potassium and calcium, the latter mainly at NMDA-Rs. These receptors consist of 4 subunits including a binding site for glutamate forming a pore across the cell membrane through which cations can pass. Whilst AMPA receptors are known to elicit fast, rapidly desensitizing currents (Mennerick & Zorumski, 2005; Roche & Isaac, 2007), NMDA receptors have a much longer opening time which results in a long depolarisation of the neuron. NMDA receptor currents are often carried not only by sodium but also by calcium ions which can potentially initiate a cascade of second messenger activity within the cell (Cull-Candy, 2007).

The calyx of Held synapse in the MNTB is a large glutamatergic synapse that generates a large excitatory postsynaptic current (EPSC) of about 10nA at a holding potential of -60mV (Barnes-Davies & Forsythe, 1995) in the principal neurons, as a consequence of large quantities of transmitter released into the synaptic cleft. This is 10-30 times the amount of current necessary to trigger an action potential. Although the large EPSC in the MNTB ensures a high fidelity transmission of information, potassium channels are needed to control the postsynaptic excitability and thereby make transmission more precise. It is clear that potassium channels have a significant impact in regulating excitability and the firing properties of MNTB neurons (Brew & Forsythe, 1995). Therefore, voltage-gated ion channels will be briefly mentioned next as they play an important role in synaptic transmission in general and in the MNTB in particular.

1.3.2 Voltage-gated ion channels

The family of voltage-gated ion channels consists mainly of Na⁺, K⁺ and Ca²⁺ channels. These are pore-forming transmembrane proteins which have a voltage-sensing domain and open and close at distinct voltages. Their main task is to gate ion-influx and –efflux across a gradient at cellular membranes, mostly of axons and neurons.

Voltage-gated sodium channels

Voltage-gated sodium channels (Na_v) are membrane crossing proteins comprised of a α -subunit forming the pore and one or more auxiliary β -subunits (Yu & Catterall, 2003; Catterall *et al.*, 2005a). The α -subunit is composed of 4 domains, each with 6 transmembrane segments. They demonstrate little diversity; so far 9 different α -subunits are known (Yu & Catterall, 2003). Na_v are responsible for fast depolarisation of neurons and axons because of their fast activation and inactivation properties. They show a short recovery time from inactivation (~2ms) (Leao *et al.*, 2005), which helps firing at high frequencies. Their activity is reflected in the fast upstroke of an action potential. Na_v1.1 and Na_v1.6 are most prominent in the MNTB (Leao *et al.*, 2005; Leao *et al.*, 2006).

Voltage-gated calcium channels

Similar to Na_v, voltage-gated calcium channels (Ca_v) consist of a α -subunit forming the pore and one or more auxiliary β -subunits. They can be differentiated by pharmacological means or by gene sequence similarities. The latter reveals three subfamilies: Ca_v1, Ca_v2 and Ca_v3. The pharmacological differentiation divides the channels into L-type (Ca_v1.1-Ca_v1.4), P/Q-type

(Ca_v2.1), N-type (Ca_v2.2), R-type (Ca_v2.3) and T-type (Ca_v3.1-3.3) channels (Catterall *et al.*, 2005b) according to the currents they produce and their specificity to different blockers. Ca_v channels trigger exocytosis of transmitter-filled vesicles at the presynaptic terminals via influx of Ca²⁺ from the extracellular space and are therefore crucial for synaptic transmission (Augustine, 2001). The removal of extracellular Ca²⁺ cations by application of Ca²⁺ free ACSF can result in a disruption of synaptic transmission (Katz & Miledi, 1970; Borst *et al.*, 1995). At the presynaptic calyx of Held P/Q, N and R type channels are present, although P-type channels (formed by the Ca_v 2.1 α -subunit) are predominant after P10 (Forsythe *et al.*, 1998; Iwasaki & Takahashi, 1998; Wu *et al.*, 1999).

Voltage-gated potassium channels

Voltage-gated potassium channels (K_v) form a broad group of ion channel families, which can be divided in three sections according to their number of transmembrane domains (TMD): 2-TMD channels, 4-TMD channels and 6-TMD channels (Coetzee *et al.*, 1999). This introduction will focus on the two voltage-gated potassium channel families so far described to be of high importance for synaptic transmission in the MNTB: K_v1, which regulate the threshold and K_v3 which determine the AP duration. Both K_v1 and K_v3 channels belong to the 6-TMD section. These proteins consist of a pore-forming tetramer, where each part of the tetramer is comprised of 6 transmembrane domains.

K_v1 homologue channels were the first to be cloned in the *Drosophila Shaker* mutant, and named after it. They are found throughout the body but – depending on the subtype – mainly in brain, heart and muscle tissue (Gutman *et al.*, 2005).

K_v channels contribute to the determination of action potentials, by enabling the efflux of K^+ -ions out of the neuron or axon. While K_v3 channels open at voltages ranges from +3 to +16mV (Gutman *et al.*, 2005), channels of the K_v1 subfamily open at ranges of far lower voltages. Due to these different opening probabilities, high voltage activated K_v3 channels are more directly involved in determination and thereby duration (width) of APs by contributing to a very fast repolarisation (Rudy & McBain, 2001; Dodson, 2003), while K_v1 channels prevent the formation and backpropagation of action potentials in a certain time slot via hyperpolarisation. The principal MNTB neurons abundantly express voltage-gated potassium channel $K_v3.1b$ (Wang *et al.*, 1998a) and heteromeric $K_v1.1$ and $K_v1.2$ channels, the latter especially in the axon initial segment (Dodson *et al.*, 2002b). Due to presynaptic $K_v3.1$ presynaptic APs have nearly half the half-width of postsynaptic APs (Dodson, 2003), which allows a more precise following of the synapse to high-frequency firing. Both K_v3 and K_v1 channels tightly regulate postsynaptic excitability by ensuring the firing of a single AP upon synaptic stimulation (Brew & Forsythe, 1995), instead of a train of action potentials.

If the function of these ion channel families is impaired by high levels of bilirubin, this could explain for some of the hearing deficits accompanying kernicterus in newborn babies. This question will be addressed in the following chapters.

1.4 Aims and Objective

Deafness is associated with bilirubin exposure during jaundice. The central hypothesis was that this hearing loss is caused by failure of synaptic transmission in the central auditory pathway. ABRs as a functional hearing test are impaired after severe jaundice in humans and in the Gunn rat. Because the MNTB is a generator of wave III of the ABR and has been so well studied in the past, it was used as a model on which to investigate potential toxic effects of bilirubin.

The initial approach was to study the effect of bilirubin on synaptic transmission in the central auditory system. With each new data set, it was possible to refine the questions and perform more and more specific experiments. Findings on abnormal ABRs in Gunn rats by Shapiro and colleagues led to the hypothesis that synaptic transmission at the level of the MNTB could be impaired. The aim was to verify this and to investigate if this potential impairment was due to a pre- and/or postsynaptic failure to propagate action potentials. Subsequently, the focus moved to investigating the underlying mechanism at the level of the MNTB that leads to hearing impairment.

The anteroventral cochlear nucleus (AVCN) is – as part of the cochlear nucleus (CN) – the first processing station in the auditory system after the cochlea. The VCN as a generator of wave II in ABRs shows signs of bilirubin-induced neurodegeneration and increased synaptic delays. Because of this, and because it is home to the globular bushy cells that give rise to the calyces of Held, the VCN was included at a later stage of this PhD project when light and electron microscopic examinations were performed.

2. Material and Methods

2.1 The Gunn rat model of hyperbilirubinaemia

In 1934, Charles K. Gunn discovered that in the Wistar rat colony he was taking care of, some rats displayed a yellow coat colour whereas the majority of them were white. Gunn singled out the yellow rats, bred them separately and found that the yellow coat colour is caused by bilirubin and is homozygote recessive (Gunn, 1938, 1944). Since then, the Gunn rat has been used as model for hyperbilirubinaemia and Crigler-Najjar syndrome.

Bilirubin is lipophilic (Mustafa & King, 1970) and difficult to excrete. It is therefore conjugated with glucuronic acid in the liver and excreted as the more water-soluble bilirubin-di-glucuronide (Lathe & Walker, 1958). In human babies and in the Gunn rat strain, this glucuronidation is decreased (Jj) or absent (jj) (Blanckaert *et al.*, 1980). The defect in glucuronidation (Schmid *et al.*, 1958) is caused by a frame-shift mutation in the enzyme UDP-glucuronosyl-transferase (Iyanagi *et al.*, 1989; Iyanagi, 1991; Roy-Chowdhury *et al.*, 1991), leading to a lack of hepatic UDP- glucuronosyl-transferase enzymes in Gunn rats (Scragg *et al.*, 1985). This causes heterozygous (Jj) Gunn rats to have ~50% of enzyme activity in comparison to Wistar rats (Strebel & Odell, 1971) and homozygous (jj) Gunn rats to have virtually none (Strebel & Odell, 1971; Chowdhury *et al.*, 1986). This decreased glucuronidation of bilirubin results in a reduced excretion of bilirubin through the bile and an increase in free bilirubin in the blood. This in turn leads to the accumulation of bilirubin in the body and its deposition in other parts of the body, including the skin and the sclera of the eyes.

Diamond and Schmid reported that, indeed, only free (unbound, unconjugated) bilirubin can cross the blood-brain-barrier (Diamond & Schmid, 1966). These authors also showed that mitochondrial uncoupling, which was previously suggested as a mechanism for bilirubin toxicity, did not occur in experimental bilirubin encephalopathy in guinea pigs (Diamond & Schmid, 1967). Uncoupling of oxidative phosphorylation in vitro only occurred at bilirubin concentrations much higher (Diamond & Schmid, 1967) than found in the brains of animals with experimental bilirubin encephalopathy (Diamond & Schmid, 1966).

Silverman and colleagues (Silverman *et al.*, 1956) reported that preterm babies treated with a sulfonamide antibiotic (sulfisoxazole) are 6x more likely to develop kernicterus. This finding was supported by experiments in jj-Gunn rats (Blanc & Johnson, 1959; Johnson *et al.*, 1959). These experiments showed that sulfonamide treatment in Gunn rats led to a steep decrease of unconjugated bilirubin concentrations in the blood within 4-6 hours. These concentrations stayed low for more than 36 hours but were accompanied by the appearance of kernicterus, marked by intense yellow staining of the brain. These experiments also suggested that unconjugated bilirubin is the toxic bilirubin form.

Odell demonstrated that sulfisoxazole (a sulfonamide) and salicylate displace albumin-bound bilirubin (Odell, 1959). Free bilirubin then enters tissue like the intestines (Schutta & Johnson, 1969) or the brain (Johnson *et al.*, 1959; Johnson *et al.*, 1961; Schutta & Johnson, 1969). The latter leads to symptoms such as ataxia (Schutta & Johnson, 1969) and auditory neuropathy (Shapiro, 1988; Shaia *et al.*, 2005) in Gunn rats and so mimics closely what happens in severely jaundiced or kernicteric human babies.

This is yet another reason to use Gunn rats as they are a good model for auditory neuropathy because, as in humans:

- The cochlea and hair cells are intact (Uziel *et al.*, 1983)
- The organ of Corti and spiral ganglion cells are normal (Belal, 1975)
- the auditory nerve shows a normal discharge rate distribution and interspike intervals (Barbary, 1991)
- an EM study on 8th nerve showed no evidence for degeneration (Barbary, 1991)
- there was no difference in fibre diameter, axon diameter and myelin thickness between jj-Gunn, Jj-Gunn and Long-Evans rats (Barbary, 1991). Although jj-Gunn rats had a smaller total fibre count and mean surface area, the mean fibre density (i.e. fibres/mm²) was not different between jj-Gunn and Jj-Gunn rats (Barbary, 1991)
- 'large neurons' in the AVCN show signs of damage at EM level, e.g. inclusion-bodies in mitochondria, vacuoles, abnormally increased extracellular space, darkening of presynaptic terminals (Jew & Williams, 1977; Jew & Sandquist, 1979).

Sulfa-treated jj-Gunn rats, which resemble severely jaundiced or kernicteric infants, show:

- a loss of ABRs after bilirubin toxicity (Shapiro, 1988; Haustein *et al.*, 2010) similar to that which is seen in humans (Chisin *et al.*, 1979; Kaga *et al.*, 1979)
- intact hair cells, decrease in calcium-binding proteins (Shaia *et al.*, 2002; Shaia *et al.*, 2005), damaged spiral ganglion cells, reduction in the

number of large diameter axons in auditory nerve 3-5 days after sulfa-treatment suggesting it as a model for auditory neuropathy/ auditory dys-synchrony (AN/AD)(Shaia *et al.*, 2005)

- reduced volume size of MNTB and CN 4-5 days after sulfa-treatment as well as reduction in mean cross-sectional area, i.e. cell size of spherical bushy cells and MNTB neurons, but not in globular cells of the AVCN (Conlee & Shapiro, 1991).

As in humans (Becker & Vogel, 1948; Ahdab-Barmada & Moossy, 1984) the cerebellum, hippocampus and basal ganglia are mainly affected (Blanc & Johnson, 1959; Jew & Sandquist, 1979), in addition to the auditory brainstem nuclei. The cerebellum, with the Purkinje cells almost exclusively degenerating, has especially been investigated in detail over the last 4 decades (Schutta & Johnson, 1967; Mikoshiba *et al.*, 1980; Takagishi & Yamamura, 1989; Takagishi & Yamamura, 1994).

Phototherapy has long been successfully used to reduce concentrations of unconjugated bilirubin in humans (Cremer *et al.*, 1958; Dobbs & Cremer, 1975) and Gunn rats (Sisson *et al.*, 1974; Calvert *et al.*, 1978). It is still the first method of choice in order to decrease free bilirubin in human neonates (Kapoor *et al.*, 2008; Maisels & McDonagh, 2008).

Gunn rats as models for Crigler-Najjar syndrome are also used to test ways to genetically re-instate the complete gene for UDP-glucurononyl-transferase by using viral vectors (Toietta *et al.*, 2005) and non-viral delivery systems (Wang *et al.*, 2009).

2.1.1 Use of Gunn rats in this thesis

For the work in this thesis all animal procedures were conducted in accordance with the 1986 Animal (Scientific Procedures) Act under Project license Wo 80/2100 at the University of Leicester, United Kingdom. Gunn rats were bought from Harlan UK (strain: HsdBlu:GUNN-UDPGT¹) and bred in-house, mating male homozygous with female heterozygous Gunn rats (Strebel & Odell, 1971; Takagishi & Yamamura, 1994). Rats between postnatal day 13 and 21 (P13-21) were used because blood bilirubin levels (unconjugated bilirubin) naturally peak between 2 and 3 weeks of life in homozygous (jj) Gunn rats (Johnson *et al.*, 1959; Schutta & Johnson, 1969). Wistar rats of the same age served as wild-type controls (Gunn, 1938).

Homo- and heterozygous Gunn rats are easy to tell apart by simply looking at them (Figure 2.1). From a few days after birth (Figure 2.1a) and throughout development (Figure 2.1b), homozygous Gunn rats are recognised by the yellow discoloration of skin and fur, whilst heterozygous littermates have a white coat colour and the skin which is visible on ears and paws appears pink. We did not simply rely on the fact that the genotype is visible through the phenotype. Sue Robinson, the research officer in the lab of Ian Forsythe also genotyped tissue samples of yellow and white Gunn rats. The tests confirmed that all 50 rats with yellow discoloration were homozygous (100%) and 48 of 49 white rats were heterozygous Gunn rats (98%). One rat from the very first litter was classed as “white coat colour” but genotyped as homozygous. This could be due to the inexperience of the animal technician who, at that time, had never handled Gunn rats before and may have misjudged the coat colour. Therefore it

was decided to take the genotyping as confirmation and after that point Gunn rats were classed by their coat colour as either *jj* or *Jj*, as others have done before (Gunn, 1938; Conlee & Shapiro, 1991).

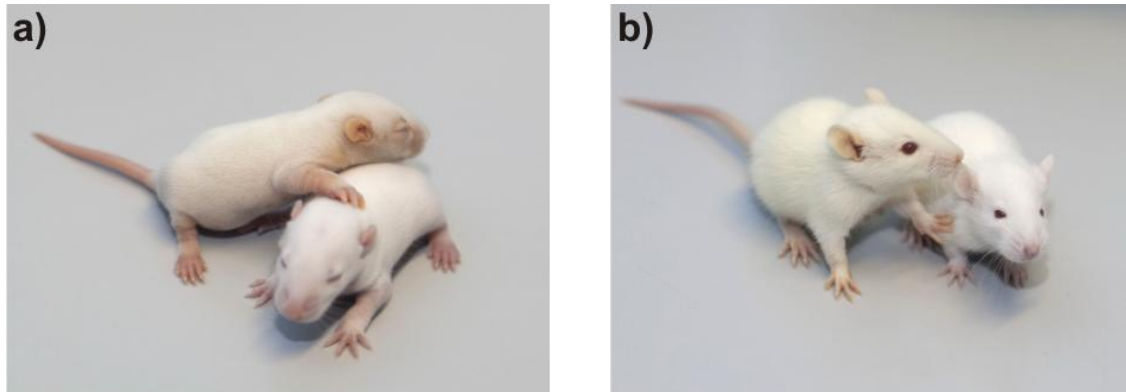


Figure 2.1 The phenotype tells the genotype of homo- and heterozygous Gunn rats.
a) 4 day old *jj*-Gunn rat pup (left) already shows distinct discoloration compared to its *Jj*-Gunn littermate (right). b) 16 day old *jj*-Gunn rat (left) shows strong yellow discoloration of skin and fur, best visible at paws and ears. The *Jj*-Gunn littermate (right) appears white like the wild-type Wistar background rats without any discoloration.

2.2 Auditory Brainstem Responses (ABRs)

Auditory brainstem responses are a functional, non-invasive hearing test frequently used in humans (Sohmer *et al.*, 1974; Starr & Hamilton, 1976; Kraus *et al.*, 1984; Agrawal *et al.*, 1998) and also in rats (Karplus *et al.*, 1988; Shapiro, 1988; Shaw, 1988) to detect retro-cochlear abnormalities underlying hearing impairments. The individual waves of an ABR reflect the activation of subsequent auditory processing stations. In humans, wave I originates from the auditory nerve, waves II and III reflect activity of cochlear nucleus, trapezoid body and superior olivary complex and wave V represents the activity of the midbrain, i.e. lateral lemniscus and inferior colliculus (Lev & Sohmer, 1972; Starr & Hamilton, 1976). In rats (Chen & Chen, 1991) and cats (Melcher & Kiang, 1996; Melcher *et al.*, 1996b), wave I reflects the activity of the auditory nerve; wave II the cochlear nucleus and wave III the superior olivary nucleus, including the MNTB. Severe jaundice in newborns can lead to sensorineural hearing loss, reflected by decreased ABRs and elevated thresholds (Chisin *et al.*, 1979; Kaga *et al.*, 1979) yet unaltered oto-acoustic emissions (Rhee *et al.*, 1999). While homozygous Gunn rats have normal ABR waveforms (Levi *et al.*, 1981; Shapiro, 1988), the displacement of bilirubin into the brain leads to decreasing ABRs (Shapiro, 1988; Shapiro, 1993).

Homozygous Gunn rats and Wistar rats were weighed and then anaesthetized with an intraperitoneal (i/p) injection of a 35-50% dose of Hypnorm/Midazolam (2.7ml/kg bodyweight; VetaPharma Ltd., UK). This dose anaesthetised the rats for 45-60 minutes, long enough to perform the ABRs. The success of the

anaesthesia was checked by the loss of the leg withdrawal reflex when pinching the hind paws. Saline (0.2ml) was injected subcutaneously before the recordings, to prevent dehydration. Rats were placed on a heating pad to help them maintain their normal body temperature. One subdermal recording electrode was placed above the mastoid bone next to the ear and the subdermal reference electrode on the middle of the scalp. A subdermal electrode needle was placed in the thigh to provide the earth. Recordings were made before (control) and 18h after (treated) administration of sulfadimethoxine (200mg/kg, Sigma) using a Medelec Sapphire 2A amplifier. Two recordings with 200-400 counts each were done for each frequency tested at the respective intensities. The data was sampled at 16 kHz and an ADC converter fed the analogue signal from the amplifier into a PC. Due to the fact that the hearing of rats is most sensitive in the area of 8-32kHz (Kelly & Masterton, 1977) ABRs were evoked using pure-tone (12, 24, 30 kHz) and 'click' stimuli delivered via a reverse-driven microphone (B&K 4134) placed directly over the left ear over a range of intensities (34-94dB) using a digital attenuator (Tucker Davies Technologies, USA). Breathing was monitored continuously and, in case of irregular breathing or signs that the anaesthetics were wearing off, the recording was stopped. After the recording the rat was put into a cage and allowed to wake up properly under observation. During the whole time the cage was placed on a heat pad, ensuring the animals would not experience hypothermia. Once the rat was moving around in its cage again it was put back into its litter because at the age tested rats are not weaned. Before being put back to their cage, experimental rats were tail-marked and/or ear-marked to identify them again the next day. Sulfa was weighted according to the individual body weight,

dissolved in 0.3ml saline and injected intraperitoneal after the control recording. For the experiments using the neuronal nitric oxide synthase (nNOS) antagonist 7-nitroindazole (7-NI), 150mg/kg 7-NI was dissolved in peanut oil, sonicated for 2 minutes to help the dissolving and injected i/p 30 minutes before i/p injection of sulfa. Eighteen hours later, ABRs were taken from the same rat in order to test for effects of hyperbilirubinaemia on the hearing system.

2.3 Preparation of *in vitro* brain slices from the MNTB

For the experiments, brain slices were prepared from tissue from Lister Hooded and Wistar rats (Biomedical Services, University of Leicester, UK) or Jj and jj Gunn rats. All procedures were in accordance with the 1986 Animal (Scientific Procedures) Act and were conducted under Project license Wo 80/2100. Animals aged 14 to 21 days old were killed by decapitation (so the brainstem would not be damaged as would be by cervical dislocation) and the brain was quickly removed. Since the brain slices were not cut in the designated procedure room, the whole brain was submerged in ice cold low Na⁺ ACSF (see Table 1 for composition) used for preparation and rapidly brought to the lab. The cortex was then separated from the mid- and hindbrain with a single scalpel cut between the superior and inferior colliculi under visual control with the help of a stereo microscope (Leica, Germany).

It should be noted that ensuring the right cutting angle of ~30° for the scalpel cut that separates the cortex is absolutely crucial (Figure 2.2). If the angle is too steep or too shallow not enough incoming fibres connected to MNTB cells are

preserved and, therefore it is not possible to elicit synaptic responses in that area.

Using the wrong cutting angle was the main reason for not getting evoked responses in the MNTB in the preparation for multi-electrode array (MEA) recordings or evoked synaptic single cell EPSCs. Since spontaneous activity could not be recorded in acute auditory brainstem slices using multi-electrode arrays, evoked responses were the only way of getting reliable, stable signals for experiments.

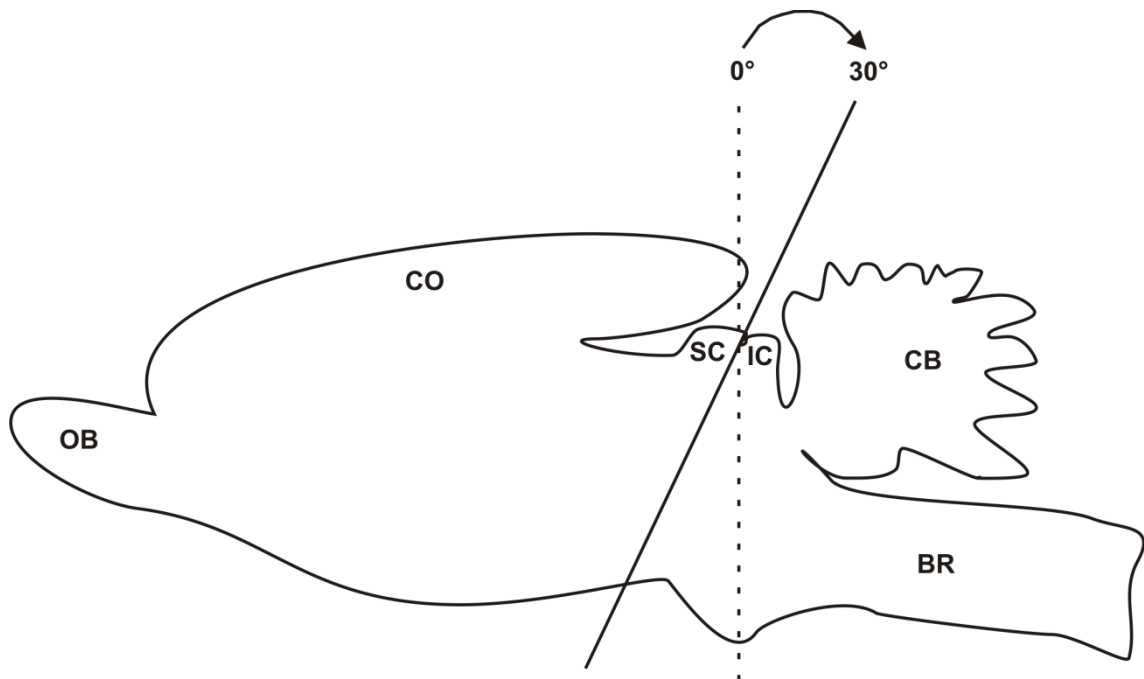


Figure 2.2 Schematic drawing of a rodent brain.

Schematic drawing of a rodent brain and the first cutting angle when collecting acute brainstem slices. OB: olfactory bulb; CO: cortex; SC: superior colliculus; IC: inferior colliculus; CB: cerebellum; BR: brainstem.

Subsequently, the cut surface of the tissue block was dried quickly using fine filter paper and the brainstem with attached cerebellum was glued onto a mobile tray which was then fixed to a vibratome stage (Microslicer DTK-1000, DSK, Japan). The brainstem was placed so that the ventral side faced the blade

(Campden Instruments Limited, UK) and the tray was filled with ice cold low Na^+ ACSF, which was continually gassed with Carbogen (95% oxygen, 5% carbon dioxide). 300 μm thick, acute brainstem slices were cut for MEA recordings and 200 μm thick slices for patch-clamp recordings and were transferred into an incubation chamber filled with normal ACSF (see Table 1 for composition).

The incubation chamber was kept in a water bath giving a temperature of around 35°C in which the slices were incubated for 30-45 minutes. After this, the slices were stored in the incubation chamber at room temperature. All solutions were continuously bubbled with Carbogen to maintain a stable pH-value of around 7.4. To determine the origin of the various components of the recorded field potentials (FPs), a range of drugs were applied (Table 2). These drugs were chosen due to their effects being well known and for which there was considerable experience in the lab.

Pharmacological experiments with MEAs included the following consecutive steps:

- 10-30min control recording in ACSF to check for stability of signals
- If the FPs were stable then:
 - 1min recording in ACSF to be used as a reference trace underlying the later recordings
 - Wash-in of the drug (usually for 10-12 minutes, in case of NO-donor SNP 20 minutes, in case of bilirubin up to 4 hours)
- If the effect of the compound to be tested was not known, the application time could be longer than 10 minutes

- After drug application wash-out period with normal ACSF alone to check if compound could be removed from the slice and FP waveforms were restored to control level (this is mainly done for Ca^{2+} free ACSF).

The concentration at the beginning of a test of the new drug (i.e. a drug not used before with this preparation on a MEA) was usually 10 times the concentration used for patch-clamp experiments in the lab (or as reported in the literature) to check if any effect can be detected. If effects could be observed, the concentration was gradually lowered in the next slices until a drug concentration equal to other experiments is reached.

in mM	slicing ACSF	ACSF	Ca^{2+} free ACSF
NaCl	-	125	125
KCl	2.5	2.5	2.5
MgCl_2	4	1	3
CaCl_2	0.1	2	-
NaH_2PO_4	1.25	1.25	1.25
NaHCO_3	26	26	26
Na^+ pyruvate	2	2	2
Myo-inositol	3	3	3
Ascorbic acid	0.5	0.5	0.5
Glucose	10	10	10
Sucrose	250	-	-

Table 1 Overview of solutions used and their composition. All concentrations given in mM.

compound	final concentration	mode of action	supplier
TTX	1 μM	Na^+ channel antagonist	Tocris
DNQX	20 μM	AMPA receptor antagonist	Tocris
AP-5	50 μM	NMDA receptor antagonist	Tocris
Kynurenic acid	2mM	Glutamate receptor antagonist	Tocris
TEA	3mM	K_v3 channel antagonist	Sigma
DTX-I	100nM	K_v1 channel antagonist	Alomone
Bilirubin	20 μM	Unknown	Sigma
SNP	100 μM	Nitric oxide donor	Calbiochem
BAY 41-2272	1 μM	Enhancer of sGC activity	Calbiochem
7-NI	150mg/kg	nNOS antagonist	Sigma

Table 2 A list of compounds and their concentration used in the experiments of this thesis

2.3.1 Preparation of *in vitro* brain slices from the AVCN

The *in vivo* data shown in Fig 4.7a were recorded from Mongolian gerbil by Marei Typlt at University of Leipzig, Leipzig, Germany and are only shown to put the patch-clamp data (Fig 4.7b) into context which were recorded from Wistar rats in Leicester by me in collaboration with Marei Typlt.

Parasagittal AVCN brain slices from Wistar rats for patch-clamp recording were prepared as described previously (Oertel, 1983; Typlt *et al.*, 2010). Rats were killed by decapitation and the brain removed as for preparation of MNTB brainstem slices. After separating the brainstem and cerebellum from the rest of the brain as shown in Figure 2.2, an additional cut was made with an angle of approximately 15° (Figure 2.3a). This lateral brainstem section containing the cochlear nucleus was glued onto the tray of the vibratome on the freshly cut surface. One slice of 200µm was taken from the top, which contained the cochlear nucleus. A bipolar platinum electrode was used to stimulate auditory nerve fibres (3–8 V, 0.1–0.2 ms, at 50 Hz for 10 s) which give rise to the endbulbs of Held that synapse onto the bushy cells (Figure 2.3b). Simultaneous extra- and intracellular recordings from spherical bushy cells were performed using the 2 channel multi-clamp 700B amplifier (Molecular Probes, USA). The intracellular patch-electrodes had resistances of 2–5MΩ and were filled with patch solution (see MNTB for description). The extracellular electrodes were filled with 3mM KCl (identical with electrodes used for *in vivo* recordings from gerbil) and had resistances of 6–11MΩ.

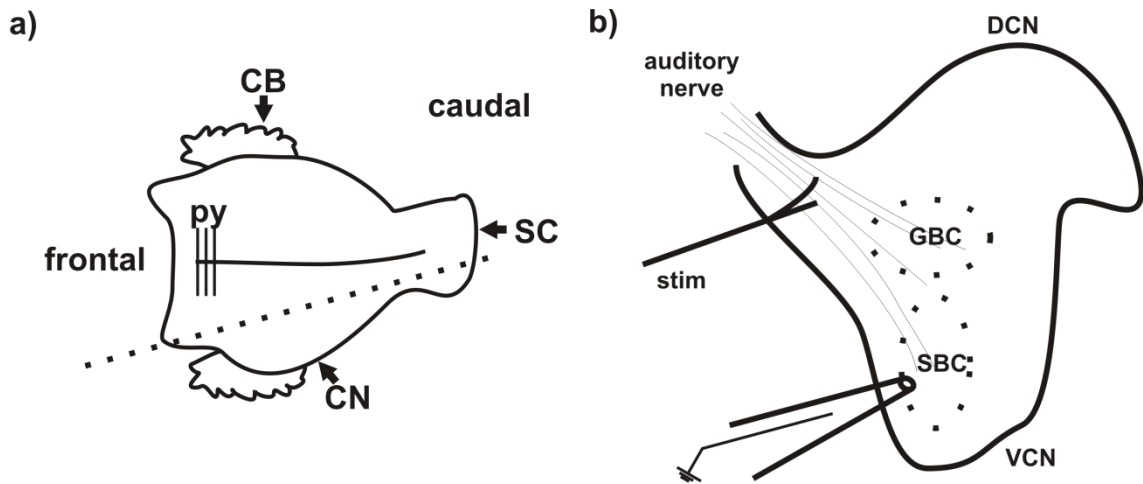


Figure 2.3 Schematic drawing of the AVCN brain slice preparation
 a) Schematic drawing of the rat brainstem from the caudal side. The cutting angle is indicated by the dotted line. CB=cerebellum, SC= spinal cord, CN= cochlear nucleus, py= pyramidal tract. b) Schematic drawing of a parasagittal slice of the cochlear nucleus and location of the bushy neurons in the ventral part. The stimulation electrode (stim) would be placed at the incoming auditory nerve fibres for synaptic stimulation. GBC= globular bushy cells, DCN= dorsal cochlear nucleus, SBC= spherical bushy cells, VCN= ventral cochlear nucleus.

2.4 Multi-electrode arrays (MED64)

The abbreviation MEA is generally used for the term “multi-electrode array”, and under this name sold by MultiChannelSystems, Reutlingen, Germany. The multi-electrode array system used here differs slightly from the MEA system and is sold by Alpha MED Science, Japan as a so-called MED system (where MED stands for “multi-electrode dish”. The abbreviations MEA and MED in this thesis both refer to the multi-electrode array by Alpha MED Science.

The MED system by Alpha MED Science, Japan consisted of: the connector plate (MED-CO3P, Alpha MED Science, Japan), which holds the MED probe (Figure 2.4b+c) itself; a 64-channel integrated amplifier (SU-MED640, Panasonic, Japan) (Figure 2.4a); 2 A/D-converter PCI-cards (National Instruments, USA); a PC (Dell, UK) and the mandatory connector cables. The stimuli were created using the software MED Connector 3.1 and Mobius 0.2.16

(Alpha MED Science, Japan), which were also used for all recordings. As the possibilities to design various stimuli with the MED Connector software are limited, an external stimulator (Master 8, A.M.P.I., Israel) was occasionally used and connected to the amplifier via a BNC cable. The MED connector sat on an inverted microscope (Zeiss Telaval 31, Zeiss, Germany) and the acute brainstem slices were placed on top of the electrodes under visual control. To avoid the slice floating off, a platinum harp with strings made out of unwaxed dental floss was placed on top of the slice to hold it in the right position. The inverted microscope, the peristaltic pump and all solutions were placed on an air table (TMC, Peabody, USA) to avoid any disturbances by vibrations.

The general design of a typical MED64 array is shown in Figure 2.4c. For all experiments MEDs with an 8x8 electrode layout with an electrode size of 50 μ m and electrode spacing of 150 μ m were used (type: MED515A, Alpha MED Science, Japan). The single electrodes are made out of platinum black and the resistance is <22k Ω . The brainstem slice lying over the electrode array is shown in Figure 2.5a. Each trace is the averaged reading from one electrode. The electrodes in the right half of the slice - within the black-dotted ellipsoid in rows 3 and 4 from top- overlay the MNTB (Figure 2.5a). One electrode located underneath the midline of the acute slice was chosen as stimulation electrode. Different electrodes along the midline were tested and the one giving the biggest response was selected. Through this electrode the stimulus pattern was delivered, which comprised of a biphasic (-/+) paired-pulse stimulus with a stimulus intensity of 100 μ A and a duration of 80 μ s per phase. The inter-pulse interval was 20ms. The whole stimulus was delivered every 5 seconds and is shown in Figure 2.5b.

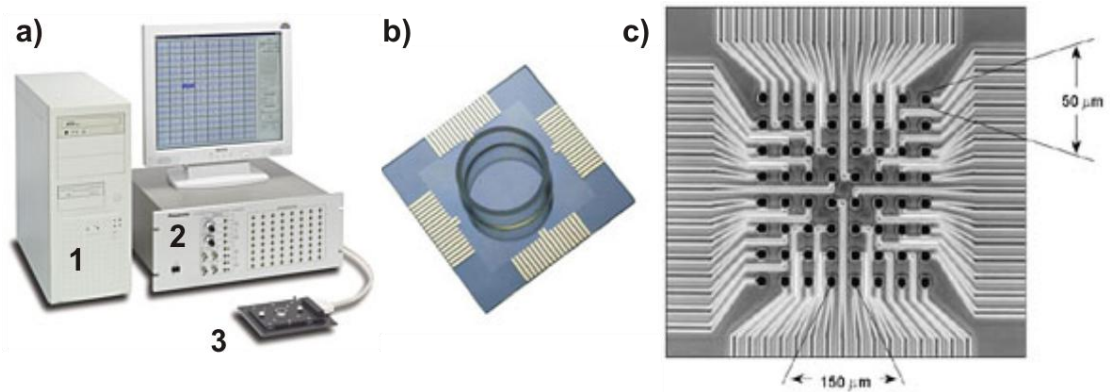


Figure 2.4 Overview of the components of the MED recording system.

a) 1: PC, 2: amplifier, 3: connector holding the MED; b) example of a typical MED probe; c) close up of MED layout that is identical to the MED515A type used in the experiments (From: www.med64.com)

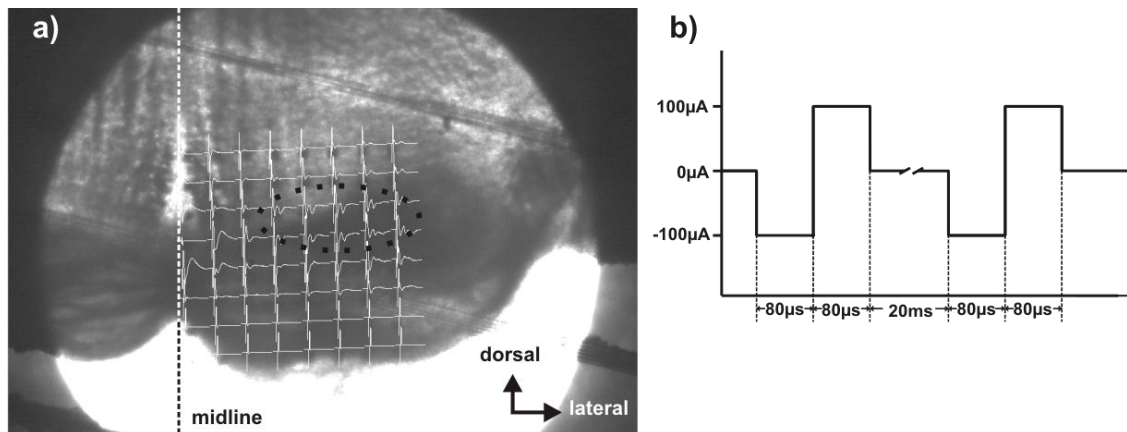


Figure 2.5 Acute brain slice on MEA and stimulus paradigm.

a) Arrangement of an acute brainstem slice on MED array as seen when looking through the microscope. The dashed straight line indicates the midline of the brainstem slice. The electrodes within the black-dotted ellipsoid are the ones overlying the MNTB. The electrodes can be seen as black dots shining through the slice. Stimulation electrode would be chosen from the electrodes of the left column which are placed at the midline of the slice. View through the microscope. b) Schematic drawing of the stimulus paradigm used for the MED experiments.

The signals were measured against the reference electrodes which are integrated in the MED probes at a sampling rate of 20kHz using the 64-channel integrated amplifier (SU-MED640, Panasonic, Japan). By midline stimulation, evoked field potentials (FP) could be recorded in the MNTB. These showed characteristic negative deflections from the baseline, which according to electrophysiological conventions, indicate membrane excitation.

All solutions used were applied using a peristaltic pump (Minipuls III, Gilson, France). To heat the MED probe and the solutions to physiological temperatures a new bottom plate containing 4 Peltier devices (design: Prof. Ian D. Forsythe, Univ. of Leicester, construction: the workshop of the Univ. of Leicester) connected to an external control unit was used. The temperature at the control unit was set in order that the temperature of the solution in the MED probe was $32^{\circ}\text{C} \pm 1^{\circ}\text{C}$.

The amplitudes (deflection from baseline) of C_1 , C_2 and $(+)C_2$ were measured against the baseline prior to the stimulus artefact. For data analysis, the following software was used: MED Conductor 3.1 (Alpha MED Science, Japan), Mobius 0.2.16 (Alpha MED Science, Japan) and MS Excel. The Students' t-test for paired data was used to test for significance and statistical significance was accepted if $p < 0.05$. Due to the huge amount of data generated whilst recording from 63 electrodes simultaneously - usually up to 2GB of raw data from experiments on a typical day - only electrodes located in the MNTB area and showing the typical evoked MNTB response (see chapter 3. results) were used for analysis.

Whole-cell patch-clamp recordings and calcium-imaging methods are widely used in the Forsythe lab and have been described in great detail several times in other papers and theses. Due to this and the numerous other different techniques used throughout this thesis which also require explanations, the description of single cell patch-clamping and calcium-imaging is given briefly below.

2.5 Patch-Clamp recordings

To investigate the effect of bilirubin on the principal neurons single-cell whole-cell patch-clamp recordings were used to test for changes in their electrical properties. Initially, the patch pipette is advanced until it touches the cell membrane and forms a seal with a resistance of several hundred mega-ohm. This recording mode is called loose-cell patch. Forming a high-resistance seal (“giga-ohm seal”) between recording pipette and cell membrane, allows for high-resolution patch-clamp recordings (Hamill *et al.*, 1981) and is called cell-attached mode. While the initial method was perfected in cell cultures it was later possible to successfully perform patch-clamp recordings in thin acute brain slices (Edwards *et al.*, 1989). After forming a ‘giga-seal’ between the solution-filled glass pipette (for composition see below) and the neuron, the membrane is ruptured by gently applying negative pressure. This recording mode is called whole-cell patch-clamp and is suitable for small cells (Hamill *et al.*, 1981), i.e. cardiomyocytes and neurons with a small dendritic tree. Once the cytoplasm is in contact with the pipette solution, the electrical properties of the neuron are controlled by the patch-clamp amplifier.

In voltage-clamp, the neuron is held at different voltages while the currents are measured. The recorded data is used to generate the so-called I-V-curve, which shows the current-voltage relationship for any given type of neuron. With the use of specific ion channel antagonists, it is then possible to make statements about the contribution of certain ion channels currents to the whole-cell current.

In current-clamp, the cell is held at different currents which can be injected via the recording pipette. In this mode, the excitability (level of current injection required for an action potential (AP) to be fired), the AP waveform and related

parameters can be investigated. Again, the use of specific blockers enables the person conducting the experiment to dissect the contributions of certain ion channels to the action potential. Acquiring this data is important, because from it it can be determined if the electrical properties change after exposure to bilirubin.

Whole-cell patch-clamp recordings were made from visually identified MNTB neurons in acute brain slices (200µm thick) of the auditory brainstem (Forsythe, 1994; Barnes-Davies & Forsythe, 1995; Dodson *et al.*, 2002a; Steinert *et al.*, 2008; Haustein *et al.*, 2010). The brain slices were prepared as described previously above. Experiments were performed at $36 \pm 1^\circ\text{C}$ using a feedback controlled Peltier device (manufactured by University of Leicester Mechanical and Electrical Workshop). Slices were held in position by a 'harp': a horseshoe-shaped 2.5cm piece of platinum wire with nylon strings glued across both long ends to hold the slice in place (Edwards *et al.*, 1989). Neurons were visualised through a 60x water immersion objective (LUMPlanFI, Olympus, NA 0.9) on a Zeiss Axioscope microscope. A monochromatic CCD camera (model 4912, COHU Inc., USA) was used to obtain live differential interference contrast (DIC) images of the neurons when patching them. Patch pipettes were pulled from glass capillaries (GC150F-7.5, OD 1.5 mm, Harvard Apparatus, Edenbridge, UK) using a 2-stage puller (Narishige PC-10, Japan) and had resistances of 2-5MΩ when filled with the pipette solution (see below). Series resistance was between 4-9MΩ (compensated by 70%). Pipettes were attached to the headstage of the Multiclamp 700B amplifier. The headstage was mounted onto an Olympus ONU 31P micromanipulator (Olympus, United Kingdom). Positive pressure was applied to the filled pipettes on approach to the brain slice to

clean the cell surface from debris and prevent blocking of the pipette. MNTB neurons were voltage-clamped at a holding potential of -60mV.

Synaptic stimulation (using a DS2A isolated stimulator (Digitimer, Welwyn Garden City, UK; 1-10 V, 0.1-0.2 ms) was delivered via a bipolar platinum electrode placed at the midline of the slice across the trapezoid body nerve fibres. Data was recorded using a Multiclamp 700B amplifier (Molecular Devices, Sunnyvale, CA, USA) sampling at 50kHz and filtering at 10kHz. Stimulation, data acquisition and analysis were performed using pCLAMP_9 and Clampfit_10.2 software (Molecular Devices). Average data is presented as mean±S.E.M. All solutions used were applied using a peristaltic pump (Minipuls 3, Gilson, France).

Pipette solution for whole-cell recordings (in mM): K-gluconate 97.5; KCl 32.5, HEPES 10, EGTA 5, MgCl₂ 1, pH was adjusted to 7.3 with KOH and osmolarity to 290 mOsm with sucrose.

2.6 Calcium-Imaging

Calcium plays an important role in many cellular processes, for example: in muscle contraction, synaptic vesicle fusion, as a second messenger, as co-factor for enzymes (i.e. in the blood clotting cascade) and in calcifying bones. Intracellular calcium accumulation is part of glutamate excitotoxicity and subsequent neuronal cell death (Manev *et al.*, 1989; Hartley *et al.*, 1993). To test if MNTB neurons were subject to excitotoxicity after bilirubin-exposure, the resting calcium concentrations in control and treated neurons were measured.

Acute brainstem slices (200µm) were prepared as for patch-clamp experiments. Slices were loaded with 5µM Fura-2 AM (Molecular Probes, Eugene, OR, USA, dissolved in DMSO with 5% pluronic acid) for 10minutes before leaving them for 30minutes in ACSF for de-esterification of the AM-dye. Fura-II was excited at 340nm (calcium bound to Fura-II) and 380nm (calcium not bound to Fura-II). Images were taken with a CCD camera (PentaMax, Princeton Instruments, Inc.) and Metafluor imaging software (Series 7, Molecular Devices) was used to display the fluorescent image (emission>505nm).

The fluorescence ratio (340nm/380nm) can be used to determine the resting intracellular calcium concentration $[Ca^{2+}]_i$. The Calcium-Imaging setup had been previously calibrated by Jörn Steinert, therefore the following formula described by Grynkiewicz (Grynkiewicz *et al.*, 1985) was used to calculate $[Ca^{2+}]_i$ in nM.

$$[Ca^{2+}] = K_d \left(\frac{(R - R_{min})}{(R_{max} - R)} \right) \left(\frac{S_{f2}}{S_{b2}} \right)$$

In this equation K_d (= 224nM, (Tong *et al.*, 2010)) is the Fura-2 dissociation constant at 37°C, R is the background-corrected fluorescent ratio F_{340}/F_{380} , R_{min} (= 0.10) and R_{max} (=0.70) are the fluorescence ratios under calcium-free and calcium-saturated conditions, respectively and $S_{f2}/S_{b2} = F_{380 \text{ in zero } Ca^{2+}} / F_{380 \text{ saturating } Ca^{2+}}$ with $S_{f2} = 346$, $S_{b2} = 153.61$. Ca^{2+} free conditions are achieved by perfusing the brain slice with 0mM Ca^{2+} ACSF, ionomycin (Billups B *et al.*, 2002) which forms pores through which Ca^{2+} leaks out of neurons and EGTA to buffer all Ca^{2+} . Ca^{2+} saturated conditions are achieved by perfusing the brain slice with high (10mM) Ca^{2+} ACSF (Billups B *et al.*, 2002), ionomycin and

depolarisation of the neurons (with high potassium ACSF). This leads to a maximum load of Ca^{2+} inside the neurons that are imaged.

2.7 Dextran-Labeling and Multi-Photon-Imaging

2.7.1 *Dextran labelling*

Calyces were anterograde labelled with Dextran-tetramethyl-rhodamine (D3308, 3000MW, Invitrogen) using a method adapted from Burger and colleagues (Burger *et al.*, 2005). Dextran-tetramethyl-rhodamine (DTMR) is known to label axons and dendrites well (Fritsch, 1993; Kaneko *et al.*, 1996). The 3000MW dye was used, as Fritsch (Fritsch, 1993) showed that 3000MW DTMR is transported quicker along axons compared to DTMRs with higher molecular weights. This method had been previously successfully used by Burger and colleagues in a similar preparation in the chick auditory brainstem (Burger *et al.*, 2005). Brainstems were dissected as for electrophysiology and trimmed down until both cochlear nuclei were visible on the same section plane. Kynurenic acid (2mM, Tocris, UK), an antagonist for NMDA and non-NMDA receptors at this concentration (Ganong & Cotman, 1986), was added to prevent excitotoxicity. Following this, 0.01M phosphate buffered saline (PBS), pH 7.4 with 5% 3000MW dextran-tetramethyl-rhodamine was pressure injected into the anteroventral cochlear nucleus on both sides in at least 3 different locations. This was done via patch-clamp glass capillaries (tip-opening: 20-30 μm), which were back-filled with DTMR and connected to a 10ml syringe through which the

pressure was applied. Immediately after dye-injection, electroporation (1x 120V pulse for 130 ms, then 60x (50ms 50V) pulses) using a bipolar tungsten electrode connected to a BTX ECM 830 electroporator (Harvard Apparatus) was employed to help the uptake of the dye into the globular bushy cells that give rise to the calyces of Held (Held, 1893). The brainstem was then maintained at room temperature for 30-60minutes before sections (350-600 μ m) containing both cochlear nuclei and MNTB were taken. Slices with a thickness of 500 μ m delivered the most reliable labelling results. These slices were then stored in the dark at room temperature in ACSF, in a slice maintenance chamber for a minimum of 3 but typically 4 hours before imaging. Slices were kept on the microscope stage using the platinum harp from patch-clamp experiments and constantly perfused with ACSF. The harp was positioned with the nylon strings facing up, so that it would not cut too deeply into the thicker slice. Images from the living slice were taken using a Zeiss Axioscope 2FS (Carl Zeiss) with Mai-Tai Deep-See multiphoton laser microscope.

2.7.2 Multi-photon imaging

Multi-photon laser scanning microscopy was invented in 1990 (Denk *et al.*, 1990) although the theory of two-photon excitation had already been established by Maria Göppert-Mayer around 1930 (Göppert, 1929; Göppert-Mayer, 1931). It has similarities with traditional confocal laser microscopy but has the great advantage that it can penetrate biological tissue up to 1000 μ m (Theer *et al.*, 2003) and produces less photo-damage, making it possible to resolve structure deep within living tissue. As the 2 photons have to excite the dye molecule at nearly exactly the same time, a pulsed laser is used to provide

short bursts (100 femto-seconds, i.e. 100×10^{-15} seconds) of photons delivered at high energy levels (1.5 W in this case).

Multi-photon laser scanning microscopy causes less photo-damage because the photons have double the wavelength and half the energy of the excitation wavelength of the chromophore, i.e. two photons $\sim 800\text{nm}$ with each having nearly half the energy of one single blue photon ($\sim 400\text{nm}$). Therefore, two photons are required at the same time to lift the electrons in the dye to a higher energy level (see Figure 2.6a). This results in less photo-damage because less energy is focused in one spot and the photons are focused on and appear in high density on the focal plane only.

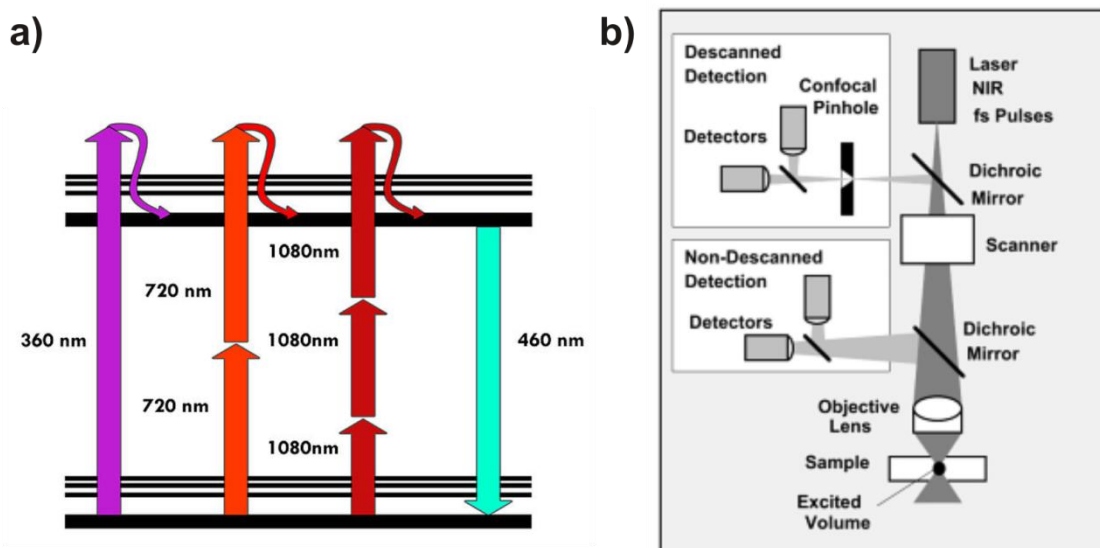


Figure 2.6 Principles of multiphoton laser microscopy.

a) Schematic drawing of the principal of multiphoton laser excitation. (from Diaspro et al, 2006 “Multi-photon excitation microscopy” *BioMedical Engineering OnLine* 5 (36)) The molecule is excited through absorption of either 1 ultra-violet photon at 360nm or 2 photons simultaneously at 720nm (near infrared) before falling onto a state where it emits light (460nm) and reaches the basic energy level again (bottom trace). b) The differences between descanned and non-descanned detection (from Becker, 2005 “Advanced time-correlated single photon counting techniques”, p.131, Copyright (2005), with permission from Springer). In the non-descanned mode all the light, including the scattered light is collected. The descanned mode only collects light directly from the focal plane and excludes scattered light by using a pinhole.

The Zeiss LSM510 microscope was fitted with a Zeiss W Plan-Apochromat water immersion 20x objective with a numerical aperture (NA) of 1.0. It was

connected to a Zeiss AxioScope 2FS (Carl Zeiss) with a LSM 510 laser module (Zeiss) and a Mai-Tai DeepSee (Spectra-Physics) mode-locked titanium sapphire femto-second laser. This is a pulsed laser used for multi-photon imaging, generating tune-able infrared light ($\lambda = 690\text{-}1020\text{nm}$) at repetition rates of 80MHz. Multiphoton laser light at 820-840nm wavelength was successfully used as excitation wavelength and produced reliable images of labelled axons and calyces (see chapter 5). The emission wavelength of dextran-tetra-methyl-rhodamine is 580nm and therefore a bandpass filter (BP) between 560-615nm was chosen to collect the emitted light.

All the following parameters were set in ZEN 2008 SP1.1 software (Zeiss, Germany). This software controls the settings for the laser as well as the filters and the pathway of the light beam in the microscope and is used for image acquisition. Before the case enclosing the microscope was built, the settings described in Table 3 were used for the 'descanned' or 'confocal' detection to capture images and z-stacks. Like in confocal microscopy, a pin-hole is used to collect only light from the confocal plane (see also Figure 2.6b) and reduce the amount of daylight 'leaked' into the objective from reaching the photo detectors (Becker, 2005).

This does however, also exclude scattered light from deeper layers of the tissue. After the case enclosing the microscope was built - making it essentially light-proof - the range of settings on the right column of Table 3 were used to obtain images and z-stacks in the non-descanned detection (NDD) mode (see also Figure 2.6b). In the NDD mode, a pin-hole is not used because all light is deflected towards very sensitive large-area photon-detectors by a mirror behind

the objective lens. This way, all the light emitted is collected, including scattered light from deeper layers of the tissue (Becker, 2005). To ensure that only the light emitted from the fluorophore is used, this method does require that no ambient light can reach the detectors.

software settings	without enclosure (descanned mode)	with enclosure (non-descanned detection (NDD) mode)
laser wavelength	820nm	840nm
master gain	740-800	~740-790
digital gain	1	1
digital offset	-0.10-0.10	-0.08-0.00
transmission	1.2-4%	1.5-3%
averages of each frame	4	4
resolution	520x520 or 1024x1024	520x520 or 1024x1024
scan time	15 seconds/frame	15 seconds/frame
filters	BP 560-615 IR	none
beam splitters	MBS: HFT KP 660 DBS1: Mirror DBS 2: NFT 545	HFT KP 660

Table 3 Software settings for multiphoton imaging in standard and non-descan-detection mode

Dextran-Tetramethyl-Rhodamine (3000MW) has an emission wavelength maximum of 580nm and an excitation wavelength maximum of 555nm (data-sheet/product description from Invitrogen).

Bilirubin is maximally excited by wavelengths between 440-530nm (McDonagh *et al.*, 1989). The emission wavelength maximum of bilirubin is 550nm (Kohashi *et al.*, 1998; Zucker *et al.*, 1999). Since the emission and excitation wavelengths of bilirubin and DTMR were so close, it was not possible to perfuse bilirubin onto the slice whilst simultaneously image the calyces and measure changes. For this experiment to be successful another dye with different excitation and emission properties would have to be chosen. An additional problem with imaging bilirubin is that light in the wavelength of 400-470nm is very effective for

phototherapy (Lightner *et al.*, 1980), changing chemical properties of bilirubin through photo-isomerisation and thereby rendering it less toxic.

z-stacks recorded with ZEN software were then imported into Volocity for analysis. To test if the calculations of the software Volocity 5.3 (Improvision, United Kingdom) were correct, fluorescent spherical beads (Focalcheck™ Fluorescent Microsphere Standards: F-7237, Molecular Probes) with a known diameter (15µm) embedded in agarose were measured and then the manually calculated surface area was compared with the computer result. The calculation of the software was identical with the manual calculations. This suggests that the surface area measurements were reliable. The following command-routine was used in Volocity to measure the calyces and calculate their surface areas after a region of interest (ROI) had been drawn around an isolated calyx: 'find object using intensity' → 'remove noise from objects' → 'clip objects to ROI'. The calyces were visually identified by their shape and great care was applied to measure only individual calyces, i.e. to avoid overlapping or adjacent structures such as axons or neighbouring calyces.

2.8 Electron microscopy

The perfusion fixation was carried out with David J Read. The embedding and staining of the tissue blocks was performed by Judy McWilliam, Tim Smith and Dr. David Dinsdale. The latter also took the images which I selected. Double-blind analysis of the EM pictures was carried out by myself and David J Read.

The first electron microscope prototype was built in 1931 by Max Knoll and Ernst Ruska in Germany. The latter built the first transmission electron microscope exceeding the resolution of a light microscope in 1933. For this work he was awarded the Nobel Prize of Physics in 1986. Electron microscopes essentially work similarly to light microscopes, in that a beam of electrons (instead of light) is focussed and guided with the help of electromagnetic and electrostatic lenses towards the sample. Electrons have much shorter wavelengths than photons (in light microscopy); therefore the resolution power of electron microscopes is far greater. An electron microscope can resolve structures up to 0.2nm and achieve magnifications of up to x2000000. The sample will scatter the electrons depending on the electron-density of its components. The scattered electrons are then refocused via lenses on a projection screen, camera film or more recently onto a digital camera.

Below is the protocol that was followed for the preparation of the EM samples:

Brains were perfusion fixed with 2% glutaraldehyde + 2% paraformaldehyde in 0.1M sodium cacodylate buffer (final pH 7.4). The brains were then embedded in low-melting point agarose and slices (500µm thick) were prepared using a vibrating blade microtome (Leica Microsystems, Milton Keynes, UK). These slices were post-fixed in 1% osmium tetroxide + 1% potassium ferrocyanide, stained en-bloc with 5% uranyl acetate and embedded in epoxy resin (TAAB

Laboratories Equipment Ltd, Aldermaston, UK). Semi-thin (1 μ m) sections were stained with toluidine blue and examined to select areas for ultramicrotomy. Ultrathin sections (70nm) were stained with lead citrate and examined in a Jeol 100-CXII transmission electron microscope (JEOL (UK) Ltd, Welwyn Garden City, UK), equipped with a 'Megaview III' digital camera (Olympus Soft Imaging Solutions GmbH, Münster, Germany). Analysis of EM images was done double-blinded using ImageJ 1.42 (NIH) or Axiovision 4.8 software (Zeiss).

For analysis, only neurons containing the nucleus were included. The idea was that in this way it could be ensured that we were looking roughly at the centre of the neuron. An example is shown in Figure 2.7a. Only neurons displaying the nucleus were analysed, while neurons not showing the nucleus (white X) were excluded. This was because it was highly possible that results could be shifted towards the impression that the cell-body is smaller and that the cell is contacted by more presynaptic profiles in relation to the cell surface. An extreme example for such a case is shown in Figure 2.7b. The cutting plane for this neuron was too far off-centre. Thereby the cell perimeter appears smaller, and a higher percentage of the cell body appears to be contacted by presynaptic profiles than might actually have been the case at the centre of the neuron. For this reason neurons not showing the nucleus in the respective section were not analysed.

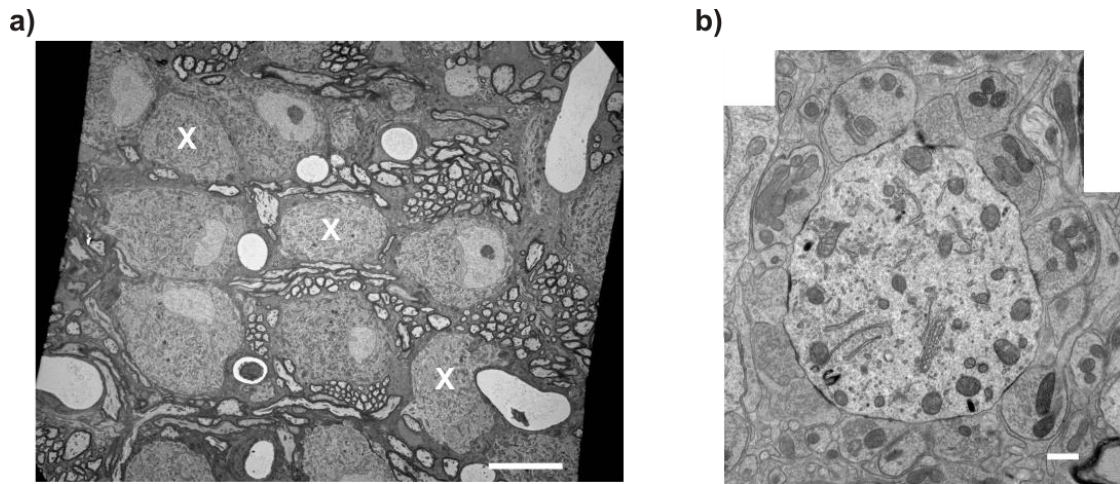


Figure 2.7 Choosing cells for EM analysis.

a) EM-image of MNTB from a control Gunn rat shows principal neurons nicely lined up in between axonal profiles. Neurons marked with an 'X' were excluded from analysis as they didn't show the nucleus (scale bar: 10µm). b) Extreme example of an off-centre Wistar rat principal neuron completely covered by presynaptic profiles but not showing the nucleus (scale bar: 2µm).

Statistical analysis was performed using SigmaPlot 11.0 software (Systat Software, Inc.). Unless otherwise stated the Student's t-test was used to test for significance. Statistical significance was accepted when $p < 0.05$.

3. Results from multi-electrode array (MEA) and auditory brainstem response (ABR) recordings

As previously described, severe hyperbilirubinaemia can lead to hearing loss in humans and the Gunn rat. *In vivo* auditory brainstem responses (ABRs) are impaired after bilirubin-toxicity and, as the MNTB contributes to wave III in ABRs, an investigation was conducted into how these neurons were affected by bilirubin. This chapter initially describes *in vitro* multi-electrode recordings (MEA) in the MNTB, including pharmacological characterisation of the evoked field potential. There will be a description of *in vitro* experiments in which perfusion of bilirubin did not produce any changes to the evoked field potentials (FPs), followed by a report on the findings of the effects of bilirubin toxicity on *in vivo* ABRs in the Gunn rat and the chapter will conclude with the effect of bilirubin toxicity (induced *in vivo*) on amplitude and synaptic delay in MEA recordings.

3.1 Extracellular Multi-electrode Array (MEA) Recordings

The initial idea was to use an *in vitro* system to study the underlying causes for the hearing loss described in severely jaundiced humans (Chisin *et al.*, 1979; Kaga *et al.*, 1979) and the Gunn rat model of hyperbilirubinaemia (Shapiro, 1988; Shapiro, 1993; Shapiro *et al.*, 2007).

For this purpose a multi-electrode array system was set up to record evoked field potentials in the MNTB in brain slices *in vitro* and the evoked MNTB responses were pharmacologically characterised. This should later aid the

interpretation of the findings from jaundiced rats. Below is a description of a typical evoked field potential in an MEA recording in the MNTB and how, by using antagonists, it is possible to distinguish between conducted and synaptically transmitted components. Earlier findings about the characterisation of the components of the evoked MNTB FB have been published in Haustein et al (2008) but using gerbils instead of rats and equipment by Multichannel Systems (MCS, Reutlingen, Germany) instead of MED64 (Alpha MED Science, Japan). For this thesis, these experiments were repeated in rat brain tissue utilizing the MED64 system (see figures 3.4-3.6). These initial experiments were crucial to later test for changes in the synaptic transmission in the MNTB of hyperbilirubinaemic *jj*-Gunn rats (3.2.1).

Based on the fact that principal neurons of the MNTB receive a single, large glutamatergic input via the calyx of Held presynaptic terminal (Held, 1893; Forsythe, 1994), it was postulated that it might be possible to distinguish between pre-and postsynaptic responses in MEA recordings if the afferent fibres could be stimulated with high precision so as to activate the population of MNTB neurons simultaneously.

Due to the high synchrony of the evoked FPs in the MNTB, the MNTB FPs are distinctly different from signals outside of this area (Haustein *et al.*, 2008). Figure 3.1a shows a schematic drawing of the position of the MEA on the brainstem slice in a typical recording situation. Figure 3.1b is the view down the inverted microscope on which the MEA-holder is mounted with an overlay of the recorded signals from the computer screen (white traces). When performing these recordings one can clearly distinguish the different waveforms within the multi-electrode array.

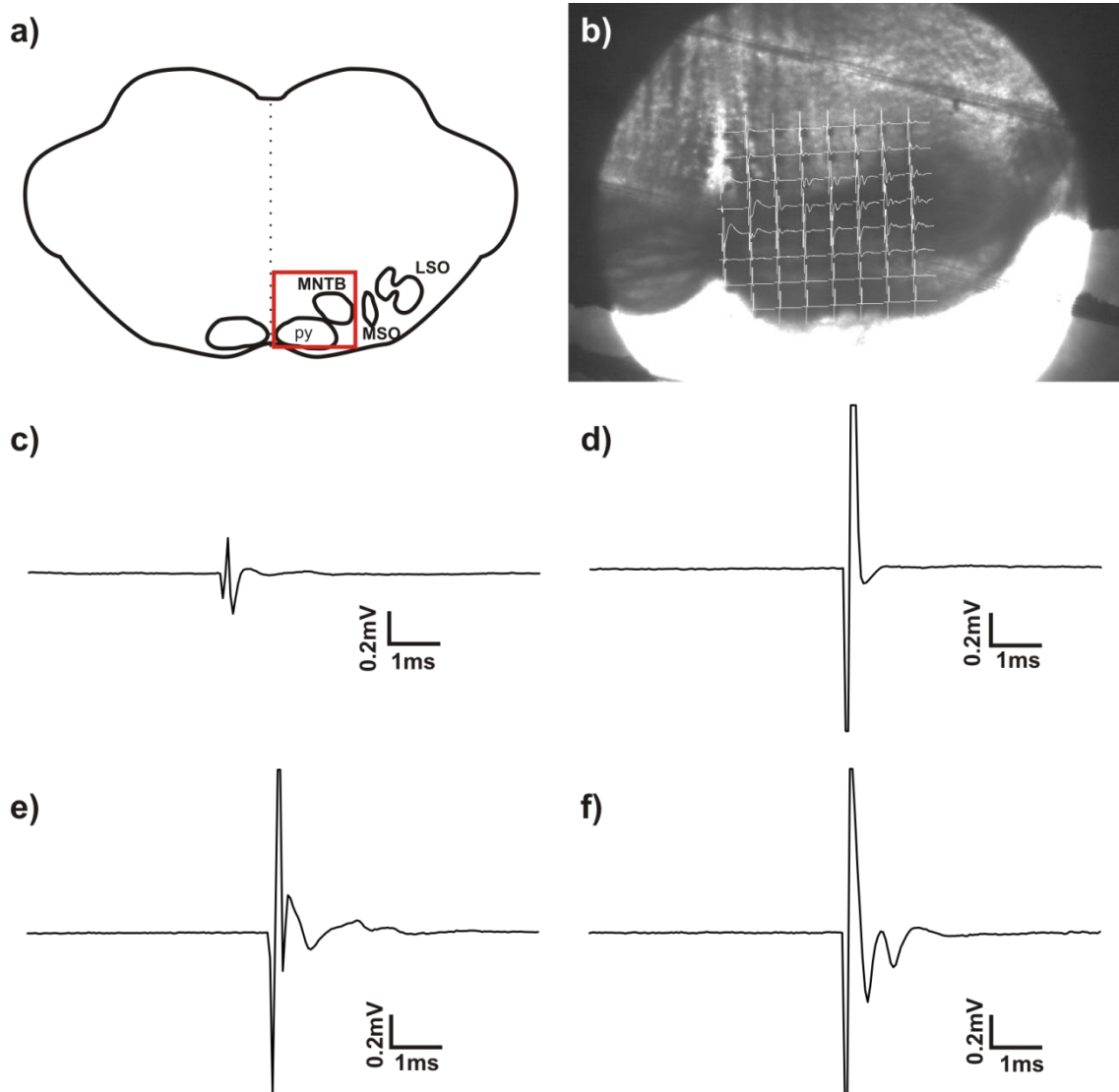


Figure 3.1 Definition of a characteristic MNTB evoked field potential as recorded with MEAs. a) A schematic drawing of the auditory brainstem with the main nuclei of the Superior Olivary Complex, the Medial Nucleus of the Trapezoid Body (MNTB), the Medial Superior Olive (MSO) and the Lateral Superior Olive (LSO). The red box marks the area where the MEA is located in b); py= pyramidal tract. b) View down the microscope shows the brainstem slice sitting on top of the multi-electrode array. The white overlay shows signals recorded from the electrodes at the different positions on the slice. The black dots are the actual electrodes c) The signal at the stimulation electrode at the midline. d) The signal from an electrode not in the slice. e) Signal from an electrode in the tissue but not in the MNTB region. f) A typical signal from an electrode placed at the MNTB area. This response is only found here and distinctly different from signals of electrodes in other areas of the brainstem slice. Stimulus artefact has been clipped.

The signal from the stimulation electrode (Figure 3.1c), for example, or an electrode that is not covered by the brain slice (Figure 3.1d) will show different deflections from the baseline after the stimulus artefact compared to an electrode recording from outside the MNTB (Figure 3.1e) or within the MNTB

area (Figure 3.1f). For analysis, only electrodes located in the MNTB area and showing the typical MNTB waveform (Figure 3.1f & Figure 3.2) were used.

Stimulation at the midline of the brain slice evoked a characteristic two-component response (Haustein *et al.*, 2008)(Figure 3.1 f &Figure 3.2).

Following the stimulus artefact there are two negative deflections from the baseline, termed component 1 (C_1) and component 2 (C_2), as well as a positive deflection directly after C_2 named the positive part of C_2 ($(+)C_2$) (Figure 3.2).

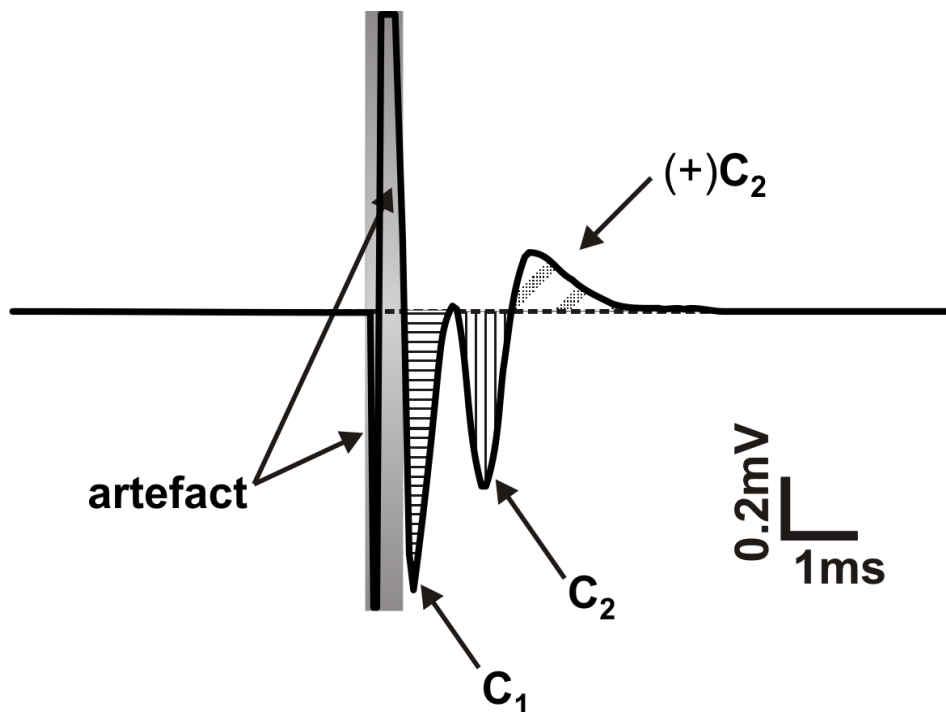


Figure 3.2 Example trace of a characteristic MNTB field potential recorded with MEA. After the stimulus artefact the waveform is characterised by two negative deflections from the baseline, named component 1 (C_1) and component 2 (C_2). The latter is followed by a positive deflection termed $(+)C_2$.

3.1.1 Effects of temperature on the evoked field potential in the MNTB

The initial experiments in the preparatory phase of the MED64 system were carried out at room temperature (generally between 21°-23°C). In order to perform experiments at more physiologically relevant temperatures, a Peltier-driven heating stage was designed by Ian D. Forsythe and manufactured by the University of Leicester mechanical workshop. This Peltier device allowed the heating of aCSF and the MED probe itself. For up to 30 minutes recordings at 36°C were stable. However, in test recordings of 60 minutes or longer, amplitudes of the evoked field potentials declined gradually. As the flow-rate could not be increased above 2ml/min without compromising the stability and position of the brain slice on the MEA, a temperature of 32°C was adopted as the most stable working temperature that was closest to the physiological temperature in rat brains (37.5°C), (Dietrich *et al.*, 1994). At 32°C recordings remained stable for up to 4 hours (longest time tested, Figure 3.14). The effect of temperature on the evoked MNTB signals is shown in Figure 3.3a. The synaptic delay, defined as the delay between minima of C₁ and C₂, was shortened significantly from 0.94±0.02ms at room temperature to 0.45±0.01ms at 32°C (Figure 3.3b). Amplitudes did not significantly differ between the two temperatures tested (Figure 3.3c). The appearance of minima for both C₁ and C₂ was significantly accelerated in 32°C compared to room temperature (Figure 3.3d).

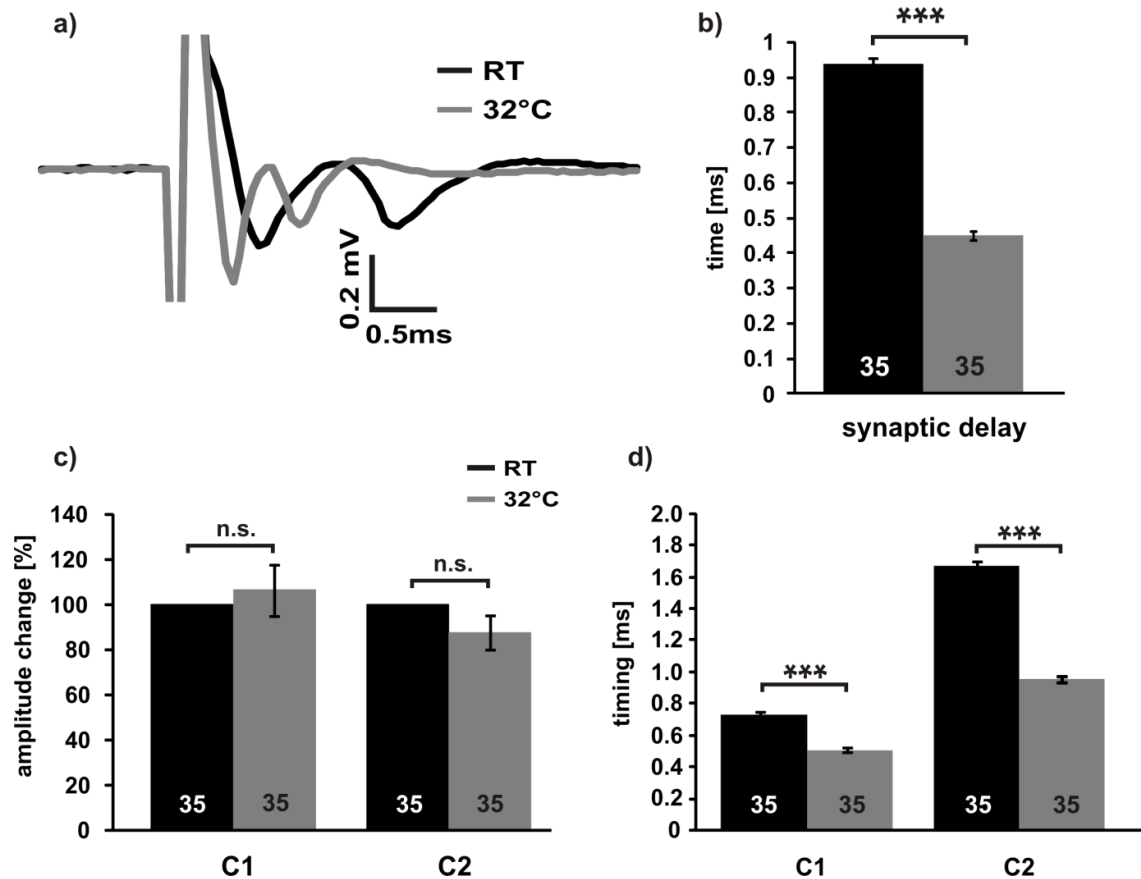


Figure 3.3 Effects of temperature on the evoked field potential in the MNTB.

Recordings at near physiological temperatures (32°C) show accelerated synaptic transmission and occurrence of both components without any effects on the signal amplitude. a) Example trace of a typical evoked MNTB field potential at room temperature (black) and 32°C (grey). b) Summary plot shows shortened synaptic delay in 32°C. c) Summary plot displays no significant difference in amplitude between the two groups. d) Summary plot shows that the appearance of both C₁ and C₂ minima is significantly sped up in 32°C. RT= room temperature. Mann-Whitney-Rank-Sum-test: n.s. = not significant, ***= p<0.001, 35 electrodes, 5 slices, 5 animals.

3.1.2 Pharmacological characterisation of the evoked field potential in the MNTB

To address the question of the origin of the individual components a number of specific pharmacological antagonists were utilised. If components are part of the stimulus artefact they should not be affected by Na⁺ channel blocker tetrodotoxin (TTX). TTX in a concentration of 1 μM did abolish both components (Figure 3.4a & b), demonstrating that they are both of cellular origin and not part of the stimulus artefact.

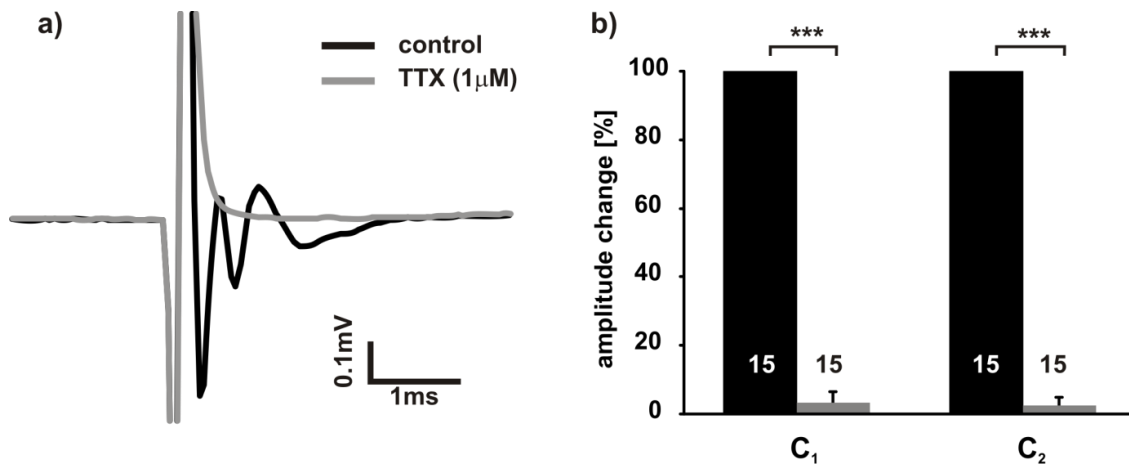


Figure 3.4 The effect of tetrodotoxin (TTX) on the evoked MNTB field potential. Both components of the evoked MNTB FP are tetrodotoxin (TTX) sensitive. a) Example trace of a typical evoked MNTB field potential before (black) and in the presence of TTX (grey). b) Summary plot shows that both C₁ and C₂ are completely blocked by TTX. ***= p<0.001, 15 electrodes, 3 slices.

It has long been understood that Ca²⁺ ions in the extracellular space in the right concentrations are necessary for synaptic transmission (Harvey & MacIntosh, 1940) or presynaptic transmitter release (Katz & Miledi, 1970). It is known that the AP arriving through the axon causes presynaptic voltage-gated calcium channels (VGCC) to open, leading to an influx of extracellular calcium into the presynaptic terminal. VGCC are in close proximity to the vesicles filled with the respective neurotransmitter, in the case of the calyx of Held, glutamate. The complex interaction of calcium-sensors such as synaptotagmin I and vesicle-associated proteins syntaxin, synaptobrevin and SNAP-25 is involved in transmitter release. It is thought that the increased calcium concentration leads to conformational changes in these protein-complexes, which in turn lead to the vesicle docking onto the presynaptic membrane and releasing its content (Augustine, 2001; Neher & Sakaba, 2008; Delaney & Stanley, 2009). The influx of extracellular calcium through voltage-gated calcium channels is crucial for synaptic transmission, therefore Ca²⁺ free ACSF was utilised to block any synaptic transmission and hence any component which reflects postsynaptic

activity. Figure 3.5a shows an example trace of a typical MNTB response in normal ACSF (black) and in Ca^{2+} free ACSF (grey). While C_1 is unaffected in this condition C_2 is completely blocked (Figure 3.5a & b). This indicates that C_2 is a synaptically transmitted component, i.e. it reflects postsynaptic activity.

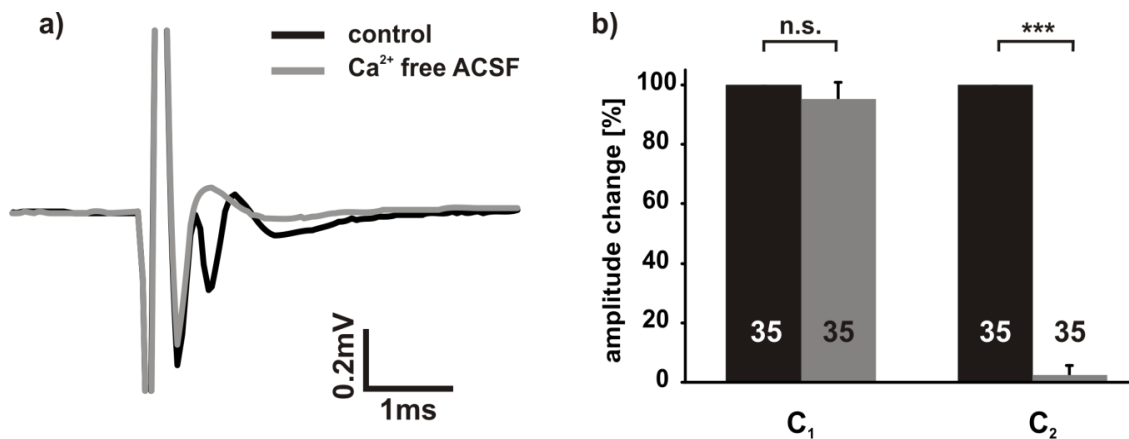


Figure 3.5 The effect of Ca^{2+} free ACSF on the evoked MNTB field potential. The block of C_2 in Ca^{2+} free ACSF reveals its postsynaptic origin. a) Example trace of a typical evoked MNTB field potential before (black) and in the presence of Ca^{2+} free ACSF (grey). b) Summary plot shows that C_2 is completely blocked and no significant effect of Ca^{2+} free ACSF on the amplitude of C_1 n.s. = not significant, *** = $p \leq 0.001$, 35 electrodes, 6 slices.

It is known that the transmission at the calyx of Held synapse is glutamatergic (Forsythe & Barnes-Davies, 1993; Barnes-Davies & Forsythe, 1995), therefore the AMPA and Kainate receptor antagonist DNQX (20 μM) was utilised to confirm this. In the presence of DNQX C_2 was completely blocked (Figure 3.6a & b), confirming its postsynaptic origin and that synaptic transmission in the MNTB is driven by glutamate.

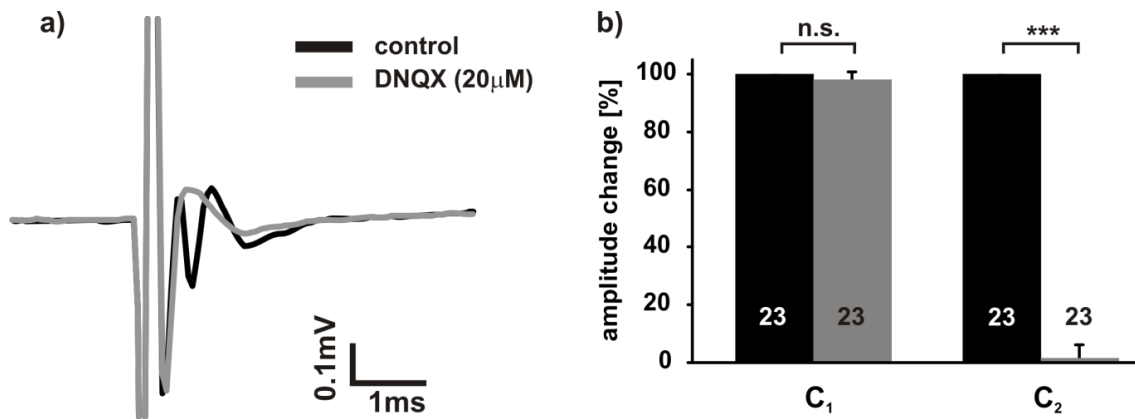


Figure 3.6 The effect of DNQX on the evoked MNTB field potential. The block of the C₂ component by glutamate receptor antagonist DNQX verifies its postsynaptic origin and confirms that synaptic transmission at this synapse is glutamatergic. a) Example trace of a typical evoked MNTB field potential before (black) and in the presence of DNQX (grey). b) Summary plot shows that C₂ is completely blocked and no effect of DNQX on the amplitude of C₁. n.s. = not significant, ***= p≤0.001, 23 electrodes, 5 slices.

Both AMPA and NMDA receptors (NMDA-R) are involved in synaptic transmission at the MNTB (Barnes-Davies & Forsythe, 1995; Steinert *et al.*, 2010b). Therefore, it was important to know to what extent NMDA receptors contribute to the C₂ component. Using NMDA-R antagonist AP-5 (50 μM) and a train of 5 pulses at 100Hz (Figure 3.7a) to release the magnesium block by depolarisation (Mayer *et al.*, 1984; Nowak *et al.*, 1984) it was discovered that AP-5 reduced the C₂ amplitude by up to 50% without affecting C₁ (Figure 3.7d+e). Through analysis of the 1st (Figure 3.7b+d) and the 5th stimulus (Figure 3.7c+e) the issue as to whether there was an effect of the stimulus itself on the outcome was investigated. There was, however, no difference between the C₂ amplitude reduction of the 1st vs. the 5th stimulus.

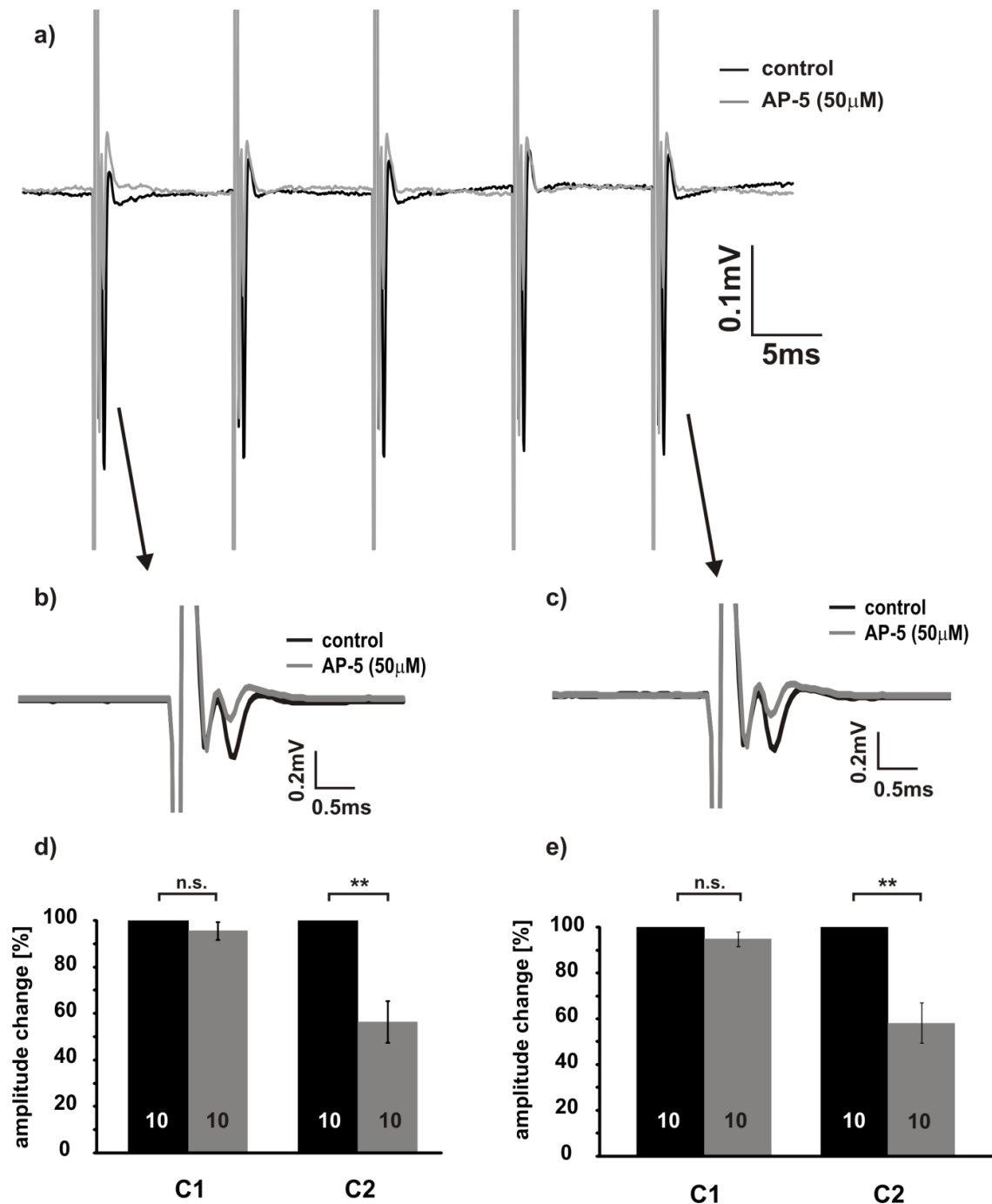


Figure 3.7 The effect of AP-5 on the evoked MNTB field potential.

A brief 100Hz train was used to remove the Mg^{2+} block of NMDA-Receptors. Partial block of C₂ component by NMDA receptor antagonist AP-5 confirms involvement of postsynaptic NMDA receptors in synaptic transmission at the Calyx of Held/MNTB synapse. a) Example trace of 100Hz train before (black) and in the presence of AP-5 (grey). b) Example of the 1st stimulus of the train before (black) and during AP-5 (grey) c) Example of the 5th stimulus of the train before (black) and during AP-5 (grey) d) Summary plot of amplitudes of 1st stimulus with (grey) and without (black) AP-5 e) Summary plot of amplitudes of 5th stimulus with (grey) and without (black) AP-5 n.s. = not significant, **= $p \leq 0.01$, 10 electrodes, 3 slices, 3 animals.

Potassium channels in the MNTB are crucial to preserve accurate timing at this auditory relay station. The voltage-gated potassium channel families K_v3 and K_v1 are especially important (Brew & Forsythe, 1995; Dodson & Forsythe, 2004) to generate a single fast action potential in the principal neurons in response to a suprathreshold glutamatergic input via the calyceal terminal. Since these two specific ion channel families are abundantly expressed in the MNTB and have such a large contribution to shaping cell excitability, it was postulated that the MEA would be sensitive enough to detect changes in the evoked field potential in the presence of K_v3 and K_v1 antagonists. In the presence of K_v1 channel antagonist dendrotoxin-I (DTX-I, 100nM), the amplitude of C_2 was significantly reduced while C_1 was not affected (Figure 3.8a & b).

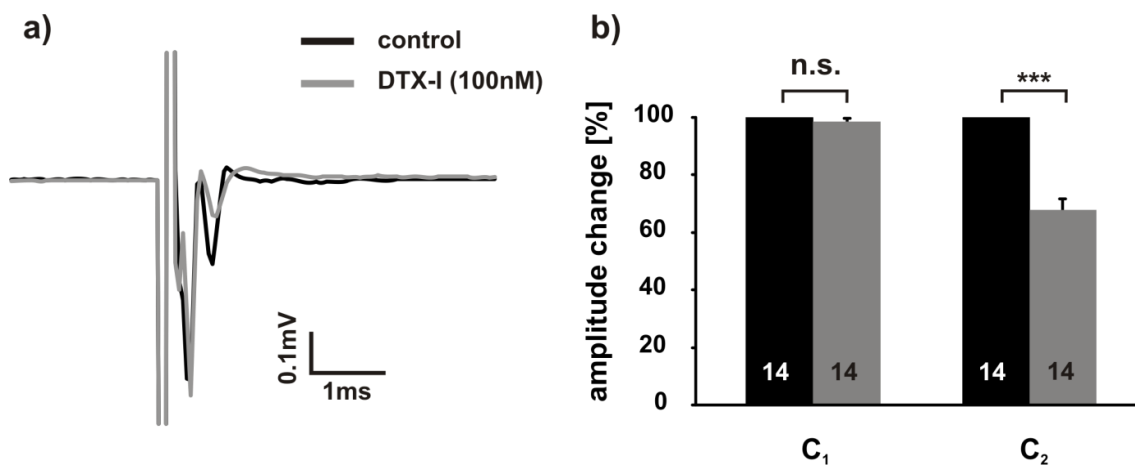


Figure 3.8 The effect of dendrotoxin-I (DTX-I) on the evoked MNTB field potential. K_v1 channel antagonist dendrotoxin-I (100nM) shows the contribution of K_v1 potassium channels in generating the postsynaptic component in extracellular MNTB recordings via MEAs from acute brainstem slices. a) Example trace of a typical evoked MNTB field potential before (black) and in the presence of DTX-I (grey). b) Summary plot shows a significantly reduced C_2 amplitude and no effect of DTX-I on the amplitude of C_1 . t-test, n.s.= not significant, ***= $p \leq 0.001$, 14 electrodes, 3 slices.

Tetraethylammonium (TEA, 3mM), which is known to block K_v3 potassium channels, led to a small yet significant decrease of the C_1 amplitude but no significant change in C_2 (Figure 3.9a b). The positive part of C_2 however, was consistently smaller in the presence of TEA (Figure 3.9a & b).

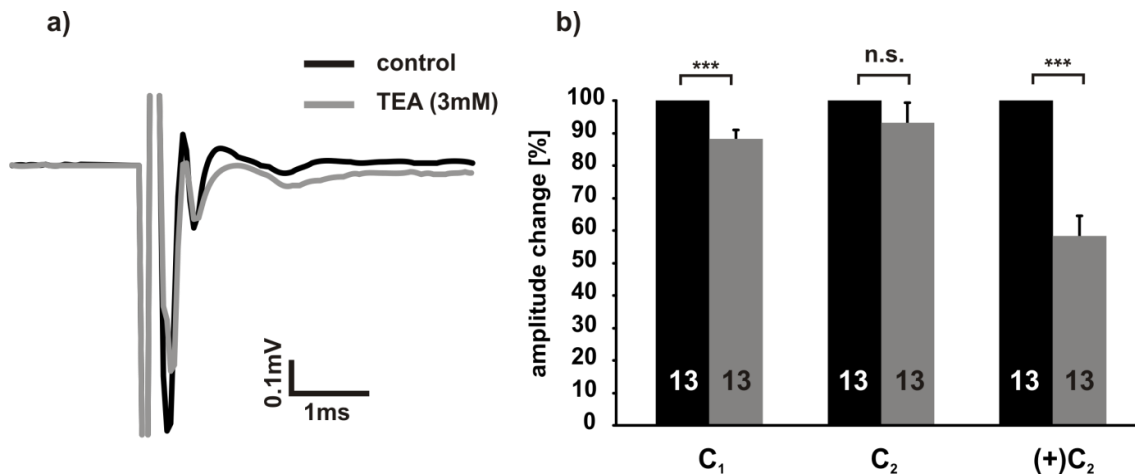


Figure 3.9 The effect of tetraethylammonium (TEA) on the evoked MNTB field potential. MEA recordings are sensitive enough to detect effects of Tetraethylammonium, a K_v3 channel antagonist, on pre- and postsynaptic components. a) Example trace of a typical evoked MNTB field potential before and in the presence of TEA (3mM). b) Summary plot shows amplitude reducing in C_1 and $(+)C_2$ but no significant change in the amplitude of C_2 through TEA. t-test, n.s.= not significant, ***= $p < 0.001$, 13 electrodes, 3 slices.

As an ongoing project in the laboratory there was an investigation into the effects of nitric oxide (NO) on the synaptic transmission in the MNTB. Whilst all other experiments for this project were carried out on mice, it was tested whether this would also occur in rats and the MEA was used to investigate this issue. As seen in the example trace (Figure 3.10a) and the summary plot (Figure 3.10b), the use of BAY 41-2272 ($1\mu\text{M}$; an enhancer of soluble guanylyl cyclase activity) and nitric oxide donor sodium nitroprusside (SNP; $100\mu\text{M}$) caused a reduction in amplitude of C_2 while not affecting C_1 . It also led to a reduction in $(+)C_2$ (Figure 3.10a), which is in accordance with the findings of the

paper that NO is suppressing K_v3 potassium currents. This data set has been published as part of the supplemental data in 2008 (Steinert *et al.*, 2008).

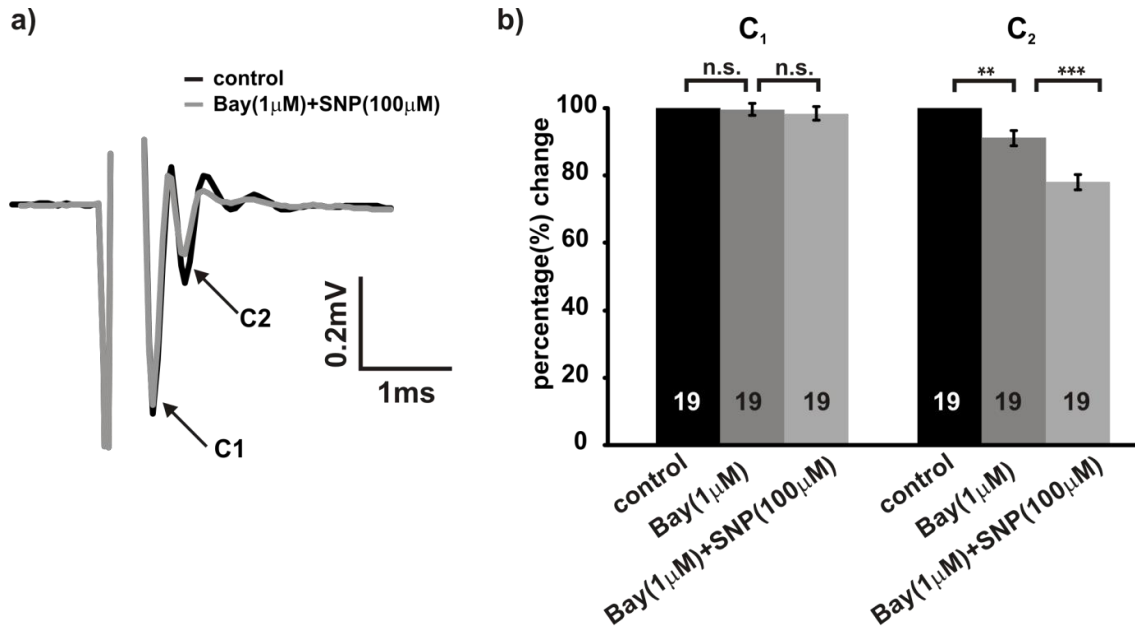


Figure 3.10 The effect of Bay 41-2272 and Sodium Nitro-Prusside (SNP) on the evoked MNTB field potential.

a) Example trace of a typical extracellular MNTB recording by means of multi-electrode arrays before (black trace) and after (grey trace) the application of Bay (1 μ M) and SNP (100 μ M). Whereas the presynaptic C₁ component is hardly affected, the amplitude of the postsynaptic C₂ component is reduced in the presence of Bay & SNP. The stimulus artefact is cut off for clarity. b) Summary of MED data obtained from 19 electrodes of 4 brain slices from 4 rats (P16-17). The C₁ components show no statistically significant change in amplitude but the C₂ components are reduced in the presence of Bay & SNP. All recordings were done at 36°C. A paired Student's t-test was used to test for statistical significance. Reprinted from Neuron 60, Steinert *et al.*, Nitric Oxide Is a Volume Transmitter Regulating Postsynaptic Excitability at a Glutamatergic Synapse, p642-656, Copyright (2008) with the permission of Elsevier.

3.1.3 Long-term recordings of the evoked field potential in the MNTB at 32°C

Having completed the pharmacological characterisation of evoked MNTB FPs, the following hypothesis was then tested: that it is possible to induce bilirubin toxicity *in vitro* by superfusing the brain slice with bilirubin while doing MEA recordings at the same time.

This set of experiments began with perfusing free bilirubin (20µM) onto the acute brain slices to test whether this would have any effects on C₁ or C₂. From the literature it is known that excess levels of bilirubin lead to hearing loss in human babies and homozygous Gunn rats. Therefore there was an expectation to see the effects at this central relay station of the auditory system which is the MNTB. Initially an increase in the C₂ amplitude (Figure 3.11a & c) was observed without any effects on C₁ (Figure 3.11b). However, this result could not be repeated and as an example (Figure 3.11d) of the numerous slices that subsequently did not show any effect during bilirubin perfusion, there is the analysis for 1 slice/9 electrodes (Figure 3.11e & f) which demonstrated that bilirubin did not have any effect on the evoked MNTB FP at room temperature.

As the results were not consistent and the temperature controller was available, it was decided to test first how long perfusion with normal ACSF could last and test for any run-down of the signals at 32°C. As there were not any values from the literature indicating how long bilirubin would have to be perfused to see effects, the experiment began with determining how long brain slices could stably be recorded. Initially, Lister Hooded rats were used to obtain stable recordings for up to 2 hours (Figure 3.12). Amplitudes of C₁ and C₂ stabilised

about 10-15mins after recording started and remained stable for the whole duration (Figure 3.12a & b).

Having established that stable recordings could be achieved for at least 2h, the focus returned to the original idea of developing an *in vitro* model of hyperbilirubinaemia. The condition was induced by perfusing bilirubin onto the slices while performing MEA recordings. Once again, the initial experiments seemed propitious, as over 3h free bilirubin perfusion led to a reduction of first C₂ (Figure 3.13b) and later also C₁ (Figure 3.13a). This result from 2 LH rats could not however be reproduced. The following brain slices from other LH rats did not respond to bilirubin and data was similar to those shown for room temperature in Figure 3.11d-f.

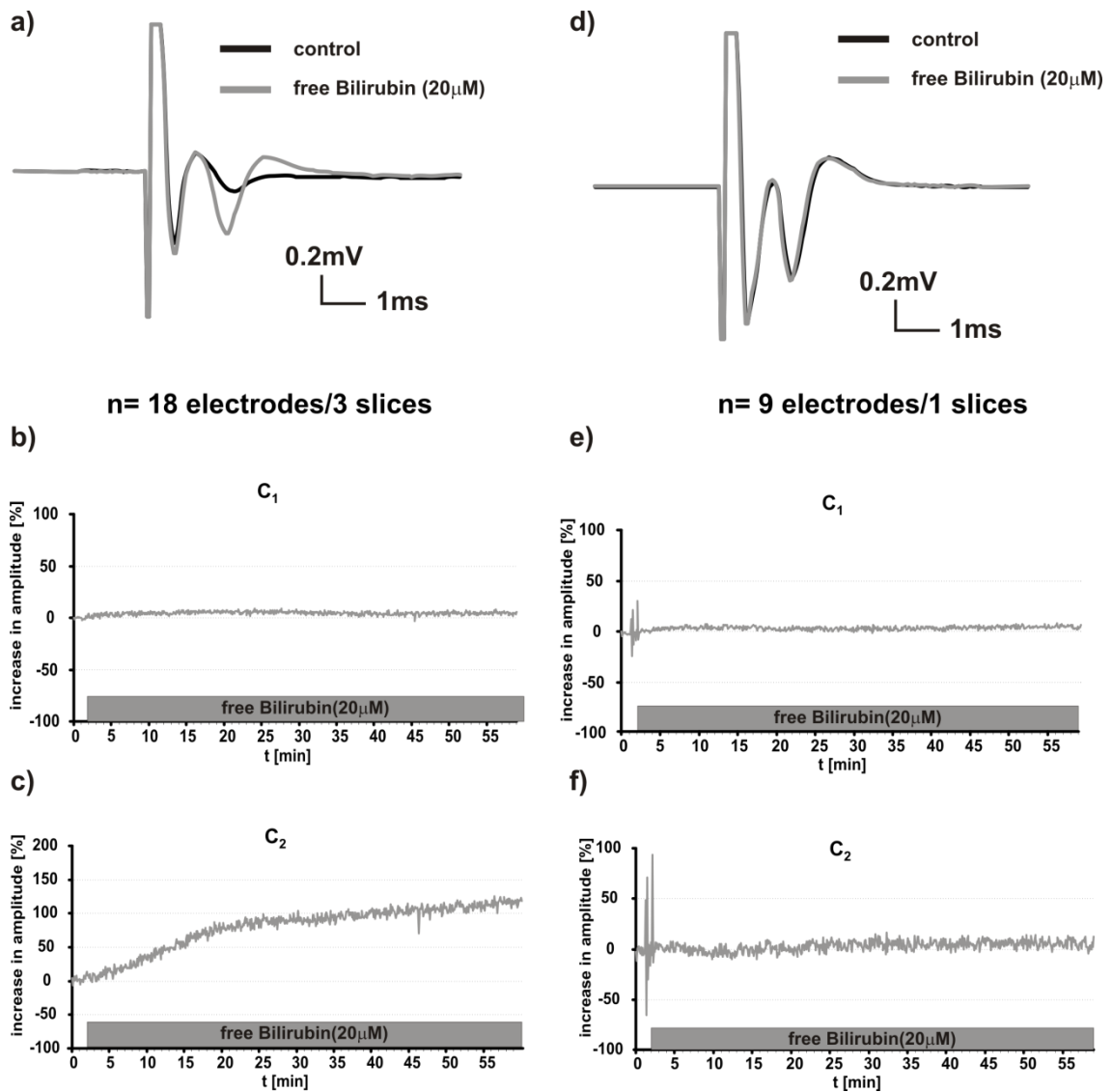


Figure 3.11 Variable effects of free bilirubin (20 μ M) on MNTB FPs in MEAs at room temperature. a) Example traces of MEA recording before (black) and at the end of (grey) bilirubin perfusion. b) Mean C₁ amplitude of 18 electrodes does not change over nearly 1h bilirubin perfusion. c) Mean C₂ amplitude of 18 electrodes increases by 100% of baseline levels over nearly 1h bilirubin perfusion. n=2 LH rats, 3 slices, 18 electrodes; d) Example trace of MEA recording before (black) and at the end of (grey) free bilirubin perfusion. e) Mean C₁ amplitude of 9 electrodes does not change over nearly 1h bilirubin perfusion. f) Mean C₂ amplitude of 9 electrodes does not change over nearly 1h bilirubin perfusion. 1 LH rat, 1 slice, 9 electrodes.

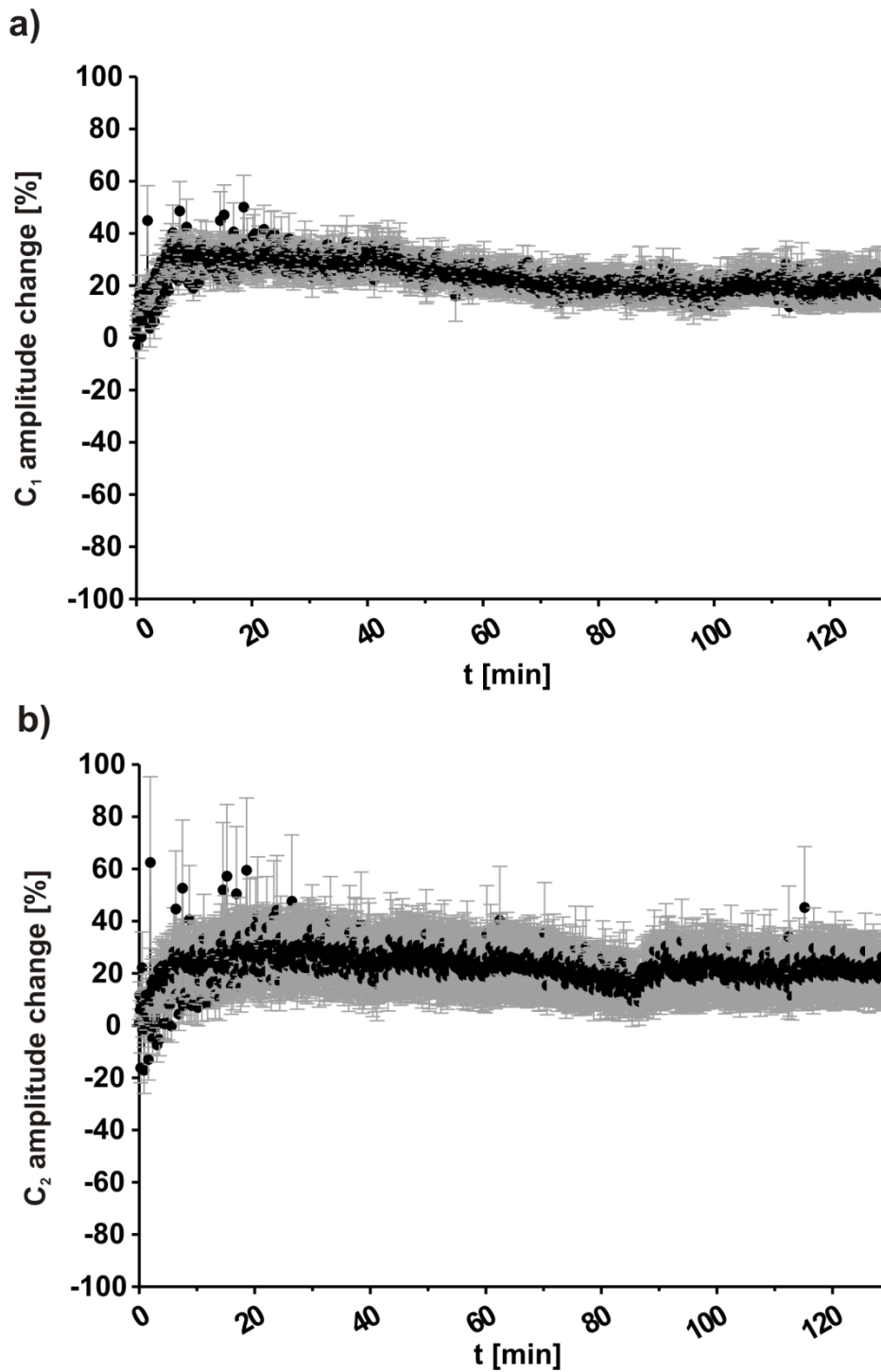


Figure 3.12 MEA recordings in the MNTB are stable for 2 hours at 32°C. MNTB recordings in ACSF at 32°C from acute brainstem slices do not alter pre- or postsynaptic amplitudes within 2h. a) C₁ amplitude remains stable for 2h in 32°C ACSF and so does C₂ (b). Data points are shown as mean \pm SEM of all electrodes; 3 Lister Hooded rats, 3 slices, 27 electrodes.

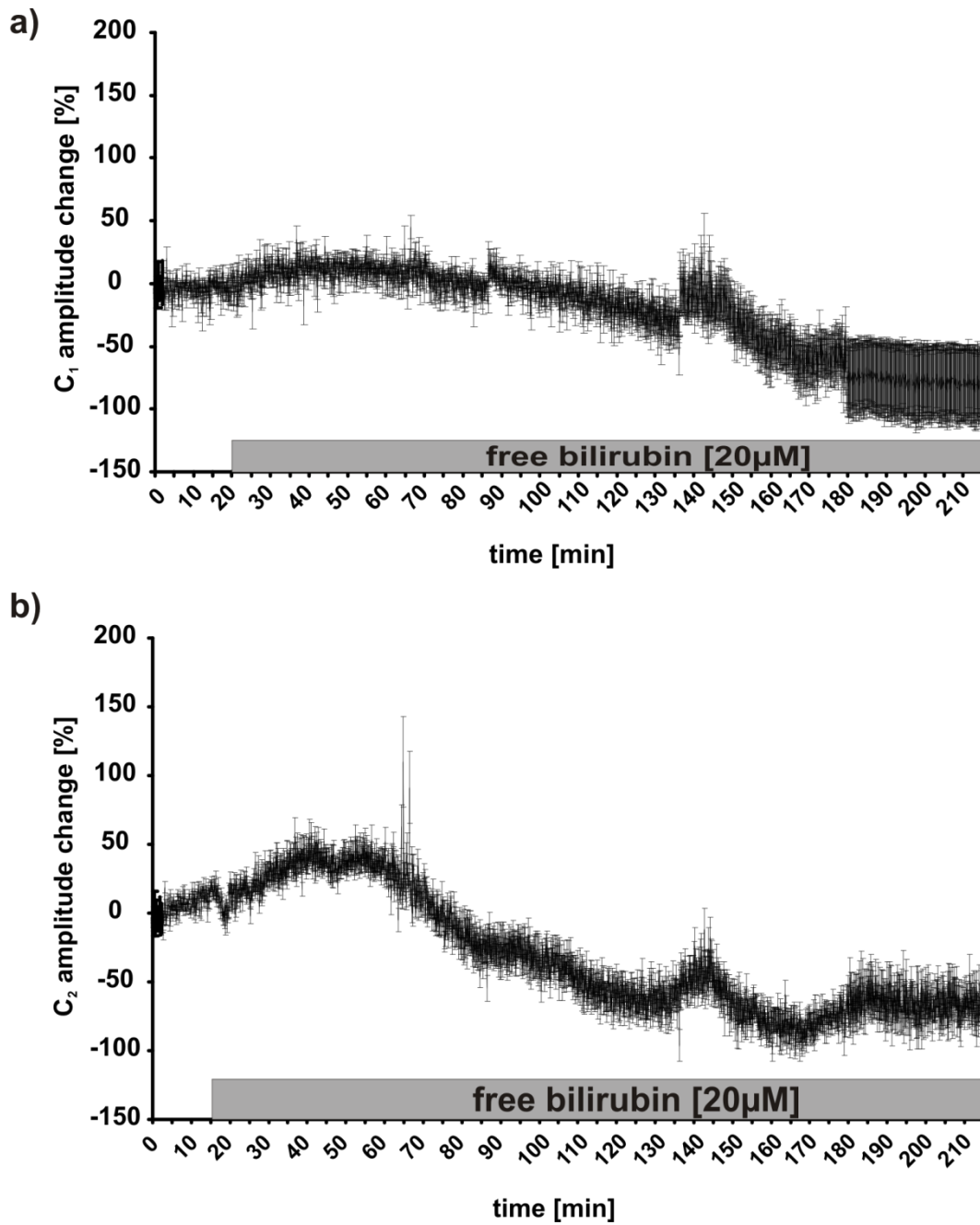


Figure 3.13 Free bilirubin (20 μM) leads to reduced field potential amplitudes in the MNTB at 31°C. a) Amplitude change of C₁. Over time C₁ decreases in the presence of free bilirubin. b) Amplitude change of C₂. After about 1h C₂ amplitude started to decline to about 50%-75% of control levels. Traces are mean ± SEM; n=2 LH rats, 2 slices, 28 electrodes.

Since perfusion of bilirubin did not produce any conclusive results in wild-type animals, it was decided to use the Gunn rat model to induce bilirubin toxicity *in vitro*.

The Gunn rat model of hyperbilirubinaemia has been used for decades to investigate effects of toxic bilirubin levels on the brain, with an emphasis on light and electron microscopic investigations particularly of the cerebellum (Schutta & Johnson, 1967, 1969, 1971; Rose & Wisniewski, 1979) but also other brain regions (Jew & Williams, 1977; Jew & Sandquist, 1979) in the 60s-80s (Fukuhara & Yamada, 1981; O'Callaghan & Miller, 1985; Sato *et al.*, 1987; Aono *et al.*, 1988; Takagishi, 1989; Takagishi & Yamamura, 1989), followed by the use of Auditory Brainstem responses to test for hearing loss (Shapiro, 1988; Shapiro, 1993) and immunohistochemistry (Shaia *et al.*, 2002; Spencer *et al.*, 2002; Shaia *et al.*, 2005) over the last 25 years.

More than 4 hours of recording MNTB FPs in ACSF at 32°C did not change amplitudes of C₁ (Figure 3.14a) or C₂ (Figure 3.14b). With this knowledge, free bilirubin was perfused (at the maximum concentration of 20µM [which is the concentration where it starts to precipitate]) onto brain slices from jj-Gunn rats whilst recording FPs for the whole time. Although there was a small tendency to amplitude decrease in both C₁ (Figure 3.15a) and C₂ (Figure 3.15b), amplitudes did not change enough to account for the dramatic changes that have been described using ABRs (Shapiro, 1988) and as was later found in the ABRs recorded from Gunn rats for this thesis.

Therefore it was concluded that the hypothesis was incorrect and it was not possible to induce bilirubin toxicity in acute brain slices by simply perfusing bilirubin onto slices.

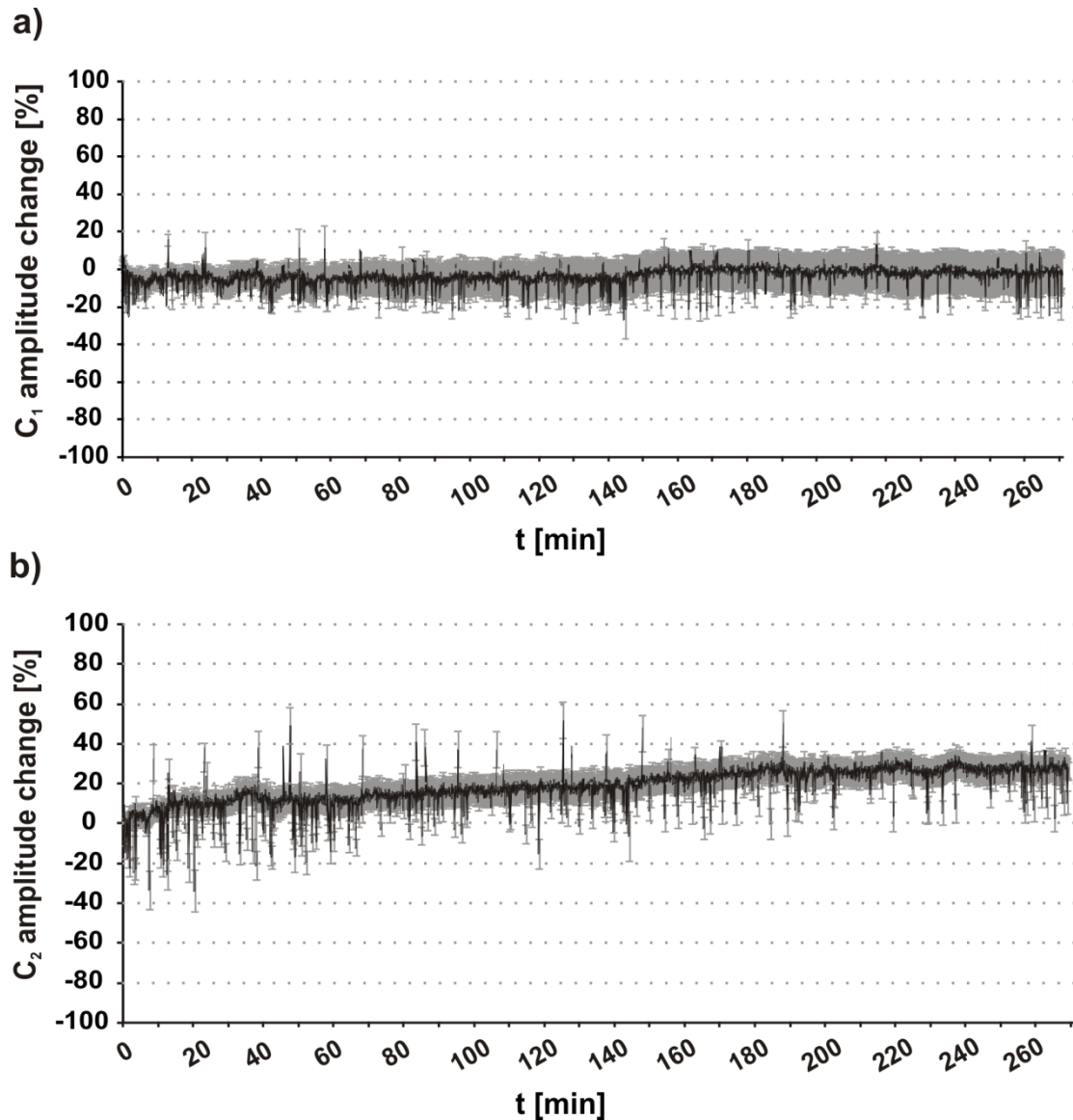


Figure 3.14 MEA recordings from the MNTB are stable for over 4h at 32°C. The effect of 4h recording at 32°C in ACSF on the amplitudes of C₁ and C₂ in acute brain slices of jj-Gunn rat. a) Over a period of more than 4h the amplitude of C₁ remains stable, while b) the amplitude of C₂ even increases slightly over time. Mean±SEM; 2 rats, 2 slices, 14 electrodes.

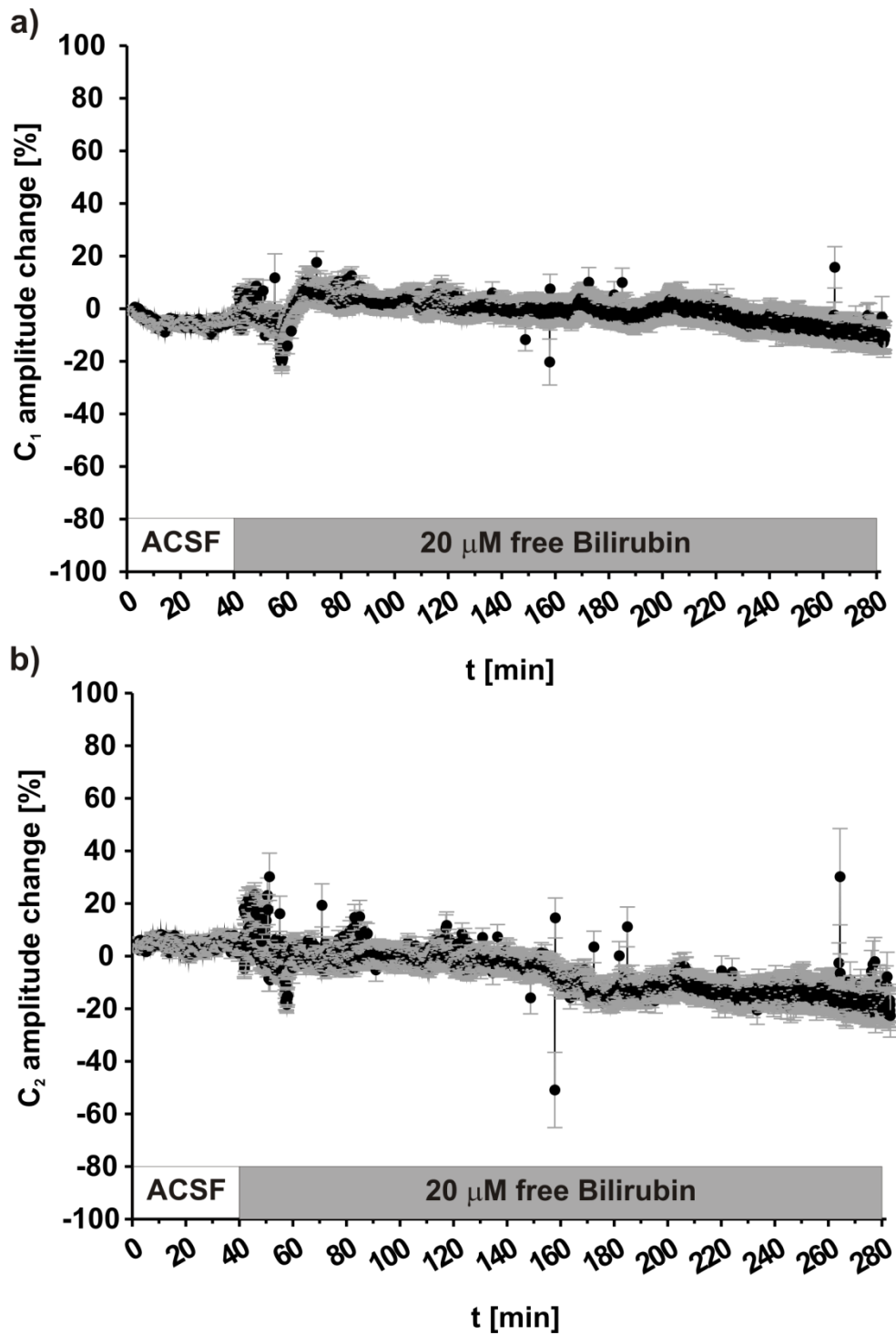


Figure 3.15 Free bilirubin has no effect onto evoked MNTB field potentials in slices of jj-Gunn rats at 32°C.

Superfusion of free bilirubin (20μM) onto acute jj-Gunn rat brainstem slices for 4 hours hardly alters the amplitudes of C₁ (a) or C₂ (b) MNTB evoked FPs at 32°C. Mean±SEM; 4 rats, 4 slices, 32 electrodes.

3.2 Auditory Brainstem Responses

After the induction of hyperbilirubinaemia *in vitro* had not been successful in either wild-type or Gunn rat brain slices, it was decided to go back to the start and try to induce it *in vivo*. After reviewing the body of literature on the Gunn rat model of hyperbilirubinaemia described in 3.1.3 it was postulated that homozygous Gunn rats would show decreased ABRs after displacement of bilirubin into the brain through a single i/p injection of sulfadimethoxine Na⁺ salt (sulfa, 200mg/kg; Sigma). This had already been demonstrated by Shapiro and colleagues (Shapiro, 1988; Shapiro, 1993; Shapiro *et al.*, 2007) and was considered to be a validation of my use of this model. If this was successful, the suggestion would then be to use acute brainstem slices for MEA recordings from these sulfa-treated Gunn rats.

Auditory Brainstem Responses have a long established use as a functional hearing test following neonatal jaundice in humans (Chisin *et al.*, 1979; Kaga *et al.*, 1979) as well as in the Gunn rat (Uziel *et al.*, 1983; Shapiro, 1988).

It has been reported that the hearing range of rats is between 0.2Hz-50kHz, with the highest sensitivity between 8-38kHz (Kelly & Masterton, 1977). The ABR system I used (see Material& Methods) allowed for testing of pure-tones between 2kHz-30kHz and 'click'-stimuli. It was decided to use the 'click' stimulus since it contains all frequencies and to test 12, 24, 30kHz pure tones as well (to determine whether there was a frequency specific loss of hearing or if it was consistent across all the frequencies).

Each rat served as its own control (black traces in Figure 3.16) and showed a normal waveform with waves I, II and IV easily identifiable (Figure 3.16a-d black traces). It was not always possible to separate wave II and III as was the

case with ABRs after the 'click' stimulus. In this case, waves II and III were treated as a single entity for the analysis (Figure 3.16a right summary graph).

For all frequencies tested ('click' and 30, 24, 12kHz), the ABRs as a result of 18h hyperbilirubinaemia following administration of sulfa straightened out and hence showed significantly decreased amplitudes of all waveforms (see Figure 3.16). Figure 3.16 shows ABR traces before (black) and after (grey) 18h hyperbilirubinaemia, which display mean \pm SEM for 'click' (Figure 3.16a), 30kHz (Figure 3.16b), 24kHz (Figure 3.16c) and 12kHz (Figure 3.16c). On the right panel a summary plot is displayed showing the amplitude changes of the individual waves at each given frequency tested. Panel b) has been published as part of figure 1 in (Haustein *et al.*, 2010).

Waveform I, representing the activity of the auditory nerve (Melcher *et al.*, 1996a; Melcher & Kiang, 1996; Melcher *et al.*, 1996b), although decreased was always visible indicating a damage occurring retrocochlear. Waveforms II and III, representing activity of the cochlear nucleus and the superior olivary complex, respectively (Melcher *et al.*, 1996a; Melcher & Kiang, 1996; Melcher *et al.*, 1996b), were either greatly reduced or indistinguishable from the background noise after 18h sulfa-treatment (see Figure 3.16a-d). This result was consistent for all 7 animals tested pre- and post sulfa-injection and confirmed that the Gunn rat is a good model to investigate bilirubin-induced hearing loss.

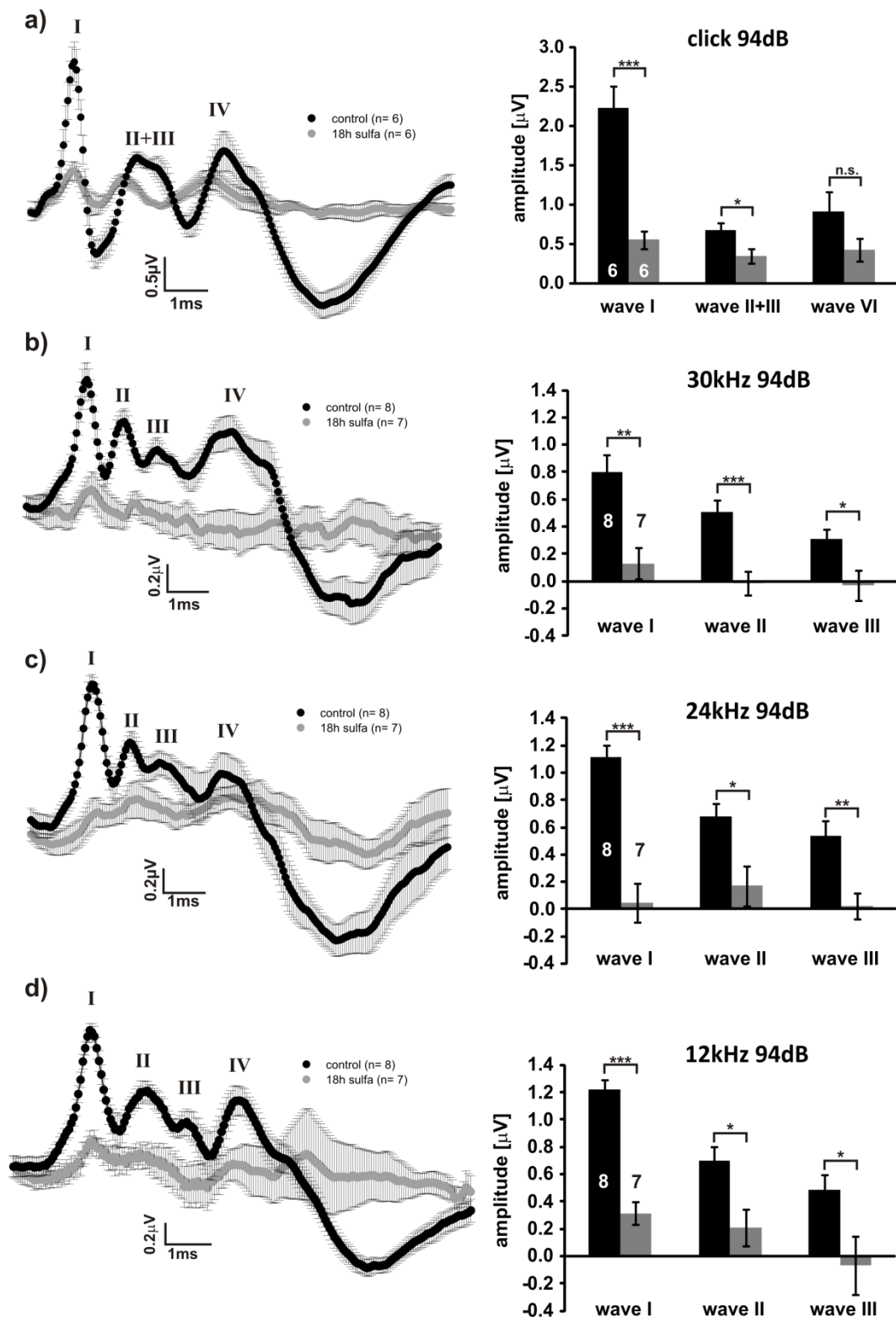


Figure 3.16 The induction of bilirubin-toxicity through sulfadimethoxine leads to decreased ABRs in jj-Gunn rats.

Following 18h sulfa-treatment, the amplitude of Auditory Brainstem Recordings in jj-Gunn rats is decreased over a range of frequencies ('click' stimulus and 30, 24, 12kHz). a) ABRs following 'click' stimulus at 94dB SPL before (black) and after (grey) sulfadimethoxine treatment leading to hyperbilirubinaemia. Roman numbers indicate the individual waves of the complex ABR response. The amplitude reduction was statistically significant (box plots). b), c), d) as in a) but for 30, 24, 12kHz pure-tone stimuli respectively. All data (traces and summary plots): mean \pm SEM; t-test, n.s. = not significant, * \leq 0.05, ** \leq 0.01, *** \leq 0.001.

It had been shown previously that sulfadimethoxine, in particular, and other sulfonamides in general have no effect on heterozygous Gunn rats but only on homozygous (Blanc & Johnson, 1959; Johnson *et al.*, 1959; Schutta & Johnson, 1971; Rose & Wisniewski, 1979). To investigate whether sulfadimethoxine did have a detrimental effect by itself, the ABRs in 4 Wistar, i.e. wild-type, rats (Gunn, 1938) were tested before and after sulfa-injection (200mg/kg; i/p). The recording confirmed that sulfa on its own did not exert non-specific effects on auditory function of wild-type rats, as shown through ABRs (Figure 3.17) across all frequencies tested (Figure 3.17a-d). In the case of 12 kHz pure-tone responses, there seemed to have been even a little increase in amplitude of waves II and III after sulfa-treatment (Figure 3.17d).

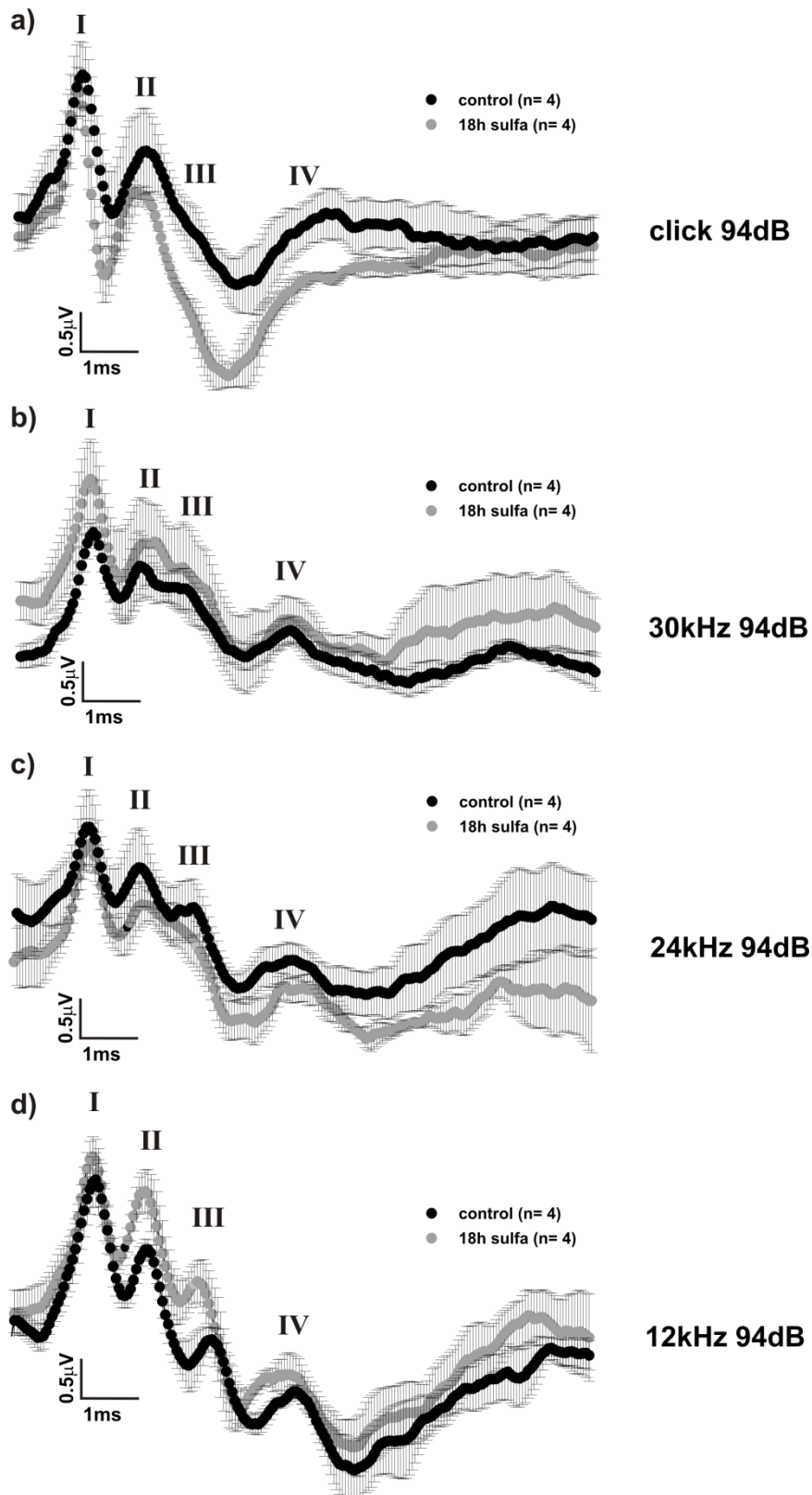


Figure 3.17 Sulfadimethoxine does not affect ABRs in Wistar rats. Wistar (wild-type) rats do not show reduction of ABRs after 18h sulfa-treatment. In 4 Wistar rats, sulfadimethoxine treatment over 18h did not reduce ABR amplitudes over a range of frequencies ('click' stimulus and 30, 24, 12kHz). Moreover, in some cases (12 kHz) is seemed to even increase amplitudes of waves II+III (d).

To quantify and summarise these findings further, the thresholds necessary to evoke ABRs at the aforementioned frequencies (Figure 3.18 & Figure 3.19) were examined. This analysis confirmed previous observations (Figure 3.16 & Figure 3.17). Thresholds in Wistar and jj-Gunn rats are initially identical (Figure 3.18a & Figure 3.19a). Sulfa-treatment had no effect on Wistar rats, but led to significantly elevated thresholds in jj-Gunn rats both for 'click' ($p \leq 0.01$, Figure 3.18b) and 12, 24, 30 kHz stimuli ($p \leq 0.001$, Figure 3.19b).

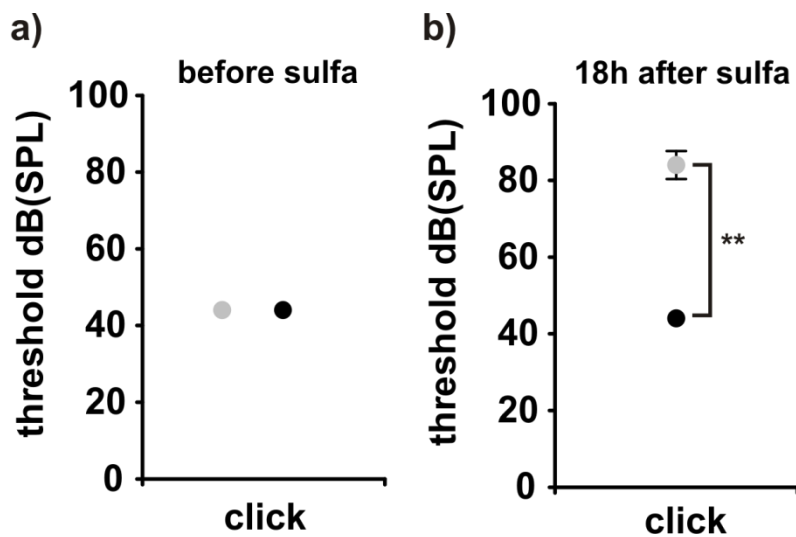


Figure 3.18 ABR thresholds following 'click' stimuli in Wistar and jj-Gunn rats before and after sulfa-treatment.

a) Both wild-type Wistar rats (black circles, $n=4$) and jj-Gunn rats (grey circles, $n=6$) have similar thresholds. b) Sulfadimethoxine (200mg/kg) does not change the ABR threshold for evoking 'click' stimuli in wild-type Wistar rat (black circles, $n=4$), but significantly elevates it in jj-Gunn rats (grey circles, $n=6$). Mann-Whitney-Rank-Sum test; **= $p \leq 0.01$

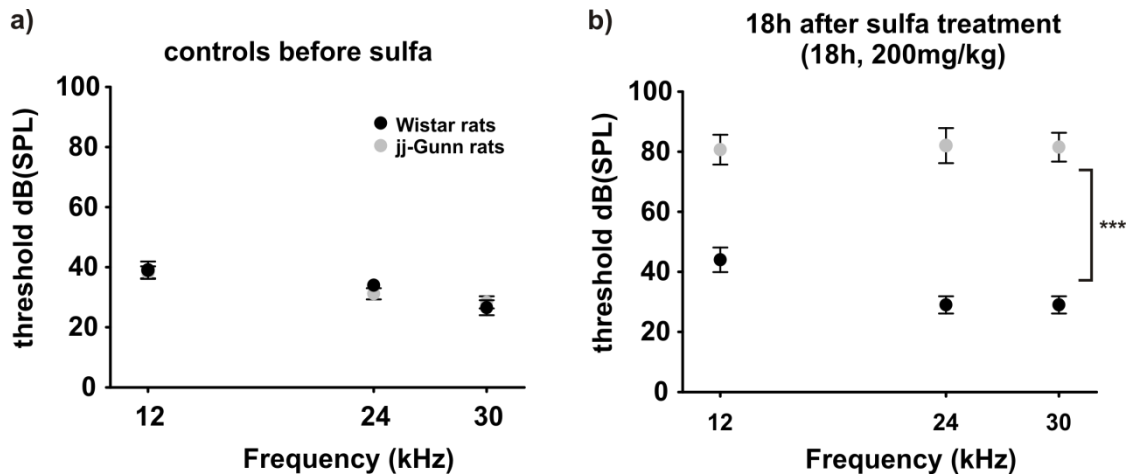


Figure 3.19 ABR thresholds following pure-tone stimuli in Wistar and jj-Gunn rats before and after sulfa-treatment.

a) Both wild-type Wistar rats (black circle, n=4) and jj-Gunn rats (grey circles, n=6) have similar thresholds at 12, 24, 30kHz. b) Sulfadimethoxine (200mg/kg) does not change the ABR threshold across all frequencies tested in wild-type Wistar rat (black circles, n=4), but significantly elevates it in jj-Gunn rats (grey circles, n=6). t-test; ***= p<0.001.

3.2.1 The effect of sulfadimethoxine on the evoked field potential in the MNTB at 32°C

With the results from ABRs (3.2) and the knowledge that perfusion of bilirubin did not provide a successful model to investigate the toxicity of bilirubin in the MNTB, the Gunn rat model was used to induce bilirubin toxicity *in vivo*.

From the ABR observations the working hypothesis was that sulfa-treatment in Wistar rats would not have an effect on the evoked MNTB response (Figure 3.20a). Indeed the C_2/C_1 ratio – a measure of how much one of the two components changes – did not show a significant difference between normal and sulfa-treated Wistar rats (Figure 3.20b). There was, rather surprisingly, a significant shortening in the synaptic delay in sulfa-treated Wistar rats (Figure 3.20c). Otherwise the typical MNTB waveform was identical in both control and sulfa-treated Wistar rats (Figure 3.20a).

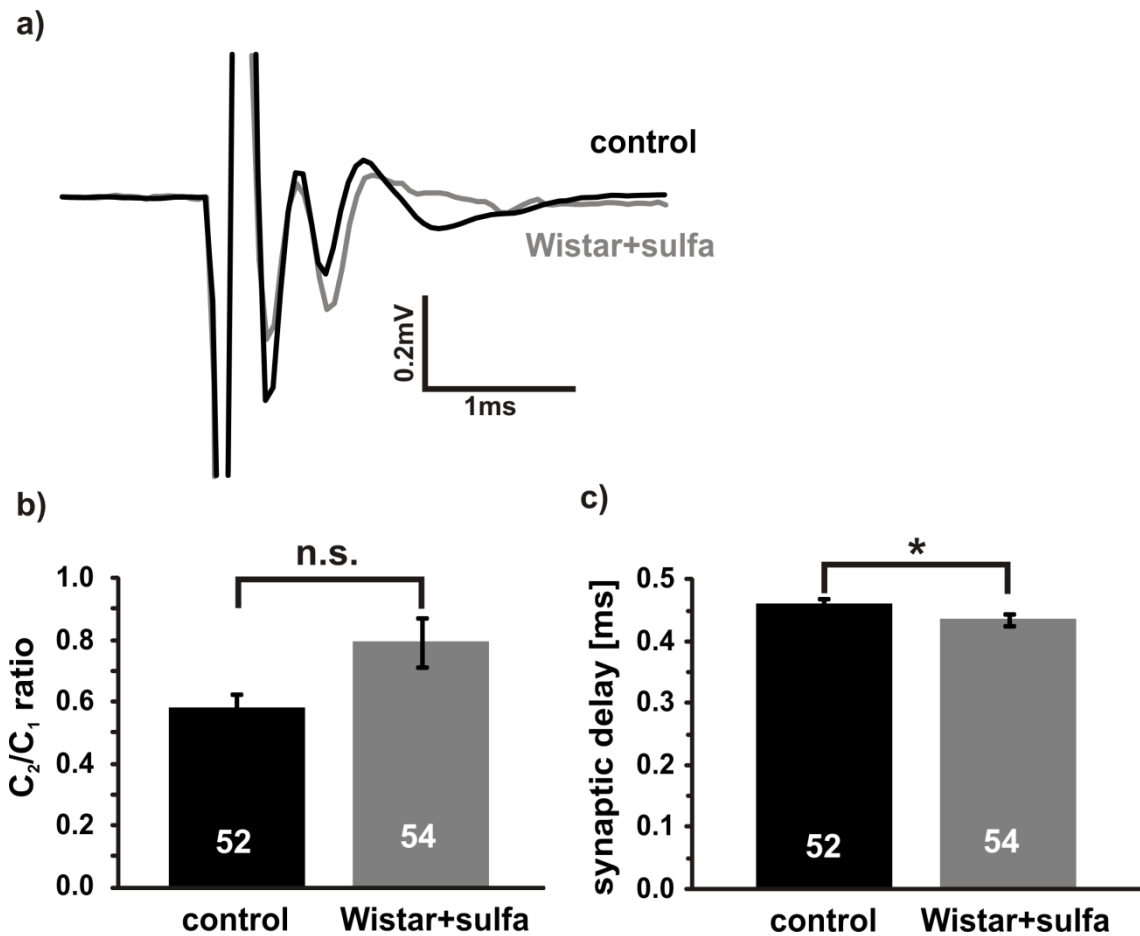


Figure 3.20 Sulfadimethoxine does not impair synaptic transmission in the MNTB of Wistar rats. Sulfadimethoxine- Na^+ salt (200mg/kg) does not significantly change C_2/C_1 ratio but improves slightly the synaptic delay in Wistar rats, indicating that sulfadimethoxine has no effect on its own on synaptic transmission in wild-type animals. Control: n=3 animals, 6 slices, 52 electrodes; Wistar+sulfa: n= 4 animals, 8 slices, 54 electrodes. t-test: synaptic delay; Mann-Whitney-Rank-Sum-test: C_2/C_1 ratio; n.s.=not significant, *= $p \leq 0.05$.

Having established the origin of the two components of the complex evoked MNTB waveform in MEA recordings and following on from the ABR experiments, brain slices were taken from 3 animals that showed reduced ABR amplitudes after 18h sulfa-treatment and recorded evoked field potentials of the MNTB using MEAs. All slices from these 3 animals and further slices from animals that had not been tested with ABRs showed increased synaptic delay (control: 0.46 ± 0.01 ms in control, n=52; treated: 1.12 ± 0.03 ms, n=55; $p < 0.001$, Mann-Whitney-Rank-Sum test) and significantly reduced or completely absent

postsynaptic component C_2 (Figure 3.21a, c, d). The increased synaptic delay is due to the appearance of the C_2 minima being significantly delayed (Figure 3.21c) while C_1 was unchanged in terms of timing (Figure 3.21c). The C_1 amplitude was not affected while the C_2 amplitude significantly decreased (control $-186.4 \pm 18.7 \mu\text{V}$ $n=52$; vs. treated $-32.1 \pm 3.2 \mu\text{V}$, $n=55$; $p < 0.001$, Mann-Whitney-Rank-Sum test) in recordings from treated animals (Figure 3.21d). This explains the decreased C_2/C_1 ratio in brain slices from treated rats (Figure 3.21b). Figure 3.21a+b have been published as part of Figure 1 in (Haustein *et al.*, 2010).

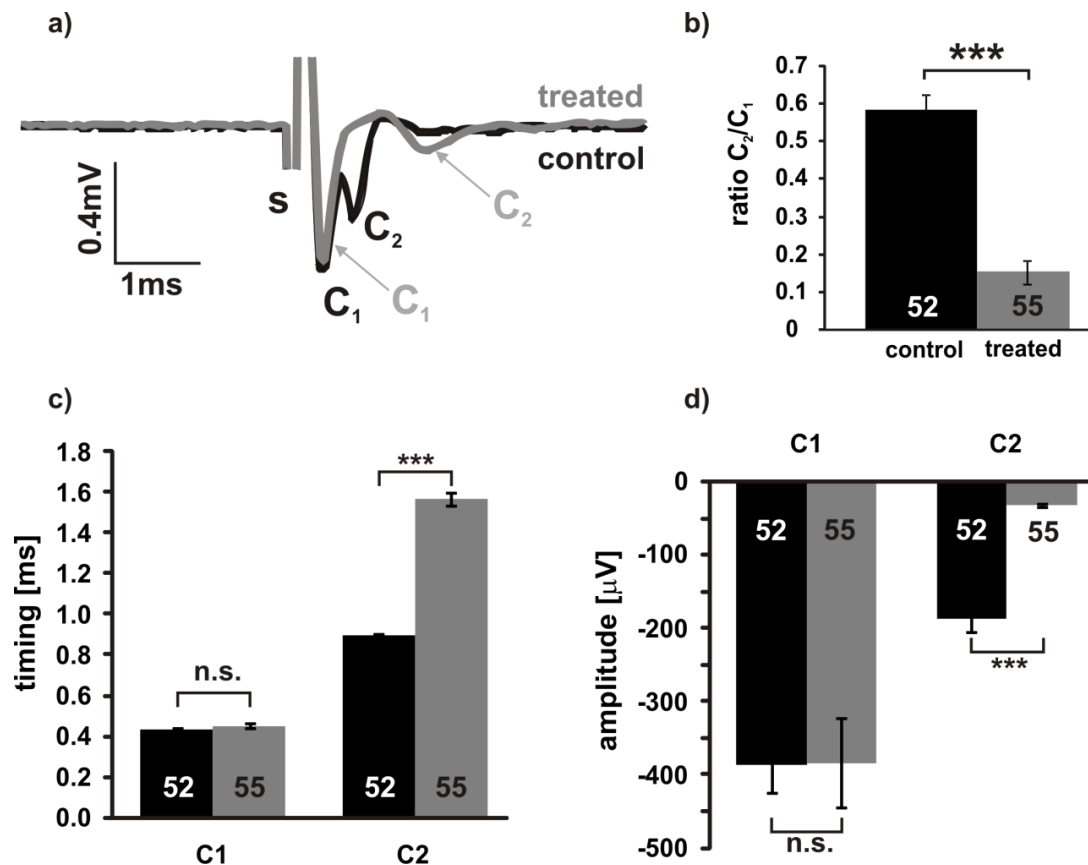


Figure 3.21 Sulfadimethoxine induced bilirubin toxicity leads to increased synaptic delay and reduction of the C_2 amplitude.

a) Example trace from a control jj-Gunn rat and from a treated jj-Gunn rat (s= clipped stimulus artefact). b) The amplitude ratio C_2/C_1 is significantly reduced in MEA recordings from treated Gunn rats. c) The time of occurrence of C_1 minima is not changed but C_2 minima occur significantly later in treated compared to control group. d) C_1 amplitude does not change between control and treated animals but C_2 is strongly reduced in treated animals. ANOVA: n.s. = not significant, ***= $p < 0.001$. control: 52electrodes/6slices/3rats; treated: 55electrodes/9slices/4rats

These findings of an underlying synaptic failure in the MNTB through *in vitro* extracellular field potential recordings in hyperbilirubinaemic jj-Gunn rats in connection with *in vivo* ABR data indicating hearing loss provide the basis for a more detailed examination of this auditory synapse in hyperbilirubinaemia on a single cell level with both electrophysiological (Chapter 4) and imaging methods (Chapter 5).

3.2.2 Summary and Conclusions:

For *in vivo* auditory brainstem responses it can be concluded that:

- Auditory brainstem responses are a reliable measure for bilirubin-induced hearing loss.
- Sulfadimethoxine has no effects on ABRs of wild-type animals, but increases bilirubin toxicity in jj-Gunn rats and leads to ABRs with decreased amplitudes and elevated thresholds.
- In experiments utilizing *in vitro* multi-electrode array recordings the following results were established: Multi-electrode array recordings can be successfully performed in the MNTB using the MED64 system.
- Pharmacological experiments reveal the typical evoked MNTB response consists of a conducted and a synaptically transmitted component which are clearly distinguishable from the stimulus artefact.
- They further demonstrate the contribution of AMPA-Rs, NMDA-Rs, K_v1s & K_v3s to the complex signal.

- MEA recordings of the MNTB are sensitive enough to show the influence of NO on synaptic transmission at this large, glutamatergic synapse.
- Stable MEA-recordings for over 4hours from brainstem-slices are possible.
- Perfusion of bilirubin is not sufficient to induce bilirubin toxicity in the acute brain slice in a reproducible manner.
- On the level of the MNTB, the hearing loss detected with ABRs is due to impaired synaptic transmission, as revealed by extracellular MED64 recordings.

The question as to whether the impaired synaptic transmission is due to failures on the pre- and/or postsynaptic site needs to be determined on a single cell level. These experiments are described in Chapters 4& 5.

4. Patch-Clamp Results

4.1 Patch-clamp recordings in the MNTB

In the previous chapter it was established that induction of bilirubin toxicity causes hearing loss and that a failure in synaptic transmission is occurring in the MNTB. The hypothesis was that a change at single-cell level had to be underlying these changes observed with ABRs and MEAs. In the next set of experiments alterations of electrophysiological properties at a single-cell level in the MNTB were investigated using patch-clamp recordings. From the ABR and MEA experiments it was expected to see changes in the MNTB but there was a need to use a more precise method to examine what led to impaired synaptic transmission. Patch-clamp recordings of MNTB neurons should help to determine if voltage-gated potassium or sodium channels were affected, if it was a block of AMPA or NMDA receptors or perhaps an impaired transmitter release at the presynaptic terminal that caused the impaired synaptic transmission. The MNTB has already been introduced in detail in chapter 1 and the patch-clamp methods used here in chapter 2. Data will be shown from combined single-cell extra-and-intracellular recordings of the AVCN, in which the somata of the bushy neurons reside that give rise to the calyces of Held. This set of experiments was part of a collaboration with the RübSamen lab in Leipzig, Germany in order to relate waveforms from *in vivo* recordings in the AVCN to waveforms obtained *in vitro* and to clarify the origin of the different components.

4.1.1 Synaptic Stimulation

From previous observations (chapter 3) the working hypothesis was that bilirubin affects synaptic transmission on a single cell level, as derived from MEA data on field potentials.

To test this hypothesis, a bipolar platinum electrode was placed at the midline of the brain slice to stimulate the synaptic inputs to the MNTB principal neurons whilst at the same time recording the synaptic responses in whole-cell mode.

The results (displayed in Figure 4.1) confirmed the finding of MEA experiments: a failure in synaptic transmission. As the whole-cell patch clamp recordings allowed more precision than the MEA, it was established that after exposure to bilirubin (i.e. sulfa-treatment), no synaptic responses driven by calyceal inputs could be evoked in postsynaptic neurons of jj-Gunn rats (Figure 4.1a, grey trace). Calyceal EPSCs (Figure 4.1a, black trace) can normally be evoked with relatively low voltage stimuli (<6V) and generate a precisely timed EPSC of a few nA amplitude (Hamann *et al.*, 2003), (Figure 4.1a, black trace & Figure 4.1b, grey area). While in control animals nearly two-thirds (9/15) but not all synaptically evoked PSCs could be classified as calyceal or low-threshold-high amplitude (Figure 4.1b), not a single giant calyceal EPSC was observed in brain slices from treated animals. Instead, small amplitude-high threshold EPSCs responses were evoked via synaptic stimulation (Figure 4.1b). Figure 4.1 was published as part of Figure 2 in (Haustein *et al.*, 2010).

Although in all animals there would be some response to midline stimulation, it is not a typical calyceal response in the cases of treated jj-Gunn rats.

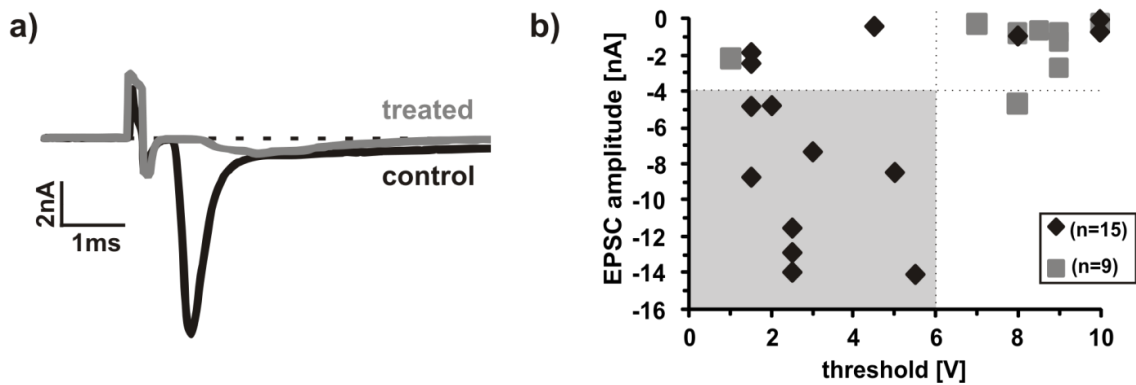


Figure 4.1 The giant calyceal EPSC is compromised in principal MNTB neurons from treated rats. a) Under voltage clamp MNTB neurons normally receive a large calyceal EPSC (black trace) but only small slow EPSCs are present following bilirubin toxicity after sulfa-treatment (grey). b) A plot of EPSC amplitude against threshold stimulus intensity shows that control calyceal EPSCs were low threshold and large amplitude (grey highlighted area), whereas the EPSCs from treated animals were small amplitude and high threshold. black diamonds= untreated, grey squares= treated.

4.1.2 Voltage-Clamp

The absent postsynaptic component in MEA recordings and the failure to evoke calyceal EPSCs in treated neurons led to the hypothesis that this was due to the fact that bilirubin impairs postsynaptic excitability. A postsynaptic site of action was proposed as previous *in vitro* studies had shown extensive cell damage in Purkinje cells of cerebellum (Schutta & Johnson, 1967; Sawasaki *et al.*, 1976; Fukuhara & Yamada, 1981; Takagishi & Yamamura, 1989; Conlee & Shapiro, 1997), CN and MNTB of Gunn rats (Jew & Williams, 1977; Jew & Sandquist, 1979; Conlee & Shapiro, 1991; Shapiro & Conlee, 1991) and CN and basal ganglia of humans (Dublin, 1951, 1974; Perlman *et al.*, 1997).

Using voltage-clamp recordings from principal MNTB neurons it was tested if the potassium currents or sodium currents were affected in treated animals. The outward potassium currents following a step-protocol were very similar in control and treated rats (Figure 4.2a). The current-voltage relationships were

almost identical in neurons from treated and control groups (Figure 4.2b). No difference was observed between MNTB neurons from control and treated animals with respect to inward sodium currents (control: 13 ± 1 nA, $n=9$ vs. treated: 12 ± 1 nA, $n=18$; at -100 mV) or outward potassium currents (Figure 4.2). This demonstrated that bilirubin did not affect sodium or potassium currents of the MNTB neurons. Figure 4.2 was published as part of Figure 2 in (Haustein *et al.*, 2010).

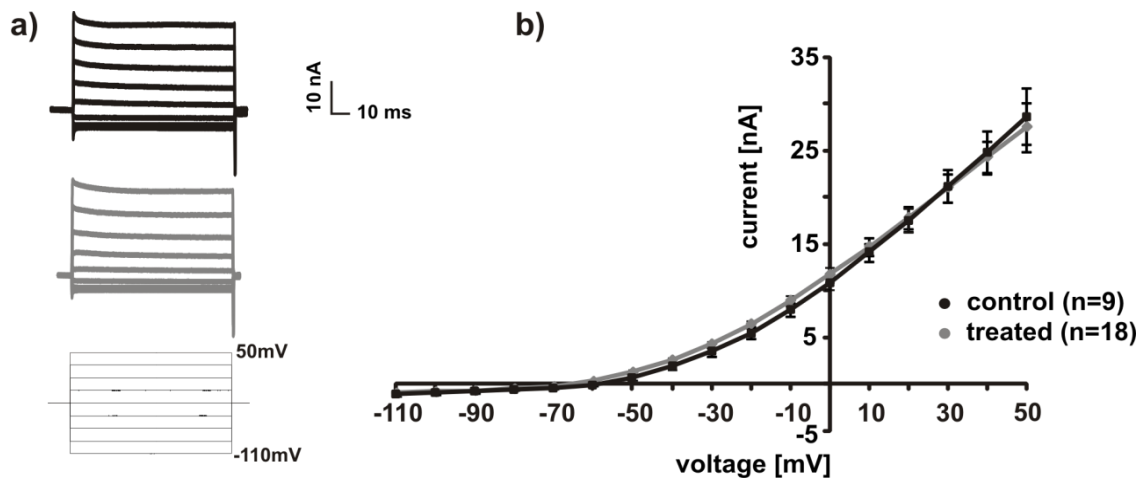


Figure 4.2 Current-Voltage relationships in control and treated neurons show no effect of high bilirubin levels on potassium channels.

a) Example traces of a control MNTB neuron (black) and a MNTB neuron from a treated Gunn rat (grey) following a voltage-step protocol (below). b) Summary plot of I-V-curves from control (9 neurons) and treated (18neurons) animal are nearly identical. Data points are means \pm SEM for control and treated condition.

4.1.3 Current-Clamp

In current-clamp configuration properties of the action potential waveform were investigated for any compromise that would account for the failure in synaptic transmission in treated rats.

Action potential waveforms from control and treated rats were very similar (Figure 4.3a). There was a slight increase in AP amplitude ($p=0.014$, Mann-Whitney-Rank-Sum test; Figure 4.3d) in treated ($70.3\pm 1.4\text{mV}$) compared to control neurons ($64.1\pm 2.6\text{mV}$). The AP halfwidth (control: $0.30\pm 0.01\text{ms}$ vs. $0.37\pm 0.05\text{ms}$ treated, $p=0.423$, Mann-Whitney-Rank-Sum test) was not statistically significantly different between the two groups (Figure 4.3b). Figure 4.3a, b+d was published as part of Figure 2 in (Haustein *et al.*, 2010).

The action potential thresholds in current-clamp were $388.9\pm 44\text{pA}$ (18 cells/7 animals) and $519.2\pm 48\text{pA}$ (26 cells/10 animals) for treated and control group, respectively (Figure 4.3c). The difference between the two groups was not statistically significant ($p=0.066$, Mann-Whitney-Rank-Sum test), although there seems to be a tendency towards lower AP thresholds in treated animals.

Thus far, there was no effect of bilirubin on the postsynaptic cells. There was however, the possibility that bilirubin might affect AMPA or NMDA receptors and so cause failures in synaptic transmission. However, a paper published by David Attwell's group did not find evidence for bilirubin influencing AMPA-Rs or NMDA-Rs or glutamate transporters (Warr *et al.*, 2000). Therefore the decision was made not to test this again in the Gunn rat MNTB but focus instead on other experiments.

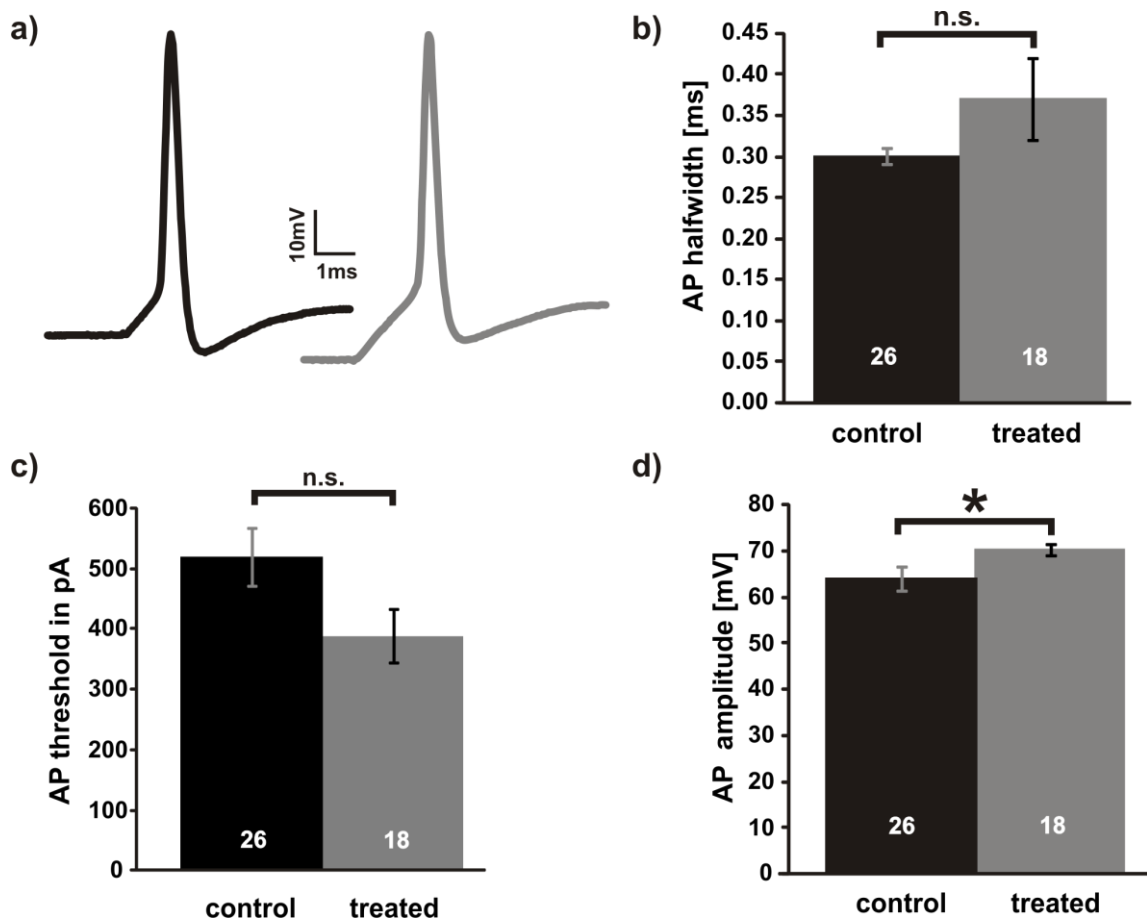


Figure 4.3 Hyperbilirubinaemia does not change action potential properties.

a) Postsynaptic MNTB neuron excitability was unchanged by high bilirubin concentrations, as seen in the similar AP waveforms. b) No significant differences in AP halfwidth between the 2 groups was found c) d) Summary bar graphs show slightly elevated AP amplitude in treated MNTB neurons. control: 26cells, 10 rats, treated: 18cells, 7rats; All values are mean±SEM; Mann-Whitney-Rank-Sum test, n.s. = not significant, * = p<0.05

In summary, no change in postsynaptic principal neurons after short-term exposure to bilirubin *in vivo* was observed that could explain the synaptic failures observed in the MEA and whole-cell patch clamp experiments with synaptic stimulation.

4.1.4 Miniature EPSCs

Another hypothesis was that bilirubin impairs the spontaneous transmitter release from the presynaptic calyx of Held, as measured by miniature EPSCs (Figure 4.4), and thereby influences synaptic transmission at this synapse.

Recordings from control (Figure 4.4a) and treated animals (Figure 4.4b) appeared to be very similar and statistical analysis of mEPSCs showed no significant change in either amplitude (Figure 4.5a), frequency (Figure 4.5b), decay tau (Figure 4.5c) or rise-time of miniature EPSCs (Figure 4.5d) between the control and treated group. It seems that bilirubin does not influence transmitter release from the presynaptic site at this acute stage in hyperbilirubinaemia.

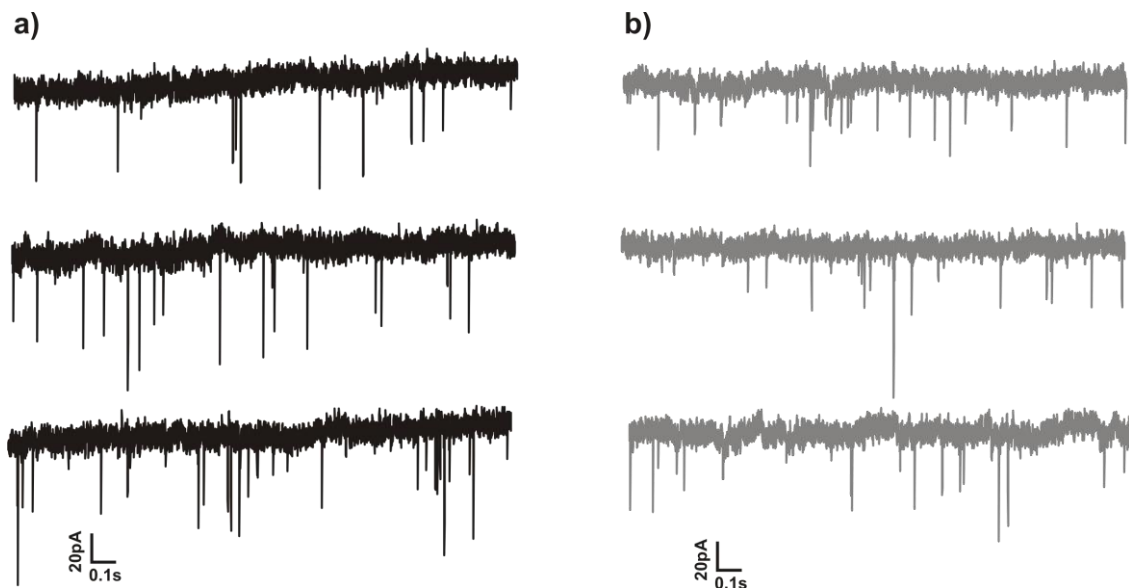


Figure 4.4 Miniature EPSCs are not changed by hyperbilirubinaemia. Example traces of miniature EPSCs from control (black traces, a) and treated rats (grey traces, b) appear very similar. The holding potential was -60mV.

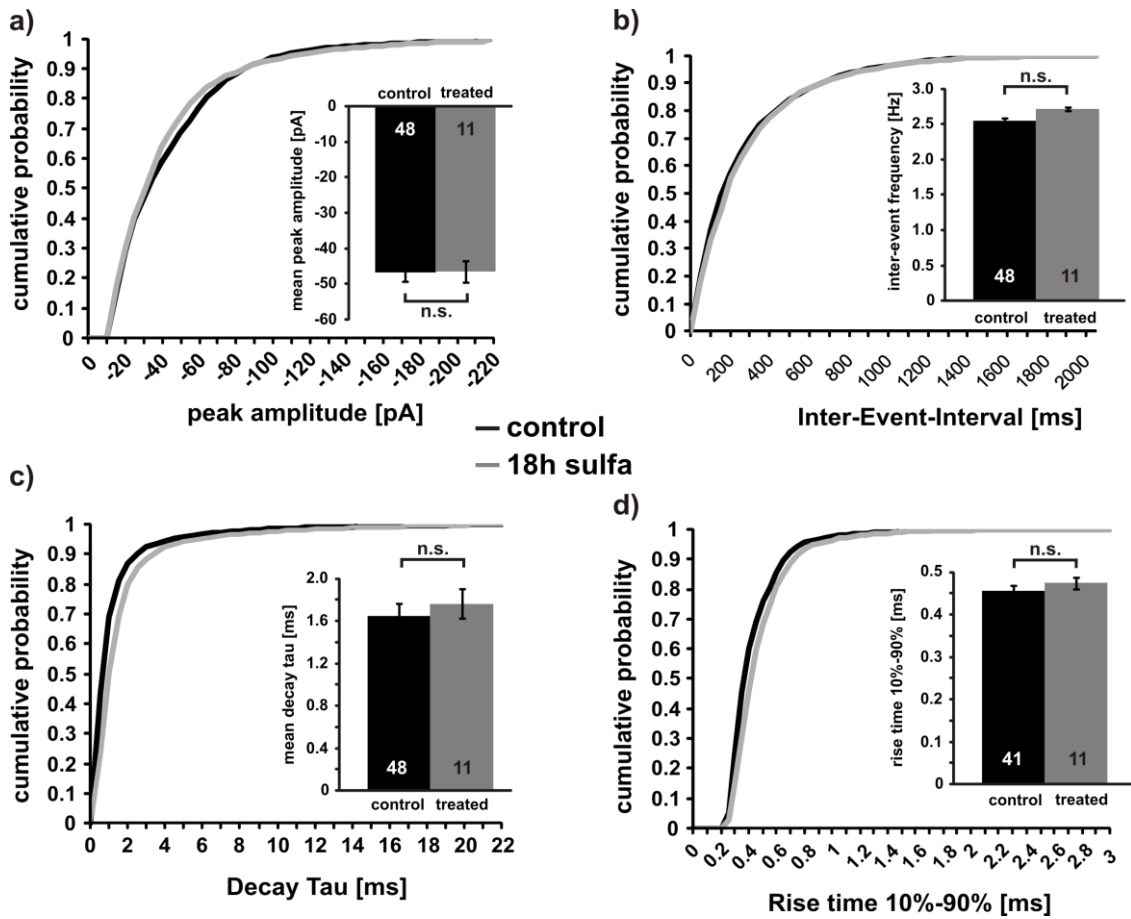


Figure 4.5 Hyperbilirubinaemia does not cause significant changes in the properties of miniature EPSCs.

No significant changes were found in the properties of miniature EPSCs between MNTB neurons from control and treated group. Summary plots for Miniature EPSC analysis show no differences in: a) peak mEPSC amplitude; b) inter-event-interval between mEPSCs; c) decay tau of mEPSCs; d) mEPSC rise time. Kolmogorov-Smirnov-Test, n.s.= not significant; control: n=48 cells/11 animals; treated: n= 11 cells/5 animals.

4.2 Patch-Clamp recordings in the AVCN

A collaboration project with Marei Typlt from Rudolf Rübtsamen lab at University of Leipzig, Leipzig, Germany, set out to determine the origin of individual components of intra- and extracellular recordings of spherical bushy neurons *in vitro* and relate them to *in vivo* recordings from endbulb of Held/spherical bushy neuron (SBC) synapses.

The signals of simultaneous extra-and intracellular patch-clamp recordings in the AVCN brain slice could be linked to help interpret data from *in vivo* and MEA experiments and the results have been published in (Typlt *et al.*, 2010). Figure 4.6 shows a current-clamp recording from a typical AVCN bushy neuron with the typical sag at negative current injections and single AP to large positive current injections.

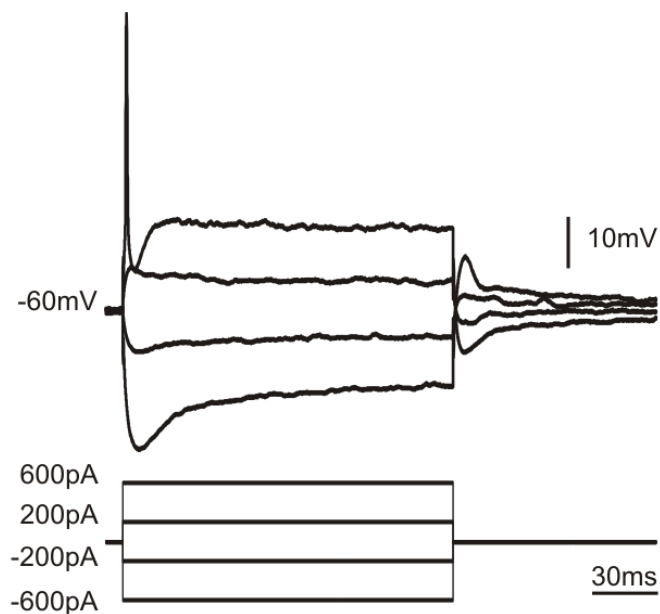


Figure 4.6 Current-clamp recording of a AVCN bushy neuron. Current-clamp protocol of a typical bushy cell of the AVCN shows the well-known sag at negative current injections. On top is the example trace of a recorded bushy cell from a Wistar rat. Below is the current clamp protocol used for this recording. Figure adapted from Typlt *et al.*, 2010.

This was used to ensure that the recording was made from the correct cell type, as bushy cells display at hyperpolarising currents a characteristic ‘sag’ and single action potential at depolarising currents (Cao *et al.*, 2007; Milenkovic *et al.*, 2009)

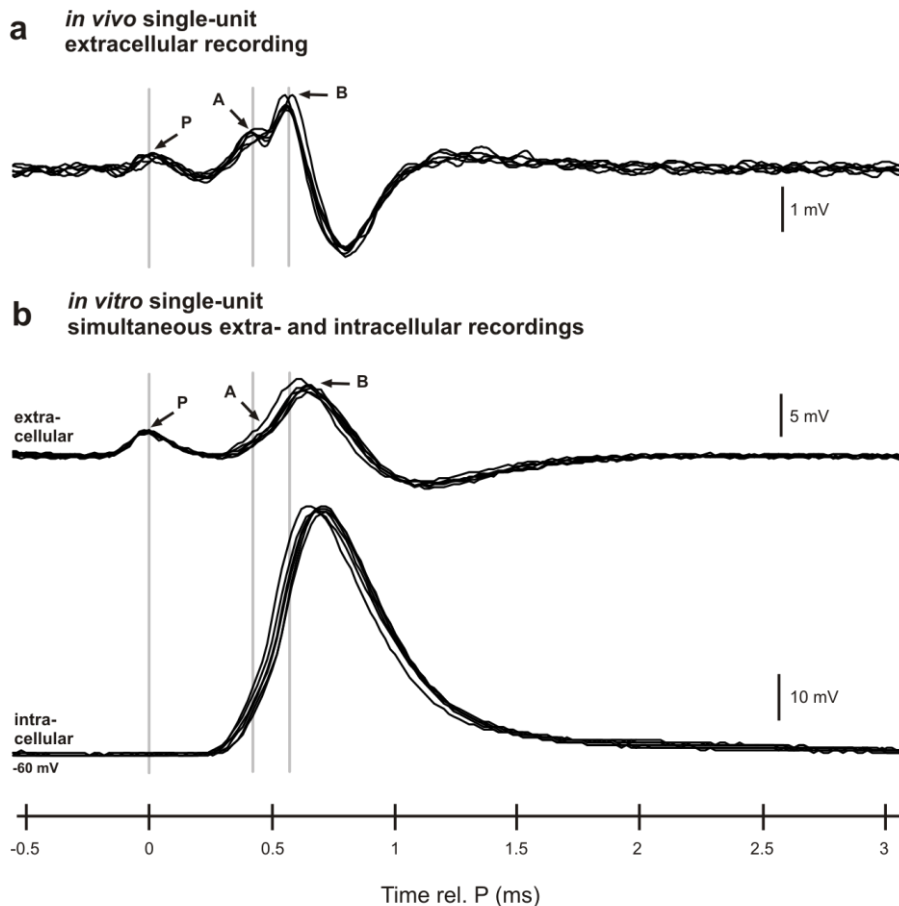


Figure 4.7 Comparison of *in vivo* and *in vitro* single-unit recordings from the AVCN. Individual components of the complex waveforms from single-cell recordings *in vivo* and *in vitro* show the same time-course. a) Overlay of 5 traces of a single-unit SBC recording from Gerbil *in vivo* shows components P, A and B. b) Simultaneous extra- (top) and intracellular (bottom) whole-cell recording from a AVCN bushy neuron in the Wistar rat brain slice at physiological temperature show all three components with a similar time-course to *in vivo*. The intracellular AP coincides with the extracellular A-B components, indicating that they are both of postsynaptic origin. Traces have been aligned relative to the P-component. Figure adapted from Typlt *et al.*, 2010.

In extracellular *in vivo* recordings from bushy cells of the AVCN (Figure 4.7a) it is possible to record a complex signal comprised of either three (P, A, B) (Pfeiffer, 1966a) or two components (P, A). The fact that not all components

can be recorded at all times has lead to different theories about their origin (Typlt *et al.*, 2010). The working hypothesis was that P is the presynaptic AP, A is the postsynaptic EPSP and B is the postsynaptic AP. The reason for not always seeing the B component in *in vivo* recordings would be the failure of the EPSP to trigger an AP. To establish for certain which component reflects what kind of activity is important for interpreting the data and linking it to *in vitro* recordings. To clarify the origin of the 3 possible components combined intra- and extracellular recordings were performed *in vitro* while synaptically stimulating the inputs to the bushy cells. This experiment was carried out in the brain slice because it is much easier than it is *in vivo* to use pharmacological means, i.e. antagonists for the component characterisation. Depending on the place of the extracellular electrode, it was possible to pick up all 3 components (Figure 4.7b and Figure 4.8a upper trace) *in vitro*. However, this was not always the case (Figure 4.8b upper trace). The P-component is by definition not detectable in the corresponding intracellular recordings from the postsynaptic neuron (Figure 4.8a lower trace). If an AP is triggered, it will mask the EPSP so there is only 1 component visible. The fact that components A and B were sensitive to glutamate receptor antagonist kynurenic acid (5mM, Figure 4.8a & b, middle panel) confirmed that they were of postsynaptic origin, whereas P was presynaptic and therefore not affected by kynurenic acid (Figure 4.8a & b). Figure 4.8c shows the summary of 6 cells for parameters such as rise time or amplitude for EPSPs (A-component) and APs (B-component) before, during and after application of kynurenic acid. It confirmed the postsynaptic origin of components A and B that the examples of 2 individual cells (Figure 4.8a & b) already showed. Taken together, the experiment demonstrated that the working

hypothesis (P = presynaptic AP, A = postsynaptic EPSP, B = postsynaptic AP) was correct. This allows now to better interpret *in vivo* recordings from the SBCs of the AVCN.

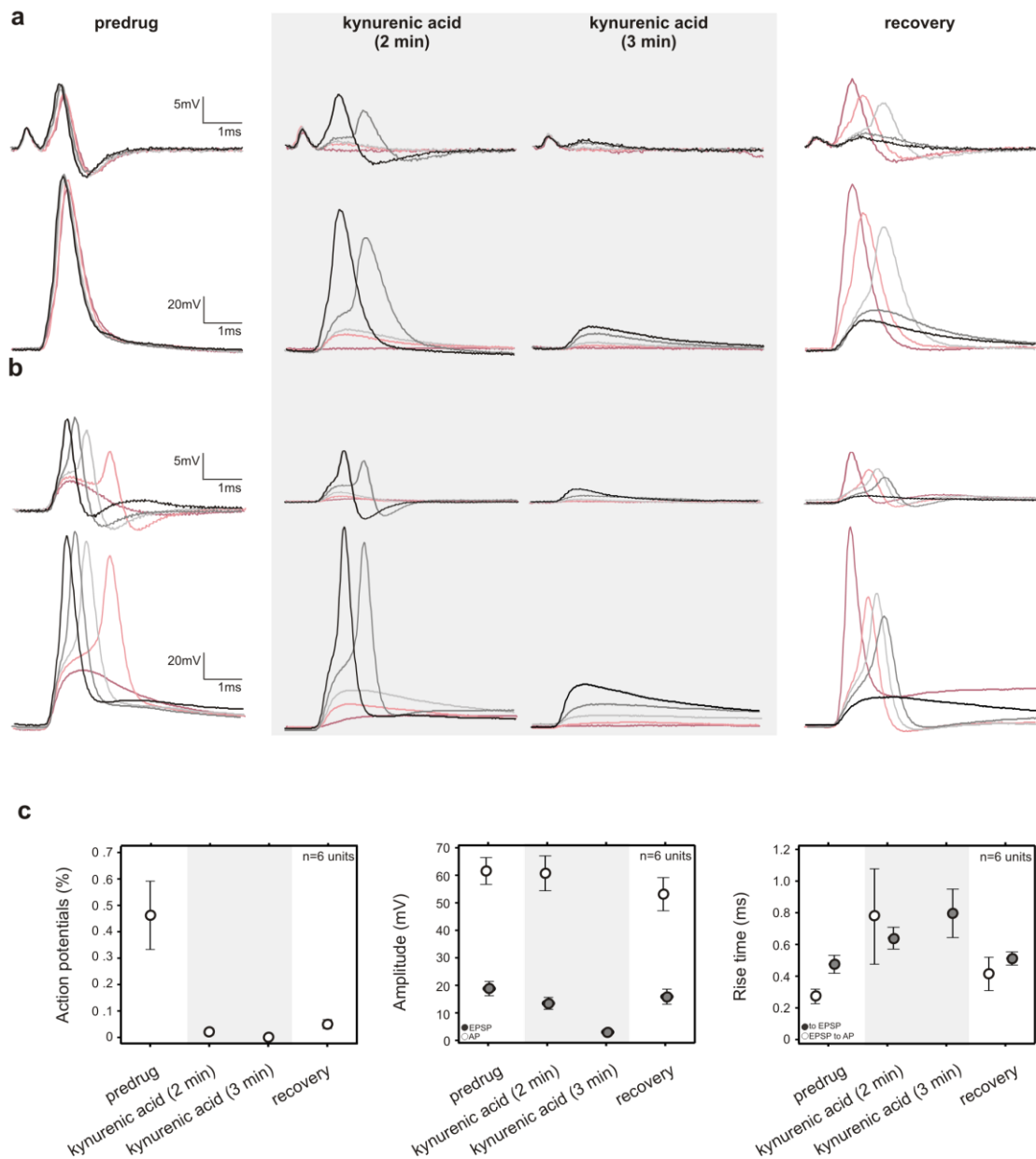


Figure 4.8 Pharmacology reveals pre- and postsynaptic origin of components in combined intra- and extracellular recordings.

Simultaneous intra- and extracellular recordings show that P-component is presynaptic EPSC which is not affected by GluR-antagonist kynurenic acid (5mM), while A+B-component are sensitive to kynurenic acid, hence the postsynaptic action potential. Upper trace: extracellular recording, lower trace intracellular recording. b) Not all cells show the pre-potential (P-component). Upper trace: extracellular recording, lower trace intracellular recording. c) Summary plot to distinguish between EPSPs and APs before, during and after Glu-R antagonist kynurenic acid. Figure from Typlt et al, 2010.

4.2.1 Summary and Conclusions:

Bilirubin distorts synaptic transmission without significantly affecting the postsynaptic site. In the light of existing literature this is a surprising finding which will be discussed in detail in Chapter 8. It also implies that bilirubin acts presynaptically and not postsynaptically. The experiments investigating the likely effects on the presynaptic site in the MNTB are described in chapter 5.

For the AVCN recordings it could be shown that the P-component reflects presynaptic action potential, component A the postsynaptic EPSP and component B the postsynaptic AP of the spherical bushy cells. These results have been published and the characterisation of the bushy cell neurons, which give rise to the calyces of Held, could become useful if the project gets extended to investigate acute effects of bilirubin on the AVCN. Even though time-constraints did not allow the extension of the research to investigate potential toxic effects of bilirubin on synaptic transmission in the VCN of jj-Gunn rats, this study was the initial stage of that investigation. The next chapter will – in addition to EM data from the MNTB and cerebellum- also present some EM data for the VCN from treated jj-Gunn rats. This data could indicate a potential direction for future experiments.

5. Results from Imaging, Light and Electron Microscopy

In the previous two chapters it was shown that bilirubin-toxicity led to hearing loss, indicated by decreased ABR and elevated ABR thresholds. It was established that in the MNTB impaired synaptic transmission was a consequence of bilirubin-toxicity and patch-clamp recordings demonstrated that the postsynaptic neurons were unaffected. With the methods used we could not yet be certain whether or not the site of action was pre- or postsynaptic or both, although the results suggested a predominantly presynaptic failure. To answer this question a number of techniques were used including: calcium-imaging of postsynaptic neurons to determine basal calcium levels, anterograde labelling of calyceal terminals to reveal possible structural changes and light and electron microscopy to investigate potential signs of neurodegeneration pre- and postsynaptically, not only in the MNTB, but also in the cerebellum and the VCN.

5.1 Calcium-Imaging

After no differences were found in the electrophysiological properties of the postsynaptic MNTB principal neurons (see chapter 4), the next step was to test for potential differences in resting intracellular calcium concentrations $[Ca^{2+}]_i$. The idea was that bilirubin might lead to toxically high calcium concentrations in the postsynaptic neuron, potentially involving NMDA receptors. Principal neurons were loaded with the ratiometric calcium indicator Fura-2 AM and the

fluorescence intensity was measured at 340nm & 380nm. An example image at 380nm excitation wavelength is shown in Figure 5.1a. Intracellular calcium concentrations $[Ca^{2+}]_i$ were calculated from Fura-2 fluorescence intensity at 340nm and 380nm (Figure 5.1a) as described in Material & Methods using the equation by (Grynkiewicz *et al.*, 1985). While there was a difference between heterozygous and homozygous Gunn rats in intracellular calcium concentration $[Ca^{2+}]_i$ (236.4 ± 12.8 nM vs. 110.8 ± 6.5 nM, $p \leq 0.001$; Figure 5.1b) there was no significant difference between control and treated jj-Gunn rats (110.8 ± 6.5 nM vs. 111.3 ± 10 nM, $p = 0.649$; Figure 5.1b).

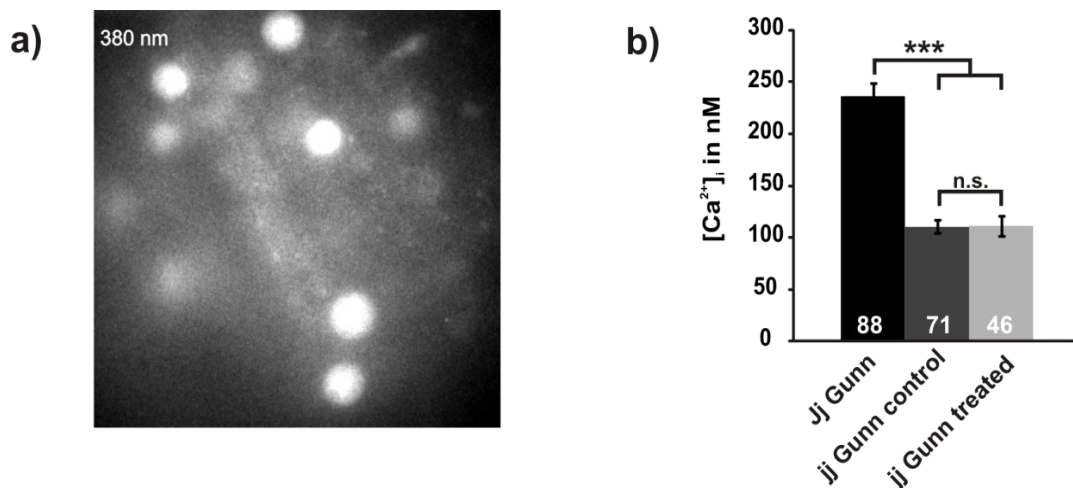


Figure 5.1 Bilirubin does not change intracellular calcium concentrations. Bilirubin does not raise basal $[Ca^{2+}]_i$ in MNTB principal neurons of Gunn rats as shown with calcium-imaging. a) A typical image of MNTB principal neurons loaded with ratiometric calcium indicator Fura-2-AM and excited with light at 380nm wavelength. b) Summary bar graph showing the calculated intracellular resting calcium concentration in MNTB principal neurons. While heterozygous Gunn rats have a significantly higher $[Ca^{2+}]_i$ there is no difference between principal neurons from treated and control homozygous Gunn rats. All values are displayed as mean \pm SEM. ANOVA on ranks, n.s.= not significant, *** ≤ 0.001 . The number of cells tested is indicated in the respective box.

This result shows that for $[Ca^{2+}]_i$ there are differences between Jj and jj Gunn rats. Interestingly $[Ca^{2+}]_i$ did not change any further in treated jj Gunn rats, that is, bilirubin-toxicity did not influence $[Ca^{2+}]_i$ in MNTB principal neurons at this acute stage of hyperbilirubinaemia. However, considering the patch-clamp

results, especially that there was no difference in the I-V-curves between control and treated rats, the difference in $[Ca^{2+}]_i$ between Jj and jj-Gunn rats cannot explain the differences in synaptic transmission between the control and treated group.

5.2 Anterograde dextran-labelling of calyces of Held

There was no difference in the properties of MNTB principal neurons that could account for the dramatic impairment in synaptic transmission in treated jj-Gunn rats. It therefore became necessary to investigate the presynaptic terminal. It is apparently not trivial but rather technically demanding to do patch-clamp recordings from the calyx of Held (personal communication with Ian D. Forsythe) though it is possible (Forsythe, 1994; Borst *et al.*, 1995). For this reason it was decided to make use of the new multi-photon laser microscope. This allows imaging of fluorescent dyes in tissue depths not reachable by conventional confocal microscopy. The new approach was to label the calyces of Held with dextran-tetramethyl-rhodamine (MW 3000) to investigate any morphological changes which might explain the loss in synaptic transmission 18h after induction of bilirubin toxicity. In the case that there would be no visible difference, calyceal patch-clamp recordings would be the next step. Calyces were successfully labelled in living brain slices from control jj-Gunn rats (Figure 5.2a+b); their morphology was identical with images made from Dil and Lucifer Yellow labelled calyces (Forsythe, 1994). In this current preparation, axons are usually well labelled in control and treated animals (Figure 5.2a, b, e, f); the

ones giving rise to the calyx as well as axons not terminating in the MNTB. In contrast to the control rats, no healthy calyces were found in treated rats. The area of the MNTB was marked by huge amounts of debris where calyces would have been expected (Figure 5.2d, e). Occasionally, structures that resembled calyceal remnants were found (Figure 5.2e, f, marked with asterisk). These calyceal remnants were used for analysis. As seen in Figure 5.2c there is a significant reduction in surface area in the calyceal remnants ($1117 \pm 318 \mu\text{m}^2$, $n=13$, $p \leq 0.001$) compared to healthy calyces ($2334 \pm 301 \mu\text{m}^2$, $n=20$). The smaller number of calyceal remnants compared to healthy calyces is due to the fact that only structures that roughly resembled a calyx were chosen for analysis. It was very difficult to find these remnants whereas labelled healthy calyces were there in abundance. The difficulty to ascertain the origin of structures resembling damaged calyces lead to the exclusion of a number of damaged structures which could have potentially been presynaptic terminals and biased us towards partially intact terminals. This will have led to an overestimation of the mean surface area for calyceal remnants.

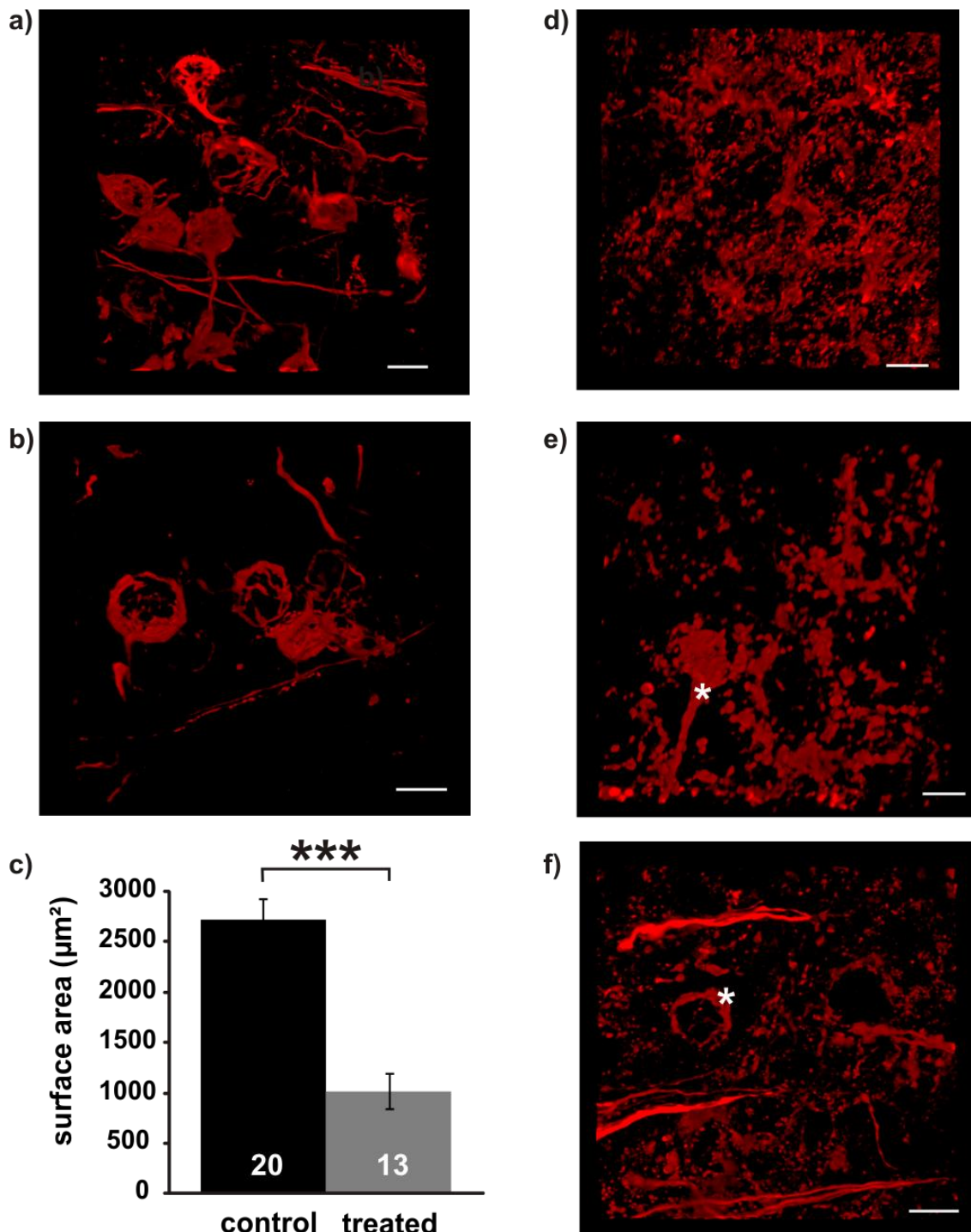


Figure 5.2 Multiphoton imaging reveals presynaptic degeneration in treated Gunn rats. Multiphoton imaging of calyces of Held in live tissue shows healthy calyces in control animals but in treated animals calyces are completely absent or severely damaged. a)+b) Examples of calyces labelled with Dextran-Tetramethyl-Rhodamine (MW 3000) from a control rat (P14, jj-Gunn) show clearly labelled calyces and axons passing by. c) Summary plot showing that the surface area of calyces or calyceal remnants (treated group) is significantly reduced in treated compared to control rats. d)-f) 18h after sulfa-treatment no healthy calyces could be found, but instead a lot of debris (d) and occasionally structures that were identified as calyceal remnants (*: e+f). Note that axons are still clearly labelled (f), indicating normal transport of the dye from the AVCN into the MNTB. All values are displayed as mean \pm SEM; Mann-Whitney-Rank-Sum test, ***=p \leq 0.001; Scale bars: 20 μm

5.3 Light and Electron Microscopy

Parallel to the dextran-labelling experiments, the brains of control and treated rats were perfusion-fixed and prepared for electron microscopy (EM) to investigate possible changes at the pre- and/or postsynaptic site. In the process of preparing the samples for the electron microscopy, semi-thin fixed brain slices are cut, stained with toluidine blue and examined before the exact area of interest for EM is selected. This way, gross changes which are already visible at light microscopic (LM) level can be detected earlier and the affected areas can be selected for a more detailed examination at EM level.

5.3.1 *Cerebellum*

It is a well established fact that, besides the brainstem and the basal ganglia, the cerebellum is one of the main affected areas in kernicterus (Blanc & Johnson, 1959; Rose & Wisniewski, 1979; Ahdab-Barmada & Moossy, 1984). A lot of work has already been done on the cerebellum in hyperbilirubinaemia. The reason for looking at the cerebellum again was to confirm previous findings and thereby confirming our animal model. For this reason, the data of the cerebellum was not quantified and statistically analysed; the focus of this thesis remains the auditory brainstem. The light microscopic images from the cerebellum showed granular bodies within the Purkinje cells of control and treated Gunn rats. At 10x magnification the Purkinje cells (PCs) appeared similar in control (Figure 5.3a) compared to treated jj-Gunn rats (Figure 5.3b). At 40x magnification, it became evident that only PCs and not granular cells

were affected in both groups (Figure 5.3c+d). At 100x magnification, it could be seen that membranous cytoplasmic bodies (MCBs) would normally accumulate at one end of the soma and not be randomly distributed through the cytoplasm (Figure 5.3e+f). It should be noted that in LM images of Wistar (Figure 5.3g) and Jj-Gunn rats (Figure 5.3h) PCs or other cells of the cerebellum did not show any changes. The result that numerous PCs in jj-Gunn rats – and nearly all neurons in the substantia nigra (Batty & Millhouse, 1976) – had MCBs was a confirmation of findings published by (Rose & Wisniewski, 1979; Fukuhara & Yamada, 1981) and a further confirmation that the right model was selected for this study. MCBs have been reported to occur in treated as well as untreated jj-Gunn rats (Rose & Wisniewski, 1979) and are seen to be a feature of this jaundice model.

Electron microscopy confirmed the light microscopic observations. In PCs of Wistar (Figure 5.4a+c) and Jj-Gunn rats, MCBs were never observed. Purkinje cells in particular and the cerebellum in general looked normal and did not show any signs of degeneration (Figure 5.4c). In treated jj-Gunn rats, EM confirmed the existence of the MCBs in the cytoplasm, with almost all PCs being affected to some degree. MCBs accumulated at one pole of the PC soma (Figure 5.4b). In the close vicinity of MCBs it was difficult to find other cell organelles (Figure 5.4d), e.g. mitochondria and endoplasmic reticulum. Despite earlier studies the origin and composition of these MCBs is still unknown.

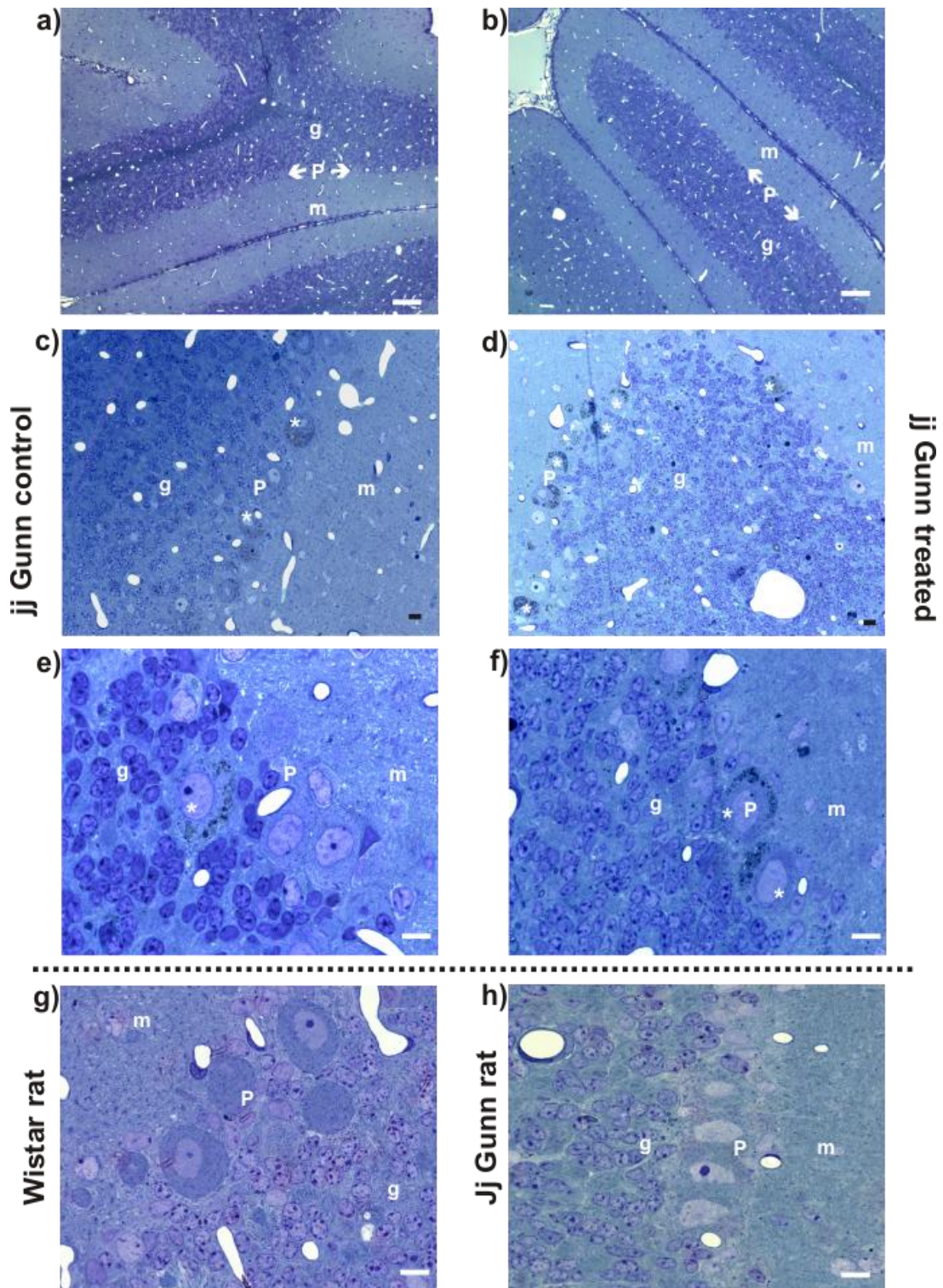


Figure 5.3 Light microscopic images from fixed cerebellar brain slices show aberrant Purkinje cells in jj-Gunn rats.

Light microscopy images from fixed cerebellar brain slices stained with toluidine-blue show aberrant Purkinje cells in control and treated jj-Gunn, but not in Jj-Gunn or Wistar rats. Note that only Purkinje cells show inclusion bodies (*); a)+b): 10x magnification of the cerebellum. c)+d): 40x magnification. Inclusion bodies (*) are visible in both control (c) and treated (d) tissue. e)+f) 100x magnification shows that only Purkinje cells have inclusion bodies (*), no other cells. g)+h) Purkinje cells in Wistar (g) and Jj-Gunn rats (h) do not show any inclusion bodies. m=molecular layer, g=granule cell layer, P= Purkinje cell layer; Scale bars: a+b= 100 μ m; c-h= 10 μ m.

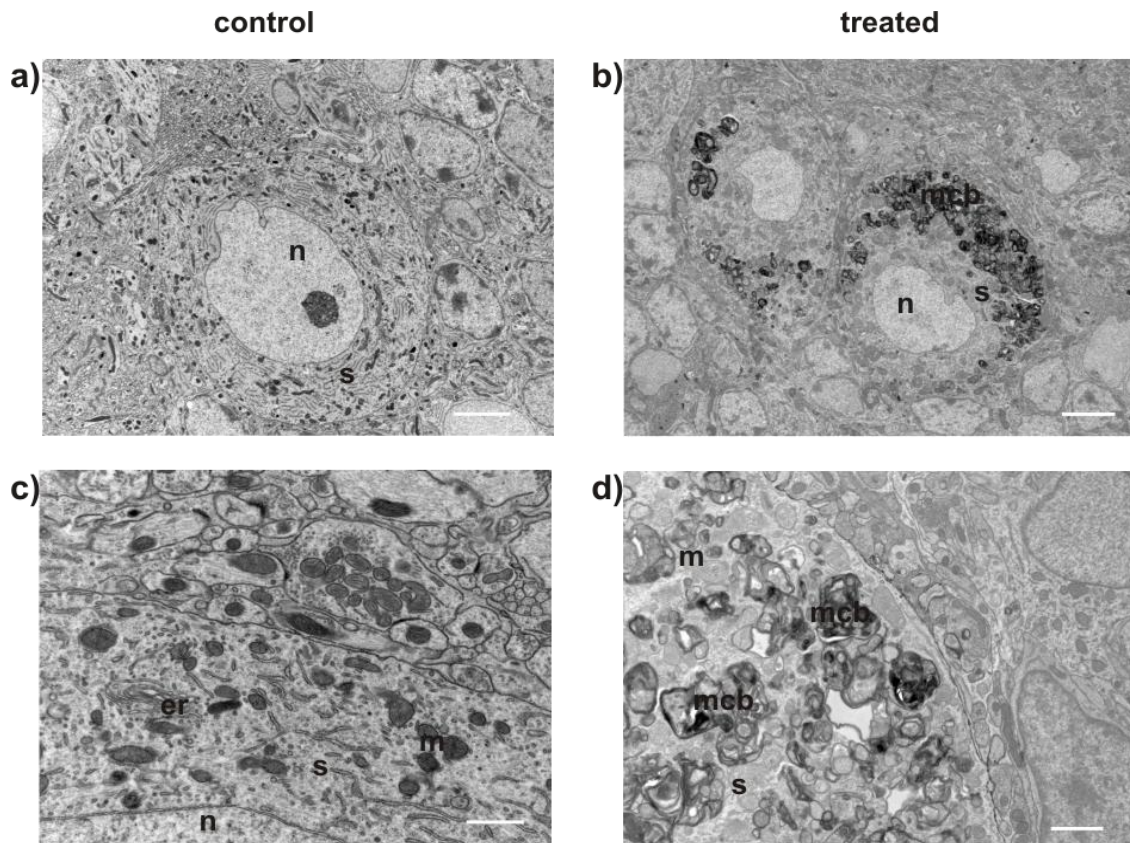


Figure 5.4 Electron microscopic images from the cerebellum of control and treated rats. Electron microscopic images from the cerebellum showing normal granular cells & Purkinje cell in control animals. In treated rats Purkinje cells had inclusion bodies, while granular cells were not affected. a) Purkinje cell from a Wistar rat with clearly distinguishable nucleus (n) and cell soma (s) next to granular cell. b) 2 Purkinje cells (from a treated jj-Gunn rat) showing membranous cytoplasmic bodies (mcb) in the soma; c) High magnification image of Purkinje cell without mcbs. Nucleus (n), soma (s) mitochondria (m) and endoplasmatic reticulum (er) can be seen. d) High magnification image of Purkinje cell soma (s) filled with mcbs. A normal mitochondrion (m) can also be seen Scale bar: a)+b)= 5 μ m; c)+d)= 2 μ m.

5.3.2 Medial Nucleus of the Trapezoid Body

Given the findings of degenerated calyces in the dextran-labelling experiments and the membraneous cytoplasmic bodies in cerebellar Purkinje neurons, the project went on to investigate any signs of degeneration at LM or EM level in the MNTB. In all the LM images analysed, it was not possible to tell the control animals (Figure 5.5a-d) from the treated ones (Figure 5.5e+f). At low magnification (Figure 5.5a, c, e) there was no sign of neurodegeneration nor at higher magnifications (100x, Figure 5.5b, d, f). Unlike in the cerebellum, there

was also no difference between jj-Gunns and Wistar or Jj-Gunn rats (Figure 5.5).

Even at EM level the MNTB did not show many differences between control and treated jj-Gunn rats. On one occasion glycogen-bodies were observed in mitochondria of principal MNTB neurons in a control jj-Gunn rat. Cell organelles, especially mitochondria did not show any signs of damage (Figure 5.6b+d). Membranous cytoplasmic bodies as seen in the cerebellum were not observed. Axonal profiles were also without signs of degeneration (Figure 5.6a+c). There were incidences where darkened presynaptic profiles in treated animals appeared (Figure 5.6c+d). This has been described for the cochlear nucleus of treated Gunn rats as a sign of neurodegeneration (Jew & Williams, 1977; Jew & Sandquist, 1979). However, the striking difference between the control (Figure 5.7a) and the treated group (Figure 5.7b) was the significantly reduced number of presynaptic profiles (control 11 ± 1 , $n = 24$; vs. treated 7 ± 1 , $n = 18$; $p \leq 0.006$; Figure 5.7b+d) and the length of their apposition at the postsynaptic neuron (control $23 \pm 2 \mu\text{m}$, vs. treated $14 \pm 2 \mu\text{m}$; $p \leq 0.006$; Figure 5.7c) in the treated group. This confirmed the results from the dextran-labelling experiments and also showed that the degeneration at this acute stage was only presynaptic with the postsynaptic MNTB principal neurons not being affected. The integrity of the postsynaptic MNTB neurons seen in the EM images confirmed the findings of patch-clamp and calcium-imaging experiments. Parts of Figure 5.7 have been published as part of Figure 3 in (Haustein *et al.*, 2010).

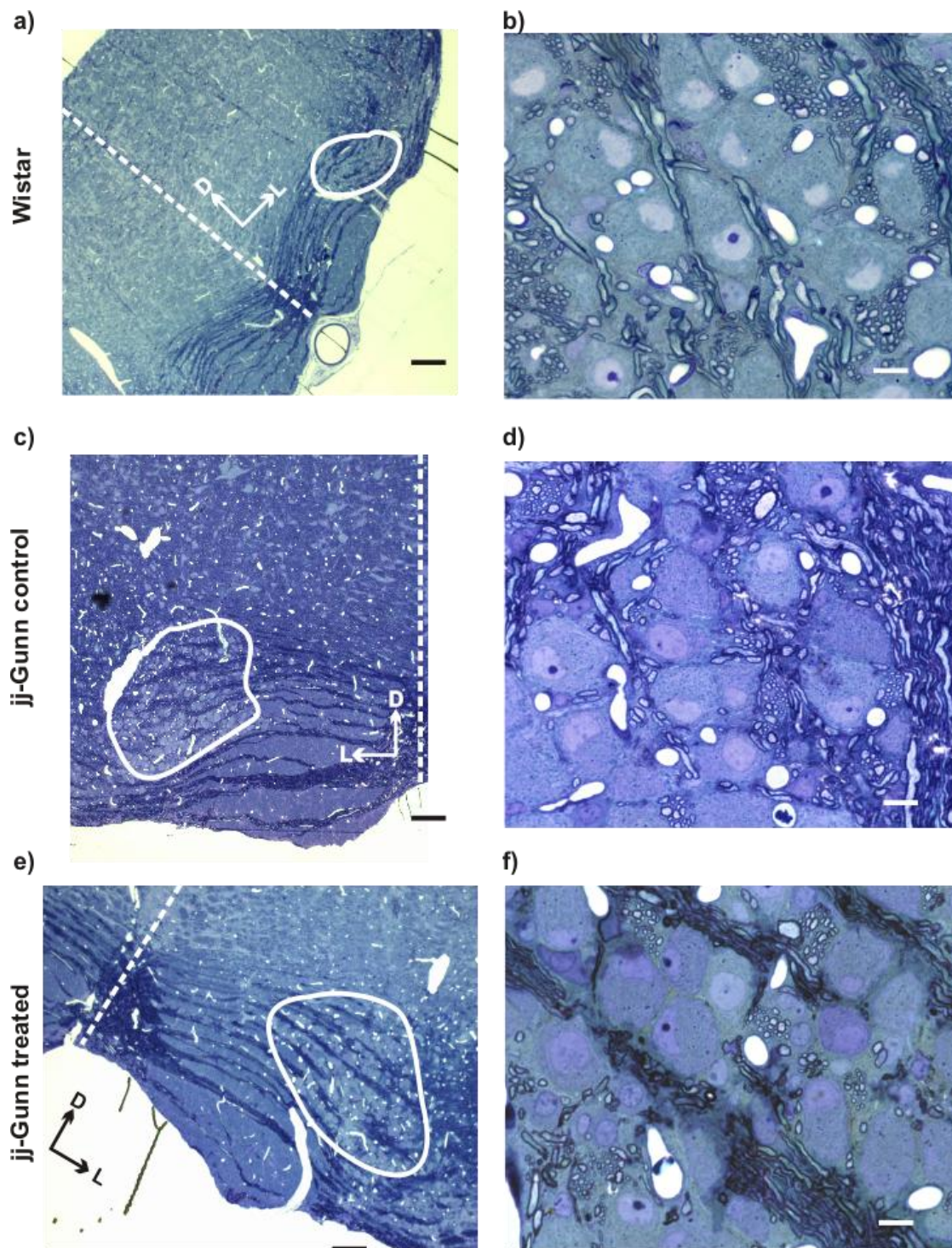


Figure 5.5 Light microscopic images of the MNTB show no differences between control and treated rats.

Light microscopy images from fixed brainstem slices stained with toluidine-blue show no obvious differences between control (a-d) and treated (e-f) animals. The left column shows low magnification images, while the right column shows MNTB principal neurons at higher magnification. a)+b) Wistar rat; c)+d) control jj-Gunn rat; e)+f) treated jj-Gunn rat. Encircled area in a,c,e marks the location of the MNTB. D=dorsal, L=lateral, dashed line= midline of the brain slice; Scale bars: a, c, e= 100 μ m; b, d, f= 10 μ m.

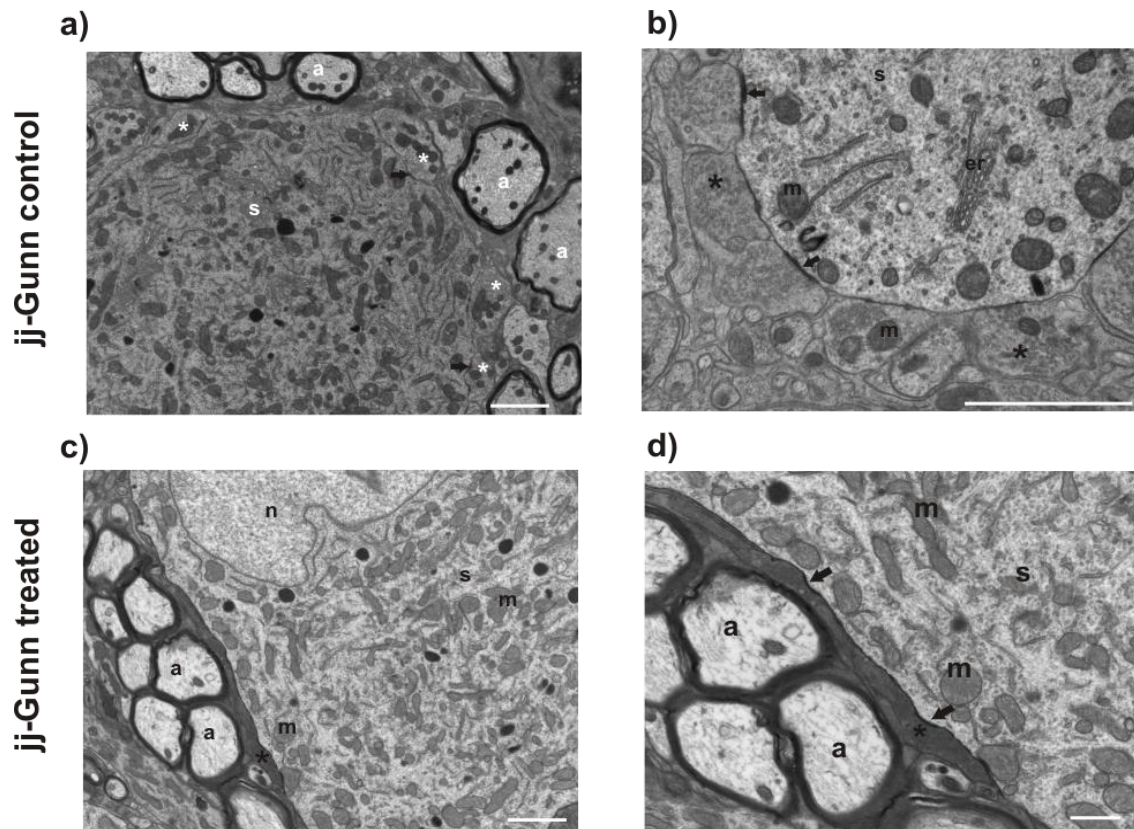


Figure 5.6 Electron microscopic images from the MNTB of control and treated rats. Electron microscopic images from the MNTB of control and treated rats show healthy postsynaptic neurons in both groups but signs of presynaptic degeneration in treated rats. a) Axonal profiles (a), presynaptic profiles (*) and the soma of MNTB principal neurons (s) do not show any signs of degeneration. b) Higher magnification image confirms this observation. Mitochondria (m) and endoplasmic reticulum (er) look healthy. PSD (arrow) can be seen between the principal neuron and the presynaptic profiles (*). c) The principal neurons from a treated MNTB present a similar picture: there were no signs of degeneration in the axonal profiles (a) or the postsynaptic soma (s). Mitochondria (m) appeared healthy, i.e. without swellings. However, in this case the presynaptic profile (*) was darkened, as can be more clearly seen at higher magnification (d). Note that the PSD (arrows) is still present, but that the presynaptic profile appears very thin and unusually dark (*). a=axonal profile, m=mitochondrion, n=nucleus, s=soma, *=presynaptic profile, arrows= Postsynaptic density; Scale bars: 2 μ m.

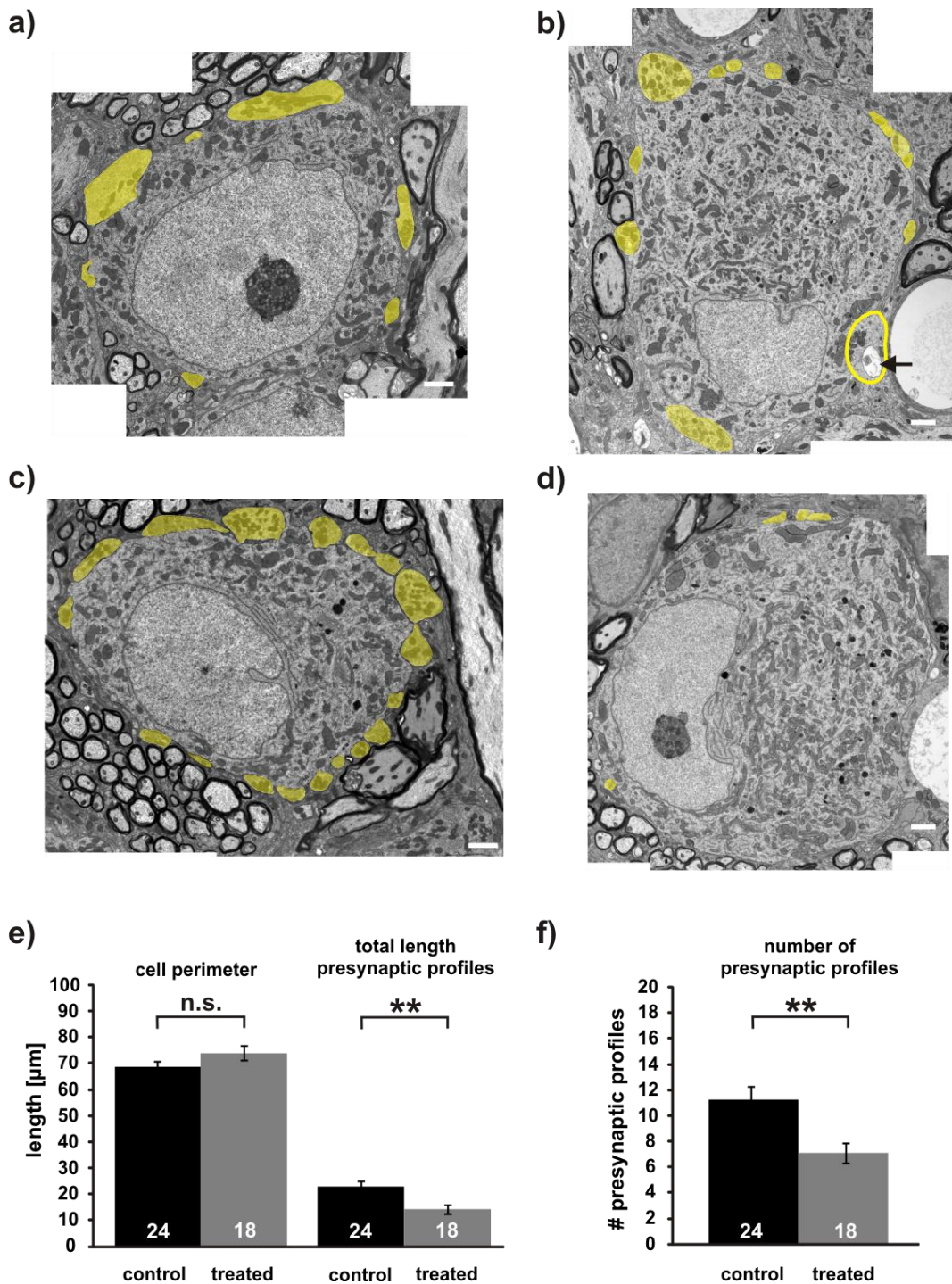


Figure 5.7 Electron micrographs of MNTB principal neurons reveal no signs of postsynaptic degeneration but confirm loss of presynaptic profiles in treated jj-Gunn rats.

a) +c) Examples of a control MNTB neurons showing no signs of postsynaptic degeneration and confirms the presence of a calyceal presynaptic terminal (high-lighted yellow) at a MNTB principal neuron. b) Example of a treated MNTB neuron that has comparable number of presynaptic profiles to control neurons and no signs of postsynaptic degeneration. Note the vacuole in one of the presynaptic profiles (arrow) which is a sign of neurodegeneration. d) MNTB principal neurons from treated group look very similar to control neurons and cell organelles seem to be intact, but it shows loss of the calyceal presynaptic terminal (yellow). e) There was no significant change in cell perimeter between control and treated group but the total length of presynaptic profiles was significantly reduced in treated animals. f) Summary bar graph shows the significantly reduced number of presynaptic profiles in treated jj-Gunn rats. Scale bars: 2μm. All values are displayed as mean±SEM; Mann-Whitney-Rank-Sum test; n.s.=not significant, **=p<0.01.

5.3.3 Cochlear Nucleus

Thus far it has been established that, 18h after induction of bilirubin toxicity, presynaptic degeneration in the MNTB is the reason for failure in synaptic transmission without effects on the postsynaptic neuron. This inevitably raises two questions:

1. Does this phenomenon occur in other areas of the auditory brainstem? (it clearly does not occur in the cerebellum, as the results show a post- rather than presynaptic degeneration problem there)
2. What is the underlying mechanism?

To answer the latter the initial findings of a pilot study in the next chapter will be described. To begin to answer the first question, LM and EM images of the ventral cochlear nucleus (VCN) from control and treated jj-Gunn rats were taken. The VCN was chosen for several reasons. Firstly, the CN shows signs of neurodegeneration in humans (Crabtree & Gerrard, 1950; Dublin, 1951; Gerrard, 1952; Dublin, 1974) and Gunn rats (Jew & Williams, 1977; Jew & Sandquist, 1979; Zhang *et al.*, 1989; Conlee & Shapiro, 1991; Shapiro & Conlee, 1991) suffering from severe hyperbilirubinaemia. Secondly, because it is home to the globular bushy cells who, with the endbulbs of Held, form synapses similar to that in the MNTB. The globular bushy cells send axons across the midline which give rise to calyx of Held in the MNTB. Could the degenerating calyces be the first signs of dying bushy cells? Thirdly, the cochlear nucleus is a generator of wave II in the ABR (Melcher *et al.*, 1996a). As wave II was also reduced 18h after induction of bilirubin toxicity (see chapter 3) it was of interest to investigate and find an explanation at the cellular level that could account for this event.

Light microscopic images showed healthy looking cell bodies in the VCN of control animals (Figure 5.8a+b). At low magnification the VCN of treated jj-Gunn rats also looked normal (Figure 5.8c), but higher magnification (100x) revealed that the cytoplasm of the bushy neurons appeared very grainy (Figure 5.8d+e). We wanted to rule out that this difference was a general feature of treated jj-Gunn rats rather than specific for the bushy neurons in the VCN. The appearance of neurons located close to the trigeminal nerve (indicated in Figure 5.8c with a white square) was therefore inspected in the same brain slice (Figure 5.8f). These neurons, like the principal neurons of the MNTB, did not show any abnormalities indicating damage or degeneration. Therefore the granular/grainy appearance of the cytoplasm can be seen as specific to the bushy neurons of the VCN and as a consequence of 18h exposure to toxic bilirubin concentrations.

At the electron microscopic level, there were some differences in the VCN compared to the MNTB. The grainy/granulous appearance of the cytoplasm in bushy cells of treated rats (Figure 5.8d+e) was a result of distorted mitochondria (i.e. glycogen bodies, vacuolation or both; Figure 5.9e+f). While most bushy neurons from control jj-Gunn rats showed no such abnormal cell organelles (Figure 5.9a+b), a small number of control bushy neurons did (Figure 5.9c+d). It should be noted that in control bushy neurons not all mitochondria showed abnormal changes (Figure 5.9c+d, arrowheads, Figure 5.10b). The majority of mitochondria remained intact. However, in treated neurons almost all mitochondria were affected (Figure 5.9e+f, arrowheads only on selected mitochondria because labelling all distorted mitochondria would

make the cell disappear beneath the arrowheads). Hence distorted mitochondria could not be used as an exclusive criterion to distinguish between control and treated VCN neurons, although almost all treated neurons and only a small number of control neurons showed distorted mitochondria. It is important to note that only in treated jj-Gunn rats but not in control rats axonal profiles showed signs of neurodegeneration (Figure 5.9g). Axonal degeneration was not observed in the MNTB. Axonal profiles showed distorted mitochondria and vacuolisation (Figure 5.9g, arrows). Also in preparations from treated rats but not in controls autophagosomes were seen (Figure 5.9h). Autophagosomes are a sign of cellular damage as they clear up debris and damaged cells.

Some bushy neurons were sectioned so that they showed long presynaptic terminals, the endbulbs of Held (Figure 5.10a). This was a further confirmation that the cells that were analysed were indeed bushy neurons; in addition to the right location and that the cells seemed identical to published EM images of bushy neurons of the VCN (Ryugo *et al.*, 1996; Wang *et al.*, 1998b; Nicol & Walmsley, 2002; Lee *et al.*, 2003; Baker *et al.*, 2010). Applying the criteria previously used in the MNTB, the analysis of the ventral cochlear nucleus revealed that here, as in the MNTB, the number (control 13 ± 2 , $n = 16$; vs. treated 7 ± 1 , $n = 16$; $p = 0.019$) and total length of presynaptic profiles of bushy cells (control $35 \pm 5 \mu\text{m}$, vs. treated $19 \pm 3 \mu\text{m}$; $p = 0.01$) was significantly reduced in treated jj-Gunn rats (Figure 5.10b-d). The circumference of the neuronal somata was, as in the MNTB, unchanged between the 2 groups (control $87 \pm 4 \mu\text{m}$ vs. treated $79 \pm 3 \mu\text{m}$; $p = 0.094$; Figure 5.10c).

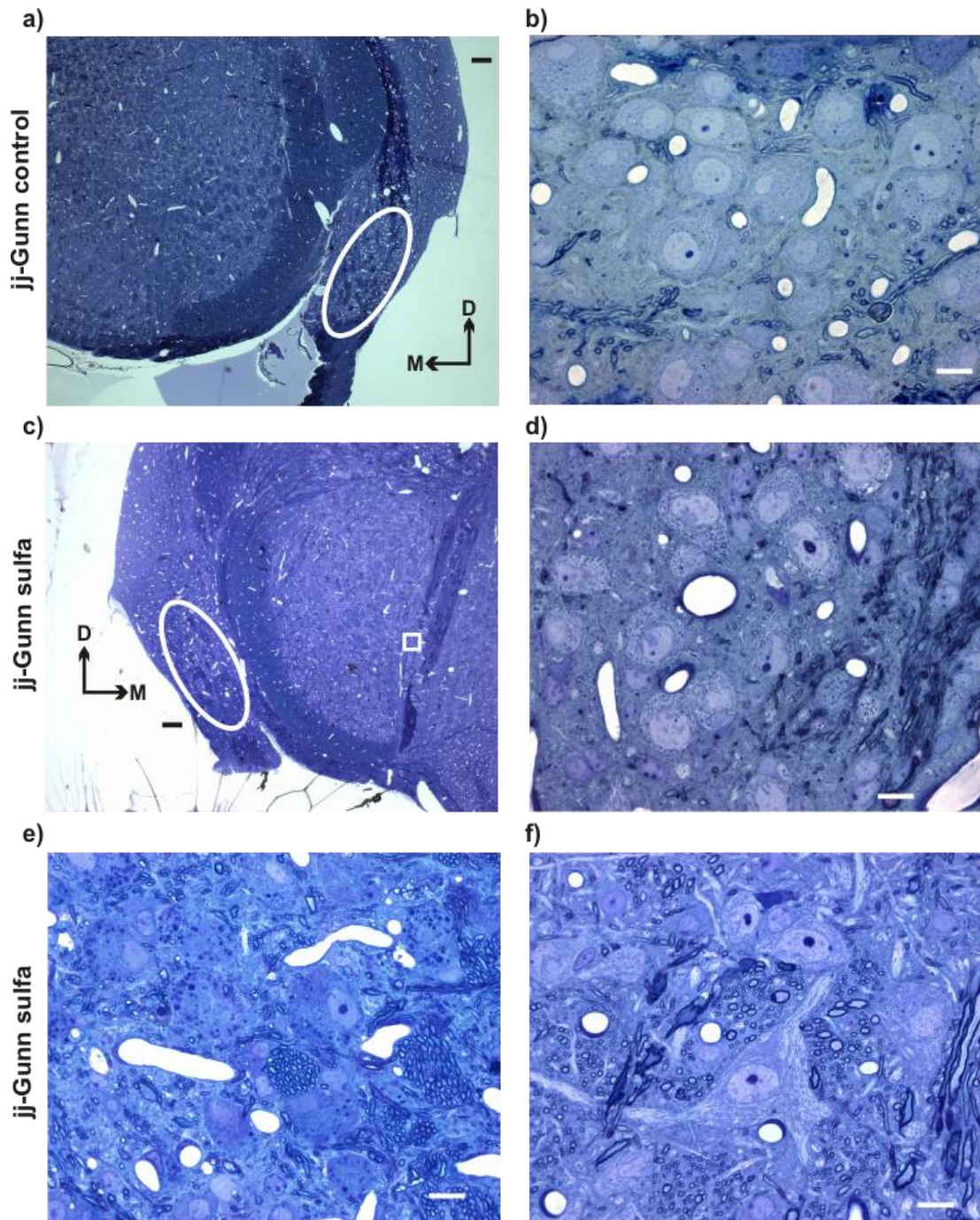


Figure 5.8 Light microscopy reveals differences between the VCN of control and treated Gunn rats. Light microscopy images from fixed brainstem slices stained with toluidine-blue show differences between control (a+b) and treated (c-f) Gunn rats in the VCN. a) Low magnification image of the CN from a control rat. b) shows VCN bushy neurons at higher magnification. c) Low magnification image of the CN from a treated rat. d+e) Show VCN bushy neurons at higher magnification. Note the more granular cytoplasm compared to controls. f) Neurons from the area marked with a white square in c) do not show granular cytoplasm, indicating that changes are confined to the VCN and do not occur generally in treated jj-Gunn rats. a)+b) control jj-Gunn; c)-f) treated jj-Gunn rat. Encircled area in a+c marks the location of the VCN. D=dorsal, M=medial; Scale bars: a+c= 100 μ m; b, d, e, f= 10 μ m.

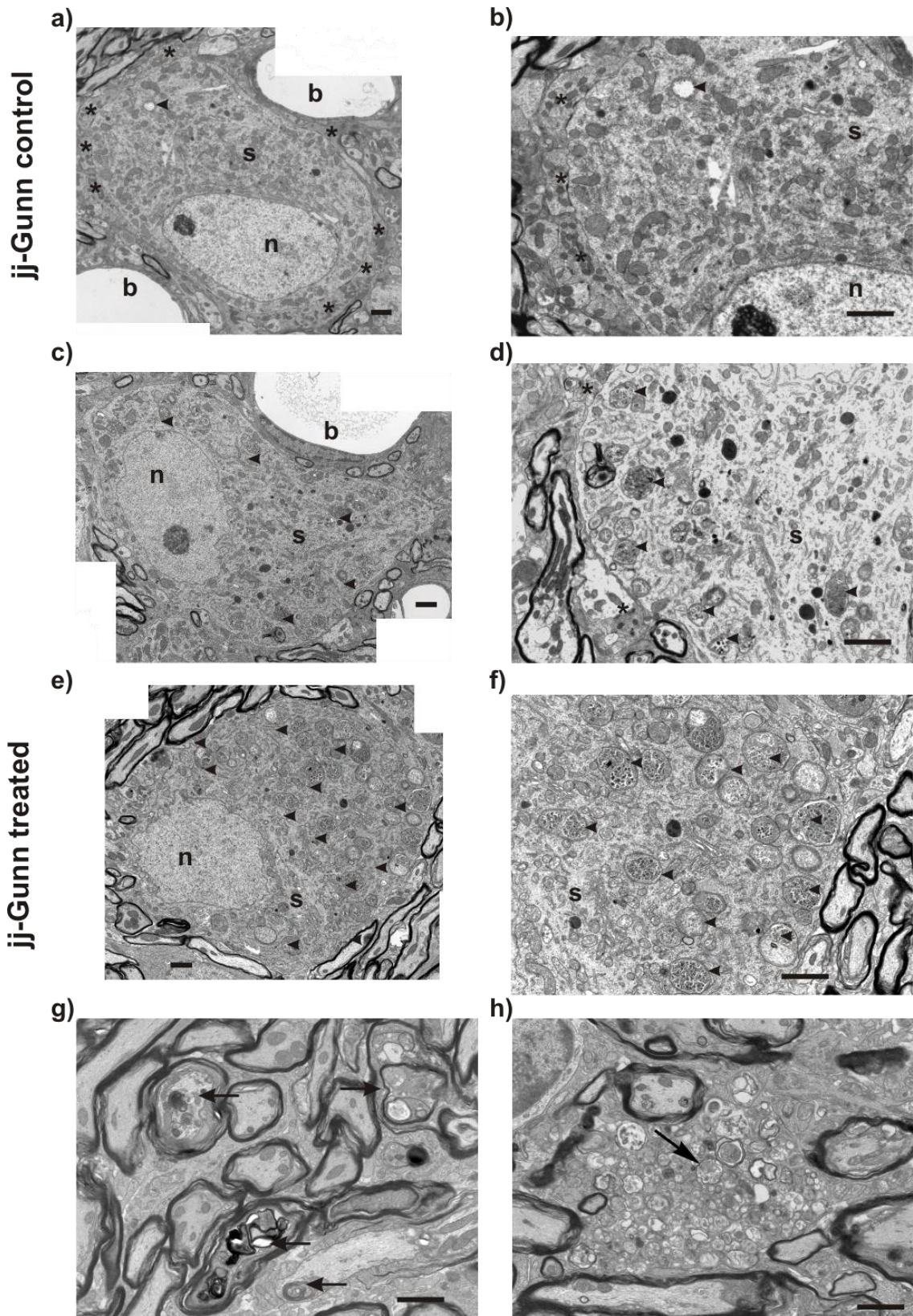


Figure 5.9 Electron microscopic images of the VCN from control Gunn rats (a-d) and treated Gunn rats (e-h) show stark signs of neurodegeneration.

a) Low magnification of a bushy cell neuron in the VCN shows virtually no signs of neurodegeneration. A mitochondrion shows vacuolisation (arrowhead), as seen at higher magnification in b). c) Another bushy cell showing some damaged mitochondria (arrowheads), as seen at higher magnification in d). e) A bushy cell from a treated rat surrounded by axonal profiles. Note that almost all mitochondria contain glycogen bodies or vacuoles, as seen in f). g)

Mitochondria in axonal profiles show signs of degeneration (arrows), like vacuoles, membrane whirls and dense bodies. h) Autophagosome (arrow) in the VCN of a treated rat indicating clearance of damage cells. These autophagosomes are almost exclusively found in treated animals. n=nucleus, s=soma, *=presynaptic profile; Scale bars: 2 μ m

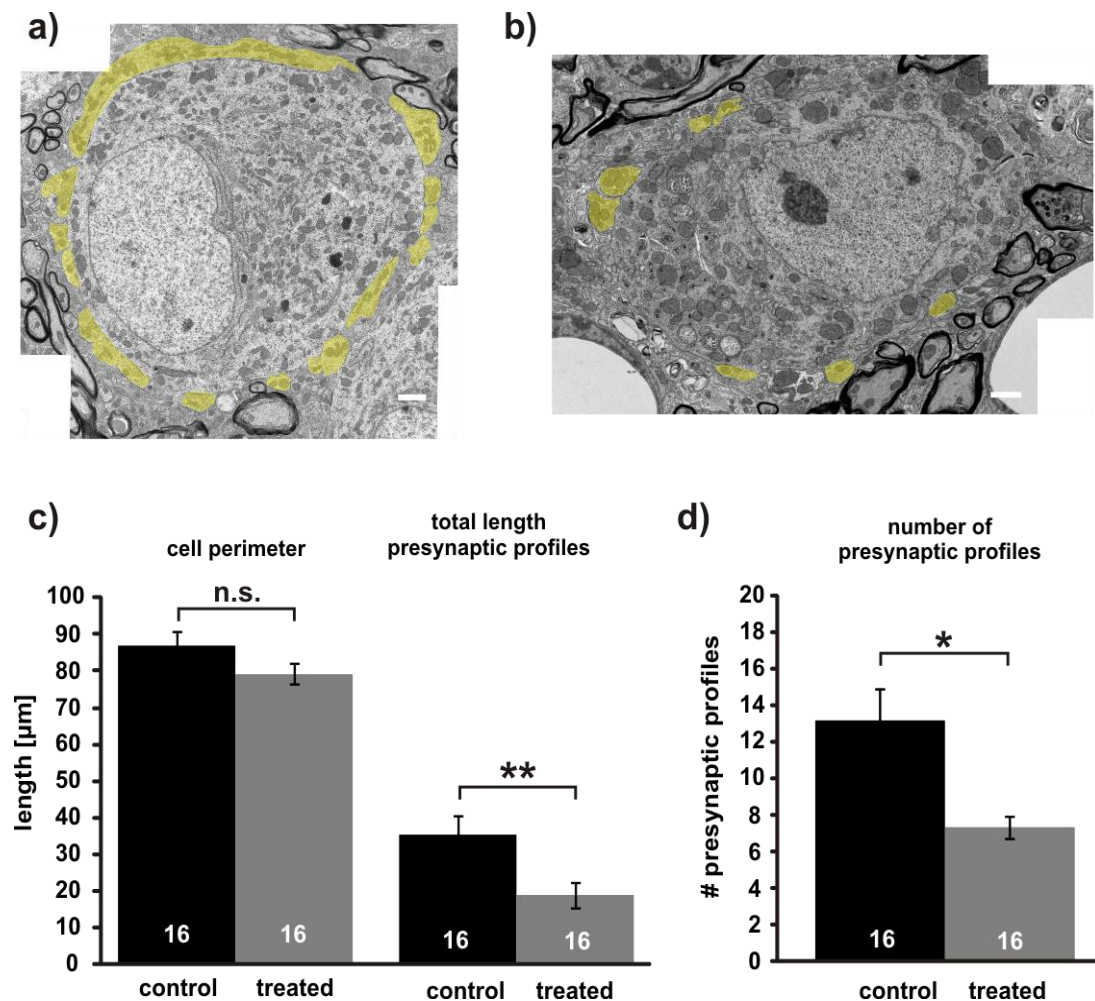


Figure 5.10 Electron microscopy reveals differences in VCN bushy neurons between control and treated jj-Gunn rats.

a) A bushy neuron from a control jj-Gunn rat shows no signs of neurodegeneration. b) A bushy neuron from a treated animal shows a reduced number of presynaptic profiles (yellow) and also mitochondria with accumulation of glycogen bodies or with vacuoles, both of which are signs of neurodegeneration. c) There was no difference in cell perimeter between the groups, but the total length of presynaptic profiles was significantly reduced in the treated group as was the number of presynaptic profiles (d). Scale bars: 2 μ m. All values are displayed as mean \pm SEM; c) t-test, d) Mann-Whitney-Rank-Sum test; n.s.=not significant, *=p \leq 0.05, **=p \leq 0.01.

5.3.4 Summary and Conclusions:

Bilirubin did not elevate $[Ca^{2+}]_i$ in MNTB neurons, but calcium-imaging revealed a difference in basal $[Ca^{2+}]_i$ between Jj and jj-Gunn rats. Multiphoton-Imaging of dextran-labelled calyces showed healthy presynaptic terminals in control and severely damaged calyces in treated animals. Axons were well labelled in both groups. Light and electron microscopic images from the cerebellum confirmed the degeneration of Purkinje neurons. While light microscopy in the MNTB showed no differences between control and treated rats, electron microscopy revealed intact neurons and reduced numbers of presynaptic terminals. The reduction of presynaptic profiles in EM images confirmed the results from multiphoton-imaging of calyces in treated rats. In the VCN, presynaptic terminals were also reduced in number compared to controls. In addition, bushy neurons and axons also displayed signs of degeneration.

From these findings it is concluded that bilirubin toxicity causes degeneration of the glutamatergic, presynaptic terminals without affecting the postsynaptic neurons in the MNTB. In the VCN pre- AND postsynaptic degeneration, as well as axonal degeneration, were results of bilirubin toxicity.

6. Nitric oxide and bilirubin neurotoxicity

Over the last 3 chapters it has been described how acute hyperbilirubinaemia leads to decreased ABRs and impairs synaptic transmission at the calyx of Held/MNTB synapse without affecting postsynaptic excitability, but rather by degeneration of the presynaptic calyx of Held terminal. These findings inevitably raise the question of the underlying mechanisms.

The more recent literature on bilirubin neurotoxicity suggests the involvement of astrocytes in the disease process via increased release of cytokines (Fernandes *et al.*, 2004), for example TNF- α , IL-1 & IL-6 stimulated by bilirubin or the inhibited glutamate uptake by astrocytes after exposure to bilirubin (Silva *et al.*, 1999), with microglia being the most reactive cell-type to bilirubin insult (Gordo *et al.*, 2006). NMDA receptors (McDonald *et al.*, 1998; Brito *et al.*, 2010) and more recently nitric oxide (NO) (Brito *et al.*, 2007; Brito *et al.*, 2010) have been implicated to play a role in what seems to be a rather complex phenomenon. It has been reported that both the block of NMDA-Rs (McDonald *et al.*, 1998; Brito *et al.*, 2010) and NO (Brito *et al.*, 2007; Brito *et al.*, 2008a; Brito *et al.*, 2010) lead to a significant reduction in bilirubin-induced cell death. The same group (Brito *et al.*, 2008a) also showed that preincubation of neuronal cell cultures with L-NAME (a neuronal nitric oxide synthase (nNOS) inhibitor) significantly reduced the amount of lactate dehydrogenase (LDH) release from nonviable cells (LDH is a measure for cell death), an indication for reduced cell death.

NMDA-Rs have been implicated in the pathology of the condition ever since (McDonald *et al.*, 1998) published results showing the block of NMDA-Rs by MK-801 reduced the number of dead neurons in the hippocampus, after exposure to high bilirubin concentrations *in vivo*. These findings were disputed by papers from (Warr *et al.*, 2000) who showed that free bilirubin has no direct effect on AMPA-Rs, NMDA-Rs and Glu-transporters, as well as (Shapiro *et al.*, 2007) who did not see protective effects of NMDA-R antagonist MK-801 in the Gunn rat model of hyperbilirubinaemia (namely, no protected ABRs and no reduction in cell death in the cerebellar cultures). However, the AMPA receptors in the MNTB contain high levels of the GluR4 subunit, low levels of the GluR2 subunit and are highly Ca²⁺-permeable (Geiger *et al.*, 1995; Joshi *et al.*, 2004). Therefore, a block of NMDA-Rs only would not be sufficient to prevent elevated intracellular calcium-concentration due to excitotoxicity.

In one of their more recent papers, (Brito *et al.*, 2010) demonstrated in primary cell cultures of cortical neurons incubated with bilirubin (100µM plus 100µM human serum albumin) that block of either NMDA-Rs, neuronal nitric oxide synthase (nNOS) or scavenging of NO (by haemoglobin) reduced the number of apoptotic cells. These results are intriguing as it was shown that MNTB neurons have a high expression of nNOS (Steinert *et al.*, 2008). That is why it was decided to test for protective effects of nNOS blocker in the homozygous Gunn rat *in vivo*, rather than trying an NMDA antagonist.

6.1 The nNOS blocker 7-nitroindazole (7-NI) leads to a partial rescue of the ABRs & MEA recordings

With the results from (Brito *et al.*, 2010) in mind, the following hypothesis was tested: the block of NO will protect from bilirubin-induced neurodegeneration causing hearing loss. If the hypothesis was correct, blocking the enzyme that synthesises NO should alleviate the symptoms and protect hearing.

To test whether this would also be the case *in vivo* and not solely in cell cultures, 150mg/kg 7-NI – a nNOS antagonist – suspended in peanut oil was injected *i/p* 30 minutes before giving the 200mg/kg sulfa *i/p*. 18 hours later the ABRs were preserved a great deal better (Figure 6.1b) than in homozygous animals treated with sulfa alone (Figure 6.1a). The ABR thresholds of 5 groups of animals were compared. The thresholds for ‘click’ stimuli were identical between Wistar rats, jj-Gunn control rats and sulfa-treated Wistar rats (Figure 6.1c). In jj-Gunn rats with 7-NI+sulfa, the thresholds were significantly lower than in those homozygous animals with sulfa alone (Figure 6.1c). Figure 6.1 was published as Figure 4 in (Haustein *et al.*, 2010).

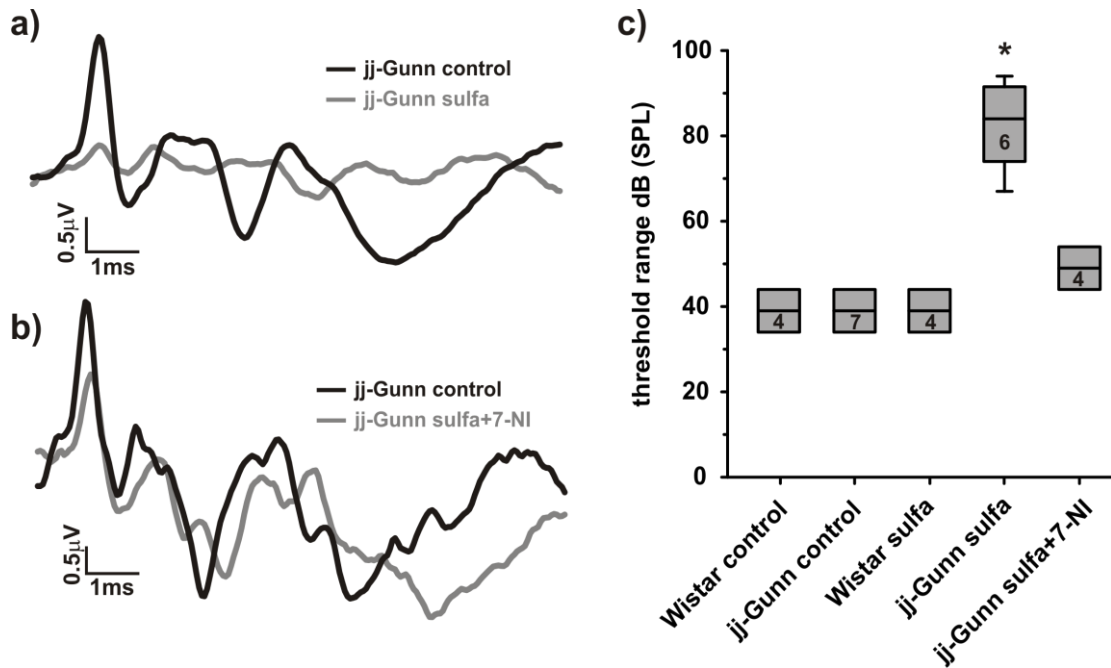


Figure 6.1 Protection from bilirubin-induced hearing loss by the nNOS antagonist 7-nitroindazole (7-NI).

a) ABRs from a jj-Gunn rat in response to a 94 dB ‘click’ stimulus before (black) and after (grey) induction of bilirubin toxicity (18 h after sulfadimethoxine, 200 mg kg⁻¹). b) ABRs from a jj-Gunn rat in response to a 94 dB ‘click’ stimulus before (black) and after (grey) induction of bilirubin toxicity (18 h after sulfadimethoxine, 200 mg/kg, and 7-NI, 150 mg/kg). c) Summary plot of ABR thresholds in response to a ‘click’ stimulus. Wild-type Wistar rats and the jj-Gunn rats have similar auditory thresholds under control conditions. The Wistar rats suffered no auditory deficit after 18 h sulfadimethoxine, whereas jj-Gunn rats show significantly elevated thresholds after sulfa treatment. 7-NI protected the hearing from this threshold elevation. Box plots show mean \pm upper and lower threshold range; ANOVA, * \leq 0.05. The number of animals tested is indicated in the respective box.

Not only were the thresholds for ‘click’ stimuli partially protected in jj-Gunn rats pre-treated with 7-NI. Across the tested pure-tone range (12, 24, 30kHz), there was a significant threshold decrease (Figure 6.2b) compared to treated jj-Gunn rats. Wistar and jj-Gunn rats have very similar ABR thresholds at 12, 24 & 30kHz (Figure 6.2a). Wistar rats showed no significant elevation of threshold, while treated jj-Gunn rats displayed threshold elevations from around 40dB to around 80dB (Figure 6.2b). jj-Gunn rats injected with the nNOS antagonist 7-NI before sulfa-treatment show a significant reduction (7-NI vs. sulfa: 12kHz: $p=0.005$; 24kHz: $p=0.016$; 30kHz: $p\leq 0.001$) in threshold elevation compared to jj-Gunn rats without 7-NI pre-treatment (Figure 6.2b). The protection here too

was improved, but not yet complete. This is evident by the fact that there were significant differences between sulfa-treated Wistar rats and 7-NI+sulfa jj Gunn rats at thresholds for 24kHz (Wistar vs. 7-NI: $p=0.001$) and 30kHz (Wistar vs. 7-NI: $p\leq 0.001$), whilst there was no significant difference at 12kHz (Wistar vs. 7-NI: $p=0.051$).

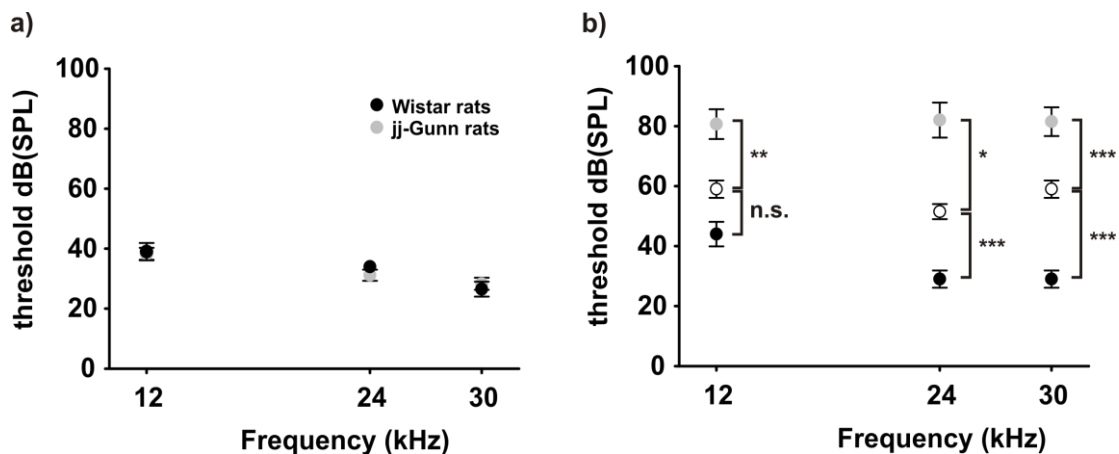


Figure 6.2 The nNOS antagonist 7-NI decreases threshold elevation by sulfa in jj-Gunn rats. a) Wistar and jj-Gunn rats have very similar ABR thresholds across the tested frequencies. jj-Gunn rats (grey circles, $n=7$), Wistar rats (black circles, $n=4$). b) 7-nitroindazole (150mg/kg) reduced the threshold elevation caused by sulfa treatment in jj-Gunn rats across all tested frequencies. Sulfa-treated jj-Gunn rats (grey circles, $n=6$ for 12kHz, $n=5$ for 24kHz, $n=4$ for 30kHz), sulfa-treated Wistar rats (black circles, $n=4$), sulfa- and 7-NI treated jj-Gunn rats 7-NI+sulfa (open circles, $n=4$). All values are displayed as mean \pm SEM; ANOVA, n.s.=not significant, $*=p\leq 0.05$, $**=p\leq 0.01$, $***=p\leq 0.001$

To follow up on the 7-NI effects *in vivo*, brain slices were taken from all 4 jj-Gunn rats that had been ABR-tested before and after 7-NI and sulfa treatment. MEA data from acute brainstem slices from jj-Gunn rats that received 7-NI 30mins prior to sulfa showed improved results compared to ‘sulfa only’ treated jj-Gunn rats. MEA recordings from these brain slices showed both a C_1 and a C_2 component (Figure 6.3a). Due to the almost total protection, a significantly improved C_2/C_1 ratio (Figure 6.3b) was found in MEA recordings from acute brainstem slices of 7-NI+sulfa treated jj-Gunn rats. More importantly, the timing of the synaptic delay was protected (i.e. not prolonged like in treated jj-Gunn

rats; Figure 6.3c) in 7-NI treated rats (control, n=52 electrodes: 0.46 ± 0.01 ms vs. 7-NI, n=30 electrodes: 0.55 ± 0.05 ms, ANOVA, not significant), which indicates that a next to normal information transmission across the calyx of Held/MNTB synapse is possible in this condition (in sulfa-treated jj-Gunn rats C₂ was frequently absent and always delayed).

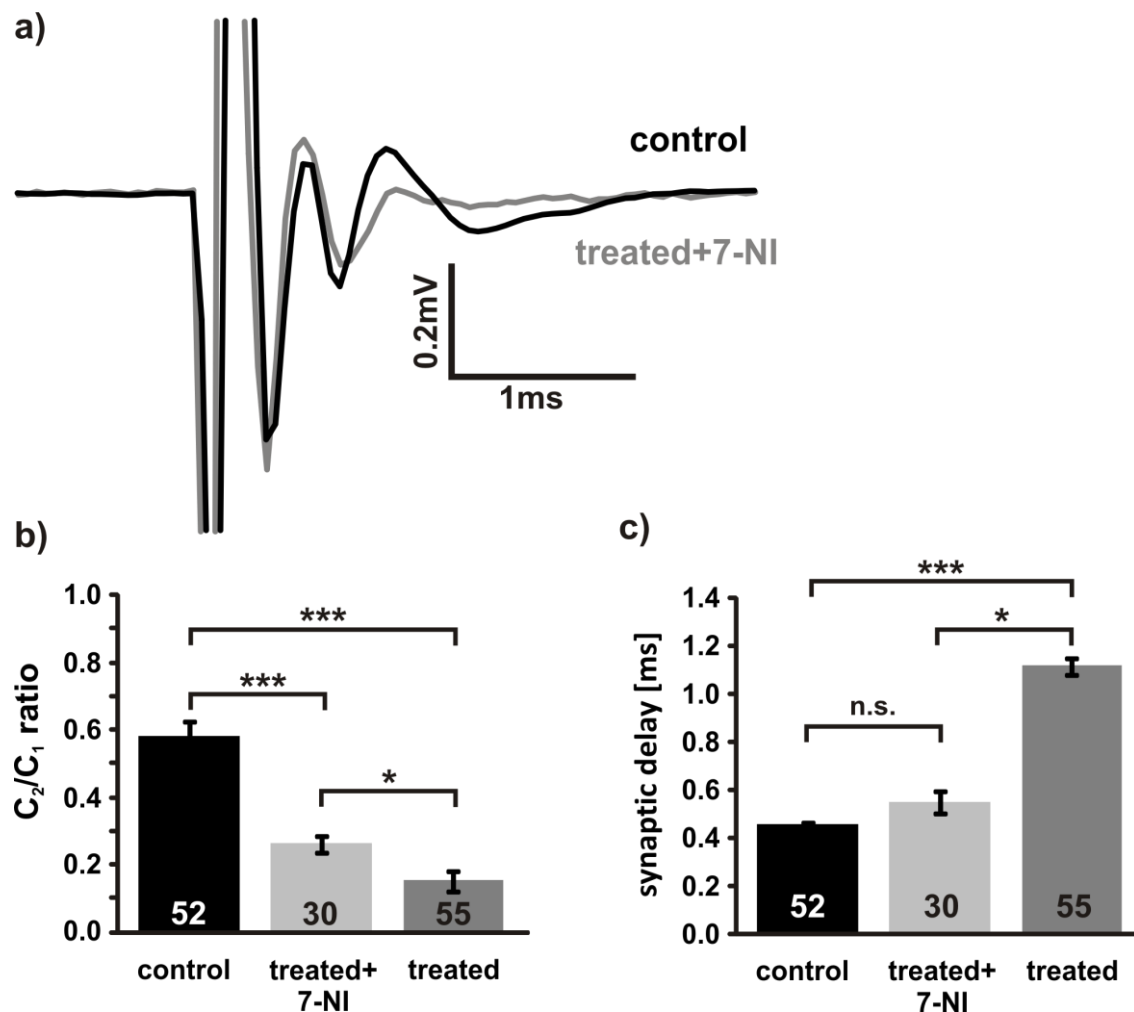


Figure 6.3 MEA recordings from acute brainstem slices of 7-NI treated Gunn rats show protected synaptic delay times but decreased C₂ amplitudes.

a) Example traces from a control (black) and 7-NI/sulfa treated rat. b) The C₂/C₁ ratio, though significantly decreased compared to control, is still significantly bigger in the 7-NI group compared to the treated group. c) The synaptic delay is not significantly increased in the treated+7-NI group compared to control, whereas the delay in the treated group is significantly longer compared to control and treated+7-NI. 7-NI: n= 4 animals, 6 slices, 30 electrodes; treated: 4 animals, 9 slices, 55 electrodes; control: 3 animals, 6 slices, 52 electrodes. All values are displayed as mean±SEM; ANOVA, n.s.=not significant, *= $p\leq 0.05$, **= $p\leq 0.001$

6.1.1 Summary and Conclusions:

The presence of nNOS antagonist 7-NI causes a partial protection of ABRs of jj-Gunn rats *in vivo* after 18h sulfa treatment. This indicates the involvement of NO in the neurodegenerative process during acute hyperbilirubinaemia in the jj-Gunn rat. Not only ABRs but also MEA recordings *in vitro* show protection from damage during hyperbilirubinaemia after 7-NI administration. This protection manifests itself in the protected timing for the synaptic delay and the appearance of both C₁ and C₂ components. This demonstrates that NO is involved in the degeneration process. However, the way in which the block of nNOS and thereby NO leads to partial protection remains elusive. The implications of these findings, potential future experiments and obstacles to overcome will be detailed in the discussion.

7. Summary of results

- MNTB field potential (FP) consists of 2 components (Figures 3.1 & 3.2)
- FPs change with temperature & recordings are stable for over 4h at 31°C (Figure 3.3 & Figure 3.14)
- C₁ was the conducted and C₂ the postsynaptic component as shown by TTX, DNQX and Ca²⁺ free ACSF (Figures 3.4-3.6)
- Synaptic transmission in MNTB is glutamatergic (Figures 3.6)
- C₂ amplitude was reduced in presence of NMDA-R blocker AP-5, confirming that NMDA-Rs are present at postsynaptic neurons and involved in synaptic transmission (Figure 3.7)
- Presence of K_v1 antagonist DTX-I led to reduction of only postsynaptic component of FPs (Figure 3.8)
- Presence of K_v3 antagonist TEA led to presynaptic reduction and reduction of (+)C₂ part of FPs (Figure 3.9)
- MNTB FPs showed effect of NO on postsynaptic signal and indicate involvement of K_v3 (Figure 3.10)
- Bilirubin perfusion onto brain slices of wild-type and Gunn rats did not have consistent effects on MEA recordings. There were no effects at all at 4h perfusion of bilirubin onto brain slices of jj-Gunn rats. Therefore this is not usable as a model to induce hyperbilirubinaemia *in vitro*

- ABR of sulfa-treated jj-Gunn rats: significant reduction of all waves and increase in threshold (Figures 3.16, 3.18 & 3.19)
- No effect of sulfa on waveform or threshold of Wistar ABR (Figures 3.17-3.19)
- Sulfa-treated Gunn rats: impaired synaptic transmission in MNTB shown by reduced or absent C_2 and longer synaptic delay (Figure 3.21)
- Sulfa-treated Wistar rats: show no significant effects, apart from slightly shorter synaptic delay in MNTB FPs (Figure 3.20)
- No calyceal EPSCs in treated group upon synaptic stimulation of the MNTB (Figure 4.1)
- I-V curves were identical between control and treated group (Figure 4.2)
- AP waveforms, half-width, threshold & amplitude, were not different between control and treated group apart from amplitude (Figure 4.3)
- Miniature EPSCs: no differences between control and treated group (Figures 4.4 & 4.5)
- AVCN: simultaneous intra- and extracellular recordings from bushy cells helped to link *in vivo* to *in vitro* recordings and helped with interpretation of waveform shapes previously published (Figures 4.6-4.8)
- Bilirubin had no effect on intracellular calcium concentration but there is a difference between Jj and jj-Gunn rats (Figure 5.1)

- Dextran labelling revealed degenerated or completely absent presynaptic terminals in treated rats and healthy calyces in control group (Figure 5.2)
- Dextran labelling also showed intact axons in both groups (Figure 5.2)
- Cerebellum showed inclusion bodies (sign of neurodegeneration) in Purkinje neurons of control and treated jj-Gunns but not in Jj-Gunn or Wistar rats (LM cerebellum, Figure 5.3; EM cerebellum, Figure 5.4)
- At light microscopic level there was no difference between control vs. treated tissue visible (LM MNTB, Figure 5.5)
- Electron microscopic images revealed healthy neuron somata in MNTB, but reduced numbers of presynaptic profiles contacting them in treated rats (EM MNTB, Figures 5.6 & 5.7)
- Light microscopic images showed granular appearance of the cytoplasm in bushy neurons of the VCN in treated, but not control rats (Figure 5.8)
- EM showed that granular appearance was due to glycogen bodies in mitochondria in treated rats and to a small extent also in control rats (Figure 5.9)
- EM revealed – like in the MNTB - a reduced number of presynaptic profiles surrounding the neuronal somata in treated jj-Gunn rats (Figure 5.10)
- Antagonist of nNOS, 7-NI, protected ABR waveforms and threshold in treated jj-Gunn rats from bilirubin toxicity (Figure 6.1 & 6.2)

- 7-NI also protected the synaptic delay in the MNTB from increase due to bilirubin-induced neurotoxicity (Figure 6.3)

8. Discussion

Severe hyperbilirubinaemia causes hearing loss in the human newborn and in an animal model. Using the Gunn rat as an experimental model for neonatal jaundice, the experiments presented in this thesis demonstrated that presynaptic neurodegeneration underlies this hearing loss and that this can be prevented by inhibition of NO production. Techniques used to investigate this issue included: *in vivo* Auditory Brainstem Responses, *in vitro* multi-electrode arrays, single-cell patch-clamp recordings, calcium-imaging, live-multiphoton laser microscopy, light and electron microscopy. Over the previous chapters it was described how these different methods have shed light on the mechanism of hearing loss in severe jaundice. The main findings, published in the Journal of Physiology (Haustein *et al.*, 2010) show that hyperbilirubinaemia causes degeneration of the central presynaptic terminals (in the MNTB and the VCN) and that block of nNOS largely protects from the bilirubin-induced hearing deficits. This chapter will discuss these findings in the light of the current and past literature and also suggest possible future experiments and directions for further studies.

8.1 MEA recordings

8.1.1 The effects of temperature on evoked field potentials in the MNTB

Extracellular multi-electrode arrays (MEAs) were used to investigate conducted and synaptically transmitted events across the MNTB. The complex evoked field potential had two components (Figure 3.2), similar to *in vivo* MNTB recordings during electrical stimulation (Guinan & Li, 1990). Previously, recordings from the MNTB in Mongolian gerbils also described an evoked field potential made up of two distinct components (Haustein *et al.*, 2008). According to these two papers the MNTB FP components were termed C₁ and C₂.

At near physiological temperatures (32±1°C) both components reached their minima faster than at room temperature (Figure 3.3). The observation of an accelerated C₁ is in good accordance with earlier papers describing that conduction velocity in myelinated nerves increases linear with temperature in the giant squid axon (Hodgkin & Katz, 1949) and in vertebrates (Hutchinson *et al.*, 1970). This increase in conduction velocity with temperature is related to the faster gating of sodium channels (Collins & Rojas, 1982). Not only was the presynaptic component faster, but also the synaptic delay was shorter at 32°C than at room temperature. Such a decrease in synaptic transmission delay with rising temperatures has been described at the neuromuscular junction (Katz & Miledi, 1965) and in the cerebellum (Sabatini & Regehr, 1996). Based on these papers, our data showed changes that would have been expected and are in good accordance with previous findings. The amplitudes of both C₁ and C₂ did not change with temperature. This was expected since the same number of

cells contributing to the extracellular signals was not thought to change with temperature. Increased temperatures did not show and were not expected to show a better synchronisation of APs, only faster transmission as described above. The synaptic delay was with 0.45ms (at 32°C) in accordance with what had been reported from *in vivo* MNTB recordings (0.46ms) (Kopp-Scheinflug *et al.*, 2003), *in vitro* dual patch-clamp experiments (0.44ms at 36°C) (Borst *et al.*, 1995) and *in vitro* MEA recordings in the MNTB of gerbil (0.45ms at 35°C) (Haustein *et al.*, 2008). At 32°C MEA recordings were stable for up to 4h, enabling long-term recordings (Figure 3.14). This was an important finding which was the basis for the subsequent study of the effects of long-term perfusion of bilirubin on pre- and postsynaptic activity in the MNTB. It would be difficult to perform whole-cell patch-clamp recordings over this time-course because of run-down and stability issues.

8.1.2 Pharmacological characterisation of evoked MNTB field potentials

There was a clear distinction between pre- (C₁) and postsynaptic (C₂) components, since the sodium-channel antagonist TTX blocked all conducted activity (Figure 3.4), whilst Ca²⁺ free ACSF (Figure 3.5) blocked synaptic transmission (Borst *et al.*, 1995) and the AMPA/kainate receptor antagonist DNQX (Figure 3.6) also blocked glutamatergic synaptic transmission (Forsythe & Barnes-Davies, 1993; Barnes-Davies & Forsythe, 1995). NMDA receptors in the MNTB were blocked (Figure 3.7) by the antagonist AP-5 (Forsythe & Barnes-Davies, 1993), confirming the well-established presence of NMDA-Rs

on the principal neurons (Forsythe & Barnes-Davies, 1993; Barnes-Davies & Forsythe, 1995; Futai *et al.*, 2001; Steinert *et al.*, 2010b).

The K_v1 channel antagonist Dendrotoxin-I affected only post- and not presynaptic components (Figure 3.8), suggesting that axonal K_v1 s do not contribute much to the C_1 signal in MEA recordings. Another reason, which seems more likely, could be that K_v1 channels are localised juxtaparanodal at the Nodes of Ranvier in myelinated CNS axons (Rasband & Trimmer, 2001; Rasband, 2004). The localisation of K_v1 channels underneath the myelin sheath (Chiu & Ritchie, 1980) might shield them from DTX (as shown by (Devaux *et al.*, 2002)), because the paranode is thought to act as a diffusion barrier (Rasband, 2004). DTX-I used in these experiments blocked $K_v1.1$ and $K_v1.2$ channels, which led to multiple firing of the principal neurons in the MNTB (Brew & Forsythe, 1995; Dodson *et al.*, 2002b). This could cause more de-synchronised firing of the neurons, leading to a reduction in FP amplitude of C_2 . In the TEA experiment (Figure 3.9), a block of both pre- and postsynaptic K_v3 channels can be seen in the presence of 3mM TEA. $K_v3.1$ channels are present at the nodes of Ranvier (Devaux *et al.*, 2003) which are not covered by myelin. Therefore, TEA can block $K_v3.1$ s more easily compared to K_v1 s. Since the MEAs recorded field potentials, it was not possible to distinguish between axonal (Devaux *et al.*, 2003) or calyceal K_v3 channels (Dodson *et al.*, 2003; Elezgarai *et al.*, 2003; Ishikawa *et al.*, 2003). For this reason, they are here referred to as presynaptic, which in this case does not have to mean exclusively calyceal. The reduced (+) C_2 amplitude showed that TEA also blocked postsynaptic K_v3 channels (Brew & Forsythe, 1995; Elezgarai *et al.*, 2003; Steinert *et al.*, 2008). It is interesting to note that the (+) C_2 is reflecting the

activity of K_v3 potassium channels. This is in accordance with work from (Gold *et al.*, 2007) who showed that in recordings of extracellular APs the positive shoulder of the AP waveform ($(+)C_2$; see also Figure 3.2) represents the contribution of K^+ currents. This positive overshoot ($(+)C_2$) is seen mostly when the recording electrodes are close to the neuronal somata (Gold *et al.*, 2006). Modulatory effects of nitric oxide on MNTB postsynaptic AMPA receptors, NMDA receptors and K_v3 channels were first observed in whole-cell patch-clamp recordings in mice (Steinert *et al.*, 2008). The MEA recordings in the presence of NO-donor SNP showed a decreased C_2 component (Figure 3.10), indicating that in rat postsynaptic AMPA-R and NMDA-R were also depressed by NO. The TEA experiment showed that the $(+)C_2$ component reflects the contribution of K_v3 channels to the complex evoked response (Figure 3.9). In the presence of NO $(+)C_2$ was also reduced, confirming the inhibitory effects of NO on postsynaptic K_v3 channels in the MNTB also in rat brain slices (Steinert *et al.*, 2008).

The high variability of results during bilirubin perfusion in brainstem slices (Figures 3.11 & 3.13) and the absence of any effect on the jj-Gunn rat brain slices (Figure 3.15) were unexpected. These results suggest that inducing bilirubin toxicity *in vitro* may be indirect and/ or the presence of bilirubin alone might not be sufficient. It is possible that some kind of “priming” *in vivo* is necessary to see the detrimental effects of severe hyperbilirubinaemia over a short time-course. This is supported by Shapiro’s work showing decreased ABRs in jj-Gunn rats as early as 2 hours after sulfa administration *in vivo* (Shapiro, 1988), while in MEA experiments on slices it was not possible to see

consistent changes in the MNTB field potentials within 4 hours of bilirubin perfusion. As shown with the last set of experiments (Figures 6.1-6.3), NO is likely to play a crucial role in bilirubin-induced neurodegeneration. It could be speculated that free bilirubin activates eNOS before or during crossing the blood brain barrier. This source of NO is not available in *in vitro* brain slices. It still needs to be determined which pathways are actually activated that will lead to such a rapid neurodegeneration, which is detected by ABRs as early as 2h after sulfa administration (Shapiro, 1988). The inability to induce bilirubin toxicity *in vitro* by perfusing bilirubin onto the brain slices suggests at least two possibilities. First, there are factors available *in vivo* which are crucial for bilirubin-induced neurodegeneration (like NO) and that these factors are not available in the acute brainstem slice. Second, neuronal activity could play an important role for bilirubin to unfold its toxicity. Bilirubin has been shown to interact with cellular membranes and impair transmitter uptake into (Vazquez *et al.*, 1988; Ochoa *et al.*, 1993; Roseth *et al.*, 1998) and release from synaptic vesicles (Ochoa *et al.*, 1993; Hansen *et al.*, 1999). The MNTB is spontaneously active *in vivo* with mean firing rates of ~30Hz and maximal firing rates of ~130Hz in rat (Kopp-Scheinflug *et al.*, 2008). However, spontaneous activity in the MNTB has not been observed *in vitro*. If bilirubin needs to be taken up into the presynaptic terminals via endocytosis to cause degeneration, then the low stimulation frequency of MEA recordings (0.2Hz) might not be sufficient to cause enough bilirubin uptake into the presynaptic terminals.

8.2 Auditory brainstem recordings

Since the induction of bilirubin toxicity in *in vitro* slices was unsuccessful, the next best option of induction *in vivo* was chosen. Inducing severe bilirubin toxicity in jj-Gunn rats through administration of sulfadimethoxine or other sulfonamides has been done successfully for decades. The ABRs in jj-Gunn rats showed the well described decline in amplitude and increase in threshold of waves I, II and III (Shapiro, 1988; Shapiro, 1993; Shapiro *et al.*, 2007) 18 hours after sulfa-administration across all frequencies (Figure 3.16, 3.18 & 3.19). This was a positive confirmation that the right model for hyperbilirubinaemia was used. The most likely explanation for the decline in wave III was the finding that MNTB calyces are degenerated (Figure 5.2) and therefore do not transmit information across the synapse anymore. The EM results of the VCN showed degenerating endbulbs of Held and bushy neurons. This could explain the reduction in amplitude of wave II after 18h of acute hyperbilirubinaemia. Shapiro's group reported degenerated spiral ganglion cells in jj-Gunn rats 3 days after sulfa-injection (200mg/kg) (Shaia *et al.*, 2005). They also observed a significant loss of thick, myelinated axons in the auditory nerve of those treated jj-Gunn rats but could find no evidence of degenerated hair cells. Should these deficits already occur during the first 18h of acute bilirubin toxicity, this could explain why wave I is also reduced (Figure 3.16).

In accordance with earlier reports (Blanc & Johnson, 1959; Johnson *et al.*, 1959; Schutta & Johnson, 1971; Rose & Wisniewski, 1979; Shaia *et al.*, 2005), sulfadimethoxine only exerted its effects on homozygous Gunn rats. ABRs of wild-type Wistar rats were not affected (Figure 3.17-3.19). There is a theoretical possibility that sulfa may have beneficial effects on rats as it is an antibiotic; but

we are not aware of any reports of effects – beneficial or detrimental – of sulfadimethoxine on ABRs of heterozygous Gunn rats or wild-type rats. It has already been shown that sulfa has no effect on Jj Gunn rat ABRs (Shapiro, 1988). This is confirmed by the findings that Wistar (i.e. wild-type) rat ABRs were not altered after 18h sulfa-administration (Figure 3.17-3.19). That ABR responses in Wistar rats showed some variation is most likely explained with different positions of the subdermal recording electrodes. Even with great care, it could not be guaranteed that the recording electrode was in the exact same place 18h after the first recording, since it was removed whilst the animal was put back with its mother after recovery from anaesthesia. The same is of course true for the treated jj-Gunn rats. In their case an equivalent variation cannot be seen, as the individual components show such a strong reduction in amplitude.

8.3 MEA recordings from acute brainstem slices of treated jj-Gunn rats

Although the *in vitro* induction of bilirubin toxicity was unsuccessful, using the *in vivo* Gunn rat model was successful. Having confirmed that sulfa treatment reproducibly led to the typical symptoms of bilirubin encephalopathy (e.g. hearing impairment, ataxia), it was decided to continue the induction *in vivo* and use the brain tissue 18h after sulfa treatment for electrophysiological examinations and imaging experiments. The MEA recording from brain slices of treated jj-Gunn rats brought the first evidence that synaptic transmission at the level of the MNTB was disrupted (Figure 3.21). This was indicated by the significantly increased synaptic delay (from 0.45ms to 1.12ms) and vastly

reduced or absent C_2 component (Figure 3.21). The increased synaptic delay to 1.12ms in the MNTB in treated jj-Gunn rats was similar to the prolonged synaptic delay reported for the VCN in treated jj-Gunn rats (Zhang *et al.*, 1989). From their observations, the authors suggested a presynaptic failure as the cause for this significantly prolonged synaptic delay, which is very probable considering our EM data on the VCN. Interestingly, the timing and amplitude of C_1 was not different from the control group (Figure 3.21). This indicated that the AP conduction along the axon was not affected by toxic bilirubin levels. The structural integrity of the axons innervating the MNTB, which would account for the unchanged C_1 , was later confirmed by the dextran-labelling experiments (Figure 5.2). The conclusion one can draw from this data set is that it is only the calyces that are degenerating and that the contribution of activity from calyces to C_1 is rather small. Although MEA recordings showed a clear deficit in synaptic transmission in treated jj-Gunn rats, this method was not sufficient to tell whether the deficit originated pre- or postsynaptically or in both sites.

It is not clear what caused the small (0.02ms) yet significant ($p=0.03$, t-test) decrease in synaptic delay in sulfa-treated Wistar (wild-type) rats (0.44 ± 0.01 ms) compared to control rats (0.46 ± 0.01 ms) (Figure 3.20). One possibility could be slightly altered temperatures. Whilst the settings on the temperature control were such that the bath should always maintain $32\pm 1^\circ\text{C}$, the ambient temperatures can fluctuate between $19\text{-}24^\circ\text{C}$. As the heating system cannot perform any rapid temperature changes, an increased ambient temperature might have led to a slightly increased bath temperature. This could account for the small (0.02ms) decrease in synaptic delay in sulfa-treated Wistar rats, which were recorded during the summer months. Whilst for the *in*

vivo ABR recordings one could envisage a potential influence of sulfadimethoxine on the ABRs (which was not the case), it is not fathomable how this could be the case in the *in vitro* MEA recordings which show a shorter synaptic delay compared to control Wistar rats.

8.4 Patch-clamp recordings

After MEA recordings clearly showed bilirubin-induced distortion of synaptic transmission, single-cell recordings were performed to determine whether postsynaptic neurons were affected. With the existing literature on kernicterus in mind, the prediction was to find damaged neurons as the reason for synaptic failures, because in the cerebellum, the most extensively researched brain region affected in bilirubin encephalopathy, the Purkinje neurons are degenerating. It was therefore even more surprising to find no evidence of bilirubin-induced damage to the MNTB principal neurons, suggesting a presynaptic site of action for bilirubin.

The identical I-V-curves of control and treated rats (Figure 4.2) gave no indication that voltage-gated potassium channels were compromised in this acute phase of hyperbilirubinaemia. Combined with the finding that synaptic stimulation in treated Gunn rats did not yield any EPSCs that could be characterised as calyceal (Figure 4.1), i.e. low threshold, high amplitude (Hamann *et al.*, 2003), it indicated a presynaptic rather than a postsynaptic site of bilirubin damage. This is in stark contrast to other brain areas heavily affected during kernicterus, such as the cerebellum and basal ganglia, where the damage is postsynaptic.

It was interesting to see the decreased action potential threshold in the treated group (Figure 4.3). Although this decrease was not significant between controls and treated animals there still was a tendency. If the control group were subdivided into individual groups and the differences in threshold compared again, then the following result would occur: control jj-Gunn vs. treated jj-Gunn: n.s. $p=0.41$; control jj-Gunn vs. Wistar: n.s. $p=0.141$; and treated jj-Gunn vs. Wistar: * $p=0.025$ (t-test). This indicates that, although there was no significant change between the homozygous Gunn rat and the wild-type Wistar rat ($p=0.141$), the sulfa-treated Gunn rat has a significantly lower AP-threshold compared to Wistar rats ($p=0.025$). It could be speculated that the loss of input, i.e. the loss of the calyces as shown in chapter 5, could make the principal neurons more excitable. To clarify this issue, further experiments would be necessary. It should be controlled for the fact whether or not the wild-type principal neurons are synaptically connected or not. Since this was not controlled for in all of the current-clamp experiments, it would be desirable to determine whether this affects the result. Although interesting, this observation does not provide any new information since bilirubin toxicity did not cause a difference between control and treated jj-Gunn rats ($p=0.41$). This might have been expected on the assumption that bilirubin has a direct effect on the AP threshold by affecting ion channels. Since it had been shown before (Warr *et al.*, 2000) that bilirubin does not affect AMPA receptors, NMDA receptors or glutamate transporters directly, it was not tested again whether this was also true for the MNTB.

Another unexpected result is the apparent lack of difference in the properties of miniature EPSCs between control and treated group (Figures 4.4-4.5). From

the experiments in chapter 5 it is clear that the calyx terminals degenerate. This should lead to a decrease in miniature EPSCs. From the mini result it could be concluded that bilirubin does not directly influence neurotransmitter release. This was very surprising, since a number of papers showed that bilirubin directly affects the release of neurotransmitters such as acetylcholine (Ochoa *et al.*, 1993) and norepinephrine (Hansen *et al.*, 1999) or re-uptake of neurotransmitters into synaptic vesicles such as dopamine (Ochoa *et al.*, 1993; Roseth *et al.*, 1998) or glutamate (Roseth *et al.*, 1998). In addition, work from David Attwell's lab showed that bilirubin does not directly influence AMPA and NMDA receptors or glutamate transporters (Warr *et al.*, 2000). For this reason, a degenerated calyceal terminal was expected to show a reduced number of miniature EPSCs in principal neurons.

However, there have been a number of issues in the design of this particular experiment. It is known that the MNTB principal neurons receive non-calyceal glycinergic (Banks & Smith, 1992; Forsythe & Barnes-Davies, 1993; Wu & Kelly, 1995) and GABAergic (Adams & Mugnaini, 1990; Suneja *et al.*, 1995; Wu & Kelly, 1995) inputs, but neither GABA nor glycine receptors were blocked in this experiment. Therefore it is not possible to distinguish between calyceal and non-calyceal miniature EPSCs. Secondly, it was not checked if the control principal neurons were synaptically connected after the slicing process. Therefore, recordings from control neurons without intact calyces might have been made and it is not possible to make any statements about the influence of bilirubin on miniature EPSCs. In summary, the mini recordings were merely a by-product of the other voltage-clamp experiments, not a separately designed study with the aim of investigating the influence of bilirubin on transmitter

release. For this reason, the data cannot be used to help answer the question of bilirubin toxicity at the calyx of Held synapse and are only shown for completion.

Taken together, the results of *in vivo* and *in vitro* experiments at this stage point towards a presynaptic failure but different approaches are required to prove that. The imaging experiments and their relevance to the overall findings are discussed next.

8.5 Calcium-Imaging

The results presented in chapter 5 demonstrated that the presynaptic terminals degenerated, whilst postsynaptic principal neurons stayed intact – as indicated through electrophysiology in chapter 4. Before the light and electron microscopy examinations of MNTB and VCN were conducted, calcium-imaging was employed to test if basal postsynaptic intracellular calcium levels were changed by bilirubin (Figure 5.1). The values for basal $[Ca^{2+}]_i$ of MNTB neurons in Jj-Gunn rats (236nM) were similar to values recently published for MNTB neurons in acute slices from Lister Hooded rats (283nM, (Tong *et al.*, 2010)). The small difference might be due to the different ages used by Tong and colleagues (P9-12) and in this thesis (P15). The MNTB expresses both parvalbumin and calbindin (Caicedo *et al.*, 1996). Friauf demonstrated that there is a strong developmental increase in the expression of calbindin in the MNTB from P10 onwards until about P21 (Friauf, 1993) with a pronounced increase between P11 and P15. This increased calcium-buffer capacity could explain why basal

$[Ca^{2+}]_i$ in the older Jj-Gunn rats was slightly lower compared to the relatively young Lister Hooded rats.

The calcium-imaging results revealed a difference between Jj and jj-Gunn rats in resting $[Ca^{2+}]_i$. Interestingly, 18h acute hyperbilirubinaemia did not change the basal $[Ca^{2+}]_i$ between control and treated jj-Gunn rats (Figure 5.1). It is not clear what causes the different resting intracellular calcium concentrations between hetero- and homozygous Gunn rats. Since jj-Gunn rats are exposed to constant small doses of bilirubin (as seen in the spontaneous occurrence of inclusion bodies in the cerebellum) the low resting $[Ca^{2+}]_i$ in jj-Gunn rats could be a sign that Ca^{2+} is well buffered to minimise toxic effects.

An increased expression of calcium-binding proteins in jj-Gunn rats is unlikely to account for the decreased basal $[Ca^{2+}]_i$, since it was shown that there is no change in expression of calbindin and parvalbumin in the MNTB between Jj and treated jj-Gunn rats (Spencer *et al.*, 2002). However, the work by Spencer and colleagues did not use quantitative methods like western blots or quantitative PCR, but used immunohistochemistry. There may after all be a change in the availability of parvalbumin and calbindin which was not detected by immunohistochemistry. Also, the paper by (Spencer *et al.*, 2002) did not compare expression levels of calcium-binding proteins between control and treated jj-Gunn rats, the result of which would be interesting to know. In addition, the numbers of animals used in this thesis for calcium imaging were low ($n=2$), although the cell numbers were double-digits. We have seen that jj-Gunn rats can display very individual susceptibility to the sulfa-treatment: some show strong signs of severe hyperbilirubinaemia, while others seem to be hardly affected with the same dose of sulfadimethoxine. To rule out the

possibility that the 2 tested control jj-Gunn rats were highly susceptible, it would be worth testing 2 more animals for each condition to see if the low numbers might have introduced any bias. So far, the exact cause of the different $[Ca^{2+}]_i$ remains unknown and a more detailed study would be necessary to clarify if this is a real difference caused by the different genetic background. More importantly, the differences in $[Ca^{2+}]_i$ did not influence the measured electrophysiological properties of MNTB principal neurons and it is evident that acute bilirubin encephalopathy did not change $[Ca^{2+}]_i$ in jj-Gunn rats.

8.6 Dextran labelling and live multi-photon imaging

The dextran-labelling of calyceal terminals was the crucial experiment that revealed the structural loss of the calyx terminal as a result of 18 hours hyperbilirubinaemia (Figure 5.2). It demonstrated that 3h incubation was long enough to transport dextran-tetramethyl-rhodamine (MW 3000 (Fritsch, 1993)) from the globular bushy cells in the AVCN to the calyceal terminals in the MNTB (Kuwabara *et al.*, 1991). The mean surface area of the healthy calyces ($2334 \pm 301 \mu m^2$) was very similar to previously published results ($2484 \mu m^2$) (Sätzler *et al.*, 2002). Whilst control animals showed healthy, dye-filled calyces, treated animals showed either debris or infrequently damaged calyces. This raised the question if the degenerated calyces might be a consequence of axonal degeneration. No evidence was found for axonal degeneration, since axons were well labelled also in treated animals. This indicated that the lack of dye-filled calyces was not a failure of active dye-transport along the axons due to degeneration. In addition, it would be expected to observe changes in the C_1

component of MEA recordings if the axons were damaged and thus unable to propagate APs. This was not the case, since MEA recordings from treated jj-Gunn rats did not show any changes in timing or amplitude of the conducted component C_1 (Figure 3.21). The dye-containing debris, which was visible in treated animals, might be remains of broken-up calyces, or even dye leaked from axons after destruction of the calyces.

8.7 Light and electron microscopy in the cerebellum

Light microscopy confirmed that damage in the cerebellum was purely limited to Purkinje neurons. It was striking to see the inclusion bodies in degenerating Purkinje neurons already at lower magnifications in control and treated jj-Gunn rats, whilst all other cells did not show any signs of damage, even at higher magnifications (Figure 5.3).

Light and electron microscopic images from the cerebellum were used as a built-in control, to check that bilirubin had actually entered the brain after sulfa administration, in addition to behavioural signs. Comparing the work presented here with earlier papers using electron microscopy in the cerebellum revealed that images presented in this thesis were identical with previously published data (Schutta & Johnson, 1969; Rose & Wisniewski, 1979; Takagishi, 1989; Takagishi & Yamamura, 1989). This demonstrated that the tissue preparation methods used in this thesis worked well and did not introduce any distortions. This increased the confidence that the changes observed between control and treated animals were real and not artefacts of the tissue preparation. The fact that no inclusion bodies were found in Purkinje cells of Wistar and Jj-Gunn rats

(Figure 5.4), but always some in control jj-Gunn rats was further confirmation that the right animal model in the correct conditions was used as this had been described before (Schutta & Johnson, 1967). It had also been demonstrated previously that untreated jj-Gunn rats show spontaneous inclusion bodies in the cerebellum (Schutta & Johnson, 1967, 1969; Rose & Wisniewski, 1979; Takagishi, 1989) and substantia nigra (Batty & Millhouse, 1976). Since the cerebellum has long been the aim of investigations in hyperbilirubinaemia and kernicterus (Schutta & Johnson, 1967; Silberberg & Schutta, 1967; Schutta & Johnson, 1969, 1971; Sawasaki *et al.*, 1976; Rose & Wisniewski, 1979; Mikoshiba *et al.*, 1980; Moore & Karp, 1980; Takagishi & Yamamura, 1989; Conlee & Shapiro, 1997), it was decided not to analyse the data as this had already been done many times. The focus for analysis was instead put on the MNTB and later also on the VCN.

8.8 Light and electron microscopy in the MNTB

It was surprising to find no changes between control and treated MNTBs at the light microscopic level (Figure 5.5). The images in this thesis were identical with previous work (Casey & Feldman, 1982). Perhaps it was this apparent lack of signs of postsynaptic degeneration in the treated MNTB that has caused no other group to test if the presynaptic terminals are still intact in hyperbilirubinaemic Gunn rats. Comparing the work presented here with previous papers using electron microscopy in the MNTB showed that images from this thesis are identical with earlier data (Lenn & Reese, 1966; Casey & Feldman, 1985; Casey & Feldman, 1988; Smith *et al.*, 1998). This confirmed

that tissue preparation methods worked well and did not introduce any distortions. Therefore it was concluded that the observed abnormalities were not due to the tissue processing methods but real changes that occurred in the living animal. EM images confirmed the findings at LM level, namely the lack of postsynaptic hallmarks of degeneration in the MNTB of the treated group (Figures 5.6-5.7). The imaging results also confirmed patch-clamp and calcium-imaging results of no apparent changes in the principal neurons as a result of bilirubin exposure. The LM and EM results could not confirm work done by Shapiro and Conlee (Conlee & Shapiro, 1991; Shapiro & Conlee, 1991) who described a reduction in size of both MNTB and CN, implying a loss of cells. In the present study no signs of postsynaptic degeneration or cell death were observed in the MNTB. However, their studies and the analysis were not done acutely but 5 days after sulfa injection. It is feasible to assume that, during this time period, the degeneration could have also affected the neurons and astrocytes, thereby leading to increased numbers of dead cells. The reduced number of presynaptic profiles in the EM images (Figure 5.7) was the most striking finding. This loss of presynaptic terminals confirmed the dextran-labelling results and can explain the impaired synaptic transmission, as seen with MEAs, Patch-Clamp recordings during synaptic stimulation and eventually the ABR failures of waveform III.

8.9 Light and electron microscopy in the VCN

In the VCN, differences between control and treated Gunn rats were already visible at the level of light microscopy. In contrast to the MNTB, the cytoplasm of VCN bushy neurons had a grainy appearance, as opposed to the smooth appearance of bushy cells from control jj-Gunn rats (Figure 5.8). That this grainy appearance of the cytoplasm was confined to the bushy cells and did not affect other cell types (Figure 5.8) indicated a particular vulnerability of these cells. EM images of the same neurons then revealed that the grainy appearance was due to distorted mitochondria with glycogen bodies.

The EM images of large spherical neurons of the VCN closely resembled those published previously (Ryugo *et al.*, 1996; Wang *et al.*, 1998b; Nicol & Walmsley, 2002; Baker *et al.*, 2010) as images of bushy neurons of the AVCN. This increased the confidence that the correct cells had been chosen for analysis. Compared to the MNTB, the VCN showed a slightly different picture regarding the cellular damage. As in the MNTB, presynaptic profiles were significantly reduced in number and length in treated animals (Figure 5.10). This confirmed a suggestion made by Zhang and colleagues in 1989. After observing a significantly prolonged synaptic delay transmission in the VCN of treated jj-Gunn rats, they suggested a presynaptic failure as the most likely cause (Zhang *et al.*, 1989). In addition, also postsynaptic bushy neurons showed signs of neurodegeneration, such as glycogen bodies and vacuolation in mitochondria (Figure 5.9). These postsynaptic changes have been described earlier in EM investigations of the CN, and especially the AVCN (Jew & Williams, 1977; Jew & Sandquist, 1979). However, the aforementioned two studies used homozygous Gunn rats without additional sulfa-administration.

This means that some of the postsynaptic changes, namely glycogen bodies in mitochondria, can occur without causing any clinical symptoms. This is in accordance with the findings of this thesis, as here too signs of degeneration in the bushy neurons of control homozygous Gunn rats were observed (Figure 5.9). However, these signs of postsynaptic degeneration were less frequently found in control compared to treated jj-Gunn rats. The appearance of autophagosomes in the treated VCN also indicated that cell damage there was more severe than in control jj-Gunn rats or in the MNTB. Earlier studies found no, postsynaptic degeneration in the AVCN in heterozygous or wild-type rats (Jew & Williams, 1977; Jew & Sandquist, 1979), something that was not tested for in this thesis because of time constraints. The starting degeneration of the globular bushy neurons could be the trigger for the calyx degeneration of the calyces in the MNTB. However, this cannot be the only explanation for the degenerating calyces. Due to the short time course of only 18h, it is more feasible that the degeneration in VCN and MNTB happen simultaneously. An early paper described changes in the MNTB after ablation of the cochlear nucleus (Morest & Jean-Baptiste, 1975). After 2 days, the following changes were described in the calyces: marked increase in neurofilaments, reduced numbers of vesicles, loss of mitochondria, and appearance of vacuoles. In addition, they stated that some calyces appeared shrunken but did not provide any measurements. These changes intensified at 4 and 7 days after ablation of the cochlear nucleus. At day 7 after CN ablation, the calyces had disappeared and many large, myelinated preterminal fibres were degenerated (Morest & Jean-Baptiste, 1975). Our experiments showed the loss of calyces already after 18h. It is therefore possible that the beginning destruction of globular bushy

neurons is a contributing factor but it is unlikely to be the only reason for presynaptic degeneration in hyperbilirubinaemia. More likely, bilirubin acts simultaneously on the VCN and MNTB, most likely through the excessive production of NO (see chapter 6).

Also in contrast to the MNTB, axonal profiles in the VCN displayed signs of degeneration, for example swollen and distorted mitochondria. This axonal degeneration might be correlated with reported degeneration of spiral ganglion cells (Shaia *et al.*, 2005). Although Shaia and colleagues used 3 days exposure time between sulfa injection and data acquisition, it is possible that the damage starts to occur already within 18 hours. A degeneration of spiral ganglion cells would also explain the reduced amplitude of wave I in the ABRs.

Neuronal degeneration in severe hyperbilirubinaemia is commonly seen in many brain areas. However, it seems that different mechanisms might be involved in the processes in different brain regions. In the cerebellum, it is almost exclusively the Purkinje neurons that undergo degeneration. Presynaptic structures of parallel fibres remain even without their postsynaptic counterparts (Takagishi & Yamamura, 1994). In the MNTB (at least at this very acute stage), it is only the presynaptic terminals that are degenerating, sparing the postsynaptic neurons. In the VCN, both pre- and postsynapse show signs of neurodegeneration. This confirms the overall finding that bilirubin affects very specific structures in certain areas of the brain and does not exert a general toxic effect everywhere to the same extent.

8.10 Presynaptic degeneration

This thesis and the paper (Haustein *et al.*, 2010) were not the first reports on presynaptic degeneration in the CNS or specifically the calyx of Held synapse.

In 2004, a paper described a transgenic mouse in which the complete knock-out of synaptic vesicle protein CSP α led to degeneration of calyces of Held after 2-4 weeks of life (figure 8). This knock-out of CSP α was lethal within 2 months of life (Fernández-Chacón *et al.*, 2004).

Age-related changes have also been well described in the MNTB, especially the loss of calyceal terminals with age (Casey & Feldman, 1985; Casey & Feldman, 1988). Not only calyces were lost but there was also a decrease in the mean number of rat principal neurons by 34% with age (2-3months vs. 2 years) (Casey & Feldman, 1982). The signs of degeneration in calyces in rats older than 24months included vacuoles, multivesicular bodies, increase in electron density and presence of multiple extracellular spaces between calyx and soma (Casey & Feldman, 1985). Between 3 and 27-33 months Casey and Feldman found a reduction of neuron surface area contacted by calyces from 47.1% to 29.9% but no reduction in non-calyceal inputs (Casey & Feldman, 1988). The average number of calyceal profiles contacting principal neurons was reduced from 15.1 in young to 9.9 in old rats (Casey & Feldman, 1988). The EM experiments in this thesis demonstrated a similar reduction in the length and number (11 vs. 7) of presynaptic profiles, not over months but over hours. However, we did not distinguish between calyceal and non-calyceal inputs. So it might be that the number of calyceal profiles could be much lower, if in treated jj-Gunn rats the non-calyceal inputs are not degenerating either.

The fact that, in Gunn rats, none of the age-related signs of degeneration were found indicated that 18 hours was a time point where the degeneration was so advanced that all that was visible was the loss of calyceal terminals.

There are two other papers worth mentioning in this context which investigated changes in the MNTB after ablation of either the cochlea (Jean-Baptiste & Morest, 1975) or the cochlear nucleus (Morest & Jean-Baptiste, 1975). 15 days after cochlea ablation, specific morphological changes were found in calyceal terminals whilst no changes in terminals or neurons were observed after 11h, 2d or 4d (Jean-Baptiste & Morest, 1975). Degeneration was sped up after CN ablation (Morest & Jean-Baptiste, 1975). However, the morphological changes in calyces were similar in both experiments: depletion of synaptic vesicles and mitochondria, a marked increase in the number of neurofilaments; vacuolated remains of mitochondria, occasionally with dense bodies. Two days after CN ablation, some calyces appeared shrunken and glia cells were seen engulfing degenerating calyceal processes (Morest & Jean-Baptiste, 1975). At day 7 after the CN ablation, no calyces could be seen and many large, myelinated preterminal axons were degenerated. The fact that none of the changes in calyceal terminals described above were found in the present experiments could raise two possibilities: first, the 18h bilirubin exposure time point chosen shows a different stage of degeneration than Morest and Jean-Baptiste described. The second, more likely, explanation is that bilirubin-induced presynaptic degeneration in the MNTB occurred independently of events in the CN. This in turn suggests that different mechanisms might be involved.

All the papers mentioned above studied degeneration at the calyx of Held synapse that occurred over longer time courses of at least 2 days (Morest &

Jean-Baptiste, 1975), often over weeks (Jean-Baptiste & Morest, 1975; Fernández-Chacón *et al.*, 2004) or years (Casey & Feldman, 1982; Casey & Feldman, 1985; Casey & Feldman, 1988). The early changes in the work of (Jean-Baptiste & Morest, 1975) only appeared 15 days after cochlea ablation and slightly accelerated after 2 days of the ablation of the cochlea nucleus (Morest & Jean-Baptiste, 1975). Even though some changes appeared as early as 2 days after CN ablation, they were by no means as rapid as in the Gunn rat model of hyperbilirubinaemia with calyceal degeneration and absence of healthy presynaptic terminal within 18h. This demonstrated that the degeneration of calyceal terminals could not be caused by the damage to bushy neurons in the VCN alone. It rather implies that bilirubin acted simultaneously at many different sites.

Presynaptic degeneration has also been described in other areas of the brain and been linked to neurodegenerative disorders. In prion disease, a loss of presynaptic terminals has been observed (Gray *et al.*, 2009; Siskova *et al.*, 2009; Hugh Perry & O'Connor, 2010). Changes to alpha-synuclein and other presynaptic proteins have been linked to presynaptic terminal loss in Alzheimer's disease (AD) (Honer, 2003). Furthermore alpha-synuclein aggregation at presynaptic terminals is linked to neurotransmitter deprivation in Parkinson's disease (PD) (Schulz-Schaeffer, 2010) and loss of dendritic spines in dementia (Kramer & Schulz-Schaeffer, 2007).

Whether or not these changes in presynaptic morphology share common mechanisms (i.e. alterations to presynaptic proteins like alpha-synuclein) or are completely different from changes occurring in the MNTB during bilirubin

toxicity remains to be seen. The question of the potential role of NO in the degeneration process demands further investigation and is discussed in the following section.

8.11 The role of nitric oxide (NO) in bilirubin-induced neurodegeneration

The protection of the ABRs and the synaptic delay in the MNTB measured with MEAs by 7-NI was highly significant (Figure 6.1 & 6.3), suggesting a crucial role for NO in bilirubin-induced neurodegeneration. Significantly elevated ABR thresholds between Wistar controls and 7-NI treated jj-Gunn rats indicated that the protection from bilirubin-neurotoxicity - although very substantial - was not 100% complete (Figure 6.1 & 6.2). The difference of ABR thresholds at 12kHz between Wistar and 7-NI rats showed a 'non significant' result ($p=0.051$) (Figure 6.2). This could be down to the small sample size ($n=4$ each) or indicate very good protection by 7-NI.

8.11.1 *Practical challenges of working with 7-NI in vivo*

It was not surprising to find that 7-NI, largely but not completely, protected from bilirubin neurotoxicity. This result is most likely explained by the following: the half-life of 7-NI is only about 90mins at 50mg/kg (Bush & Pollack, 2000), but the exposure-time to bilirubin is 18 hours. The IC_{50}^2 of 7-NI is $1\mu\text{M}$ *in vitro* (Babbedge *et al.*, 1993; MacKenzie *et al.*, 1994). The serum concentration of 7-

² IC_{50} is the concentration of a compound at which it inhibits 50% of the biological activity. Here it is the concentration of 7-NI at which it inhibits 50% of the enzyme activity of neuronal nitric oxide synthase (nNOS).

NI 4-6h after i/p injection of 50mg/kg 7-NI is still above the IC₅₀ (Bush & Pollack, 2000). Since a concentration of 150mg/kg instead of 50mg/kg 7-NI was used, it is reasonable to assume that protection is provided for approximately the first 6-8 hours but not for the whole 18 hours. Due to this discrepancy, a second injection of 7-NI or even multiple doses might bring better protection as it keeps the concentration of 7-NI above the IC₅₀ (Bush & Pollack, 2001). Despite the potentially more complete protection, it was decided to not do a second injection because this would have meant a change of protocol after 2 animals had already been studied and that data might not have been comparable. Therefore, a single initial dose was used for all experiments, with a concentration that is at the upper end of concentrations used *in vivo* (Ison *et al.*, 2009).

Unfortunately, the block of NO has significant side effects. For example, NO inhibition disturbed the wake-sleep cycle by prolonging the phases (Ribeiro & Kapas, 2005). (Hermansteyne *et al.*, 2010) reported strong expression of Kv2.2 in area of brain involved in wake/sleep cycle and motivation (magnocellular preoptic nucleus (MCPO) and the horizontal limb of the diagonal band of Broca (HDB) of the basal forebrain complex). These areas also have high nNOS expression. Work in Ian Forsythe's group (Steinert *et al.*, "Nitric oxide is an activity-dependent homeostatic regulator of neuronal intrinsic excitability" *submitted*) demonstrated that NO is regulating Kv2.2 channels. A block of nNOS would therefore critically affect motivation & wake/sleep cycle, which was already observed in 7-NI treated Gunn rats.

Another side effect of blocking NO was the drooping of eye-lids (ptosis) and loss of righting reflex (Dzoljic *et al.*, 1996). Increased duration of diazepam-

induced sleep (Talarek & Fidecka, 2004) added to the challenges. As midazolam was used for the anaesthesia during ABRs, the combination with 7-NI delayed the waking up and thereby movement of the rats. An additional practical complication was that the experimental rats were between 2-3 weeks old and not yet weaned. This meant that rats undergoing ABRs and therefore anaesthesia had to be able to wake up completely to compete for food from their mother with their litter-mates. In terms of animal care and welfare, it was therefore challenging to come up with an experimental design over 18 or 24h in which the rats potentially did not have motivation or are too sleepy to feed from their mother. This hurdle will need to be overcome before further tests can be carried out. One way to increase protection from bilirubin-induced neurotoxicity might be to use a second or third dose of 7-NI with lower concentrations. However, this could potentially intensify these side effects, making it difficult to practically perform this experiment. Since a single high dose of 7-NI (150mg/kg) was used, the next experiment could be to test if halving the 7-NI concentration but giving it twice would reduce some of the side effects and still give good protection from bilirubin-induced toxicity of the hearing system.

8.11.2 Nitric oxide and neurotoxicity

It has been suggested that the combination of nNOS & NMDA receptor (NMDA-R) blocker might be another way to increase protection from bilirubin toxicity, as NMDA-Rs have been implicated as part of bilirubin-induced toxicity (McDonald *et al.*, 1998; Brito *et al.*, 2010).

The results from the 7-NI experiments added another piece to the puzzle of bilirubin encephalopathy. It strengthened the case for involvement of NO, potentially via NMDA receptors in neurons. NMDA-Rs and nNOS are tightly coupled at the postsynaptic density (PSD-95) through their mutual PDZ binding motifs (Brenman *et al.*, 1996). The activation of Ca²⁺ permeable NMDA-Rs and Ca²⁺ influx can stimulate Ca²⁺/calmodulin which in turn activates nNOS (Bredt & Snyder, 1990) to produce NO. It was shown that with increasing concentration both NMDA and sodium nitro-prusside (SNP, a NO donor) similarly increased cell death (Dawson *et al.*, 1993). The block of calmodulin in neuronal cell culture (hippocampus, cortex, striatum) attenuated cell death, indicating a link between NMDA and NO neurotoxicity (Dawson *et al.*, 1993). NO might then react with O₂ and form peroxynitrite (ONOO⁻); ONOO⁻ could lead to a wealth of neurotoxic actions, including inhibition of mitochondrial respiration, lipid peroxidation and DNA damage (Steinert *et al.*, 2010a). However, AMPA receptors in the MNTB – as well as in basket cells in the dentate gyrus of the hippocampus (Geiger *et al.*, 1995; Koh *et al.*, 1995) – have been found to be calcium-permeable (Geiger *et al.*, 1995; Joshi *et al.*, 2004). Although AMPA/kainate receptors are about 70-fold less permeable to calcium compared to NMDA receptors (Mayer & Westbrook, 1987), they would still contribute to the calcium influx. Therefore, although NMDA blockers have reduced neurotoxic effects of bilirubin in cortical cultures (Brito *et al.*, 2010) or striatum and hippocampus (McDonald *et al.*, 1998), they might not do so in the MNTB. Neuronal NOS and soluble guanylyl cyclase (sGC) are expressed in rat VCN and central fibres of auditory nerve stained positively for nNOS (Burette *et al.*, 2001). MNTB principal neurons also have a high expression of nNOS and sGC

(Fessenden *et al.*, 1999; Steinert *et al.*, 2008). In this thesis and in other papers (Conlee & Shapiro, 1991; Shapiro & Conlee, 1991; Shaia *et al.*, 2005), it has been demonstrated that VCN and MNTB are heavily affected by bilirubin-induced damage. Since bilirubin was shown to up-regulate nNOS expression (Brito *et al.*, 2010), the differential expression of nNOS and sGC throughout the brain could explain why certain brain regions are more susceptible than others. If NO was a key player in bilirubin-induced neurodegeneration, then the damage would be expected to be more severe in areas with high expression of both enzymes like the cerebellum, the MNTB and the VCN.

In the light of these findings, the fact that a block of either NO or NMDA reduces bilirubin neurotoxicity is no longer surprising. The group of Dora Brites in Lisbon suggested the following scenario for neuronal oxidative damage through bilirubin (Brito *et al.*, 2010): bilirubin leads to glutamate release, which in turn stimulates NMDA receptors. This causes activation of nNOS and release of NO. In response to NO release the neurons then activate sGC producing cGMP (Moro *et al.*, 1996), which in excess could lead to oxidative disruption, mitochondrial dysfunction and eventually cell death.

However, the initial step in this proposed cascade contradicts findings by David Attwell's group, namely that bilirubin does not directly influence AMPA receptors, NMDA receptors or glutamate transporters (Warr *et al.*, 2000). Therefore the question of how excess levels of bilirubin increase nNOS expression and activate toxic NO production is still not fully answered and needs further investigation.

The inhibition of nNOS is suggested as a novel therapeutic approach in the prevention of bilirubin-induced neurodegeneration. If 7-NI or any other suitable

nNOS antagonist could be applied locally to the CNS rather than globally as done in this thesis, this could increase the duration of protection, decrease the concentration necessary and therefore potentially reduce the side-effects described in 8.11.1. To increase clinical relevance, it should be determined how it is possible to administer nNOS antagonists many hours after the insult and still protect from neurodegeneration.

8.11.3 *Astrocytes and bilirubin-induced neurotoxicity*

It was shown that bilirubin is toxic to neurons and astrocytes in different ways. Whilst neurons were more susceptible to cell death through necrosis or apoptosis, astrocytes were more prone to inhibition of glutamate uptake (Silva *et al.*, 2002). It has been reported that neurons are more vulnerable to death through bilirubin toxicity than astrocytes (Falcão *et al.*, 2006; Brito *et al.*, 2008b). However, it could be speculated that the presynaptic degeneration in the MNTB is linked to inflammatory processes because it has been shown that unconjugated bilirubin (UCB) activates glia cells, leading to a secretion of pro-inflammatory cytokines TNF-alpha, IL-1 and IL-6 (Falcão *et al.*, 2006; Fernandes *et al.*, 2006; Gordo *et al.*, 2006; Falcão *et al.*, 2007; Fernandes *et al.*, 2007). It has also been reported that UCB induces up-regulation of the transporter multidrug resistance-associated protein 1 (Mrp1) (Gennuso *et al.*, 2004). Mrp1, an ATP dependent efflux pump, was shown to mediate UCB transport across the cell membrane (Rigato *et al.*, 2004). In cultured astrocytes, this bilirubin-induced up-regulation protects the astrocytes from bilirubin-induced damage (Gennuso *et al.*, 2004). Since Mrp1 has been shown to also

be expressed in neurons (Falcão *et al.*, 2007) and that block of Mrp1 in the presence of unconjugated bilirubin increased cell death of neurons (Falcão *et al.*, 2007), it seems reasonable to assume that the toxicity of bilirubin is determined by its concentration.

Since the involvement of NO in the degeneration process has been demonstrated, it would also be interesting to investigate to what extent the glia cells at the calyx of Held/MNTB synapse are affected. The MNTB contains both astrocytes (Reyes-Haro *et al.*, 2010) and NG2+ glia cells, the latter of which receive glutamatergic inputs in the MNTB (Müller *et al.*, 2009). *In vitro* work in cortical cell cultures of astrocytes and neurons showed that UCB activated astrocytes and led to increased cell death in astrocytes and neurons (Falcão *et al.*, 2006; Brito *et al.*, 2008b), suggesting a potential role for astrocytes in neurodegeneration also *in vivo*.

Further questions remain and could prompt new experiments in order to answer them. It is intriguing to observe the differential effects of bilirubin-induced neurotoxicity on pre- and postsynaptic sites in MNTB and VCN. Future experiments should be aimed at determining how the differential effects of NO occur and what role activity dependence plays since neurodegeneration was triggered only *in vivo* but could not be reproduced *in vitro*.

- Since nNOS is expressed in MNTB neurons and not in the calyces, but the calyces are degenerating and not the neurons: what are the differential effects of NO on the calyx and on the principal neuron?
- Does bilirubin need to be taken up into the presynaptic terminal by endocytosis to cause degeneration?

- Is synaptic activity important for bilirubin-induced presynaptic degeneration in the MNTB and VCN? If it is, could increased synaptic stimulation combined with bilirubin perfusion of the brain slices in MEA recordings create an *in vitro* model of bilirubin neurotoxicity?

Since waves I and II of the ABR are impaired after 18h sulfa treatment, the auditory pathway presents an interesting target for further tests. Experiments could be aimed to answer the following questions:

- To what extent are spiral ganglion cells and axons of the auditory nerve (Shaia *et al.*, 2005) affected after 18h hyperbilirubinaemia and to what extent does 7-NI provide protection?
- How would EM images of VCN and MNTB from jj-Gunn rats treated with 7-NI differ from those presented in this thesis (i.e., without 7-NI)? Is there any difference compared to sulfa-treated Gunn rats? If there was a difference, is it site-specific, i.e. pre and/or postsynaptic?
- What are the time-courses of pre- and postsynaptic degeneration *in vivo* in MNTB and VCN?
- What is the pathway responsible for excess levels of bilirubin to lead to production of NO at neurotoxic concentrations?

In the light of the wealth of *in vitro* data, especially recent work on cultured cortical neurons and astrocytes, further investigations should aim to determine the *in vivo* relevance of these *in vitro* data. Since Brito et al (2010) demonstrated that bilirubin leads to increased nNOS expression in neuronal cultures the following questions arise:

- Do jj-Gunn rats have higher nNOS expression compared to Jj-Gunn rats and could they be therefore more susceptible to bilirubin neurotoxicity?
- Does the scenario suggested by Brito et al (2010) (see page 159 in this thesis for a brief summary) for bilirubin toxicity also occur in the Gunn rat *in vivo*?
- To what extent are astrocytes and microglia involved *in vivo* in bilirubin-induced neurodegeneration? Is their role protective or destructive?

Finally, the clinical relevance of using certain drugs to fight bilirubin-induced neurodegeneration should be determined in a series of time-course experiments. Experiments could follow the design of a recent study (Rice *et al.*, 2011). Rice and colleagues investigated the effects of minocycline injection 30mins and 120mins after sulfa administration in jj-Gunn rats to test for neuroprotective effects on ABRs. The outcome was that 30mins did protect ABRs in the Gunn rats but 120mins did not. The questions to follow on from the data presented here would be:

- At what time point after sulfa-administration would intervention with 7-NI still be protective?
- How many injections (one, two, multiple) at which concentrations provide the best outcome with the least side effects?

To know these time-courses for nNOS inhibitors as well as concentrations which cause a minimum of side effects could become relevant in a clinical setting.

8.12 Summary:

Acute bilirubin encephalopathy causes presynaptic degeneration within 18 hours in the Gunn rat model of hyperbilirubinaemia, as shown by live multiphoton imaging of the presynaptic terminals and electron microscopy. This leads to impaired synaptic transmission in the MNTB as shown by MEA and patch-clamp recordings, without affecting the postsynaptic neurons. The integrity of postsynaptic principal neurons was confirmed by voltage- and current-clamp single-cell recordings, calcium-imaging and electron microscopy. Auditory Brainstem Responses show reduced amplitudes as a consequence of the presynaptic degeneration in VCN and MNTB. Presynaptic degeneration in the MNTB occurs most likely independently of neurodegeneration of bushy neurons in the VCN. Nitric oxide is involved in the degeneration process, since block of nNOS rescues the ABRs and synaptic transmission in the MNTB. The inhibition of nNOS is suggested as a new therapeutic approach for prevention of bilirubin-induced neurodegeneration.

REFERENCES

- Abu-Bakar Ae, Moore MR & Lang MA. (2005). Evidence for induced microsomal bilirubin degradation by cytochrome P450 2A5. *Biochemical Pharmacology* **70**, 1527-1535.
- Adams JC & Mugnaini E. (1990). Immunocytochemical evidence for inhibitory and disinhibitory circuits in the superior olive. *Hearing Research* **49**, 281-298.
- Agrawal VK, Shukla R, Misra PK, Kapoor RK & Malik GK. (1998). Brainstem auditory evoked response in newborns with hyperbilirubinemia. *Indian Pediatrics* **35**, 513-518.
- Ahdab-Barmada M & Moossy J. (1984). The Neuropathology of Kernicterus in the Premature Neonate: Diagnostic Problems. *Journal of Neuropathology & Experimental Neurology* **43**, 45-56.
- Ahlfors CE. (2010). Predicting bilirubin neurotoxicity in jaundiced newborns. *Current Opinion in Pediatrics* **22**, 129-133.
- Ahlfors CE & Parker AE. (2008). Unbound Bilirubin Concentration is Associated With Abnormal Automated Auditory Brainstem Response for Jaundiced Newborns. *Pediatrics* **121**, 976-978.
- Ahlfors CE, Wennberg RP, Ostrow JD & Tiribelli C. (2009). Unbound (Free) Bilirubin (Bf): Improving the Paradigm for Evaluating Neonatal Jaundice. *Clinical Chemistry* **55**, 1288-1299.
- Altman M, Vanpée M, Cnattingius S & Norman M. (2011). Neonatal Morbidity in Moderately Preterm Infants: A Swedish National Population-Based Study. *The Journal of Pediatrics* **158**, 239-244.
- American Academy of Pediatrics Subcommittee on Neonatal Hyperbilirubinemia. (2001). Neonatal Jaundice and Kernicterus. *Pediatrics* **108**, 763-765.
- Amin SB, Ahlfors C, Orlando MS, Dalzell LE, Merle KS & Guillet R. (2001). Bilirubin and Serial Auditory Brainstem Responses in Premature Infants. *Pediatrics* **107**, 664-670.
- Aono S, Keino H, Yamada Y, Adachi Y, Nanno T, Uyama E, Koiwai O & Sato H. (1995). Analysis of genes for bilirubin UDP-glucuronosyltransferase in Gilbert's syndrome. *The Lancet* **345**, 958-959.

- Aono S, Sato H, Semba R, Kashiwamata S, Kato K & Eng LF. (1988). Comparative Study of Glial Marker Proteins in the Hypoplastic Cerebellum of Jaundiced Gunn Rats. *Journal of Neurochemistry* **50**, 717-721.
- Arias IM & London IM. (1957). Bilirubin glucuronide formation in vitro; demonstration of a defect in Gilbert's disease. *Science* **126**, 563-564.
- Augustine GJ. (2001). How does calcium trigger neurotransmitter release? *Current Opinion in Neurobiology* **11**, 320-326.
- Babbedge R, Bland-Ward P, Hart S & Moore P. (1993). Inhibition of rat cerebellar nitric oxide synthase by 7-nitro indazole and related substituted indazoles. *British Journal of Pharmacology* **110**, 225-228.
- Baker CA, Montey KL, Pongstaporn T & Ryugo DK. (2010). Postnatal development of the endbulb of Held in congenitally deaf cats. *Frontiers in Neuroanatomy* **4**, 12.
- Banks MI & Smith PH. (1992). Intracellular recordings from neurobiotin-labeled cells in brain slices of the rat medial nucleus of the trapezoid body. *Journal of Neuroscience* **12**, 2819-2837.
- Baranano DE, Rao M, Ferris CD & Snyder SH. (2002). Biliverdin reductase: A major physiologic cytoprotectant. *Proceedings of the National Academy of Sciences of the United States of America* **99**, 16093-16098.
- Barbary AE. (1991). Auditory nerve of the normal and jaundiced rat. I. Spontaneous discharge rate and cochlear nerve histology. *Hearing Research* **54**, 75-90.
- Barnes-Davies M & Forsythe ID. (1995). Pre- and postsynaptic glutamate receptors at a giant excitatory synapse in rat auditory brainstem slices. *Journal of Physiology-London* **488**, 387-406.
- Batty HK & Millhouse OE. (1976). Ultrastructure of the Gunn rat substantia nigra 1. Cytoplasmic changes. *Acta Neuropathologica* **35**, 93-107.
- Becker PFL & Vogel P. (1948). Kernicterus: a review with a report of the findings in a study of seven cases. *Journal of Neuropathology & Experimental Neurology* **7**, 190-215.
- Becker W. (2005). Advanced Time-Correlated Single Photon Counting Techniques. In *Springer Series in Chemical Physics*, ed. Castleman AW, Toennies JP & Zinth W, pp. 401. Springer, Berlin, Heidelberg, New York.
- Belal A. (1975). Effect of hyperbilirubinemia on the inner ear in Gunn rats. *The Journal of Laryngology & Otology* **89**, 259-265.

- Bergman I, Hirsch RP, Fria TJ, Shapiro SM, Holzman I & Painter MJ. (1985). Cause of hearing loss in the high-risk premature infant. *The Journal of Pediatrics* **106**, 95-101.
- Berk PD, Howe RB, Bloomer JR & Berlin NI. (1969). Studies of bilirubin kinetics in normal adults. *The Journal of Clinical Investigation* **48**, 2176-2190.
- Billups B, Wong A & Forsythe ID. (2002). Detecting synaptic connections in the medial nucleus of the trapezoid body using calcium imaging. *Pflügers Archiv European Journal of Physiology* **444**, 663-669.
- Blanc WA & Johnson L. (1959). Studies on Kernicterus - Relationship with Sulfonamide Intoxication, Report on Kernicterus in Rats with Glucuronyl Transferase Deficiency and Review of Pathogenesis. *Journal of Neuropathology and Experimental Neurology* **18**, 165-189.
- Blanckaert N, Gollan J & Schmid R. (1980). Mechanism of Bilirubin Diglucuronide Formation in Intact Rats :bilirubin diglucuronide formation in vivo. *The Journal of Clinical Investigation* **65**, 1332-1342.
- Bledsoe JSC, Snead CR, Helfert RH, Prasad V, Wenthold RJ & Altschuler RA. (1990). Immunocytochemical and lesion studies support the hypothesis that the projection from the medial nucleus of the trapezoid body to the lateral superior olive is glycinergic. *Brain Research* **517**, 189-194.
- Borst JGG, Helmchen F & Sakmann B. (1995). Pre- and postsynaptic whole-cell recordings in the medial nucleus of the trapezoid body of the rat. *Journal of Physiology-London* **489**, 825-840.
- Borst JGG & Sakmann B. (1998). Facilitation of presynaptic calcium currents in the rat brainstem. *Journal of Physiology-London* **513**, 149-155.
- Bosma PJ. (2003). Inherited disorders of bilirubin metabolism. *Journal of Hepatology* **38**, 107-117.
- Bosma PJ, Chowdhury JR, Bakker C, Gantla S, de Boer A, Oostra BA, Lindhout D, Tytgat GNJ, Jansen PLM, Elferink RPJO & Chowdhury NR. (1995). The Genetic Basis of the Reduced Expression of Bilirubin UDP-Glucuronosyltransferase 1 in Gilbert's Syndrome. *New England Journal of Medicine* **333**, 1171-1175.
- Botelho MSeN, Silva VBd, Arruda LdS, Kuniyoshi IC, Oliveira LLRd & Oliveira ASd. (2010). Newborn hearing screening in the Limiar Clinic in Porto Velho - Rondônia. *Brazilian Journal of Otorhinolaryngology (Impresso) [online]* **76**, 605-610.
- Bredt DS & Snyder SH. (1990). Isolation of nitric oxide synthetase, a calmodulin-requiring enzyme. *Proceedings of the National Academy of Sciences of the United States of America* **87**, 682-685.

- Brenman J, Chao D, Gee S, McGee A, Craven S, Santillano D, Wu Z, Huang F, Xia H, Peters M, Froehner S & Bredt D. (1996). Interaction of nitric oxide synthase with the postsynaptic density protein PSD-95 and alpha1-syntrophin mediated by PDZ domains. *Cell* **84**, 757-767.
- Brew HM & Forsythe ID. (1995). Two voltage-dependent K⁺ conductances with complementary functions in postsynaptic integration at a central auditory synapse. *Journal of Neuroscience* **15**, 8011-8022.
- Brewster DH, Tucker JS, Fleming M, Morris C, Stockton DL, Lloyd DJ, Bhattacharya S & Chalmers JWT. (2010). Risk of skin cancer after neonatal phototherapy: retrospective cohort study. *Archives of Disease in Childhood* **95**, 826-831.
- Brito MA, Lima S, Fernandes A, Falcão AS, Silva RFM, Butterfield DA & Brites D. (2008a). Bilirubin injury to neurons: Contribution of oxidative stress and rescue by glycoconjugated bilirubin. *NeuroToxicology* **29**, 259-269.
- Brito MA, Rosa AI, Falcao AS, Fernandes A, Silva RFM, Butterfield DA & Brites D. (2008b). Unconjugated bilirubin differentially affects the redox status of neuronal and astroglial cells. *Neurobiology of Disease* **29**, 30-40.
- Brito MA, Vaz AR, Lima S, Fernandes A, Falcao AS, Silva SL, Silva RFM & Brites D. (2007). Bilirubin induces oxidative stress in neurons, which is prevented by nNOS inhibition. *Free Radical Research* **41**, S19-S19.
- Brito MA, Vaz AR, Silva SL, Falcao AS, Fernandes A, Silva RFM & Brites D. (2010). N-methyl-D-aspartate receptor and neuronal nitric oxide synthase activation mediate bilirubin-induced neurotoxicity. *Molecular Medicine* **16**, 372-380.
- Buchmayer S, Johansson S, Johansson A, Hultman CM, Sparen P & Cnattingius S. (2009). Can Association Between Preterm Birth and Autism be Explained by Maternal or Neonatal Morbidity? *Pediatrics* **124**, e817-825.
- Burette A, Petrusz P, Schmidt HHHW & Weinberg RJ. (2001). Immunohistochemical localization of nitric oxide synthase and soluble guanylyl cyclase in the ventral cochlear nucleus of the rat. *The Journal of Comparative Neurology* **431**, 1-10.
- Burger RM, Cramer KS, Pfeiffer JD & Rubel EW. (2005). Avian superior olivary nucleus provides divergent inhibitory input to parallel auditory pathways. *The Journal of Comparative Neurology* **481**, 6-18.
- Burke BL, Robbins JM, Bird TM, Hobbs CA, Nesmith C & Tilford JM. (2009). Trends in Hospitalizations for Neonatal Jaundice and Kernicterus in the United States, 1988-2005. *Pediatrics* **123**, 524-532.

- Bush MA & Pollack GM. (2000). Pharmacokinetics and protein binding of the selective neuronal nitric oxide synthase inhibitor 7-nitroindazole. *Biopharmaceutics & Drug Disposition* **21**, 221-228.
- Bush MA & Pollack GM. (2001). Pharmacokinetics and Pharmacodynamics of 7-Nitroindazole, a Selective Nitric Oxide Synthase Inhibitor, in the Rat Hippocampus. *Pharmaceutical Research* **18**, 1607-1612.
- Caicedo A, d'Aldin C, Puel J-L & Eybalin M. (1996). Distribution of calcium-binding protein immunoreactivities in the guinea pig auditory brainstem. *Anatomy and Embryology* **194**, 465-487.
- Calvert RT, Hulshoff A, Buice RG & Kostenbauder HB. (1978). Bilirubin dynamics in the Gunn rat during phototherapy. *Journal of Pharmaceutical Sciences* **67**, 205-209.
- Cant NB & Benson CG. (2003). Parallel auditory pathways: projection patterns of the different neuronal populations in the dorsal and ventral cochlear nuclei. *Brain Research Bulletin* **60**, 457-474.
- Cao X-J, Shatadal S & Oertel D. (2007). Voltage-Sensitive Conductances of Bushy Cells of the Mammalian Ventral Cochlear Nucleus. *Journal of Neurophysiology* **97**, 3961-3975.
- Casey MA & Feldman ML. (1982). Aging in the rat medial nucleus of the trapezoid body I. Light microscopy. *Neurobiology of Aging* **3**, 187-195.
- Casey MA & Feldman ML. (1985). Aging in the rat medial nucleus of the trapezoid Body. II. Electron microscopy. *The Journal of Comparative Neurology* **232**, 401-413.
- Casey MA & Feldman ML. (1988). Age-related loss of synaptic terminals in the rat medial nucleus of the trapezoid body. *Neuroscience* **24**, 189-194.
- Catterall WA, Goldin AL & Waxman SG. (2005a). International Union of Pharmacology. XLVII. Nomenclature and Structure-Function Relationships of Voltage-Gated Sodium Channels. *Pharmacol Rev* **57**, 397-409.
- Catterall WA, Perez-Reyes E, Snutch TP & Striessnig J. (2005b). International Union of Pharmacology. XLVIII. Nomenclature and Structure-Function Relationships of Voltage-Gated Calcium Channels. *Pharmacol Rev* **57**, 411-425.
- Chen TJ & Chen SS. (1991). Generator study of brainstem auditory evoked potentials by a radiofrequency lesion method in rats. *Experimental Brain Research* **85**, 537-542.

- Chen W-X, Wong VCN & Wong K-Y. (2006). Neurodevelopmental Outcome of Severe Neonatal Hemolytic Hyperbilirubinemia. *Journal of Child Neurology* **21**, 474-479.
- Chisin R, Perlman M & Sohmer H. (1979). Cochlear and brain stem responses in hearing loss following neonatal hyperbilirubinemia. *Annals of Otolaryngology, Rhinology and Laryngology* **88**, 352-357.
- Chiu SY & Ritchie JM. (1980). Potassium channels in nodal and internodal axonal membrane of mammalian myelinated fibres. *Nature* **284**, 170-171.
- Chowdhury NR, Arias IM, Lederstein M & Chowdhury JR. (1986). Substrates and products of purified rat liver bilirubin UDP - glucuronosyltransferase. *Hepatology* **6**, 123-128.
- Coetzee WA, Amarillo Y, Chiu J, Chow A, Lau D, McCormack T, Moreno H, Nadal MS, Ozaita A, Pountney D, Saganich M, Vega-Saenz de Miera E & Rudy B. (1999). Molecular diversity of K⁺ channels. In *Molecular and Functional Diversity of Ion Channels and Receptors*, pp. 233-285.
- Collins CA & Rojas E. (1982). Temperature dependence of the sodium channel gating kinetics in the node of Ranvier. *Q J Exp Physiol* **67**, 41-55.
- Conlee JW & Shapiro SM. (1991). Morphological changes in the cochlear nucleus and nucleus of the trapezoid body in Gunn rat pups. *Hearing Research* **57**, 23-30.
- Conlee JW & Shapiro SM. (1997). Development of cerebellar hypoplasia in jaundiced Gunn rats: a quantitative light microscopic analysis. *Acta Neuropathologica* **93**, 450-460.
- Cornelius CE & Arias IM. (1972). Animal model of human disease. Crigler-Najjar Syndrome. Animal model: hereditary nonhemolytic unconjugated hyperbilirubinemia in Gunn rats. *American Journal of Pathology* **69**, 369-372.
- Crabtree N & Gerrard J. (1950). Perceptive Deafness Associated with Severe Neonatal Jaundice. *The Journal of Laryngology & Otolaryngology* **64**, 482-506.
- Cremer RJ, Perryman PW & Richards DH. (1958). Influence of light on the hyperbilirubinaemia of infants. *The Lancet* **271**, 1094-1097.
- Crigler JFJ & Najjar VA. (1952). Congenital Familial Nonhemolytic Jaundice With Kernicterus. *Pediatrics* **10**, 169-180.
- Croen LA, Yoshida CK, Odouli R & Newman TB. (2005). Neonatal Hyperbilirubinemia and Risk of Autism Spectrum Disorders. *Pediatrics* **115**, e135-138.
- Cull-Candy SG. (2007). NMDA Receptors. In *Encyclopedia of Life Sciences*.

- Dani C, Poggi C, Barp J, Romagnoli C & Buonocore G. (2011). Current Italian practices regarding the management of hyperbilirubinaemia in preterm infants. *Acta Paediatrica* **100**, 666-669.
- Dawson VL, Dawson TM, Bartley DA, Uhl GR & Snyder SH. (1993). Mechanisms of nitric oxide-mediated neurotoxicity in primary brain cultures. *Journal of Neuroscience* **13**, 2651-2661.
- de Matteis F, Lord GA, Kee Lim C & Pons N. (2006). Bilirubin degradation by uncoupled cytochrome P450. Comparison with a chemical oxidation system and characterization of the products by high-performance liquid chromatography/electrospray ionization mass spectrometry. *Rapid Communications in Mass Spectrometry* **20**, 1209-1217.
- de Vries LS, Lary S & Dubowitz LMS. (1985). Relationship of Serum Bilirubin Levels to Ototoxicity and Deafness in High-Risk Low-Birth-Weight Infants. *Pediatrics* **76**, 351-354.
- de Vries LS, Lary S, Whitelaw AG & Dubowitz LMS. (1987). Relationship of serum bilirubin levels and hearing impairment in newborn infants. *Early Human Development* **15**, 269-277.
- Delaney KR & Stanley EE. (2009). Calcium and Neurotransmitter Release. In *Encyclopedia of Life Sciences (ELS)*. John Wiley & Sons, Ltd, Cichester.
- Denk W, Strickler JH & Webb WW. (1990). Two-photon laser scanning fluorescence microscopy. *Science* **248**, 73-76.
- Devaux J, Alcaraz G, Grinspan J, Bennett V, Joho R, Crest M & Scherer SS. (2003). Kv3.1b is a novel component of CNS nodes. *Journal of Neuroscience* **23**, 4509-4518.
- Devaux J, Gola M, Jacquet G & Crest M. (2002). Effects of K⁺ channel blockers on developing rat myelinated CNS axons: Identification of four types of K⁺ channels. *Journal of Neurophysiology* **87**, 1376-1385.
- Diamond I & Schmid R. (1966). Experimental bilirubin encephalopathy. The mode of entry of bilirubin-14C into the central nervous system. *Journal of Clinical Investigation* **45**, 678-689.
- Diamond I & Schmid R. (1967). Oxidative Phosphorylation in Experimental Bilirubin Encephalopathy. *Science* **155**, 1288-1289.
- Dietrich WD, Alonso O, Busto R, Globus MYT & Ginsberg MD. (1994). Post-traumatic brain hypothermia reduces histopathological damage following concussive brain injury in the rat. *Acta Neuropathologica* **87**, 250-258.
- Dobbs RH & Cremer RJ. (1975). Phototherapy. *Archives of Disease in Childhood* **50**, 833-836.

- Dodson PD. (2003). The role of voltage-gated potassium channels in regulating excitability at a central synapse. In *Department of Cell Physiology and Pharmacology*, pp. 220. University of Leicester, Leicester.
- Dodson PD, Barker MC & Forsythe ID. (2002a). Pre- and postsynaptic K⁺ currents at the Calyx of Held. *Journal of Physiology-London* **543**, 21P-21P.
- Dodson PD, Barker MC & Forsythe ID. (2002b). Two heteromeric Kv1 potassium channels differentially regulate action potential firing. *Journal of Neuroscience* **22**, 6953-6961.
- Dodson PD, Billups B, Rusznak Z, Szucs G, Barker MC & Forsythe ID. (2003). Presynaptic rat Kv1.2 channels suppress synaptic terminal hyperexcitability following action potential invasion. *Journal of Physiology-London* **550**, 27-33.
- Dodson PD & Forsythe ID. (2004). Presynaptic K⁺ channels: electrifying regulators of synaptic terminal excitability. *Trends in Neurosciences* **27**, 210-217.
- Dore S, Takahashi M, Ferris CD, Hester LD, Guastella D & Snyder SH. (1999). Bilirubin, formed by activation of heme oxygenase-2, protects neurons against oxidative stress injury. *Proceedings of the National Academy of Sciences of the United States of America* **96**, 2445-2450.
- Dublin WB. (1951). Neurologic lesions of erythroblastosis fetalis in relation to nuclear deafness. *American Journal of Clinical Pathology* **21**, 935-939.
- Dublin WB. (1974). Cytoarchitecture of the Cochlear Nuclei: Report of an Illustrative Case of Erythroblastosis. *Archives of Otolaryngology* **100**, 355-359.
- Dzoljic MR, de Vries R & van Leeuwen R. (1996). Sleep and nitric oxide: effects of 7-nitro indazole, inhibitor of brain nitric oxide synthase. *Brain Research* **718**, 145-150.
- Ebbesen F. (2000). Recurrence of kernicterus in term and near-term infants in Denmark. *Acta Paediatrica* **89**, 1213-1217.
- Ebbesen F, Andersson C, Verder H, Grytter C, Pedersen-bjergaard L, Petersen JR & Schaarup J. (2005). Extreme hyperbilirubinaemia in term and near-term infants in Denmark. *Acta Paediatrica* **94**, 59-64.
- Edwards FA, Konnerth A, Sakmann B & Takahashi T. (1989). A thin slice preparation for patch clamp recordings from neurones of the mammalian central nervous system. *Pflügers Archiv European Journal of Physiology* **414**, 600-612.

- Elezgarai I, Díez J, Puente N, Azkue JJ, Benítez R, Bilbao A, Knöpfel T, Doñate-Oliver F & Grandes P. (2003). Subcellular localization of the voltage-dependent potassium channel Kv3.1b in postnatal and adult rat medial nucleus of the trapezoid body. *Neuroscience* **118**, 889-898.
- Falcão A, Fernandes A, Brito M, Silva R & Brites D. (2006). Bilirubin-induced immunostimulant effects and toxicity vary with neural cell type and maturation state. *Acta Neuropathologica* **112**, 95-105.
- Falcão AS, Bellarosa C, Fernandes A, Brito MA, Silva RFM, Tiribelli C & Brites D. (2007). Role of multidrug resistance-associated protein 1 expression in the in vitro susceptibility of rat nerve cell to unconjugated bilirubin. *Neuroscience* **144**, 878-888.
- Fenwick JD. (1975). Neonatal jaundice as a cause of deafness. *The Journal of Laryngology & Otology* **89**, 925-932.
- Fernandes A, Falcão AS, Abranches E, Bekman E, Henrique D, Lanier LM & Brites D. (2009). Bilirubin as a determinant for altered neurogenesis, neuritogenesis, and synaptogenesis. *Developmental Neurobiology* **69**, 568-582.
- Fernandes A, Falcão AS, Silva RFM, Brito MA & Brites D. (2007). MAPKs are key players in mediating cytokine release and cell death induced by unconjugated bilirubin in cultured rat cortical astrocytes. *European Journal of Neuroscience* **25**, 1058-1068.
- Fernandes A, Falcão AS, Silva RFM, Gordo AC, Gama MJ, Brito MA & Brites D. (2006). Inflammatory signalling pathways involved in astroglial activation by unconjugated bilirubin. *Journal of Neurochemistry* **96**, 1667-1679.
- Fernandes A, Silva RFM, Falcão AS, Brito MA & Brites D. (2004). Cytokine production, glutamate release and cell death in rat cultured astrocytes treated with unconjugated bilirubin and LPS. *Journal of Neuroimmunology* **153**, 64-75.
- Fernández-Chacón R, Wölfel M, Nishimune H, Tabares L, Schmitz F, Castellano-Muñoz M, Rosenmund C, Montesinos ML, Sanes JR, Schneggenburger R & Südhof TC. (2004). The Synaptic Vesicle Protein CSP[alpha] Prevents Presynaptic Degeneration. *Neuron* **42**, 237-251.
- Fessenden JD, Altschuler RA, Seasholtz AF & Schacht J. (1999). Nitric oxide/cyclic guanosine monophosphate pathway in the peripheral and central auditory system of the rat. *The Journal of Comparative Neurology* **404**, 52-63.
- Fettiplace R & Hackney CM. (2006). The sensory and motor roles of auditory hair cells. *Nature Reviews Neuroscience* **7**, 19-29.

- Forsythe ID. (1994). Direct patch recording from identified presynaptic terminals mediating glutamatergic EPSCs in the rat CNS, in vitro. *The Journal of Physiology* **479**, 381-387.
- Forsythe ID & Barnes-Davies M. (1993). The binaural auditory pathway: excitatory amino acid receptors mediate dual timecourse excitatory postsynaptic currents in the rat medial nucleus of the trapezoid body. *Proceedings of the Royal Society of London Series B-Biological Sciences* **251**, 151-157.
- Forsythe ID, Tsujimoto T, Barnes-Davies M, Cuttle MF & Takahashi T. (1998). Inactivation of Presynaptic Calcium Current Contributes to Synaptic Depression at a Fast Central Synapse. *Neuron* **20**, 797-807.
- Friauf E. (1993). Transient appearance of calbindin-D28k-positive neurons in the superior olivary complex of developing rats. *The Journal of Comparative Neurology* **334**, 59-74.
- Friauf E & Ostwald J. (1988). Divergent projections of physiologically characterized rat ventral cochlear nucleus neurons as shown by intra-axonal injection of horseradish peroxidase. *Experimental Brain Research* **73**, 263-284.
- Fritsch B. (1993). Fast axonal diffusion of 3000 molecular weight dextran amines. *Journal of Neuroscience Methods* **50**, 95-103.
- Fukuhara T & Yamada E. (1981). Unusual cytoplasmic bodies in Purkinje cells of the Gunn rats. *Acta Neuropathologica* **55**, 269-273.
- Futai K, Okada M, Matsuyama K & Takahashi T. (2001). High-Fidelity Transmission Acquired via a Developmental Decrease in NMDA Receptor Expression at an Auditory Synapse. *Journal of Neuroscience* **21**, 3342-3349.
- Ganong AH & Cotman CW. (1986). Kynurenic acid and quinolinic acid act at N-methyl-D-aspartate receptors in the rat hippocampus. *Journal of Pharmacology and Experimental Therapeutics* **236**, 293-299.
- Geiger JRP, Melcher T, Koh DS, Sakmann B, Seeburg PH, Jonas P & Monyer H. (1995). Relative abundance of subunit mRNAs determines gating and Ca²⁺ permeability of AMPA receptors in principal neurons and interneurons in rat CNS. *Neuron* **15**, 193-204.
- Gennuso F, Ferneti C, Tirolo C, Testa N, L'Episcopo F, Caniglia S, Morale MC, Ostrow JD, Pascolo L, Tiribelli C & Marchetti B. (2004). Bilirubin protects astrocytes from its own toxicity by inducing up-regulation and translocation of multidrug resistance-associated protein 1 (Mrp1). *Proceedings of the National Academy of Sciences of the United States of America* **101**, 2470-2475.

- Gerrard J. (1952). Nuclear Jaundice and Deafness. *The Journal of Laryngology & Otology* **66**, 39-46.
- Gold C, Henze DA & Koch C. (2007). Using extracellular action potential recordings to constrain compartmental models. *Journal of Computational Neuroscience* **23**, 39-58.
- Gold C, Henze DA, Koch C & Buzsaki G. (2006). On the origin of the extracellular action potential waveform: A modeling study. *Journal of Neurophysiology* **95**, 3113-3128.
- Göppert-Mayer M. (1931). Über Elementarakte mit zwei Quantensprüngen. *Annalen der Physik* **401**, 273-294.
- Göppert M. (1929). Über die Wahrscheinlichkeit des Zusammenwirkens zweier Lichtquanten in einem Elementarakt. *Naturwissenschaften* **17**, 932-932.
- Gordo AC, Falcao AS, Fernandes A, Brito MA, Silva RFM & Brites D. (2006). Unconjugated bilirubin activates and damages microglia. *Journal of Neuroscience Research* **84**, 194-201.
- Grandes P & Streit P. (1989). Glutamate-like immunoreactivity in calyces of Held. *Journal of Neurocytology* **18**, 685-693.
- Gray BC, Siskova Z, Perry VH & O'Connor V. (2009). Selective presynaptic degeneration in the synaptopathy associated with ME7-induced hippocampal pathology. *Neurobiology of Disease* **35**, 63-74.
- Grothe B. (2000). The evolution of temporal processing in the medial superior olive, an auditory brainstem structure. *Progress in Neurobiology* **61**, 581-610.
- Grynkiewicz G, Poenie M & Tsien RY. (1985). A new generation of Ca²⁺ indicators with greatly improved fluorescence properties. *Journal of Biological Chemistry* **260**, 3440-3450.
- Guinan JJ & Li RYS. (1990). Signal processing in brainstem auditory neurons which receive giant endings (calyces of Held) in the medial nucleus of the trapezoid body of the cat. *Hearing Research* **49**, 321-334.
- Gunn CK. (1938). Hereditary acholuric jaundice in a new mutant strain of rats. *Journal of Heredity* **29**, 137-139.
- Gunn CK. (1944). Hereditary acholuric jaundice in the rat. *Canadian Medical Association Journal* **50**, 230-237.
- Gutman GA, Chandy KG, Grissmer S, Lazdunski M, McKinnon D, Pardo LA, Robertson GA, Rudy B, Sanguinetti MC, Stuhmer W & Wang XL. (2005). International Union of Pharmacology. LIII. Nomenclature and molecular

- relationships of voltage-gated potassium channels. *Pharmacological Reviews* **57**, 473-508.
- Hamann M, Billups B & Forsythe ID. (2003). Non-calyceal excitatory inputs mediate low fidelity synaptic transmission in rat auditory brainstem slices. *European Journal of Neuroscience* **18**, 2899-2902.
- Hameed NN, Na' ma AM, Vilms R & Bhutani VK. (2011). Severe Neonatal Hyperbilirubinemia and Adverse Short-Term Consequences in Baghdad, Iraq. *Neonatology* **100**, 57-63.
- Hamill OP, Marty A, Neher E, Sakmann B & Sigworth FJ. (1981). Improved patch-clamp techniques for high-resolution current recording from cells and cell-free membrane patches. *Pflügers Archiv European Journal of Physiology* **391**, 85-100.
- Hansen TWR. (2000). Pioneers in the Scientific Study of Neonatal Jaundice and Kernicterus. *Pediatrics* **106**, <http://www.pediatrics.org/cgi/content/full/106/102/e115>.
- Hansen TWR, Mathiesen SBW, Sefland I & Walaas SI. (1999). Bilirubin inhibits Ca²⁺-dependent release of norepinephrine from permeabilized nerve terminals. *Neurochemical Research* **24**, 733-738.
- Harris MC, Bernbaum JC, Polin JR, Zimmerman R & Polin RA. (2001). Developmental Follow-Up of Breastfed Term and Near-Term Infants With Marked Hyperbilirubinemia. *Pediatrics* **107**, 1075-1080.
- Hartley DM, Kurth MC, Bjerkness L, Weiss JH & Choi DW. (1993). Glutamate receptor-induced ⁴⁵Ca²⁺ accumulation in cortical cell culture correlates with subsequent neuronal degeneration. *Journal of Neuroscience* **13**, 1993-2000.
- Harvey AM & MacIntosh FC. (1940). Calcium and synaptic transmission in a sympathetic ganglion. *The Journal of Physiology* **97**, 408-416.
- Haustein MD, Read DJ, Steinert JR, Pilati N, Dinsdale D & Forsythe ID. (2010). Acute hyperbilirubinaemia induces presynaptic neurodegeneration at a central glutamatergic synapse. *The Journal of Physiology* **588**, 4683-4693.
- Haustein MD, Reinert T, Warnatsch A, Englitz B, Dietz B, Robitzki A, Rübtsamen R & Milenkovic I. (2008). Synaptic transmission and short-term plasticity at the calyx of Held synapse revealed by multielectrode array recordings. *Journal of Neuroscience Methods* **174**, 227-236.
- Held H. (1893). Die zentrale Gehörleitung. *Archiv für Anatomie und Physiologie* **17**, 201-248.

- Helfert RH, Snead CR & Altschuler RA. (1991). The ascending auditory pathways. In *Neurobiology of Hearing: The central auditory system*, ed. Altschuler RA, Bobbin RP, Clopton BM & Hoffman DW, pp. 1-25. Raven Press, New York.
- Hermansteyne TO, Kihira Y, Misono K, Deitchler A, Yanagawa Y & Misonou H. (2010). Immunolocalization of the voltage-gated potassium channel Kv2.2 in GABAergic neurons in the basal forebrain of rats and mice. *The Journal of Comparative Neurology* **518**, 4298-4310.
- Hodgkin AL & Katz B. (1949). The effect of temperature on the electrical activity of the giant axon of the squid. *The Journal of Physiology* **109**, 240-249.
- Honer WG. (2003). Pathology of presynaptic proteins in Alzheimer's disease: more than simple loss of terminals. *Neurobiology of Aging* **24**, 1047-1062.
- Hugh Perry V & O'Connor V. (2010). The role of microglia in synaptic stripping and synaptic degeneration: a revised perspective. *ASN NEURO* **2**, e00047.
- Hutchinson NA, Koles ZJ & Smith RS. (1970). Conduction velocity in myelinated nerve fibres of *Xenopus laevis*. *Journal of Physiology-London* **208**, 279-289.
- Ishikawa T, Nakamura Y, Saitoh N, Li W-B, Iwasaki S & Takahashi T. (2003). Distinct Roles of Kv1 and Kv3 Potassium Channels at the Calyx of Held Presynaptic Terminal. *Journal of Neuroscience* **23**, 10445-10453.
- Ison J, Housel N, Allen P, Kopp-Scheinflug C & Forsythe ID. (2009). Antagonists of neuronal nitric oxide synthase (nNOS) affect auditory behaviors in mice: A study of the acoustic startle reflex (ASR) and its inhibition by gaps in noise and a change in sound source location. In *Abstracts of the 32nd Annual ARO Midwinter Research Meeting* ed. Santi PA, pp. 146. Association for Research in Otolaryngology, Baltimore, Maryland, USA.
- Iwasaki S & Takahashi T. (1998). Developmental changes in calcium channel types mediating synaptic transmission in rat auditory brainstem. *The Journal of Physiology* **509**, 419-423.
- Iyanagi T. (1991). Molecular basis of multiple UDP-glucuronosyltransferase isoenzyme deficiencies in the hyperbilirubinemic rat (Gunn rat). *Journal of Biological Chemistry* **266**, 24048-24052.
- Iyanagi T, Watanabe T & Uchiyama Y. (1989). The 3-methylcholanthrene-inducible UDP-glucuronosyltransferase deficiency in the hyperbilirubinemic rat (Gunn rat) is caused by a -1 frameshift mutation. *Journal of Biological Chemistry* **264**, 21302-21307.

- Jangaard KA, Fell DB, Dodds L & Allen AC. (2008). Outcomes in a Population of Healthy Term and Near-Term Infants With Serum Bilirubin Levels of $\geq 325 \mu\text{mol/L}$ ($\geq 19 \text{ mg/dL}$) Who Were Born in Nova Scotia, Canada, Between 1994 and 2000. *Pediatrics* **122**, 119-124.
- Jean-Baptiste M & Morest DK. (1975). Transneuronal changes of synaptic endings and nuclear chromatin in the trapezoid body following cochlear ablations in cats. *The Journal of Comparative Neurology* **162**, 111-133.
- Jew JY & Sandquist D. (1979). CNS changes in Hyperbilirubinemia. Functional Implications. *Archives of Neurology* **36**, 149-154.
- Jew JY & Williams TH. (1977). Ultrastructural aspects of bilirubin encephalopathy in cochlear nuclei of the Gunn rat. *Journal of Anatomy* **124**, 599-614.
- Johnson L, Garcia ML, Figuera E & Sarmiento F. (1961). Kernicterus in rats lacking glucuronyl transferase. II. Factors which alter bilirubin concentration and frequency of kernicterus. *American journal of diseases of children* **101**, 322-349.
- Johnson L, Sarmiento F, Blanc WA & Day R. (1959). Kernicterus in rats with an inherited deficiency of glucuronyl transferase. *American journal of diseases of children* **97**, 591-608.
- Joshi I, Shokralla S, Titis P & Wang L-Y. (2004). The Role of AMPA Receptor Gating in the Development of High-Fidelity Neurotransmission at the Calyx of Held Synapse. *Journal of Neuroscience* **24**, 183-196.
- Juul-Dam N, Townsend J & Courchesne E. (2001). Prenatal, Perinatal, and Neonatal Factors in Autism, Pervasive Developmental Disorder-Not Otherwise Specified, and the General Population. *Pediatrics* **107**, e63.
- Kaga K, Kitazumi E & Kodama K. (1979). Auditory brain stem responses of kernicterus infants. *International Journal of Pediatric Otorhinolaryngology* **1**, 255-264.
- Kandler K, Clause A & Noh J. (2009). Tonotopic reorganization of developing auditory brainstem circuits. *Nature Neuroscience* **12**, 711-717.
- Kaneko T, Saeki K, Lee T & Mizuno N. (1996). Improved retrograde axonal transport and subsequent visualization of tetramethylrhodamine (TMR)-dextran amine by means of an acidic injection vehicle and antibodies against TMR. *Journal of Neuroscience Methods* **65**, 157-165.
- Kaplan M & Hammerman C. (2005). Understanding severe hyperbilirubinemia and preventing kernicterus: Adjuncts in the interpretation of neonatal serum bilirubin. *Clinica Chimica Acta* **356**, 9-21.

- Kapoor R, Csoma Z, Kemeny L, Olah J, Ostrow JD, Wennberg RP, Tiribelli C, Maisels MJ & McDonagh AF. (2008). Phototherapy for Neonatal Jaundice. *New England Journal of Medicine* **358**, 2522-2525.
- Karplus M, Lee C, Cashore WJ & Oh W. (1988). The effects of brain bilirubin deposition on auditory brain stem evoked responses in rats. *Early Human Development* **16**, 185-194.
- Katz B & Miledi R. (1965). The effect of temperature on the synaptic delay at the neuromuscular junction. *The Journal of Physiology* **181**, 656-670.
- Katz B & Miledi R. (1970). Further study of the role of calcium in synaptic transmission. *The Journal of Physiology* **207**, 789-801.
- Kelly JB & Masterton B. (1977). Auditory sensitivity of the albino rat. *Journal of Comparative and Physiological Psychology* **91**, 930-936.
- Kimura M, Saitoh N & Takahashi T. (2003). Adenosine A(1) receptor-mediated presynaptic inhibition at the calyx of Held of immature rats. *Journal of Physiology-London* **553**, 415-426.
- Koh DS, Geiger JR, Jonas P & Sakmann B. (1995). Ca(2+)-permeable AMPA and NMDA receptor channels in basket cells of rat hippocampal dentate gyrus. *The Journal of Physiology* **485**, 383-402.
- Koiwai O, Nishizawa M, Hasada K, Aono S, Adachi Y, Mamlya N & Sato H. (1995). Gilbert's syndrome is caused by a heterozygous missense mutation in the gene for bilirubin UDP-glucuronosyltransferase. *Human Molecular Genetics* **4**, 1183-1186.
- Kopp-Scheinflug C, Lippe WR, Dorrscheidt GJ & Rubsamen R. (2003). The medial nucleus of the trapezoid body in the gerbil is more than a relay: Comparison of pre- and postsynaptic activity. *Jaro* **4**, 1-23.
- Kopp-Scheinflug C, Tolnai S, Malmierca MS & RübSamen R. (2008). The medial nucleus of the trapezoid body: comparative physiology. *Neuroscience* **154**, 160-170.
- Kotak VC, Korada S, Schwartz IR & Sanes DH. (1998). A developmental shift from GABAergic to glycinergic transmission in the central auditory system. *Journal of Neuroscience* **18**, 4646-4655.
- Kramer ML & Schulz-Schaeffer WJ. (2007). Presynaptic α -Synuclein Aggregates, Not Lewy Bodies, Cause Neurodegeneration in Dementia with Lewy Bodies. *Journal of Neuroscience* **27**, 1405-1410.
- Kraus N, Ozdamar O, Stein L & Reed N. (1984). Absent Auditory Brain Stem Response: Peripheral Hearing Loss or Brain Stem Dysfunction? *Laryngoscope* **94**, 400-406.

- Kuriyama M, Tomiwa K, Konishi Y & Mikawa H. (1986). Improvement in auditory brainstem response of hyperbilirubinemic infants after exchange transfusions. *Pediatric Neurology* **2**, 127-132.
- Kuwabara N, Dicaprio RA & Zook JM. (1991). Afferents to the medial nucleus of the trapezoid body and their collateral projections. *Journal of Comparative Neurology* **314**, 684-706.
- Lathe GH. (1955). Exchange transfusion as a means of removing bilirubin in haemolytic disease of the newborn. *British Medical Journal* **1**, 192-196.
- Lathe GH & Walker M. (1958). The synthesis of bilirubin glucuronide in animal and human liver. *Biochemical Journal* **70**, 705-712.
- Leao RM, Kushmerick C, Pinaud R, Renden R, Li G-L, Taschenberger H, Spirou G, Levinson SR & von Gersdorff H. (2005). Presynaptic Na⁺ Channels: Locus, Development, and Recovery from Inactivation at a High-Fidelity Synapse. *Journal of Neuroscience* **25**, 3724-3738.
- Leao RN, Naves MM, Leao KE & Walmsley B. (2006). Altered sodium currents in auditory neurons of congenitally deaf mice. *European Journal of Neuroscience* **24**, 1137-1146.
- Lee DJ, Cahill HB & Ryugo DK. (2003). Effects of congenital deafness in the cochlear nuclei of *Shaker-2* mice: An ultrastructural analysis of synapse morphology in the endbulbs of Held. *Journal of Neurocytology* **32**, 229-243.
- Lenn NJ & Reese TS. (1966). The fine structure of nerve endings in the nucleus of the trapezoid body and the ventral cochlear nucleus. *American Journal of Anatomy* **118**, 375-389.
- Leonard M, Noy N & Zakim D. (1989). The interactions of bilirubin with model and biological membranes. *Journal of Biological Chemistry* **264**, 5648-5652.
- Lev A & Sohmer H. (1972). Sources of averaged neural responses recorded in animal and human subjects during cochlear audiometry (Electro-Cochleogram). *European Archives of Oto-Rhino-Laryngology* **201**, 79-90.
- Levi G, Sohmer H & Kapitulnik J. (1981). Auditory nerve and Brain-Stem Responses in Homozygous Jaundiced GUNN Rats. *Archives of Oto-Rhino-Laryngology-Archiv Fur Ohren-Nasen-Und Kehlkopfheilkunde* **232**, 139-143.
- Lightner DA, Wooldridge TA, Rodgers SL & Norris RD. (1980). Action spectra for bilirubin photodisappearance. *Cellular and Molecular Life Sciences* **36**, 380-382.

- London IM, West R, Shemin D & Rittenberg D. (1950). On the origin of bile pigment in normal man. *Journal of Biological Chemistry* **184**, 351-358.
- MacKenzie GM, Rose S, Bland-Ward PA, Moore PK, Jenner P & Marsden CD. (1994). Time course of inhibition of brain nitric oxide synthase by 7-nitro indazole. *Neuroreport* **5**, 1993-1996.
- Maimburg RD, Bech BH, Bjerre JV, Olsen J & Moller-Madsen B. (2009). Obstetric outcome in Danish children with a validated diagnosis of kernicterus. *Acta Obstetricia et Gynecologica Scandinavica* **88**, 1011 - 1016.
- Maimburg RD, Bech BH, Vaeth M, Moller-Madsen B & Olsen J. (2010). Neonatal Jaundice, Autism, and Other Disorders of Psychological Development. *Pediatrics*, peds.2010-0052.
- Maisels MJ & McDonagh AF. (2008). Phototherapy for Neonatal Jaundice. *New England Journal of Medicine* **358**, 920-928.
- Mancuso C, Bonsignore A, Di Stasio E, Mordente A & Motterlini R. (2003). Bilirubin and S-nitrosothiols interaction: evidence for a possible role of bilirubin as a scavenger of nitric oxide. *Biochemical Pharmacology* **66**, 2355-2363.
- Manev H, Favaron M, Guidotti A & Costa E. (1989). Delayed increase of Ca²⁺ influx elicited by glutamate: role in neuronal death. *Molecular Pharmacology* **36**, 106-112.
- Manning D, Todd P, Maxwell M & Jane Platt M. (2007). Prospective surveillance study of severe hyperbilirubinaemia in the newborn in the UK and Ireland. *Archives of Disease in Childhood - Fetal and Neonatal Edition* **92**, F342-346.
- Mayer ML & Westbrook GL. (1987). Permeation and block of N-methyl-D-aspartic acid receptor channels by divalent cations in mouse cultured central neurones. *The Journal of Physiology* **394**, 501-527.
- Mayer ML, Westbrook GL & Guthrie PB. (1984). Voltage-dependent block by Mg²⁺ of NMDA responses in spinal cord neurones. *Nature* **309**, 261-263.
- McDonagh AF, Agati G, Fusi F & Pratesi R. (1989). Quantum yields for laser photocyclization of bilirubin in the presence of human serum albumin. Dependence of quantum yield on excitation wavelength. *Photochemistry and Photobiology* **50**, 305-319.
- McDonald JW, Shapiro SM, Silverstein FS & Johnston MV. (1998). Role of glutamate receptor-mediated excitotoxicity in bilirubin-induced brain injury in the Gunn rat model. *Experimental Neurology* **150**, 21-29.

- MedlinePlus Encyclopedia. Bilirubin - blood.
<http://www.nlm.nih.gov/medlineplus/ency/article/003479.htm>.
- Melcher JR, Guinan Jr JJ, Knudson IM & Kiang NYS. (1996a). Generators of the brainstem auditory evoked potential in cat. II. Correlating lesion sites with waveform changes. *Hearing Research* **93**, 28-51.
- Melcher JR & Kiang NYS. (1996). Generators of the brainstem auditory evoked potential in cat III: identified cell populations. *Hearing Research* **93**, 52-71.
- Melcher JR, Knudson IM, Fullerton BC, Guinan Jr JJ, Norris BE & Kiang NYS. (1996b). Generators of the brainstem auditory evoked potential in cat. I. An experimental approach to their identification. *Hearing Research* **93**, 1-27.
- Mennerick S & Zorumski CF. (2005). Glutamate as a Neurotransmitter. In *Encyclopedia of Life Sciences*.
- Mikoshiba K, Kohsaka S, Takamatsu K & Tsukada Y. (1980). Cerebellar Hypoplasia in the Gunn Rat with Hereditary Hyperbilirubinemia: Immunohistochemical and Neurochemical Studies. *Journal of Neurochemistry* **35**, 1309-1318.
- Milenkovic I, Rinke I, Witte M, Dietz B & Rübsamen R. (2009). P2 Receptor-Mediated Signaling in Spherical Bushy Cells of the Mammalian Cochlear Nucleus. *Journal of Neurophysiology* **102**, 1821-1833.
- Miyaoka T, Seno H, Itoga M, Iijima M, Inagaki T & Horiguchi J. (2000). Schizophrenia-associated idiopathic unconjugated hyperbilirubinemia (Gilbert's syndrome). *The Journal of Clinical Psychiatry* **61**, 868-871.
- Monaghan G, Ryan M, Hume R, Burchell B & Seddon R. (1996). Genetic variation in bilirubin UDP-glucuronosyltransferase gene promoter and Gilbert's syndrome. *The Lancet* **347**, 578-581.
- Moore PJ & Karp WB. (1980). Further observations on the effect of bilirubin encephalopathy on the Purkinje cell population in Gunn rats. *Experimental Neurology* **69**, 408-413.
- Morest DK & Jean-Baptiste M. (1975). Degeneration and phagocytosis of synaptic endings and axons in the medial trapezoid nucleus of the cat. *The Journal of Comparative Neurology* **162**, 135-155.
- Moro MA, Russel RJ, Celtek S, Lizasoain I, Su Y, Darley-Usmar VM, Radomski MW & Moncada S. (1996). cGMP mediates the vascular and platelet actions of nitric oxide: confirmation using an inhibitor of the soluble guanylyl cyclase. *Proceedings of the National Academy of Sciences of the United States of America* **93**, 1480-1485.

- Mukhopadhyay K, Chowdhary G, Singh P, Kumar P & Narang A. (2010). Neurodevelopmental Outcome of Acute Bilirubin Encephalopathy. *Journal of Tropical Pediatrics* **55**, 333-336.
- Müller J, Reyes-Haro D, Pivneva T, Nolte C, Schaette R, Lübke J & Kettenmann H. (2009). The principal neurons of the medial nucleus of the trapezoid body and NG2+ glial cells receive coordinated excitatory synaptic input. *The Journal of General Physiology* **134**, 115-127.
- Mustafa MG & King TE. (1970). Binding of Bilirubin with Lipid. A Possible Mechanism of its Toxic Reactions in Mitochondria. *Journal of Biological Chemistry* **245**, 1084-1089.
- Nakamura H, Takada S, Shimabuku R, Matsuo M, Matsuo T & Negishi H. (1985). Auditory Nerve and Brainstem Responses in Newborn Infants with Hyperbilirubinemia. *Pediatrics* **75**, 703-708.
- National Collaborating Centre for Women's and Children's Health. (2010). Neonatal Jaundice - Clinical Guideline May 2010, ed. National Institute for Health and Clinical Excellence (NICE), pp. 1-525. Royal College of Obstetricians and Gynaecologists, London.
- Neher E & Sakaba T. (2008). Multiple Roles of Calcium Ions in the Regulation of Neurotransmitter Release. *Neuron* **59**, 861-872.
- Nickisch A, Massinger C, Ertl-Wagner B & von Voss H. (2009). Pedaudiologic findings after severe neonatal hyperbilirubinemia. *European Archives of Oto-Rhino-Laryngology* **266**, 207-212.
- Nicol MJ & Walmsley B. (2002). Ultrastructural basis of synaptic transmission between endbulbs of Held and bushy cells in the rat cochlear nucleus. *The Journal of Physiology* **539**, 713-723.
- Notter MFD & Kendig JW. (1986). Differential sensitivity of neural cells to bilirubin toxicity. *Experimental Neurology* **94**, 670-682.
- Nowak L, Bregestovski P, Ascher P, Herbet A & Prochiantz A. (1984). Magnesium gates glutamate-activated channels in mouse central neurones. *Nature* **307**, 462-465.
- Nwaesei CG, Van Aerde J, Boyden M & Perlman M. (1984). Changes in Auditory Brainstem Responses in Hyperbilirubinemic Infants Before and After Exchange Transfusion. *Pediatrics* **74**, 800-803.
- O'Callaghan JP & Miller DB. (1985). Cerebellar hypoplasia in the Gunn rat is associated with quantitative changes in neurotypic and gliotypic proteins. *Journal of Pharmacology and Experimental Therapeutics* **234**, 522-533.
- Ochoa ELM, Wennberg RP, An Y, Tandon T, Takashima T, Nguyen T & Chui A. (1993). Interactions of bilirubin with isolated presynaptic nerve terminals:

- functional effects on the uptake and release of neurotransmitters. *Cellular and Molecular Neurobiology* **13**, 69-86.
- Odell GB. (1959). Studies in Kernicterus. I. The Protein Binding of Bilirubin. *The Journal of Clinical Investigation* **38**, 823-833.
- Oertel D. (1983). Synaptic responses and electrical properties of cells in brain slices of the mouse anteroventral cochlear nucleus. *The Journal of Neuroscience* **3**, 2043-2053.
- Orth J. (1875). Ueber das Vorkommen von Bilirubinkristallen bei neugeborenen Kindern. *Virchows Archiv* **63**, 447-462.
- Oysu C, Aslan I, Ulubil A & Baserer N. (2002). Incidence of cochlear involvement in hyperbilirubinemic deafness. *Annals of Otology Rhinology and Laryngology* **111**, 1021-1025.
- Özmert E, Erdem G, Topçu M, Yurdakök M, Tekinalp G, Genç D & Renda Y. (1996). Long-term follow-up of indirect hyperbilirubinemia in full-term Turkish infants. *Acta Pædiatrica* **85**, 1440-1444.
- Perlman JM, Rogers BB & Burns D. (1997). Kernicteric Findings at Autopsy in Two Sick Near Term Infants. *Pediatrics* **99**, 612-615.
- Perlman M, Fainmesser P, Sohmer H, Tamari H, Wax Y & Pevsmer B. (1983). Auditory Nerve-Brainstem Evoked Responses in Hyperbilirubinemic Neonates. *Pediatrics* **72**, 658-664.
- Pfeiffer RR. (1966a). Anteroventral cochlear nucleus: wave forms of extracellularly recorded spike potentials. *Science* **154**, 667-668.
- Pfeiffer RR. (1966b). Classification of response patterns of spike discharges for units in the cochlear nucleus: Tone-burst stimulation. *Experimental Brain Research* **1**, 220-235.
- Rasband MN. (2004). It's "juxta" potassium channel! *Journal of Neuroscience Research* **76**, 749-757.
- Rasband MN & Trimmer JS. (2001). Developmental clustering of ion channels at and near the node of Ranvier. *Developmental Biology* **236**, 5-16.
- Rennie J, Burman-Roy S & Murphy MS. (2010). Neonatal jaundice: summary of NICE guidance. *BMJ* **340**.
- Reyes-Haro D, Mueller J, Boresch M, Pivneva T, Benedetti B, Scheller A, Nolte C & Kettenmann H. (2010). Neuron-astrocyte interactions in the medial nucleus of the trapezoid body. *The Journal of General Physiology* **135**, 583-594.

- Rhee C-K, Park H-M & Jang Y-J. (1999). Audiologic Evaluation of Neonates With Severe Hyperbilirubinemia Using Transiently Evoked Otoacoustic Emissions and Auditory Brainstem Responses. *The Laryngoscope* **109**, 2005-2008.
- Ribeiro AC & Kapas L. (2005). Day- and nighttime injection of a nitric oxide synthase inhibitor elicits opposite sleep responses in rats. *Am J Physiol Regul Integr Comp Physiol* **289**, R521-531.
- Rice AC, Chiou V, Zuckoff S & Shapiro SM. (2011). Profile of Minocycline Neuroprotection in Bilirubin-Induced Auditory System Dysfunction. *Brain Research* **1368**, 290-298.
- Rigato I, Pascolo L, Ferneti C, Ostrow JD & Tiribelli C. (2004). The human multidrug-resistance-associated protein MRP1 mediates ATP-dependent transport of unconjugated bilirubin. *Biochemical Journal* **383**, 335-341.
- Roche KW & Isaac JT. (2007). AMPA Receptors. In *Encyclopedia of Life Sciences*.
- Rodrigues CMP, Sola S, Brito MA, Brites D & Moura JJG. (2002a). Bilirubin directly disrupts membrane lipid polarity and fluidity, protein order and redox status in rat mitochondria. *Journal of Hepatology* **36**, 335-341.
- Rodrigues CMP, Sola S, Castro RE, Laires PA, Brites D & Moura JJG. (2002b). Perturbation of membrane dynamics in nerve cells as an early event during bilirubin-induced apoptosis. *Journal of Lipid Research* **43**, 885-894.
- Rose AL & Wisniewski H. (1979). Acute Bilirubin Encephalopathy Induced With Sulfadimethoxine in GUNN rats. *Journal of Neuropathology and Experimental Neurology* **38**, 152-164.
- Roseth S, Hansen TWR, Fonnum E & Walaas SI. (1998). Bilirubin inhibits transport of neurotransmitters in synaptic vesicles. *Pediatric Research* **44**, 312-316.
- Roy-Chowdhury J, Huang TJ, Kesari K, Lederstein M, Arias IM & Roy-Chowdhury N. (1991). Molecular basis for the lack of bilirubin-specific and 3-methylcholanthrene-inducible UDP-glucuronosyltransferase activities in Gunn rats. The two isoforms are encoded by distinct mRNA species that share an identical single base deletion. *Journal of Biological Chemistry* **266**, 18294-18298.
- Rudy B & McBain CJ. (2001). Kv3 channels: voltage-gated K⁺ channels designed for high-frequency repetitive firing. *Trends in Neurosciences* **24**, 517-526.

- Ryugo DK, Wu MM & Pongstaporn T. (1996). Activity-related features of synapse morphology: A study of endbulbs of Held. *The Journal of Comparative Neurology* **365**, 141-158.
- Sabatini BL & Regehr WG. (1996). Timing of neurotransmission at fast synapses in the mammalian brain. *Nature* **384**, 170-172.
- Saluja S, Agarwal A, Kler N & Amin S. (2010). Auditory neuropathy spectrum disorder in late preterm and term infants with severe jaundice. *International Journal of Pediatric Otorhinolaryngology* **74**, 1292-1297.
- Sato H, Keino H, Aono S, Semba R & Kashiwamata S. (1987). Different Behaviors Among Lysosomal Enzymes in the Cerebellum of Jaundiced Gunn Rats with Cerebellar Hypoplasia. *Journal of Neurochemistry* **48**, 1823-1825.
- Sätzler K, Söhl LF, Bollmann JH, Borst JGG, Frotzsch M, Sakmann B & Lübke JHR. (2002). Three-Dimensional reconstruction of a Calyx of Held and its postsynaptic principal neuron in the Medial Nucleus of the Trapezoid Body. *Journal of Neuroscience* **22**, 10567-10579.
- Sawasaki Y, Yamada N & Nakajima H. (1976). Developmental features of cerebellar hypoplasia and brain bilirubin levels in a mutant (GUNN) rat with hereditary hyperbilirubinaemia. *Journal of Neurochemistry* **27**, 577-583.
- Scheidt PC, Mellits ED, Hardy JB, Drage JS & Boggs TR. (1977). Toxicity to bilirubin in neonates: Infant development during first year in relation to maximum neonatal serum bilirubin concentration. *The Journal of Pediatrics* **91**, 292-297.
- Schmid R, Axelrod J, Hammaker L & Swarm RL. (1958). Congenital jaundice in rats, due to a defect in glucuronide formation. *Journal of Clinical Investigation* **37**, 1123-1130.
- Schmid R & Hammaker L. (1963). Metabolism and disposition of C¹⁴-bilirubin in congenital nonhemolytic jaundice. *The Journal of Clinical Investigation* **42**, 1720-1734.
- Schulz-Schaeffer W. (2010). The synaptic pathology of α -synuclein aggregation in dementia with Lewy bodies, Parkinson's disease and Parkinson's disease dementia. *Acta Neuropathologica* **120**, 131-143.
- Schutta HS & Johnson L. (1967). Bilirubin encephalopathy in the GUNN rat: a fine structure study of the cerebellar cortex. *Journal of Neuropathology and Experimental Neurology* **26**, 377-396.
- Schutta HS & Johnson L. (1969). Clinical signs and morphologic abnormalities in Gunn rats treated with sulfadimethoxine. *The Journal of Pediatrics* **75**, 1070-1079.

- Schutta HS & Johnson L. (1971). Electron microscopic observations on acute bilirubin encephalopathy in Gunn rats induced by sulfadimethoxine. *Laboratory Investigation* **24**, 82-89.
- Scragg I, Celier C & Burchell B. (1985). Congenital jaundice in rats due to the absence of hepatic bilirubin UDP-glucuronyltransferase enzyme protein. *FEBS Letters* **183**, 37-42.
- Sgro M, Campbell D & Shah V. (2006). Incidence and causes of severe neonatal hyperbilirubinemia in Canada. *Canadian Medical Association Journal* **175**, 587-590.
- Shaia WT, Shapiro SM, Heller AJ, Galiani DL, Sismanis A & Spencer RF. (2002). Immunohistochemical localization of calcium-binding proteins in the brainstem vestibular nuclei of the jaundiced Gunn rat. *Hearing Research* **173**, 82-90.
- Shaia WT, Shapiro SM & Spencer RF. (2005). The jaundiced Gunn rat model of auditory neuropathy/dyssynchrony. *Laryngoscope* **115**, 2167-2173.
- Shapiro SM. (1988). Acute Brainstem Auditory Evoked Potential Abnormalities in Jaundiced Gunn Rats Given Sulfonamide. *Pediatric Research* **23**, 306-310.
- Shapiro SM. (1993). Reversible brainstem auditory evoked potential abnormalities in jaundiced Gunn rats given Sulfonamide. *Pediatric Research* **34**, 629-633.
- Shapiro SM. (2010). Chronic bilirubin encephalopathy: diagnosis and outcome. *Seminars in Fetal and Neonatal Medicine* **15**, 157-163.
- Shapiro SM, Bhutani VK & Johnson L. (2006). Hyperbilirubinemia and Kernicterus. *Clinics in Perinatology* **33**, 387-410.
- Shapiro SM & Conlee JW. (1991). Brainstem auditory evoked potentials correlate with morphological changes in Gunn rat pups. *Hearing Research* **57**, 16-22.
- Shapiro SM, Sombati S, Geiger A & Rice AC. (2007). NMDA channel antagonist MK-801 does not protect against bilirubin neurotoxicity. *Neonatology* **92**, 248-257.
- Shaw NA. (1988). The auditory evoked potential in the rat - a review. *Progress in Neurobiology* **31**, 19-45.
- Sheykholeslami K & Kaga K. (2000). Otoacoustic emissions and auditory brainstem responses after neonatal hyperbilirubinemia. *International Journal of Pediatric Otorhinolaryngology* **52**, 65-73.

- Silberberg DH & Schutta HS. (1967). The effects of unconjugated bilirubin and related pigments on cultures of rat cerebellum. *Journal of Neuropathology & Experimental Neurology* **26**, 572-583.
- Silva DPCd & Martins RHG. (2009). Analysis of transient otoacoustic emissions and brainstem evoked auditory potentials in neonates with hyperbilirubinemia. *Brazilian Journal of Otorhinolaryngology (Impresso)* **75**, 381-386.
- Silva R, Mata L, Gulbenkian S, Brito MA, Tiribelli C & Brites D. (1999). Inhibition of glutamate uptake by unconjugated bilirubin in cultured cortical rat astrocytes: role of concentration and pH. *Biochemical and Biophysical Research Communications* **265**, 67-72.
- Silva RFM, Rodrigues CMP & Brites D. (2002). Rat cultured neuronal and glial cells respond differently to toxicity of unconjugated bilirubin. *Pediatric Research* **51**, 535-541.
- Silverman WA, Andersen DH, Blanc WA & Crozier DN. (1956). A difference in mortality rate and incidence of kernicterus among premature infants allotted to two prophylactic antibacterial regimens. *Pediatrics* **18**, 614-625.
- Siskova Z, Page A, O'Connor V & Perry VH. (2009). Degenerating Synaptic Boutons in Prion Disease: Microglia Activation without Synaptic Stripping. *American Journal of Pathology* **175**, 1610-1621.
- Sisson TRC, Goldberg S & Slaven B. (1974). The Effect of Visible Light on the Gunn Rat: Convulsive Threshold, Bilirubin Concentration, and Brain Color. *Pediatric Research* **8**, 647-651.
- Smith AJ, Owens S & Forsythe ID. (2000). Characterisation of inhibitory and excitatory postsynaptic currents of the rat medial superior olive. *The Journal of Physiology* **529**, 681-698.
- Smith PH, Joris PX, Carney LH & Yin TCT. (1991). Projections of physiologically characterized globular bushy cell axons from the cochlear nucleus of the cat. *Journal of Comparative Neurology* **304**, 387-407.
- Smith PH, Joris PX & Yin TCT. (1998). Anatomy and physiology of principal cells of the medial nucleus of the trapezoid body (MNTB) of the cat. *Journal of Neurophysiology* **79**, 3127-3142.
- Sohmer H, Feinmesser M & Szabo G. (1974). Sources of electrocochleographic responses as studied in patients with brain damage. *Electroencephalography and Clinical Neurophysiology* **37**, 663-669.
- Spencer RF, Shaia WT, Gleason AT, Sismanis A & Shapiro SM. (2002). Changes in calcium-binding protein expression in the auditory brainstem nuclei of the jaundiced Gunn rat. *Hearing Research* **171**, 129-141.

- Spirou GA, Brownell WE & Zidanic M. (1990). Recordings from cat trapezoid body and HRP labeling of globular bushy cell axons. *Journal of Neurophysiology* **63**, 1169-1190.
- Starr A & Hamilton AE. (1976). Correlation between confirmed sites of neurological lesions and abnormalities of far-field auditory brainstem responses. *Electroencephalography and Clinical Neurophysiology* **41**, 595-608.
- Starr A, Picton TW, Sininger Y, Hood LJ & Berlin CI. (1996). Auditory neuropathy. *Brain* **119**, 741-753.
- Steinert JR, Chernova T & Forsythe ID. (2010a). Nitric Oxide Signaling in Brain Function, Dysfunction, and Dementia. *The Neuroscientist* **16**, 435-452.
- Steinert JR, Kopp-Scheinflug C, Baker C, Challiss RAJ, Mistry R, Haustein MD, Griffin SJ, Tong H, Graham BP & Forsythe ID. (2008). Nitric Oxide Is a Volume Transmitter Regulating Postsynaptic Excitability at a Glutamatergic Synapse. *Neuron* **60**, 642-656.
- Steinert JR, Postlethwaite M, Jordan MD, Chernova T, Robinson SW & Forsythe ID. (2010b). NMDAR-mediated EPSCs are maintained and accelerate in time course during maturation of mouse and rat auditory brainstem in vitro. *The Journal of Physiology* **588**, 447-463.
- Stocker R, Yamamoto Y, McDonagh AF, Glazer AN & Ames BN. (1987). Bilirubin is a antioxidant of possible physiological importance. *Science* **235**, 1043-1046.
- Strauss K, Robinson D, Vreman H, Puffenberger E, Hart G & Morton D. (2006). Management of hyperbilirubinemia and prevention of kernicterus in 20 patients with Crigler-Najjar disease. *European Journal of Pediatrics* **165**, 306-319.
- Strebel L & Odell GB. (1971). Bilirubin Uridine Diphospho-Glucuronyltransferase in rat liver microsomes: Genetic variation and maturation. *Pediatric Research* **5**, 548-559.
- Suneja SK, Benson CG, Gross J & Potashner SJ. (1995). Uptake and Release of d-Aspartate, GABA, and Glycine in Guinea Pig Brainstem Auditory Nuclei. *Journal of Neurochemistry* **64**, 147-160.
- Takagishi Y. (1989). Development of cerebellar hypoplasia in jaundiced Gunn rats: a morphological study. *Congenital Anomalies* **29**, 275-294.
- Takagishi Y & Yamamura H. (1989). Purkinje cell abnormalities and synaptogenesis in genetically jaundiced rats (Gunn rats). *Brain Research* **492**, 116-128.

- Takagishi Y & Yamamura H. (1994). Membrane structure of parallel-fibre synaptic terminals in the cerebellum of the jaundiced Gunn rat: freeze-fracture and E-PTA study. *Journal of Neurocytology* **23**, 39-48.
- Takahashi T, Forsythe ID, Tsujimoto T, BarnesDavies M & Onodera K. (1996). Presynaptic calcium current modulation by a metabotropic glutamate receptor. *Science* **274**, 594-597.
- Talarek S & Fidecka S. (2004). Involvement of nitricoxidergic system in the hypnotic effects of benzodiazepines in mice. *Polish Journal of Pharmacology* **56**, 719-726.
- Taschenberger H & von Gersdorff H. (2000). Fine-tuning an auditory synapse for speed and fidelity: developmental changes in presynaptic waveform, EPSC kinetics, and synaptic plasticity. *Journal of Neuroscience* **20**, 9162-9173.
- Theer P, Hasan MT & Denk W. (2003). Two-photon imaging to a depth of 1000 μm in living brains by use of a Ti:Al₂O₃ regenerative amplifier. *Optics Letters* **28**, 1022-1024.
- Thoma J, Gerull G & Mrowinski D. (1986). A long-term study of hearing in children following neonatal hyperbilirubinemia. *European Archives of Oto-Rhino-Laryngology* **243**, 133-137.
- Tikmani SS, Warraich HJ, Abbasi F, Rizvi A, Darmstadt GL & Zaidi AKM. (2010). Incidence of neonatal hyperbilirubinemia: a population-based prospective study in Pakistan. *Tropical Medicine & International Health* **15**, 502-507.
- Toietta G, Mane VP, Norona WS, Finegold MJ, Ng P, McDonagh AF, Beaudet AL & Lee B. (2005). Lifelong elimination of hyperbilirubinemia in the Gunn rat with a single injection of helper-dependent adenoviral vector. *Proceedings of the National Academy of Sciences of the United States of America* **102**, 3930-3935.
- Tolbert LP & Morest DK. (1982). The neuronal architecture of the anteroventral cochlear nucleus of the cat in the region of the cochlear nerve root: Golgi and Nissl methods. *Neuroscience* **7**, 3013-3030.
- Tolbert LP, Morest DK & Yurgelun-Todd DA. (1982). The neuronal architecture of the anteroventral cochlear nucleus of the cat in the region of the cochlear nerve root: Horseradish peroxidase labelling of identified cell types. *Neuroscience* **7**, 3031-3052.
- Tong H, Steinert JR, Robinson SW, Chernova T, Read DJ, Oliver DL & Forsythe ID. (2010). Regulation of Kv channel expression and neuronal excitability in rat medial nucleus of the trapezoid body maintained in organotypic culture. *The Journal of Physiology* **588**, 1451-1468.

- Tukey RH & Strassburg CP. (2000). Human UDP-Glucuronosyltransferases: Metabolism, Expression, and Disease. *Annual Review of Pharmacology and Toxicology* **40**, 581-616.
- Typlt M, Haustein MD, Dietz B, Steinert JR, Witte M, Englitz B, Milenkovic I, Kopp-Scheinflug C, Forsythe ID & Rübsamen R. (2010). Presynaptic and postsynaptic origin of multicomponent extracellular waveforms at the endbulb of Held spherical bushy cell synapse. *European Journal of Neuroscience* **31**, 1574-1581.
- Uziel A, Marot M & Pujol R. (1983). The Gunn Rat - an Experimental Model for Central Deafness. *Acta Oto-Laryngologica* **95**, 651-656.
- van der Veere CN, Sinaasappel M, McDonagh AF, Rosenthal P, Labrune P, Odièvre M, Fevery J, Otte J, McClean P, Bürk G, Masakowski V, Sperl W, Mowat AP, Vergani GM, Heller K, Wilson JP, Shepherd R & Jansen PL. (1996). Current therapy for Crigler-Najjar syndrome type 1: Report of a world registry. *Hepatology* **24**, 311-315.
- Vazquez J, Garcia-Calvo M, Valdivieso F, Mayor F & Mayor F, Jr. (1988). Interaction of bilirubin with the synaptosomal plasma membrane. *Journal of Biological Chemistry* **263**, 1255-1265.
- Wang L-Y, Gan L, Forsythe ID & Kaczmarek LK. (1998a). Contribution of the Kv3.1 potassium channel to high-frequency firing in mouse auditory neurones. *The Journal of Physiology* **509**, 183-194.
- Wang X, Sarkar DP, Mani P, Steer CJ, Chen Y, Guha C, Chandrasekhar V, Chaudhuri A, Roy-Chowdhury N, Kren BT & Roy-Chowdhury J. (2009). Long-term reduction of jaundice in Gunn rats by nonviral liver-targeted delivery of *Sleeping Beauty* transposon. *Hepatology* **50**, 815-824.
- Wang Y-X, Wenthold RJ, Ottersen OP & Petralia RS. (1998b). Endbulb Synapses in the Anteroventral Cochlear Nucleus Express a Specific Subset of AMPA-Type Glutamate Receptor Subunits. *Journal of Neuroscience* **18**, 1148-1160.
- Warr O, Mort D & Attwell D. (2000). Bilirubin does not modulate ionotropic glutamate receptors or glutamate transporters. *Brain Research* **879**, 13-16.
- Wong V, Chen W-X & Wong K-Y. (2006). Short- and Long-Term Outcome of Severe Neonatal Nonhemolytic Hyperbilirubinemia. *Journal of Child Neurology* **21**, 309-315.
- Wu L-G, Westenbroek RE, Borst JGG, Catterall WA & Sakmann B. (1999). Calcium Channel Types with Distinct Presynaptic Localization Couple Differentially to Transmitter Release in Single Calyx-Type Synapses. *Journal of Neuroscience* **19**, 726-736.

- Wu SH & Kelly JB. (1992). Synaptic pharmacology of the superior olivary complex studied in mouse brain slice. *Journal of Neuroscience* **12**, 3084-3097.
- Wu SH & Kelly JB. (1995). Inhibition in the superior olivary complex: pharmacological evidence from mouse brain slice. *Journal of Neurophysiology* **73**, 256-269.
- Yu FH & Catterall WA. (2003). Overview of the voltage-gated sodium channel family. *Genome Biology* **4**, 207.
- Zhang S, Wickesberg RE & Oertel D. (1989). Jaundiced Gunn rats have increased synaptic delays in the ventral cochlear nucleus. *Brain Research* **501**, 194-197.
- Zucker SD, Goessling W & Hoppin AG. (1999). Unconjugated Bilirubin Exhibits Spontaneous Diffusion through Model Lipid Bilayers and Native Hepatocyte Membranes. *Journal of Biological Chemistry* **274**, 10852-10862.

LIST OF ABBREVIATIONS

7-NI	7-nitro-indazole	jj-Gunn	homozygous Gunn rat
ABR	auditory brainstem response	Jj-Gunn	heterozygous Gunn rat
ACSF	artificial cerebrospinal fluid	K _v	voltage-gated potassium channel family
AMPA	α-amino-3-hydroxy-5-methyl-isoxazole-propionate	LM	light microscopy/ light microscopic
AP	action potential	LSO	lateral superior olive
AVCN	anteroventral cochlear nucleus	MEA	multi-electrode array
CCD	charge-coupled device	MNTB	medial nucleus of the trapezoid body
CN	cochlear nucleus	MSO	medial superior olive
DNQX	6,7-dinitroquinoxaline-2,3-dione	NMDA	N-methyl-D-aspartate
DTMR	dextran-tetra-methyl-rhodamine	nNOS	neuronal nitric oxide synthase
DTX-I	dendrotoxin-I	NO	nitric oxide
EM	electron microscopy/ electron microscopic	SBC	spherical bushy cell
EPSC	excitatory post synaptic current	SOC	superior olivary complex
EPSP	excitatory post synaptic potential	TEA	tetraethylammonium
FP	field potential	TTX	tetrodotoxin
GABA	γ-amino-butyric-acid	UDP-GT	uridine-di-phosphate glucuronosyl-transferase
GBC	globular bushy cell	VCN	ventral cochlear nucleus